



Palacký University Olomouc
Faculty of Medicine and Dentistry

**IDENTIFICATION AND CHARACTERISATION OF TAU
MINIMAL REGIONS AS POTENTIAL
PHARMACOLOGICAL TARGETS AGAINST TAU
SPREADING IN TAUOPATHIES**

DISSERTATION

Presented in partial fulfilment of the requirements for the
Degree of Doctor of Philosophy in Pediatrics

By

Narendran Annadurai, M.Sc.

February 2023

Supervisor

Viswanath Das, M.Sc., Ph.D.

I, the undersigned, hereby declare that this Ph.D. dissertation has been composed solely by myself, under the supervision of Viswanath Das, M.Sc., Ph.D. Any collaborative contributions from colleagues have been explicitly acknowledged, and references to all supporting literature and resources have been duly cited. The research was carried out at the Institute of Molecular and Translational Medicine, Faculty of Medicine and Dentistry, Palacký University Olomouc.

I further declare that this dissertation has not been submitted, in whole or in part, for any other degree or professional qualification.

In Olomouc

February 2023

Narendran Annadurai, M.Sc.

Acknowledgement

First, I would like to express my deepest gratitude to my supervisor, Viswanath Das, MSc., PhD., for allowing me to pursue a PhD under his guidance. He was always there to provide his scientific insights and helped me to progress as a researcher. I am incredibly thankful to you for always trusting and believing in me and allowing me to learn from my mistakes. This endeavour would not have been possible without your guidance. I appreciate all your contributions of time, enduring support, encouragement, and words of wisdom which always helped me during challenging times in the PhD pursuit.

I am incredibly thankful to Doc. MUDr. Marián Hajdúch, PhD., the Director of the Institute of Molecular and Translational Medicine, for providing me with an excellent scientific infrastructure to carry out my research work without any hurdles. I highly appreciate your support and encouragement throughout my study period.

I sincerely thank Prof. Juan Bautista De Sanctis, PhD., for giving valuable suggestions and ideas and motivating me to pursue research. I also thank MUDr. Petr Džubák, PhD., and MUDr. Josef Srovnal, PhD., for their support during my PhD studies.

I owe thankfulness to my colleague, Mgr. Agáta Kubíčková for her support and help with my laboratory experiments. I express my gratitude to Soňa Gurská, PhD., for her help in high throughput screening experiments. Additionally, I thank Ivo Frydrych, PhD., and Ján Gurský, PhD., for helping me with fluorescence-activated cell sorting experiments. I also thank Ermin Schadich, PhD., for his support and help during my studies. I also extend my thanks to Khushboo Agrawal, PhD., and Jiří Řehulka, PhD., for their support when I joined the institute as a fresh PhD student and for technical help during my studies.

I express my special thanks to Mgr. Anna Janošťáková for providing an organized tissue culture laboratory environment to carry out my experiments without any discrepancies. I also thank Bc. Renata Buriánová for her help and support in the cell biology lab.

I owe thankfulness to my colleagues Mgr. Jana Václavková, PhD., Mgr. Jana Kotulová, PhD., Mgr. Martin Ondra, Mgr. Jarmila Stanková and Mgr. Kateřina Ječmeňová for their help and

support during my stay at IMTM. I also thank Jiří Hrubý, who was my BSc student, for his contribution to my study.

I would also like to thank Dr Maritn Mistrik and Dr Koberna Karel for letting me use some instruments in their lab. I also thank Prof. Jiří Drábek, PhD., for his support and for providing me with a thermo-shaker. I want to acknowledge all my colleagues at IMTM for helping me in various stages of my PhD.

I also want to thank Lukáš Malina, PhD., and Jakub Malohlava, PhD., from the Department of Medical Biophysics, Faculty of Medicine and Dentistry, Palacký University in Olomouc, Czech Republic, for helping me with atomic force microscopy experiments.

I sincerely thank my collaborators, Drs. Mario Salmona, Luisa Diomede, Antonio Bastone, Alfredo Cagnotto and Margherita Romeo from the Department of Molecular Biochemistry and Pharmacology, Istituto di Ricerche Farmacologiche Mario Negri IRCCS, Milan, Italy. I am grateful for their support in providing tau peptides and working with *Caenorhabditis elegans* models for my studies.

I am thankful to Prof. Michal Otyepka, PhD., and Mgr. Martin Šrejber, PhD., from Czech Advanced Technology and Research Institute (CATRIN), Regional Centre of Advanced Technologies and Materials (RCPTM), Palacký University Olomouc, Czech Republic and doc. RNDr. Karel Berka, PhD., from the Department of Physical Chemistry, Faculty of Science, Palacký University Olomouc, Czech Republic, for helping with molecular simulation studies.

I want to extend my sincere thanks to the secretaries and administrative staff of IMTM for their help with administrative matters. I also thank receptionists Jiří Krajča and Markéta Strakošová for their help. Finally, I thank Jitka Melcrová and the staff from the study department for their incredible cooperation throughout my PhD.

I could not have undertaken this journey without the support and love of my family- my parents, Jayalakshmi and Annadurai, for supporting me throughout my life. In addition, I thank my wife, Renuka, for her moral support and constant encouragement. This thesis would not be possible without you all.

Funding Acknowledgement

This work was supported by Palacký University Olomouc Doctoral Scholarship to Narendran Annadurai. The research was supported by generous funding from the Internal Student Grant Agency of the Palacký University in Olomouc (IGA_LF_2017_026, IGA_LF_2018_031, IGA_LF_2019_018, IGA_LF_2020_007, IGA_LF_2021_038 and IGA_LF_2022_033), the European Regional Development Fund (ENOCHE, CZ.02.1.01/0.0/0.0/16_019/0000868), the Czech Ministry of Education, Youth and Sports (LO1304, LM2011024, LM2018130, LM2018133 and LM2018129), the Ministry of Health of the Czech Republic (NV15-31984A, AZV 16-32105A), and the Technology Agency of the Czech Republic (PerMed, TN01000013). The study was partly supported by project nr. LX22NPO5107 (MEYS): Financed by EU – Next Generation EU.

| | |
|---|-----|
| Abbreviations | i |
| Summary | iii |
| List of tables | vi |
| List of figures | vii |
| 1 Introduction | 1 |
| 1.1. Dementia..... | 2 |
| 1.2. Proteinopathies | 6 |
| 1.3. Functions of tau protein..... | 10 |
| 1.4. Impact of tau mutations on its interaction with microtubules..... | 13 |
| 1.5. Post-translational modifications of tau..... | 18 |
| 1.6. Tauopathies | 21 |
| 1.7. Tau targeting therapy..... | 39 |
| 2 Aims of the study | 45 |
| 3 Materials and Methods | 47 |
| 3.1. Chemicals and peptides..... | 48 |
| 3.2. Tau aggregation assay..... | 50 |
| 3.3. Fluorescence imaging, atomic force microscopy, and Congo red absorbance..... | 51 |
| 3.4. Coomassie gel staining..... | 52 |
| 3.5. Preparation of models for molecular dynamics simulation..... | 53 |
| 3.6. Cell culture and DNA transfection..... | 53 |
| 3.7. Tau seeding assay..... | 53 |
| 3.8. Imaging and quantification of cell number and seeding..... | 55 |
| 3.9. Quantification of internalised R3 fibrils..... | 56 |
| 3.10. Cytotoxicity assay | 57 |
| 3.11. Determining the IC ₅₀ value of compounds..... | 57 |
| 3.12. Triton X-100 cell fractionation and Western blot analysis..... | 57 |
| 3.13. Sample processing and protein quantification..... | 58 |

| | |
|---|------------|
| 3.14. SDS-PAGE Electrophoresis and Western blotting | 60 |
| 3.15. Cellular re-seeding assay..... | 62 |
| 3.16. <i>Caenorhabditis elegans</i> studies..... | 62 |
| 3.17. Statistical analysis..... | 62 |
| 4 Identification of minimal regions in the tau repeat microtubule-binding domain that defines seeding and its impact on intracellular tau phosphorylation and aggregation..... | 65 |
| Results..... | 66 |
| 4.1.R3 repeat region of the tau RD is essential for self-assembly of tau..... | 66 |
| 4.2.Seed-competent R2 and R3 fibrils induce tau RD P301S aggregation..... | 69 |
| 4.3.R2 and R3 seeds increase triton-insoluble phospho-tau levels and reseed intracellular tau..... | 72 |
| Discussion..... | 78 |
| 5 Targeting the minimal regions with small molecules to abrogate the generation of prion-like tau aggregates..... | 81 |
| Results..... | 82 |
| 5.1.R3 aggregation and effects of antitumour drugs on their fibrillisation..... | 82 |
| 5.2.Inhibition of polymerisation of preformed R3 fibrils..... | 88 |
| 5.3.Mechanisms of drug effect on R3 fibrillisation..... | 90 |
| 5.4.Molecular dynamics simulation of drug-peptide interaction..... | 93 |
| 5.5.Exogenous R3Ag effect on intracellular Tau-RD seeding..... | 95 |
| 5.6.Drug treatment abrogates R3Ag-mediated intracellular tau seeding..... | 98 |
| 5.7.Drugs protect <i>C. elegans</i> from R3Ag-mediated toxicity..... | 106 |
| Discussion..... | 111 |
| 6 Comparison of clearance of intracellular aggregates in tau cell model seeded with aggregates of tau repeat peptides..... | 114 |
| Results..... | 115 |
| 6.1.R2 and R3 fibrils affect autophagy in tau biosensor cells..... | 115 |
| 6.2.Screening of autophagy-inducing compounds that reduce intracellular tau aggregation in R3 fibrils..... | 115 |

| | |
|---|------------|
| 6.3. EGCG and RSV reduced intracellular tau aggregation in R3 fibrils seeded tau biosensor cells..... | 117 |
| 6.4. EGCG and RSV induced autophagy in R3 fibrils seeded tau biosensor cells..... | 117 |
| 6.5. CQ inhibited autophagy in R3 fibrils seeded tau biosensor cells..... | 122 |
| 6.6. Effect of EGCG, RSV and CQ on triton-insoluble total and phosphorylated Ser262 tau..... | 122 |
| Discussion..... | 126 |
| 7 General Discussion | 130 |
| References | 135 |
| Publications | 155 |
| Appendix | 156 |
| Materials (Instruments and equipment) | 158 |
| Curriculum vitae | 160 |

Abbreviations

A β – Amyloid beta

AFM – Atomic Force Microscopy

AD – Alzheimer's disease

ANS – 8-anilino-1-naphthalenesulfonic acid

BSA – Bovine serum albumin

CBS – Corticobasal syndrome

CJD – Creutzfeldt-Jakob disease

CNS – Central Nervous System

CTE – Chronic Traumatic Encephalopathy

DMSO – Dimethyl Sulfoxide

DMF – Dimethylformamide

DTT – Dithiothreitol

EDTA – Ethylenediaminetetraacetic acid

FTDP-17 – Frontotemporal dementia with parkinsonism linked to chromosome 17

FRET – Förster resonance energy transfer

HPLC – High-performance liquid chromatography

MAPT – Microtubule Associated Protein Tau

MTBD – Microtubule-binding domain

MCI – mild cognitive impairment

MS – Multiple sclerosis

NPH – Normal pressure hydrocephalus

NFTs – Neurofibrillary tangles

NGM – Nematode growth media

PAGE – Polyacrylamide gel electrophoresis

PBS – Phosphate-buffered saline

PiD – Pick's disease

PHFs – Paired helical filaments

PVDF – Polyvinylidene difluoride

R3Ag – R3 aggregates

RT – Room temperature

SDS – Sodium dodecyl sulfate

TBS – Tris-buffered saline

TFA – Trifluoroacetic acid

ThT – Thioflavin T

Tau, a microtubule-associated protein present abundantly in neurons of the central nervous system, stabilizes axonal microtubules, providing structural architecture to axons. Tau aggregation occurs in many neurodegenerative diseases collectively termed ‘tauopathies’, including Alzheimer's disease (AD) and frontotemporal dementia (FTD). These diseases are characterized by the intracellular deposits of fibrillar tau tangles. The spreading of tau aggregates *via* transcellular propagation is a common feature of several tauopathies, where synaptic tau seeding precedes the pathological spreading of tau¹⁻⁴. Tau seeding, the ability of prion-like tau to recruit and misfold inert tau to generate new seeds, is detected early in AD human brains before the development of significant tau pathology. Circumstantial evidence shows that pathological ‘tau seeds’ spread across the brain through synaptically connected neurons, potentially contributing to AD pathogenesis^{1,5-10}. Clinically, the presence of tau precedes significant grey matter atrophy in the AD brain, suggesting that tau aggregation acts as a critical inducer of neurodegeneration¹¹. Microtubule-binding domain in tau plays a pivotal role in its aggregation^{12,13}. Two amyloid hexapeptide motifs in the tau repeat domain, VQIINK (PHF6*) of repeat 2 (R2) and VQIVYK (PHF6) of repeat 3 (R3), assemble into β -sheet-rich fibrils *in vitro*, but these fibrils are not prion-like¹⁴. On the contrary, the 31-amino acid R3 self-assembles into prion-like aggregates^{15,16}. Rapid tau fibrillisation is also mediated by phosphorylation of Ser202/Thr205/Ser208 sites in the proline-rich domain¹⁷. Inclusive evidence proves that changes induced by pathological hyperphosphorylation affect tau seeding, resulting in tau propagation and subsequent AD progression^{5,18-20}.

Our study aimed at the identification of the minimal regions within the tau repeat domain that define seeding potency and the subsequent impact on intracellular native tau. By using individual tau repeat peptides, we first showed that R2 and R3 form seed-competent fibrils in the presence of heparin. Though R2 and R3 hold identical N-terminal hexapeptide and cysteine residue sequences, R3 but not R2 formed prion-like fibrils in the absence of heparin. Besides, cysteine to alanine substitution in R3 (C322A) abrogated its self-aggregation and seeding potency. However, despite this substitution, R3 (C322A) assembled into prion-like fibrils, but only in the presence of heparin. Next, prion-like aggregates of R2 and R3 induced aggregation, pathological phosphorylation and

oligomerization of native tau in tau cell models expressing P301S or P301L tau. Protein fractions prepared from biosensor cells, previously seeded with R2 and R3 aggregates, resulted in the aggregation of native tau upon introduction into a fresh set of cells. Our findings suggest that under physiological conditions, while R3 may be the minimal region essential for pathological seed generation, R2 needs polyanionic cofactors to initiate pathogenic seeds. R2 and R3 fibrils induce template-induced misfolding and pathological hyperphosphorylation of intracellular inert tau, making intracellular tau seed-competent. These findings shed light on potential molecular mechanisms of aggregation of native tau by exogenous prion-like aggregates. Overall, the results of our study identify N-terminal hexapeptides and cysteine residue of R2 and R3 as druggable targets for early inhibition of prion-like seeds.

Next, to prove our above hypothesis, we targeted the minimal regions (VQIVYK and cysteine) of self-aggregating R3 with small molecules to abolish the prion-like activity of R3 aggregates. Antitumour drugs have been suggested to confer protection against neurodegeneration, supporting the idea of repurposing approved and experimental or investigational oncology drugs for AD therapy²¹. Therefore, we evaluated whether antitumour drugs that abrogate the generation of prion-like aggregates of tau R3 prevent tau seeding and toxicity in the tau cell model and *Caenorhabditis elegans*. We demonstrated that small molecules that interact with the N-terminal VQIVYK or the C-terminal region housing the cysteine residue (C322) prevent tau R3 dimerisation and abolish the generation of prion-like R3 aggregates. Preformed R3 seeds capped with, or R3 seeds formed in the presence of VQIVYK- or C322-targeting drugs, have a reduced prion-like potency to cause aggregation of endogenous tau in tau biosensor cells. These findings indicate that VQIVYK- or C322-targeting drugs may act as prophylactic agents against tau seeding.

Since we found the prion-like potential of R2 and R3, we next wanted to explore the mechanisms associated with the clearance of intracellular aggregates in biosensor cells seeded with R2 and R3 aggregates. First, we found that both R2 and R3 seeds increased p62 levels in response to the build-up of intracellular tau aggregates. Next, R2 and R3 seeds reduced the autophagy marker indicated by the conversion of LC3-I to -II. These findings indicate a failure in autophagy initiation and autophagy flux in tau biosensor cells, causing a failure in the clearance of intracellular aggregates. Thus, we studied whether autophagy-inducing compounds can remove intracellular tau aggregates. We showed that autophagy inducers such as EGCG, RSV and VITC reduced intracellular tau

aggregates. Alternatively, we also found that autophagy inhibition by CQ failed to clear the intracellular aggregates. As we proved in our previous study, the seeding process involves the build-up of intracellular phosphorylated tau aggregates. Therefore, we checked the insoluble total and phosphorylated tau levels in the EGCG, RSV and CQ-treated biosensor cells seeded with R3 seeds. We found that EGCG reduced both triton-insoluble total and phosphorylated Ser262 tau. As expected, CQ treatment did not affect the triton-insoluble total and phosphorylated Ser262 tau levels. These findings indicate that autophagy induction can be used to target the clearance of intracellular tau aggregates.

Altogether, evidence from this thesis supports the importance of targeting N-terminal hexapeptides or cysteines of R2 or R3 and enhancing cell clearance mechanisms for developing tau-targeted therapies.

List of tables

| | |
|---|-----|
| Table 1.1. Tau isoforms..... | 11 |
| Table 3.1. Source of antitumour drugs and solvent concentrations..... | 63 |
| Table 3.2. Sources of compounds, stock and working concentrations..... | 64 |
| Table 5.1. List of antitumor drugs classified into six groups based on their primary mechanism of action..... | 84 |
| Table 5.2. Comparison of ThT fluorescence reading from Fig. 5.1C..... | 86 |
| Table 5.3. P-value summary from Fig. 5.16..... | 109 |
| Table 6.1. List of compounds and their mechanism of autophagy induction or inhibition..... | 116 |

List of figures

| | |
|---|----|
| Fig. 1.1. Timeline showing the approval years of AD drugs since the discovery of the first case of AD in 1906 by Alois Alzheimer by the US FDA..... | 5 |
| Fig. 1.2. Six tau isoforms generated by alternative splicing of MAPT genes 16 exons..... | 9 |
| Fig. 1.3. Tau-microtubule dynamics under healthy and pathological conditions..... | 12 |
| Fig. 1.4. Tau mutations associated with dominant familial frontotemporal dementia..... | 14 |
| Fig. 1.5. Post-translational modification sites of human tau..... | 19 |
| Fig. 1.6. Composition of tau isoforms reported in tau pathologies..... | 23 |
| Fig. 1.7. Schematic representation of tau aggregation kinetic reactions..... | 27 |
| Fig. 1.8. Mechanism of tau secretion and spreading | 32 |
| Fig. 1.9. Transcellular propagation of protein misfolding mechanism..... | 35 |
| Fig. 1.10. Cell-to-cell tau spreading by prion-like mechanism and potential areas for therapeutic interventions | 37 |
| Fig. 1.11. Tau-related therapeutic targets..... | 41 |
| Fig. 3.1. Tau protein domain organization and tau repeat peptides sequence..... | 49 |
| Fig. 3.2. Experimental procedure of seeding, fractionation, and re-seeding..... | 61 |
| Fig. 4.1. <i>In vitro</i> aggregation of tau repeat peptides in the presence of heparin..... | 67 |
| Fig. 4.2. Concentration-dependent aggregation of tau repeat peptides in the presence of heparin and Coomassie gel staining..... | 68 |
| Fig. 4.3. R3 self-assembles in the absence of heparin | 70 |
| Fig. 4.4. Seeding potential of tau repeat peptide aggregates..... | 71 |
| Fig. 4.5. Cellular internalisation of tau R3 aggregates..... | 73 |

| | |
|---|-----|
| Fig. 4.6. Effect of tau R2 and R3 aggregates on intracellular tau phosphorylation and aggregation in Tau RD P301S biosensor cells..... | 74 |
| Fig. 4.7. Effect of tau R2 and R3 aggregates on intracellular tau phosphorylation and aggregation in Tau P301L (0N4R) HEK293 cells..... | 76 |
| Fig. 4.8. Cellular re-seeding assay..... | 77 |
| Fig. 5.1. Drug effect on R3 aggregation..... | 83 |
| Fig. 5.2. Dose-dependent effect of DMSO and drugs on R3 aggregation..... | 87 |
| Fig. 5.3. Inhibition of elongation of preformed R3Ag or protofilaments..... | 89 |
| Fig. 5.4. Drug effect on R3 dimerisation..... | 91 |
| Fig. 5.5. Data on mutant R3 peptide aggregation..... | 92 |
| Fig. 5.6. Molecular dynamics simulation of drugs with R3 dimer..... | 94 |
| Fig. 5.7. Effect of R3Ag on seeding and viability..... | 96 |
| Fig. 5.8. Effect of Lipofectamine transfection reagent on cell density and seeding..... | 97 |
| Fig. 5.9. Schematic representation of the seeding experiments..... | 99 |
| Fig. 5.10. Drug treatment abrogates seed-competent R3Ag formation..... | 100 |
| Fig. 5.11. Raw data of seeding from Fig. 5.10..... | 101 |
| Fig. 5.12. Raw data of drug-only effect from Fig. 5.10..... | 103 |
| Fig. 5.13. Drug pretreatment (2 h) of cells prevents seeding by exogenous R3Ag..... | 104 |
| Fig. 5.14. Drug pretreatment (24 h) of cells prevents seeding by exogenous R3Ag..... | 105 |
| Fig. 5.15. R3Ag causes pharyngeal impairment in <i>C. elegans</i> | 107 |
| Fig. 5.16. Drug treatment reverses the toxicity of R3Ag in <i>C. elegans</i> | 108 |
| Fig. 5.17. Effect of drug pretreatment on R3Ag toxicity in <i>C. elegans</i> | 110 |

| | |
|---|-----|
| Fig. 6.1. Time-dependent changes in the autophagy-related proteins in biosensor cells seeded with R2 fibrils..... | 118 |
| Fig. 6.2. Time-dependent changes in the autophagy-related proteins in biosensor cells seeded with R3 fibrils..... | 119 |
| Fig. 6.3. Effect of compounds on the viability of tau biosensor cells. Data is mean \pm SEM of 2 independent experiments..... | 120 |
| Fig. 6.4. EGCG and RSV reduced intracellular tau aggregation in R3 fibrils seeded cells..... | 121 |
| Fig. 6.5. EGCG and RSV induced autophagy in tau biosensor cells seeded with R3 fibrils..... | 123 |
| Fig. 6.6. CQ inhibited autophagy in R3 fibrils seeded tau biosensor cells..... | 124 |
| Fig. 6.7. Effect of EGCG, RSV and CQ on the solubility and phosphorylation of intracellular seeded tau..... | 125 |

Chapter 1

Introduction

1.1 Dementia

Dementia results in deterioration in multiple cognitive domains and is accompanied by functional impairment. Individuals diagnosed with dementia cannot perform their daily activities independently. A memory decline and at least one cognitive dysfunction are sufficient to compromise daily function. There are different types of dementia, and the word ‘dementia’ is often used as an umbrella term²². One of the most commonly characterized dementia in the ageing population is Alzheimer's disease (AD), a neurodegenerative disorder. AD is characterized by the deposition of misfolded tau-containing neurofibrillary tangles (NFTs) amyloid beta (A β)-rich plaques in the brain²³.

1.1.1. Global burden

Currently, 55 million people worldwide are diagnosed with dementia, of which the most common variation is AD which accounts for around 60-70% of dementia cases²⁴. The World Health Organisation (WHO) suggests that by 2050, about 139 million people will have dementia²⁴. In addition to AD, chronic traumatic encephalopathy (CTE), Corticobasal syndrome (CBS), Progressive supranuclear palsy (PSP), Creutzfeldt-Jakob disease (CJD), Huntington's disease, HIV-related cognitive impairment, Hypothyroidism, Multiple sclerosis (MS), Niemann-Pick disease type C, Normal pressure hydrocephalus (NPH), Vitamin B12 deficiency, Alcohol-related cognitive impairment and Wernicke-Korsakoff syndrome are other rare causes of dementia reported so far²⁵. Studies also linked the growing incidence of diabetes as an associated cause for the increase in people with dementia globally^{26,27}. Dementia has significant social and economic implications regarding direct medical and social care costs and informal care costs. As per the WHO report, in 2019, the estimated global societal cost was US\$ 1.3 trillion. An increase in dementia cases and associated care costs might raise the cost to US\$ 2.8 trillion by 2030²⁴.

1.1.2. Prevalence and incidence of AD in Europe

As per statistical data presented by the global burden of disease study 2013, AD remained the leading cause of life loss between 1990 and 2013²⁸. In 2006, nearly 26.6 million patients were diagnosed with AD worldwide. The number is expected to rise to 106.8 million by 2050, with 16.51 million European patients²⁹. Factors like age, sex, smoking, obesity, low education level,

the APOE ϵ 4 allele and diabetes are identified as risk factors associated with AD³⁰. Furthermore, a progressive upward trend in the incidence of dementia was confirmed by various studies, with an increase of 87 % in Europe between 2010-2050³¹. Thus, a better understanding of AD epidemiology is essential for early diagnosis and for reducing AD's impact on the elderly population.

1.1.3 Social and healthcare economic burden of people with AD in the Czech Republic

Advanced scientific contributions in medicine, improved healthcare, and a healthy lifestyle contributes to the prolongation of life expectancy of the general population. However, health issues associated with the ageing population remain a significant concern of the present century in many countries³². As per data published by the Czech Statistical Office, one-fifth of the Czech population comprises seniors aged 65 and above, and the share will increase to 22.3-28.6 % by 2030-2050³². With high prevalence among the elderly, AD progression remains unnoticed until the first sign of mild cognitive impairment (MCI), when it is already too late to stop or reverse the disease³³. According to Czech Alzheimer's Society, 183,000 patients were diagnosed with dementia in 2020, and these numbers are expected to increase two-fold by 2050 (amounting to 383,000 AD patients)³². Symptomatic drugs employed for AD treatment improve symptoms but pose no or minimal impact on the disease progression. Thus, patients diagnosed with AD has only a perspective of a few years and need to rely on their family and health or social system for their existence. Furthermore, among the reported diseased conditions, AD significantly impacts the financial sustainability of the diseased population³².

AD's economic burden on social and healthcare services was demonstrated in two selected regions in the Czech Republic: Kralovehradecky Kraj and Kraj Vysocina. These two regions were chosen as they share a higher percentage of AD patients than other Czech regions. More precisely, a 20% increase in the population of people aged 65+ between 2002 and 2017 in the Kralovehradecky Kraj region corresponds to a 40% increase in the economic load index. Similar circumstances were reported in the Kraj Vysocina Region, wherein an economic load index is expected to increase by nearly 100% by 2050. However, the average age is expected to be 49.9 compared to the present age of 41. The regions mentioned above are considered representative areas of the Czech Republic with an ageing population³².

The Czech Alzheimer's Society and the Czech Statistical Office have published a report that provides forecasts of patient population development and raises awareness of the unpreparedness of the Czech health and social system to accommodate the growing number of AD patients. Currently, to treat patients with dementia and AD, 21,000 beds in 341 senior homes and social care clinics are available. Nevertheless, it remains below the EU average though there has been an increase since 2005 according to health spending per capita in the Czech Republic. Contributing to more than 250 billion EUR, the cost associated with dementia in Europe is expected to rise roughly to 43% from 2008-2030³². As per data provided by World Alzheimer Report, between 2010 and 2015, the cost associated with dementia in the individual European region was EUR 210.1 billion, 14.3 billion, and 14.2 billion in Western, Eastern and Central Europe, respectively. Whereas the total cost in Europe in 2010 was EUR 238.6 billion, the forecast for 2015 was EUR 301.2 billion³⁴. However, the lack of consistent data on the prevalence and incidence of AD in Europe and elsewhere might make the estimate biased³².

1.1.4 Dementia treatment

Drug regulatory agencies such as the Food and Drug Administration of the USA (FDA USA) and the European Medicines Agency (EMA) have approved acetylcholinesterase inhibitors, such as tacrine, donepezil, rivastigmine, galantamine, and N-methyl-D-aspartate receptor antagonists, memantine, and A β -targeting monoclonal antibody, aducanumab, for AD treatment (Fig. 1.1)³⁵. While the former treats mild to moderate AD, the latter treats moderate to severe AD. Therapy with these drugs is not definitive or cost-effective, though they are reported to control dementia-related symptoms by slowing disease progression³⁶. Thus, there is a significant interest in developing effective disease-modifying therapies targeting A β , a significant component of senile plaques, and tau aggregate-containing NFTs for AD treatment³⁷.

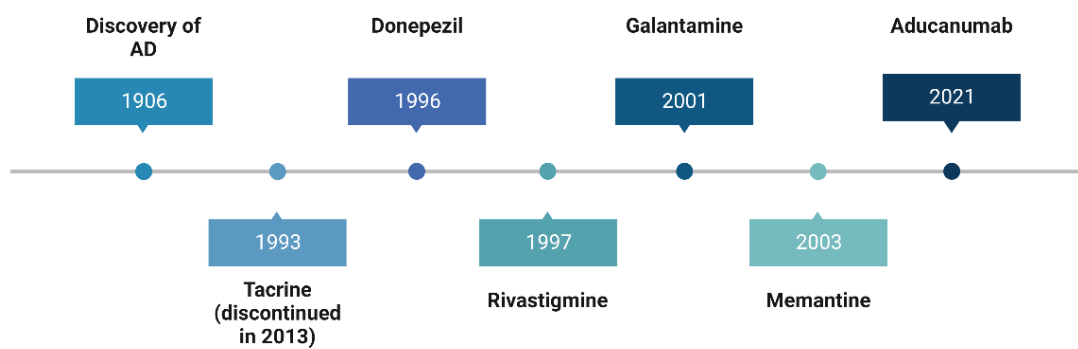


Fig. 1.1. Timeline showing the approval years of AD drugs since the discovery of the first case of AD in 1906 by Alois Alzheimer by the US FDA. Timeline figure was created with BioRender.com.

1.2 Proteinopathies

Neurodegenerative diseases, collectively termed proteinopathies, are characterized by aggregation of the misfolded proteins caused by genetic mutations and are also generally reported in elderly populations due to metabolic stress and proteostasis failure³⁸. AD and systemic amyloidoses have been known for decades, and growing evidence links these diseases with inappropriate deposition of protein aggregates³⁹. Additionally, apart from extracellular space, ordered aggregation of pathogenic proteins is reported in the cytoplasm and nucleus, qualifying as amyloidoses⁴⁰. In general, complex cellular quality control mechanisms inhibit protein aggregation. However, protein tends to aggregate within or around cells under certain circumstances. Though proteins pose a diverse amino acid sequence, they tend to adopt a highly ordered and insoluble structure when aggregated, known as ‘cross- β spine’, resulting in protein deposits termed ‘amyloid’^{41,42}. Though the amino acid sequence-based prediction of protein tends to form amyloid is highly possible, amyloid formation is far from a simple function of protein sequences and secondary structures⁴³. Amyloid proteins remain in various highly ordered aggregated forms and exist in equilibrium between soluble monomeric or oligomeric states. Multiple factors like protein concentration, interaction with other proteins, and cellular environment define aggregate formation. Thus, a thorough study of factors involved in maintaining the equilibrium is essential to understand protein aggregation disorders better and develop effective therapies. A better understanding of this protein aggregation disease and its pathogenic features provides opportunities for comprehensive therapeutic approaches like inhibition of aggregation and cellular toxicity pathways, enhancement of aggregation clearance and depletion of monomeric precursor proteins⁴⁰.

1.2.1 Neurodegenerative diseases

Neurodegeneration is a selective, slow, and progressive loss of neuronal structure and function, including neuronal cell death³⁸. $A\beta$ and tau accumulation in AD and α -synuclein in Parkinson's disease (PD) are examples of neurodegenerative diseases, though the exact mechanism behind neurodegenerative processes is poorly understood⁴⁴.

1.2.2. Protein toxicity in neurodegenerative diseases

Many protein aggregations are known to affect the nervous system, wherein the formation of aggregates is toxic to the central nervous system (CNS) even though they are ubiquitously expressed⁴⁵. Moreover, pathological accumulation of the protein aggregates is reported within the nucleus or cytoplasmic compartments, as in the case of polyglutamine expansion diseases or PD and both intracellularly and extracellularly in AD⁴⁶. Furthermore, the prevalence of neurodegenerative diseases such as AD, PD, amyotrophic lateral sclerosis, frontotemporal dementia, and Huntington's disease are increasing at an alarming rate, and protein toxicity remains a vital pathogenic manifestation⁴⁷. Furthermore, patients with these disease conditions exhibit neurological disabilities, namely motor problems and memory impairment⁴⁷.

Neurons affected by proteinopathies display cellular defects like mitochondrial dysfunction, transcriptional alteration and impaired RNA/protein quality control system contributing to the initiation and progression of neurodegenerative diseases^{48,49}. These cellular defects are not specific to a particular disorder but are commonly associated with multiple disease conditions. Furthermore, though cell death remains the outcome of the disease process, they are often preceded by neurological deficits in animal models and patients⁵⁰. Thus, characterizing the mechanism behind protein toxicity from one subcellular compartment to another, for example, nucleus and mitochondria, will aid in understanding protein toxicity and is indispensable for the future development of rational and effective therapeutics for these diseases. Furthermore, accumulation, oligomerization, and multimerization of disease-associated toxic proteins cause pathological alteration of proteins; thus, elucidating the toxic protein nature will aid in developing therapeutic strategies⁵⁰.

1.2.3. Tau protein structure and function

Tau protein is abundantly present in the axonal compartment of neurons and stabilizes microtubule bundles⁵¹⁻⁵³. Alternative splicing of the Microtubule Associated Protein Tau (MAPT) gene on chromosome 17q21 in the adult human brain results in six tau isoforms (352-441 amino acid residues; 37-46 kDa (Fig. 1.2; Table 1.1)^{54,55}. Due to the larger diameter of axons, a "big Tau" isoform with 695 amino acids is predominantly expressed in the peripheral nervous system. It is equivalent to 2N4R plus 242 residues from exon 4a⁵⁶. The extended tau isoform (441 amino acid residues) in the human central nervous system is subdivided into various domains, which include

an N-terminal projection domain (1-165), proline-rich domain (166-242), microtubule-binding domain (MTBD) (243-367) and C-terminal domain (368- 441). MTBD comprises four partially repeated sequences R1(244-274), R2(275-305), R3(306-336), and R4(337-368). Half of the N-terminal domain projects away from microtubules and thus remains unbound, termed the "projection domain". The C-terminal is termed the assembly domain since most of it interacts with microtubules, facilitating its assembly. Under normal physiological conditions, tau remains as unfolded soluble protein with a paperclip-like structure wherein the N-terminal, C-terminal and repeat domains are in proximity, protecting tau from aggregation⁵⁷.

Reported six tau isoforms are distinguished either by the presence or absence of one or two N-terminal inserts and the three or four microtubule-binding repeats in the C-terminal domain of tau⁵¹. The three-repeat (3R) and four-repeat (4R) tau isoforms are expressed in a one-to-one ratio in adult brain regions. Any deviation from this ratio is a characteristic of neurodegenerative tauopathies⁵⁸. Compared to 3R tau, 4R tau poses a higher affinity assembly toward microtubules and a higher propensity for self-aggregation^{59,60}. Other isoforms like 2N, 0N and 1N are underrepresented at a ratio of ~9%, 37%, and 54% of total tau, respectively⁶¹. The splicing and expression pattern of tau differs between brain regions. For example, protein levels are reported to be enhanced twice in the neocortex compared to white matter and cerebellum, which explains the differential vulnerability of brain regions observed in tau pathology⁶².

The six tau isoforms present in the human brain are produced via alternative splicing of the MAPT gene's 16 exons. Alternative splicing results in 6 isoforms that vary by the number of N-terminal inserts and the presence or absence of R2. Exons 2 and 3 encode the two possible N-terminal inserts, N1 and N2. Exon 10 encodes R2 in the microtubule-binding domain. Tau lacks significant amounts of a secondary structure under normal conditions. Events like truncation prevent the formation of hairpin structures, thus facilitating tau aggregation⁶³. In contrast to the full-length tau, MTBD repeats, more specifically, 2R and 3R display an enhanced propensity to form an ordered β - sheet structure⁶⁴. Although tau is an intrinsically disordered protein, the tau C terminus folds over the MTBD, and the N terminal folds back over the C terminus, bringing both termini nearby, forming a "paperclip" conformation⁵⁷. However, tau binding to microtubules reduced the association between the N and C terminus of tau.

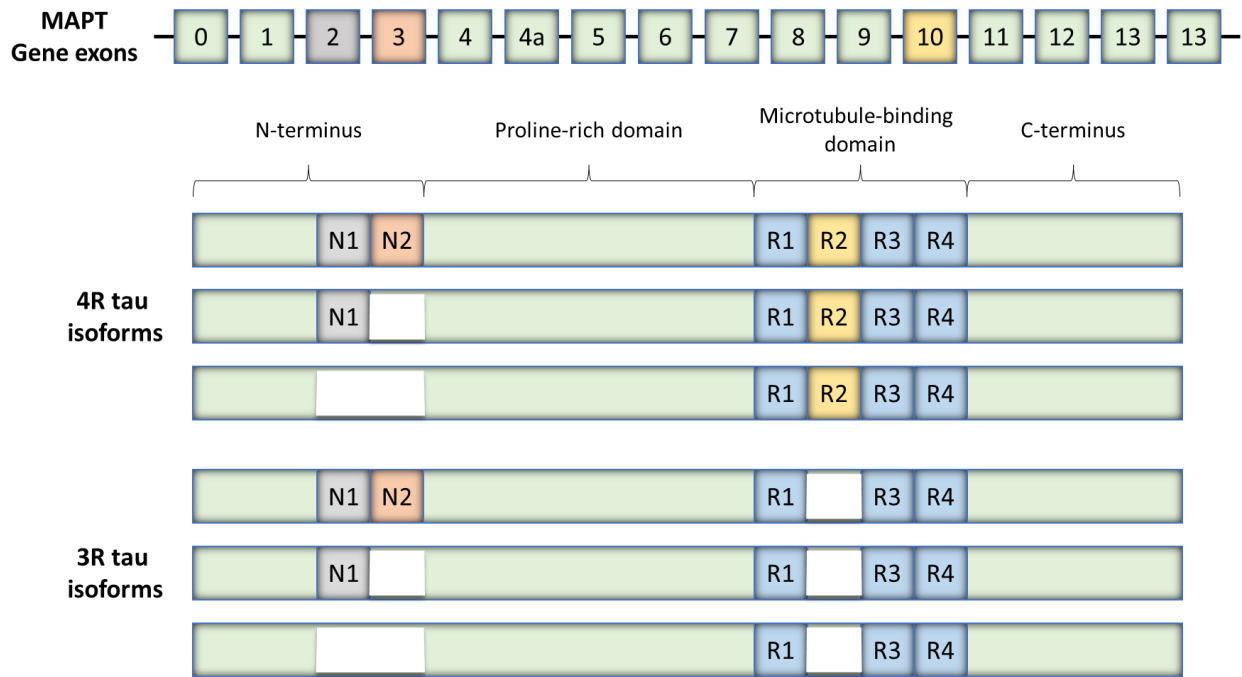


Fig. 1.2. Six tau isoforms generated by alternative splicing of MAPT genes 16 exons. N1 and N2 N-terminal inserts (shown in grey and orange) are encoded by exons 2 and 3. R2, the second microtubule binding repeat (shown in yellow) in the microtubule-binding domain, is encoded by Exon 10. Variations in the number of N-terminal inserts (0N, 1N or 2N) and the presence or absence of R2 (4R isoforms or 3R isoforms) are observed in six isoforms due to alternative splicing.

Several cofactors, including ions like zinc, induce structural changes, potentially regulating tau functions⁶⁵. Additionally, proline-directed tau phosphorylation readily disrupts tau conformation resulting in the loosening and tightening of the paperclip structure depending on the site of phosphorylation⁶⁶. The zinc-binding tau also regulates tau aggregation and toxicity independent of phosphorylation⁶⁷.

1.3 Functions of tau protein

Microtubules assembled as polymers of α - β -tubulin heterodimers carry out functions like cytoskeleton architecture maintenance, separation of chromosomes during mitosis, or as tracks for intracellular transport by motor proteins. Additionally, the tau repeat domain and its flanking regions promote the assembly and stabilization of microtubules^{12,68}. Tau plays a predominant role in regulating microtubule dynamics and spatial arrangements. Tau binding towards microtubules occurs at α - and β - tubulin heterodimer interface withholding stretches with specific amino acids in repeat domain regions responsible for its function residues 224-237 and 245-253 in R1, 275-284 in R2, and 300-317 between R2 and R3 (Fig. 1.3)⁶⁹. Furthermore, a local hairpin structure with 275VQIINK280 and 306VQIVYK311 residues becomes evident post-formation of a tau-microtubule complex, and these hexapeptides motifs are essential for tau aggregation. Thus, tau poses a conflicting function of microtubule binding and self-aggregation. Furthermore, the binding of the projection domain to the neuronal plasma membrane might contribute to neurite development⁷⁰. The length of the projection domain is a determining factor of microtubule filament spacing length and axon diameter⁷¹.

Numerous factors, including post-translational modifications, ensure good system dynamics by regulating the binding ability of tau and other microtubule-associated proteins towards microtubules. However, the exact mechanism for deciphering the assembly and stabilization of microtubules by tau remains challenging due to the disordered nature of tau and the inherent dynamics of the system. Deletion or reduction of MAPT expression results in impaired microtubule density and morphology underlying the essential role of tau in cellular function⁷². Throughout neuron development, tau promotes neurite outgrowth independently without microtubule via interaction with actin⁷³. Additionally, tau is reportedly involved in DNA repair and heat shock responses in the nucleolar organizing region of the cell⁷⁴. Finally, post-translational modification events like phosphorylations can modulate tau-mediated microtubule assembly⁷⁵.

Table 1.1. Tau isoforms. htau - human tau. The number designates the clone number⁵².

| Clone | Inserts/repeats | Number of amino acids | MW (kDa) |
|----------------|------------------------|------------------------------|-----------------|
| htau40 | 2N4R | 441 | 45.9 |
| htau39 | 2N3R | 410 | 42.6 |
| htau34 | 1N4R | 412 | 43.0 |
| htau37 | 1N3R | 381 | 39.7 |
| htau24 | 0N4R | 383 | 40.0 |
| htau23 | 0N3R | 352 | 36.7 |
| Big tau | 2N4R+ exon 4a | 695 | 72.7 |

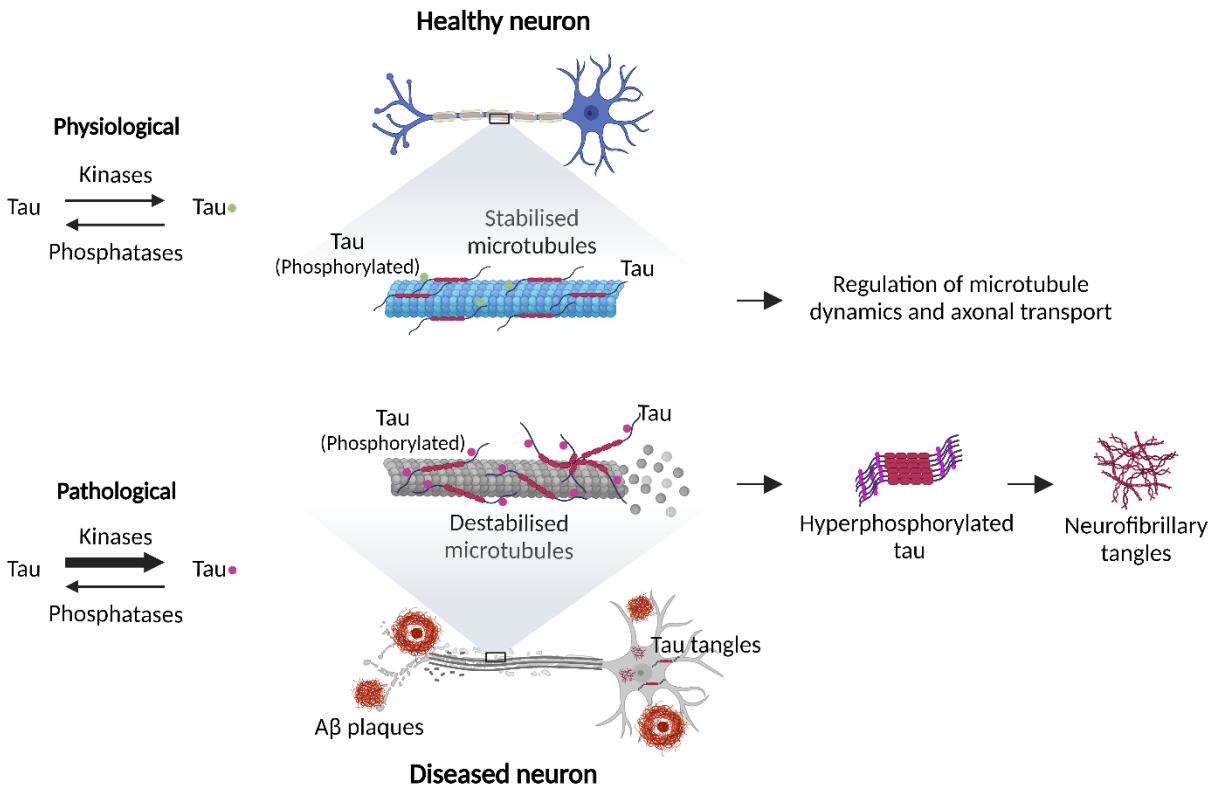


Fig. 1.3. Tau-microtubule dynamics under healthy and pathological conditions. Physiologically phosphorylated tau forms (green sphere) can interact with microtubules normally, whereas increased phosphorylation by disease-specific kinase leads to microtubule destabilisation under pathological conditions. Tau hyperphosphorylation (pink sphere) leads to the formation of intracellular tau deposits and, eventually, neurofibrillary tangles. Created with BioRender.com.

Motor proteins dynein and kinesin regulate efficient protein trafficking retrograde from the axon to soma and anterograde from soma to the axon, respectively. Tau can control this axonal transport through competitive binding with dynein and kinesin for microtubules, resulting in protein cargo accumulation in the soma^{76,77}. Furthermore, tau influences the number of kinesins bound to microtubules either by occupying binding sites on microtubules or by the interaction of the N-terminus with specific enzymes that regulate microtubule-kinesin binding⁷⁸. Additionally, tau can modulate axonal transport by binding to dynactin, a dynein-interacting partner⁷⁹. Finally, as dynein and kinesin oppose each other, tau can contribute to controlling both anterograde and retrograde transport⁸⁰. Though neuronal tau is known to be profoundly located in axons, small quantities of dendritic tau have been reported and are anticipated to play an essential role in the regulation of synaptic plasticity. For example, electrical stimulation of synapses causes tau in cultured mouse neurons to migrate to dendritic spines, where its interaction with actin may contribute to spine remodelling that triggers synaptic plasticity⁸¹.

1.4 Impact of tau mutations on its interaction with microtubules

Pathogenic variants within the MAPT gene cause various neurodegenerative diseases characterized by the accumulation of hyperphosphorylated tau aggregates in the neurons. The frontotemporal dementia mutations in the MAPT gene alter tau biochemical properties and the ratio of tau isoforms⁸². Change in the isoform ratio indirectly impacts microtubule assembly and the dynamics of the microtubule networks because the 3R-tau is known to have a lower capacity for microtubule stabilization and tubulin polymerization than the 4R-tau (Fig. 1.3)^{83,84}. In addition, the frontotemporal dementia-associated tau mutations (Fig. 1.4) also influence the post-translational modifications of tau, which represent another indirect effect on tau-microtubule interactions⁸².

The effect of R5L, P301L, and R406W mutation differ regarding their impact on tau microtubule stabilization, tau sequence localization and the number of N-terminal inserts of 0, 1, or 2 N isoforms in 4R-tau isoforms⁸⁵. For example, the tau R406W mutation is consistently reported to diminish tau phosphorylation. More precisely, tau with R5L mutation poses a reduced tendency to polymerize tubulin, lower rate, and longer lag time, specifically for the 0N4R-tau isoform, compared to the 1N and 2N-tau that are wild-type tau⁸⁵.

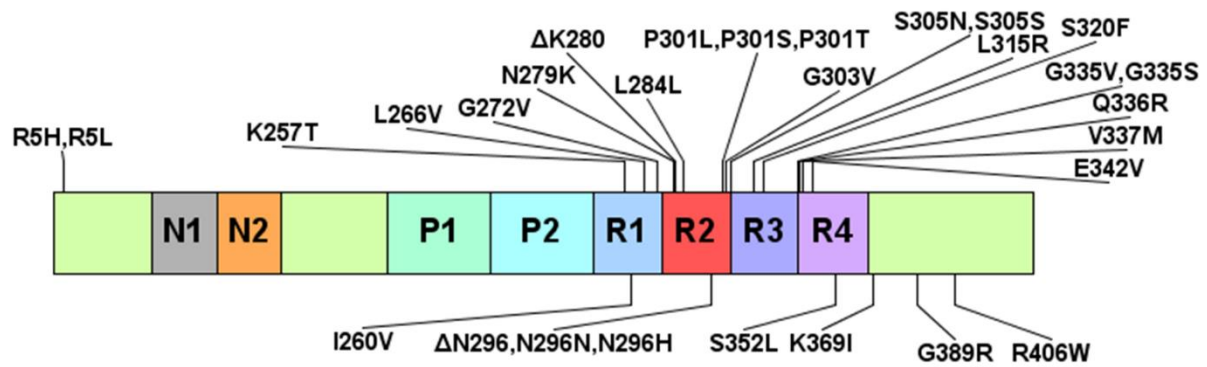


Fig. 1.4. Tau mutations associated with dominant familial frontotemporal dementia. Most of the mutations reported in the coding region are reported around the microtubule-binding domains and in the C-terminal region. Diagram was created with IBS: an illustrator for the presentation and visualization of biological sequences⁸⁶.

Surprisingly, the R406W mutation is reported to be the most affected, although the mutation is not near the MTBD, suggesting an alternative conformation might be involved⁵⁸. In addition, tau with P301L, V337M or R406W mutations has reduced binding to microtubules and decreased efficiency in initiating tubulin assembly⁸². On the contrary, with the P301L mutation, the tau-dependent defect in microtubules weakens with the removal of each N-terminal insert, as contributed by the differential effect of mutations-induced conformational changes on the global hairpin-like tau conformation. This brings the N-terminal region close to the MTBD⁸⁵.

Mammalian cells expressing tau P301L have a lesser amount of tau bound to microtubules. Nevertheless, a strong consensus on the impact of frontotemporal mutations in a cellular context has not yet been elucidated. CHO and neuroblastoma cells, transfected with tau tagged with GFP, microtubule co-localization and microtubule bundle generation remain identical with mutant and wild-type tau⁸⁷. Furthermore, the site-dependent and isoform-dependent effect of the tau mutations on microtubule stabilization was observed in COS cells transfected with 3R- or 4R-tau isoforms. For instance, the V337M mutation poses a significant effect when introduced in 3R-tau but not in 4R-tau, showing disruption of the microtubule networks and diminished co-localization of tau and tubulin⁸⁸. This isoform-specific effect of mutations might explain the discrepancies reported on the impact of tau in frontotemporal dementia-associated mutations on its microtubule-associated functions.

1.4.1 Neurotoxicity from loss of tau function

Tau loss of function is capable of structural and functional dysfunction of axonal microtubules leading to axonal transport deficit. Experiments carried out so far in animal models underlie that other redundant microtubule-associated proteins can only partially compensate for the function of tau. For example, aged tau knockout mice exhibited behavioural impairments and structural abnormalities, suggesting a vital role of tau in neuronal and brain physiological functions⁸⁹. Furthermore, tau functional loss leads to post-translational modifications that may affect tau aggregation. Therapeutic strategies targeted at long-term suppression of tau might increase the disease complication.

Factors like functional motor proteins, intact microtubules and adequate ATP from mitochondria are essential for axonal transport and regulation of microtubule dynamics within a cellular environment. However, tau influences the activity of motor proteins dynein and kinesin by

reducing their binding frequency toward microtubules and anterograde and retrograde axonal transport of cargo⁹⁰. It affects the axonal transport of protein and organelles resulting in synapse degeneration. Furthermore, the accumulation of untransported

organelles, for example, mitochondria in neuronal soma, leads to energy deprivation and oxidative stress, thereby contributing to pathology and neuronal loss in tauopathies⁵¹. Besides, proteins and organelles accumulation in axon and cell body give rise to spheroids and axonal swellings as observed in neurodegenerative diseases⁹¹.

1.4.2 Neurotoxicity from a gain of function

In aggregated form, tau gain of function results in compromised neuronal function, wherein the release of aggregates into extracellular space mediates its interaction with cell receptors facilitating spreading. Earlier, NFTs are considered toxic tau species as the severity of cognitive deficits corresponds to its regional distribution in the AD brain. Nevertheless, growing evidence reports that NFTs formation is neither decisive nor adequate for neurodegeneration⁹². Instead, they pose a protective response wherein cells can scavenge toxic monomeric or oligomeric tau species, protecting neurons from acute assaults⁹³. Furthermore, results obtained from various transgenic mouse models demonstrate that tangle formation does not correlate with neuronal loss; instead, they appear to survive with tangles without any functional impairments^{94,95}.

Among the hyperphosphorylated tau reported in both human and mouse neurons, MC-1 positive tau, a misfolded earliest alteration of tau in AD, is reported only in human neurons⁹⁶. Instead, these tau aggregates might indirectly cause toxicity by depletion of functionally significant proteins, disturbing cytoplasm organization and subcellular organelles and axonal transport interference, ultimately leading to neurodegeneration by neuronal loss. Furthermore, results from various studies claim soluble tau oligomers as toxic rather than NFTs, wherein SDS-stable tau oligomer levels are high in AD and PSP brains^{97,98}. Nevertheless, the role played by tau oligomers in tauopathies yet controversial due to poor understanding and characterisation wherein methods concerning standardisation of oligomer preparation and assay methods among different groups are required to pinpoint the toxic tau species; additionally, the possibility of *in vitro* generation of various tau species with disease-relevant properties as present *in vivo*.

1.4.3 Neurotoxicity from mislocalisation

Under normal physiological conditions, neurons pose small tau localized in dendritic compartments. However, in AD brains and other tauopathies, tau hyperphosphorylation, mutation, and overexpression lead to tau mislocalisation into dendrites, presynaptic terminals and postsynaptic spines resulting in microtubules destabilisation and synaptic dysfunction, which microtubule-stabilising drugs can rescue^{99–101}. Furthermore, mutated tau in fly and rat neurons binds to synaptic vesicles through its N-terminal domain, thereby reducing synaptic transmission, including interference with presynaptic functions like synaptic vesicle mobility and release rate¹⁰². Missorted dendritic tau mediates A β -induced neurotoxicity *via* numerous mechanisms as dendritic tau's ability to promote microtubule depolymerisation, wherein dendritic tau mediates translocation of tubulin tyrosine ligase-like 6 into dendrites, where it polyglutamylates the microtubules increasing their susceptibility to severing by spastin¹⁰³. Additionally, they act as scaffolding proteins to mediate the delivery of Fyn kinase to postsynaptic sites. Fyn, in turn, phosphorylates the NMDA receptor 2 subunit, stabilising the interaction between receptor with postsynaptic density protein 95, potentiating glutamatergic signalling and rendering neurons susceptible to A β mediated excitotoxicity^{104–106}.

Recent findings reveal tau's new physiological role besides its well-known role in microtubule stabilisation and axonal transport. The pathogenicity of tau remains a subject of debate as it can induce both losses of its normal function and novel toxic gain of function. Both loss and gain of tau function may contribute to neurodegeneration, ultimately resulting in the onset and progression of tauopathies. Therefore, it will be critical to develop effective tau therapeutic strategies to overcome tau loss of function and minimise gain-of-function caused by toxic multimeric tau species, depending on which mechanism prevails in each tauopathy. For example, strategies targeting microtubule stabilization will be a promising approach in conditions where tau mutation causes loss of function but not in case of loss of function as they are microtubule independent and do not report any accumulation of toxic tau aggregate.

Conversely, tauopathies mainly caused by tau gain of functions can be enhanced by therapeutic strategies reducing tau *via* increasing its proteolysis and clearance. In contrast, such an approach could harm the loss of function mechanisms of tau toxicity, as the treatment would exacerbate the sequestration of soluble tau. A study in transgenic mice with inducible tau expression showed that

after the suppression of transgenic tau expression, memory function recovered, and neuronal loss ceased, but NFTs continued to accumulate¹⁰⁷. Therapeutic strategies to reduce tau would have to be prolonged enough to remove any residual seed-competent tau species from human brains. Still, this long-term reduction of tau levels may pose safety concerns¹⁰⁸.

1.5 Post-translational modifications of tau

Various post-translational modifications of tau, including acetylation, phosphorylation, nitration, glycation, oxidation, polyamination, sumoylation, ubiquitination and addition of β -linked N-acetylglucosamine (O-GlcNAcylation) were reported (Fig. 1.5)^{109,110}. Herein we discuss the mechanism of post-translational modification of tau, its function and its relationship to disease in detail.

1.5.1 Tau phosphorylation

In AD brains, NFTs comprise paired helical and straight filaments of hyperphosphorylated tau¹¹¹. Phosphorylation is reported as the most common tau post-translational modification. There are 85 phosphorylation sites, including 45 serine residues, 35 threonine residues, and 5 tyrosine residues¹¹². Phosphorylations at residues S262, S293, S324, and S356 dissociate tau from microtubule binding^{109,113}. Thus, phosphorylations regulate tau binding to microtubules^{109,113,114}.

An average of 2-3 moles of phosphate per tau molecule is present in normal conditions, whereas, in AD, the ratio is 3-4 times higher¹¹⁴. Self-aggregation and accumulation of tau in the somatodendritic compartment and defects of axonal mitochondrial trafficking, which result in neuronal toxicity, are known to be induced by tau hyperphosphorylation events¹¹⁵⁻¹¹⁷. Furthermore, tau phosphorylation precedes the formation of tau fibrils in the AD brain¹¹⁸. These observations demonstrate that tau hyperphosphorylation plays a crucial role in the development and pathogenesis of tauopathies and that its inhibition may be a therapeutic strategy. A balance between protein kinase and phosphatase activity controls tau phosphorylations¹¹². Tau is a crucial substrate for protein phosphatase 2A (PP2A), whose activity is turned down in the AD brain¹¹⁹⁻¹²². PP2A pose increased substrate specificity and withholds several regulatory subunits, thus making it a not quickly responsive target for drug design and therapies. Therefore, efforts are underway to develop protein kinase inhibitors that can reduce tau aggregation and neuronal death in tauopathies¹¹².

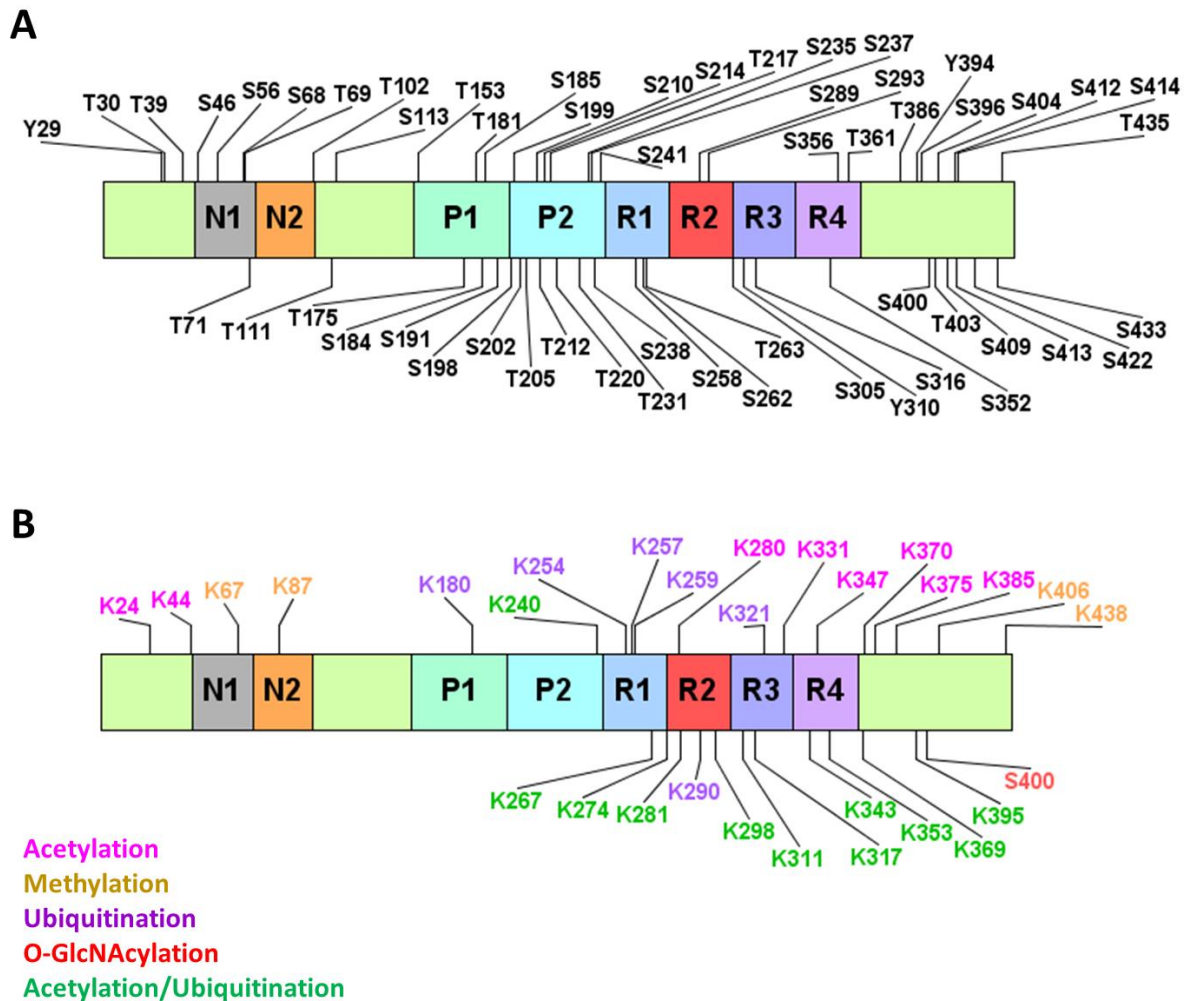


Fig. 1.5. Post-translational modification sites of human tau. Diagrams were created with IBS: an illustrator for the presentation and visualization of biological sequences⁸⁶. The post-translational modification sites were derived and adapted from Wesseling H et al. *Cell*, 2020¹²³ and Wegmann S et al. *Current Opinion in Neurobiology*, 2021¹²⁴. (A) Post-translational modification sites identified in human AD brains mapped on the longest tau isoform sequence (2N4R, UniprotKB P10636-8). Phosphorylation sites along residues are displayed in grey (above and below the domain structure), with the most abundant phosphorylation sites clustering in P1 and P2 of the proline-rich domain between residues T181 and S235 and regions C-terminally of the repeat domain (repeats R1–R4) in between residues S396 and S404 (R0 and C-terminal). Inserts N1 and N2, the N-terminal projection domain is also often phosphorylated. (B) most of the Acetylation (pink) and ubiquitination (violet) occur within the MT-assembly domain and often alternatively at the same residues (green). Methylation (brown) is rare and found only in the C-terminal and projection domains. Only one O-GlcNAcylation was found in the C-terminal domain¹¹⁰.

1.5.2 Tau acetylation

Tau protein withholds more than 30 lysine residues, possibly acetylated, located in the MTBD, a proline-rich domain, and the C-terminal domain¹²⁵. Acetyltransferases such as p300 and CBP acetyltransferase and deacetylases such as histone deacetylase 6 and sirtuin 1 regulate the acetylation level in tau^{126–128}. In addition, with the help of catalytic cysteine residues C291 and C322, tau promotes the self-acetylation of autologous lysine residues in the MTBD¹²⁹. Highly acetylated lysine residues are reported in the brains of AD and other tauopathies compared to healthy brains^{130,131}. Furthermore, acetylation at K280/K281 residues inhibits microtubule stabilization and promotes tau aggregation¹³². Deleting sirtuin 1 increases tau acetylation and inhibits its degradation, thereby accumulating pathogenic phospho-tau *in vivo*¹²⁸. These facts underlie the importance of acetylation and its significance in tau-induced toxicity. An old salicylate derivative with anti-inflammatory properties, salsalate is reported to inhibit tau acetylation by blocking p300 acetyltransferase activity and acetylation of K174 in the PS19 transgenic mouse line overexpressing P301S-tau.

Additionally, salsalate prevents hippocampal atrophy and memory impairment^{133,134}. Though reported to be safe and well tolerated, a pilot study by administering progressive supranuclear palsy patients failed to improve cognitive performance. Factors attributing to this failure include poor penetration ability into the brain and an increase in tau aggregation¹³⁵.

1.5.3 Tau ubiquitination

Apart from acetylation, tau lysine residues undergo ubiquitination, a process closely associated with the proteasomal degradation pathway¹³⁶. Interestingly, hyperphosphorylated tau is ubiquitinated in AD patients^{137–139}. Thus dysfunction of either proteasomal or lysosomal degradation pathways might lead to excessive accumulation of ubiquitinated tau, thereby contributing to the formation of NFTs¹⁴⁰.

1.5.4 O-GlcNAcylation

Paired helical filaments (PHFs) from AD brains are reported to contain glycosylated tau¹⁴¹. The non-canonical form of glycosylation involves the addition of β -linked N-acetylglucosamine (O-GlcNAcylation), and the events are tightly regulated by O-GlcNAc transferase and neutral β -hexosaminidase known as O-GlcNAcase¹⁴². An O-GlcNAcase inhibitor was reported to enhance

tau O-GlcNAcylation, thereby inhibiting the formation of tau aggregates and neuronal loss in P301L tau transgenic mice¹⁴³. Reduction in tau O-GlcNAcylation is related to neurofibrillary pathology in AD brains^{144–146}. On the contrary, an increase in tau phosphorylation, neurodegeneration and cognitive impairment was observed in mice with forebrain-specific O-GlcNAc transferase conditional knockout¹⁴⁶. Thiamet G, an inhibitor of O-GlcNAcase with good bioavailability, decreased site-specific phosphorylation of T181, T212, S214, S262/S356, S404, and S409 residues upon acute injection into the lateral ventricle of wild-type tau transgenic mice^{143,147,148}. Furthermore, oral administration of Thiamet G in drinking water enhanced O-GlcNAcylation and inhibited tau aggregation and neuronal cell loss¹⁴³. Administration of MK-8719, a low molecular weight O-GlcNAcase inhibitor developed in collaboration with Alectos Therapeutics and Merck, was found to enhance brain O-GlcNAc levels, reduce pathological tau and improve brain atrophy in an rTg4510 mouse model of tauopathy¹⁴⁹. Results from these findings substantiate the upregulation of tau O-GlcNAcylation as a therapeutic strategy for tau-related neurodegeneration.

1.6 Tauopathies

Tau is reported to form intracellular aggregates in various neurodegenerative diseases, which include AD, frontotemporal dementia, corticobasal degeneration (CBD), and PSP, termed ‘tauopathies’⁵². In tauopathies, tau self-assembles into neurotoxic oligomers and fibrillar aggregates as it detaches from microtubules⁹³. The discovery of tau mutation and its correlation with aggregation and cognitive decline has emphasised the hypothesis that tau mutation plays a causative role in AD or frontotemporal dementia-associated neurodegeneration^{52,150–153}. As a central molecular player in neurodegenerative diseases, including AD and other tauopathies, tau remains an attractive and challenging therapeutic target^{150,154,155}. In contrast to amyloid plaques, NFTs remain distinctive proteinaceous lesions of AD and correlate well with clinical disease progression⁹³. In AD staging, immunostaining methods employed AT8, a monoclonal antibody that binds to hyperphosphorylated tau¹⁵⁶. Nevertheless, metastable tau oligomers remain a significant neurotoxic agent and possibly the main culprit responsible for impairing and eventually killing susceptible neurons, similar to other proteinopathies¹⁵⁷.

Tauopathies are characterized by aberrant tau aggregates (NFTs and tau inclusions) in neurons and glial cells^{158,159}. In tauopathies, the formation of misfolded and oligomerized tau is reported to be

the onset characteristic feature wherein the appearance of NFTs marks the disease progression¹⁶⁰. Although the mechanism underlying the tau pathological process is not precise, human tau pathology progresses from one brain region to another in a disease-specific manner^{161–164}. Deposition of tau remains a distinctive pathological sign associated with many tauopathies, and the Braak system has used the same to classify disease progression stages¹⁵⁶. Furthermore, as tau accumulates into hyperphosphorylated NFTs, the visualization of tangles in the entorhinal cortex that transverse through the brain along the neuronal network to the rest of the brain regions remains a histopathologic marker for AD⁵². Moreover, neuronal loss and dementia reported in AD patients are hypothesized to be associated with damages along this neuronal connections¹⁶⁵.

Among the reported tauopathies characterized by aggregated tau, AD remains a well-known disease wherein tau protein is aggregated into NFTs within neurons and the selective loss of neurons and synapses¹⁶⁶. Both extracellular amyloid plaques comprising fibrillar A β and NFTs consisting of hyperphosphorylated tau were reported to be the signature trait of the disease in 1906 by German psychiatrist Alois Alzheimer^{167–171}. A heterogeneous group of disorders of frontotemporal dementia with parkinsonism linked to chromosome 17(FTDP-17) are pathogenic to a mutation in the tau gene and display prominent tau pathologies rather than senile plaques or disease-specific inclusions^{172,173}.

NFTs and other tau pathologies can induce neurodegeneration in the worm, fly and mouse models of neurodegenerative tauopathies with convincing plausibility to their authentic human counterparts^{172,174}. Most tauopathy patients also show depositions of A β , α -synuclein, or huntingtin⁵¹. These observations suggest that tau abnormalities have a typical pathological role across neurodegenerative diseases. Furthermore, abnormal changes in tau and its pathological aggregation are standard features of neurodegenerative diseases^{93,175,176}. Thus more efforts have been carried out to search for *in vitro* tau aggregation inhibitors^{177–183}.

1.6.1 Classification of tauopathies

Though tauopathies display a common molecular mechanism and characteristics of lesions like nerve cell loss, gliosis, superficial spongiosis, gross brain atrophy and ballooned neurons, they differ in isoform and cell involved, inclusion morphology, cellular tau pathology and its clinical presentation significantly vary among the disease type (Fig. 1.6)^{184,185}. In addition, tauopathies are distinguished by the tau isoforms involved. The neuronal inclusion comprises 3R- and 4R-tau

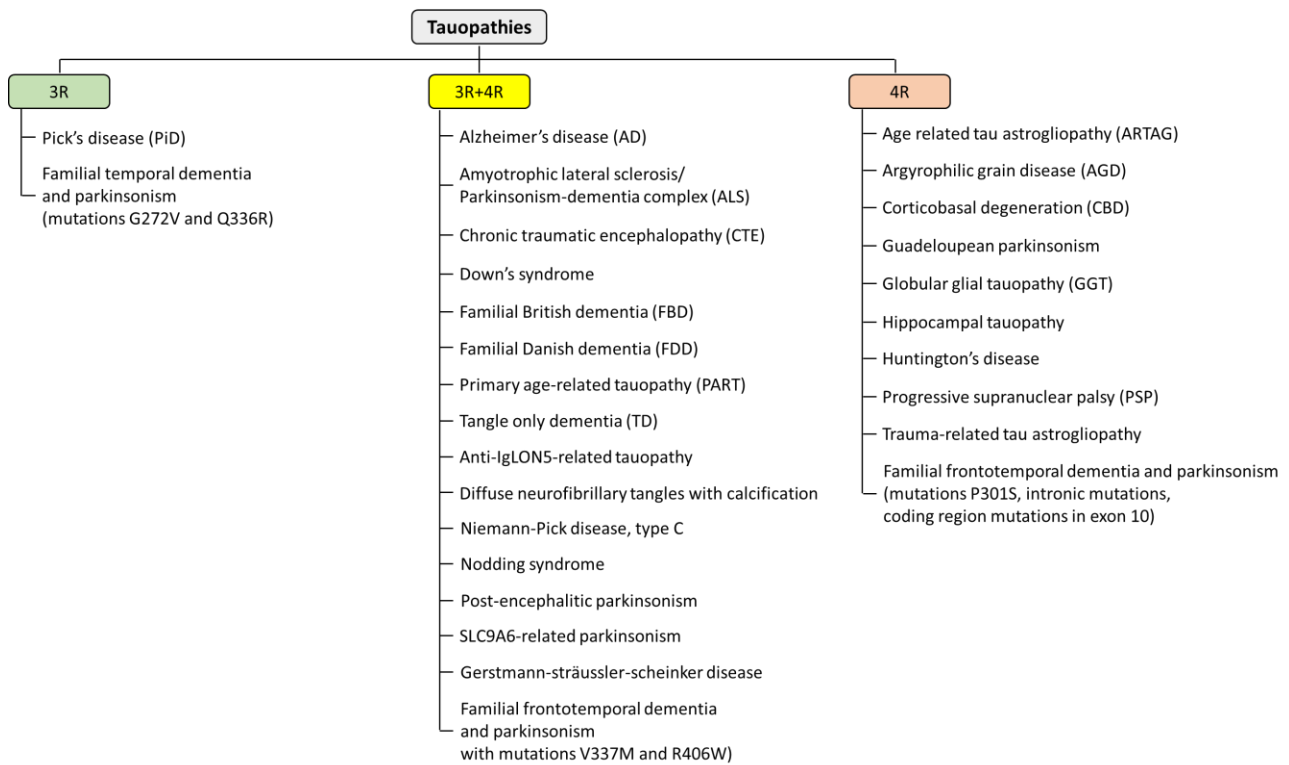


Fig. 1.6. Composition of tau isoforms reported in tau pathologies. Tauopathies with known tau isoform composition are mixed tauopathies (3R+4R), mainly 3R and 4R. List adapted from Limorenko G and Lashuel HA, *Neurobiology of Disease*, 2021¹⁸⁶.

isoforms in AD and CTE, British familial dementia, and Danish familial dementia^{187,188}. Depending on MAPT mutation, tau inclusion in FTDP-17 comprises six tau isoforms, predominantly with 3R, 4R or both 3R- and 4R- tau isoforms¹⁸⁹. In Pick's disease, the inclusions were composed of a 3R-tau isoform. Furthermore, in PSP, globular glial tauopathy, CBD, ageing-related tau astroglialopathy and argyrophilic grain disease, 4R-tau isoforms predominate in neuronal deposits^{187,188,190}.

Tauopathies are also classified based on the distinct migration pattern of full-length tau species. Though corticobasal degeneration and PSP are reported to be composed of 4R tauopathies, their cleavage products vary in size. Detergent insoluble cleaved tau from corticobasal degeneration migrates as 37 kDa doublet, whereas in the case of PSP, it migrates as a single band of 33 kDa¹⁹¹. In AD, the six tau isoforms are detected as tau triplet (tau 60, 64 and 69 kDa) with immunoblotting, wherein corticobasal degeneration and PSP appear as tau doublet (tau 64 and 69 kDa) with 4R-tau isoforms forming aggregates. In the case of Pick's disease, the tau deposits were made of 3R isoforms and appeared as doublet tau 60 and 64 kDa¹⁹². Concerning the morphological characteristics of the filaments, tau inclusions appear to be in the form of NFTs and neuropil threads in the somatodendritic compartment and distal axons and dendrites, respectively. In argyrophilic grain disease, glial tau inclusions in astrocytes, oligodendrocytes, and pre-tangle neurons in limbic areas contribute to hallmark lesions observed^{193,194}. Globose-type NFTs and neuropil threads, along with glial changes in tufted astrocytes and oligodendroglial coiled bodies, are reported in PSP¹⁹⁵⁻¹⁹⁷. In addition, corticobasal degeneration was distinguished with pre-tangle neurons, intracytoplasmic pathological tau in neuropil threads, astrocytic plaques and coiled bodies¹⁹⁸. Furthermore, FTDP-17 brains are characterized by filamentous tau inclusions in nerve and glial cells, astrocytic gliosis and spongiosis and Pick's disease with pick bodies, more specifically in neocortical, hippocampal and subcortical nerve cells^{151,199}.

1.6.2 Alzheimer's disease

Two types of lesions were first observed and described by Alois Alzheimer in the grey matter of a demented patient's brain in 1906¹⁷¹. The disease was named after him, defining neuropathological characteristics like lesions, senile plaques and NFTs. Reported as the third most frequent widespread dementia syndrome with pathology affecting humans apart from cancer and cardiovascular diseases, AD displays abundant deposits of extracellular senile A β plaques and

intracellular NFTs consisting of tau^{200,201}. Despite the prevalent hypothesis underlying misfolding and fibrillisation events as the cause of disease-specific inclusions, the exact mechanism behind brain degeneration in AD remains poorly understood.

AD, a degenerative tauopathy, is characterized by abnormal hyperphosphorylation of the tau, thereby leading to its aggregation through its repeat domain to form intraneuronal PHFs. Correlation between the quantity of aggregated tau, the spread of neurofibrillary tangle pathology, the extent of clinical dementia, and functional molecular imaging deficits was confirmed by various studies²⁰²⁻²⁰⁵. Though the close spatial correlation between neuronal loss and tau-based NFTs in patients' brains is evident, the correlation is overlooked, points to a higher layer of complexity, and supports the hypothesis that tau might play a prominent role in AD neurodegeneration²⁰⁶. Disease progression involves MCI at early stages to advanced dementia at later stages. Non-availability of drugs for disease treatment leaves physicians with no other option besides symptom-alleviating medications, placing patients under stress.

1.6.3 Tau aggregation

With a highly hydrophilic nature (solubility to ~650 μ M), unfolded tau protein aggregates into well-structured fibres in AD and other tauopathies²⁰⁷. Furthermore, significantly advanced studies in this field identified tau protein comprised of isolated short peptide motifs embedded within a hydrophilic environment, with a high tendency for β -structure and aggregation²⁰⁸. Two hexapeptide motifs, PHF6*(VQIINK) and PHF6(VQIVYK), enriched in hydrophobic amino acids, are present within the tau R2 and R3 repeat domains, respectively and are responsible for aggregation, forming the core of the PHFs²⁰⁸. The presence of β -hairpin structure in regions, including the PHF6 segment in intact tau monomer, was confirmed by *in vitro* and *in silico* studies. Mutation in hexapeptide motifs disrupts β -structure (e.g., an inserted proline), rendering the protein incompetent for assembly. PHF6, located in R3, is present in all tau isoforms, whereas PHF6* is present only in the 4R-tau isoform due to its presence in R2. Interaction of PHF6- PHF6, PHF6*-PHF6*, or PHF6-PHF6* motif²⁰⁹ mediates abnormal self-assembly of tau *via* dimerization. Recruitment of tau monomer forms nucleation seeds which in turn elongate into oligomers, eventually leading to tau filaments formation in a dose and time-dependent manner^{209,210}. Several biophysical and microscopic techniques confirm the presence of β -sheet structure and twisted helical structure in tau aggregates^{12,64,211,212}. The core region of PHFs

consists of a tau repeat domain wherein the N- and C-terminal regions spread away from the core structure representing paired helical filament's fuzzy coat²¹³. Even in the aggregated state, the fuzzy coat is highly mobile and poses a characteristic "soft polymer brush" extending from the paired helical filament core and interacting with other cellular components²¹⁴⁻²¹⁶. Besides enhancing the β -propensity of the motifs, the Δ K280 and P301L mutation increases tau aggregation in FTDP-17²¹⁷. P301L mutation shifts PHF6, disturbs the local compact structure and enhances the propensity for aggregation²¹⁸. Disulfide bridges formed between cysteine residues withhold protein-protein interaction or protein structure. Though cysteine residues (C291 and C322) play a controversial role in tau aggregation, results from some studies claim an intermolecular disulfide bond is involved in the seed formation to initiate tau polymerization and tau oligomer formation²¹⁹⁻²²¹. Additionally, the capping of cysteine residues with 1,2-dihydroxybenzene inhibits tau oligomer formation underlying the role played by cysteine residues in tau oligomer formation²²².

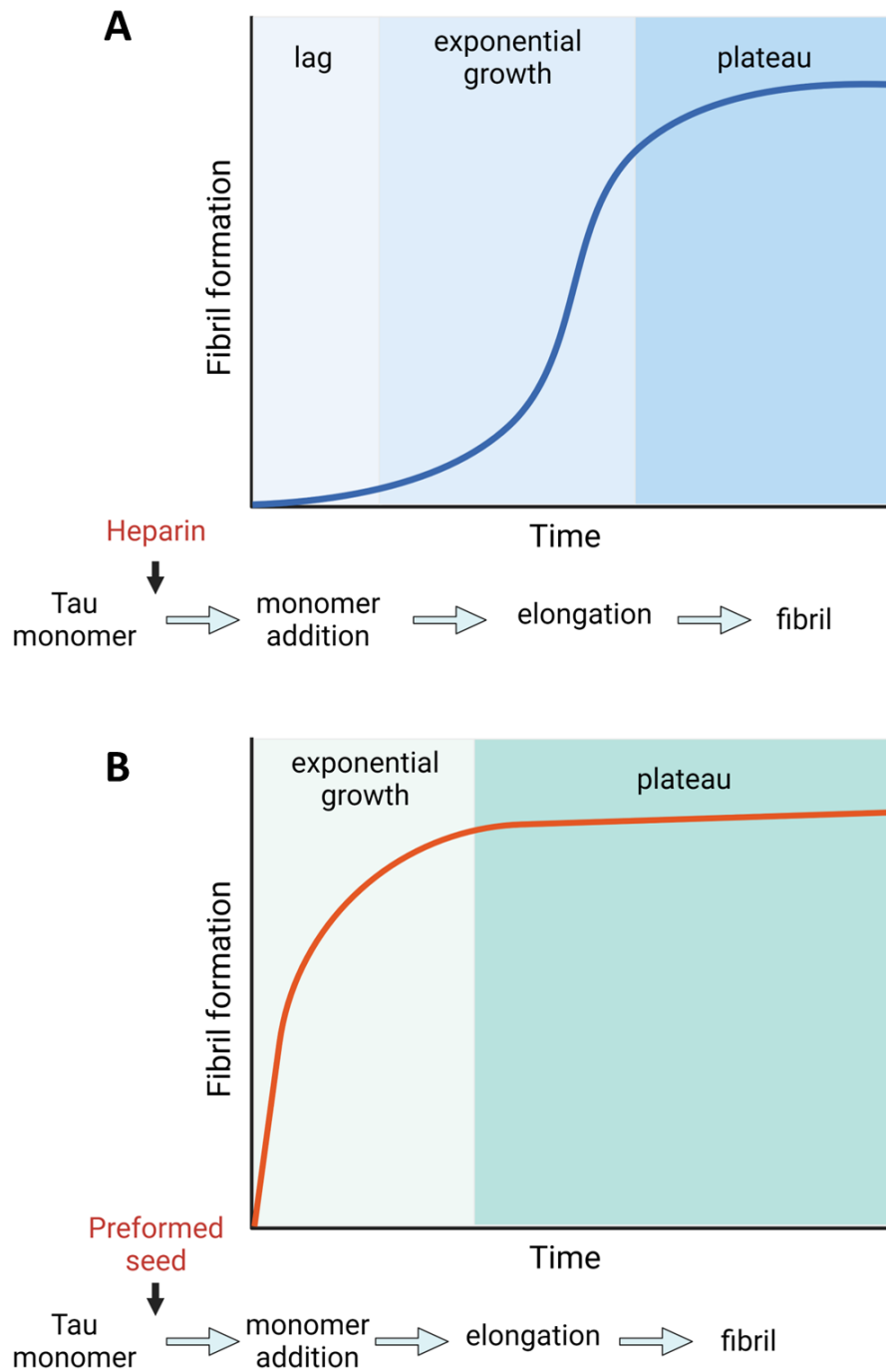


Fig. 1.7. Schematic representation of tau aggregation kinetic reactions. (A) Cofactor-induced tau aggregation displays a sigmoidal curve consisting of lag, exponential and plateau phases. (B) Preformed Tau nucleus-induced aggregation follows faster kinetics through the bypass of the lag phase. Created with BioRender.com.

NFTs consist of various hyperphosphorylated sites, and the implications of tau kinase inhibitors reduced tau phosphorylation, thereby inhibiting tau aggregation^{223,224}. It has been demonstrated that tau aggregation mediated by tau phosphorylation are site-specific, and phosphorylation at some sites inhibits tau aggregation^{17,225,226}. Therefore, the compounds directly targeting tau aggregation may be more effective tauopathies than tau kinase inhibitors. In tauopathies, including AD, aberrant tau post-translational modification results in self-assembly into neurotoxic oligomers and fibrils. Among the post-translational modifications reported so far, hyperphosphorylation remains the often-reported modification that initiates aberrant tau self-assembly. Thus, artificial models utilizing heparin and other polyanions were employed to induce aggregation *in vitro*, as it is challenging to introduce post-translational modification in cell culture models. These experimental systems are specifically convenient for screening tau aggregation inhibitors and disaggregation inducers²²⁷. However, structures resolved by cryo-electron microscopy display heparin-induced 4R- and 3R-tau fibrils that are structurally distinct from those reported in AD and Pick's disease questioning the relevance of such *in vitro* assays²²⁸. Heparin and RNA co-assemble with tau to induce fibril formation *in vitro*²²⁹.

Recent findings report that cofactors are not essential for tau fibrillisation and hyperphosphorylation is sufficient to induce fibril formation^{17,230}. Though the tau self-assembly process has been reported in many *in vitro* studies, the difficulty associated with the process of obtaining purified tau hyperphosphorylated forms, tau forms devoid of post-translational modification that does not aggregate spontaneously, were employed. Tau fragments comprising full-length or part of the MTBD are aggregation-prone, and their fibrils can serve as a template for tau aggregation^{183,231–234}. However, this strategy does not alleviate the concern about the lack of pathologically relevant post-translational modifications.

Polyanionic cofactors like heparin and other polyanionic nucleation factors, including nucleic acids, acidic lipid micelles, and acidic peptides, can initiate *in vitro* aggregation by compensating the basic charge of tau²³⁵. Under *in vitro* conditions, the fluorescent dye Thioflavin T monitored the tau aggregation level, and recombinant tau was polymerized with heparin or RNA. Researchers utilized this *in vitro* system mentioned above to screen for inhibitors targeting tau aggregation^{182,236}. Most aggregation tau inhibitors reported so far share a characteristic feature such as a negative or positive charge in their structure, antioxidant properties, and compounds of

natural origin. *In vitro* aggregation assays employ polyanions, RNA and fatty acids, such as arachidonic acid, or small anionic molecules as external inducers to stimulate tau aggregation, and the mechanism behind this process is still unclear. Though the fibrils generated from these assays are morphologically similar to PHFs, the mechanism involved along the aggregation process and structural details of these fibrils are pretty distinct from disease-relevant tau aggregates²³⁷. Tau fibrils formed in the presence of heparin or RNA disaggregate upon adding heparinase or RNase, respectively²²⁹. These findings are of particular concern as distinct conformational tau generated by inducers display different biological and pathological behaviour and might not recapitulate the structure of tau found in patient brains^{238,239}. Thus, an alternative approach focusing on phosphorylated tau production for *in vitro* studies involving aggregation, structure and pathological effects has to be carried out. Nevertheless, only a few studies reported this strategy and were focused on fibril formation and morphology^{17,240,241}. The mechanism of tau aggregation is briefly presented in Fig. 1.7.

1.6.4 Propagation of protein aggregation in neurodegenerative diseases

Neurodegenerative diseases remain a significant health concern for the world's aging population with the accumulation of amyloid proteins inside or outside cells. The most common neurodegenerative disease characteristics include protein amyloid deposition and degeneration of brain networks. Under experimental systems, amyloid protein, such as A β , tau, and α -synuclein, display properties similar to infectious prion³. As examined by X-rays, the term 'amyloid' refers to long, unbranched protein fibrils that display cross- β fibre diffraction. Identified as ordered protein assemblies, these amyloids act as a template for their replication through monomer addition, like small molecules or protein crystallization, which might trigger the progression of disease pathology in neurodegenerative diseases^{242,243}.

Numerous models explain the mechanism of amyloid growth, and a few are discussed below. The first model suggests a nucleated polymerization event, wherein the monomer is transformed into a seed, and fibrils grow *via* monomer addition²⁴³⁻²⁴⁶. Recent work specifies that for tau, the pathogenic seed can be a single molecule²⁴⁷. The second model proposes an induced fit wherein monomers get converted into aggregates failing to grow into ordered amyloid fibrils^{243,248}. Thus, aggregates serve as substrates for other proteins to bind and undergo a conformational change that enables subsequent amyloid growth. In both models mentioned above, fibrils grown are subjected

to fragmentation and secondary nucleation events that rapidly amplify protein amyloids. This provides an understanding of the origin and progression of multiple neurodegenerative diseases based on the self-replication mechanism through template formation. Mutation leading to dominantly inherited neurodegenerative diseases significantly alters proteins that accumulate in sporadic cases, usually through structural destabilization that promotes amyloid formation or *via* overproduction. Though the factors involved in triggering protein aggregation in sporadic diseases remain unknown, results from many studies report that diminished protein quality control in aging organisms could play a possible role²⁴⁹. Ubiquitin-proteasome system and the endosomal/lysosomal pathways are vital for keeping aggregation-prone proteins under control^{250,251}. Perhaps genome-wide association studies report that proteins associated with these pathways are linked to AD. Both sporadic and dominantly inherited AD show a primary pathogenic role in protein aggregation and accumulation.

Prions, known as the infectious assembly of proteins, serve as a template to convert normal proteins into pathogenic conformation, mediating disease transmission between individuals²⁵². Stanley Prusiner was awarded the Nobel prize in physiology or medicine in 1997 for explaining this novel and frightening basis of neurodegenerative disease. Nevertheless, with the principal goal to confirm protein-based infectious propagation of pathology, in some aspects, the field was distracted from investigating the molecular and cellular mechanisms of pathogenesis wherein a tiny inoculum progressively amplifies its structure within individual cells and then spreads throughout the nervous system. Cases of Prion disease are sporadic and not infectious, underlying that the process can begin and proceed based on endogenous mechanisms. Prion disease exhibit characteristics similar to non-infectious diseases like AD, amyotrophic lateral sclerosis and PD with amyloid protein deposition, progressive neurodegeneration and genetic and sporadic causes.

Additionally, results from the last decade are compelling and link prion mechanisms to common amyloid diseases^{5,19,239,253–255}. Deciphering the primary mechanism behind cell-cell propagation of pathology promises to introduce new therapeutic and diagnostic strategies. A significant understanding of prion biology and the role of discrete amyloid structures in driving specific pathology patterns might provide insights into pathogenic mechanisms.

1.6.5 Trans-cellular propagation of tau and seeding

Tau pathology propagates through the brain in a reproducible temporal and regional manner⁸. In tauopathies, disease progression is marked by the release of tau seed from one cell to another, leading to pathological tau aggregation. Tau propagation is hypothesized to be through a prion-like mechanism, which utilizes an initial seed to recruit normal monomeric tau and facilitates autocatalytic amplification²⁵⁶. Initial tau seed could be undigested cellular components, such as lipofuscin deposits or tau in an oligomeric state²⁵⁶. Tau undergoes active cell-to-cell (trans-cellular) transfer and initiates tau aggregates propagation in unaffected neurons^{239,257}. The mechanism underlying the spread of pathological tau is of significant focus for dementia research, thus remaining a potential therapeutic target for the attenuation of tau propagation (Mechanism of tau secretion and spreading is briefly explained in Fig. 1.8).

According to the observation, recombinant tau fibrils induce aggregation of full-length tau in cultured cells, which in turn gets transferred between cells¹⁹. In addition, the prion hypothesis explains that aggregated tau escapes from its origin cell and enters adjacent cells and seeds, further propagating pathology²⁵⁸. Additionally, it has been reported that intracellular tau fibrils propagate aggregation upon release into media by direct interaction with native tau in recipient cells. The ability of the anti-tau monoclonal antibody (HJ9.3) to interrupt this aggregation process by preventing recipient cells from tau aggregate uptake was reported²⁵⁷.

Apart from experimentation with recombinant tau, several groups deciphered the ability of PHFs from the AD brain to induce cytoplasmic tau aggregation²⁵⁹. In addition, brain extract from human P301S tau transgenic mice was injected into mice expressing wild-type tau and found to initiate pathological features⁵. Similar findings were reported wherein propagation of NFTs-like inclusions was observed from injected site to adjacent brain regions in a time-dependent manner²⁶⁰. Selective expression of tau in the entorhinal cortex cause late pathology onset in the axonal terminal zones in the dentate gyrus and hippocampus^{261,262}. Thus, a growing body of evidence supports the mechanism of tau aggregate transfer between cells and underlies the possibility of targeting these aggregates with therapeutic antibodies.

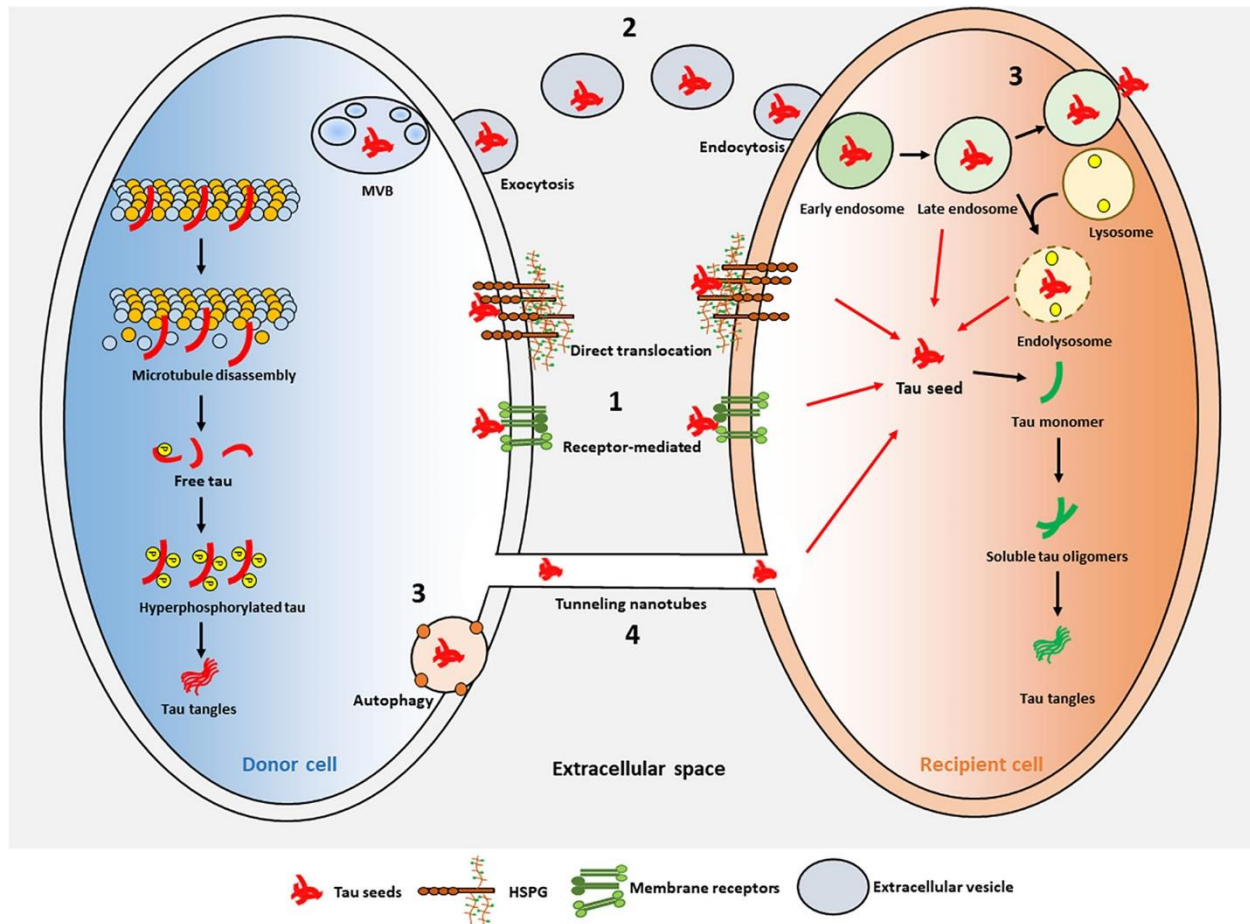


Fig. 1.8. Mechanism of tau secretion and spreading. Schematic representation of pathological tau transfer from a donor cell to a recipient cell by [1] Type I HSPG (heparan sulfate proteoglycans)- or receptor-mediated direct secretion and uptake of tau seeds, [2] Type III multivesicular bodies (MVB)-, and extracellular vesicle-mediated exocytosis and endocytosis, [3] endolysosomal and autophagy release, or [4] tunnelling nanotube-mediated direct cell-to-cell transfer of tau seeds. Irrespective spreading module, exogenous tau seeds the templated misfolding and aggregation of native tau once internalized by the recipient cell. This figure is reused from Annadurai N *et al.* Tau secretion and propagation: Perspectives for potential preventive interventions in Alzheimer’s disease and other tauopathies, *Experimental Neurology*, 2021⁴.

In vitro and *in vivo* studies demonstrate extracellular tau's ability to seed assembly and induce intracellular tau aggregate formation in adjacent cells^{5,19}. In addition, co-cultured cells were reported to uptake released intracellular tau aggregates and promote fibrillisation, illustrating prion-like tau propagation^{97,239,257}. Synaptic connections between neurons facilitate trans-cellular propagation of tau stimulated by depolarisation during neuronal activity, which can accelerate the spread of tauopathies^{262–267}. As seen in AD, the stereotypical staging of tau pathology can be described by trans-synaptic propagation *via* specifically connected neurons. Nevertheless, the exact mechanism behind tau propagation events like intracellular tau uptake and secretion is not fully understood. In comparison, several studies specify vesicle-mediated tau secretion *via* exosomes and ectosomes^{264,268}. Microglial cells also promote tau propagation through an exosome-dependent mechanism²⁶⁸.

In contrast, results from other findings demonstrate tau propagation as exosome independent process that requires heat shock cognate 70, chaperone DnaJ and synaptosomal-associated protein 23²⁶⁹. In addition, secreted pathological tau undergoes cellular uptake to enter neighbouring cells, linked to multiple cellular uptake mechanisms. The reported mechanisms include dynamin-driven and receptor-mediated endocytosis and actin-dependent proteoglycan-mediated micropinocytosis^{266,270,271}. In addition to the factors that regulate intercellular propagation, it is also important to consider the tau species responsible for initiating seeding. As the most widely recognized species, proteolytically stable oligomers have strong seeding potential, triggering tau self-assembly cascades in unaffected brain regions^{5,19,97,266,272}. While recent studies support that tau 297-391, the stable core of the PHF, known as '*dGAE*', in its soluble form, gets internalized into neuronal cells and recruits endogenous tau, some evidence supports fibril-induced tau propagation²⁷³. However, oligomeric tau is believed to be crucial species that provide tau with its 'prion-like' characteristic features.

Understanding the self-propagation of tau and the seeding abilities of pathogenic tau species in tauopathies has opened up new opportunities for therapeutic targets and interventions for treating tauopathies. Disruption of the tau propagation mechanism with anti-tau antibody infusions and small molecules are attractive therapeutic strategy. Treatment with anti-tau antibody infusion reduced oligomeric tau levels and improved cognitive function. Increasing evidence suggests that cytotoxicity associated with tauopathies might not result from larger aggregates of NFTs, even

though it is considered a histopathological hallmark of AD. In AD patients, apart from trans-cellular propagation, oligomers are known to be involved in cognitive decline and molecular dysfunctions that underlie neurodegeneration. Overexpression of tau *in vivo* displayed neuronal loss, behavioural abnormalities, and synaptic dysfunction without NFTs²⁷⁴⁻²⁷⁷. These findings are further supported by evidence from studies involving the injection of tau oligomers into wild-type mice which exhibited memory impairment, synaptic loss, and mitochondrial dysfunction²⁷⁸. These studies substantiate the pathological role of pre-tangle tau species in the dysfunction of neurons compared to tau fibrils. In response to these research findings, it has been proposed that tau fibrils are generated as a protective response wherein the toxic oligomeric species are absorbed and cleared *via* protease activity or autophagy^{279,280}.

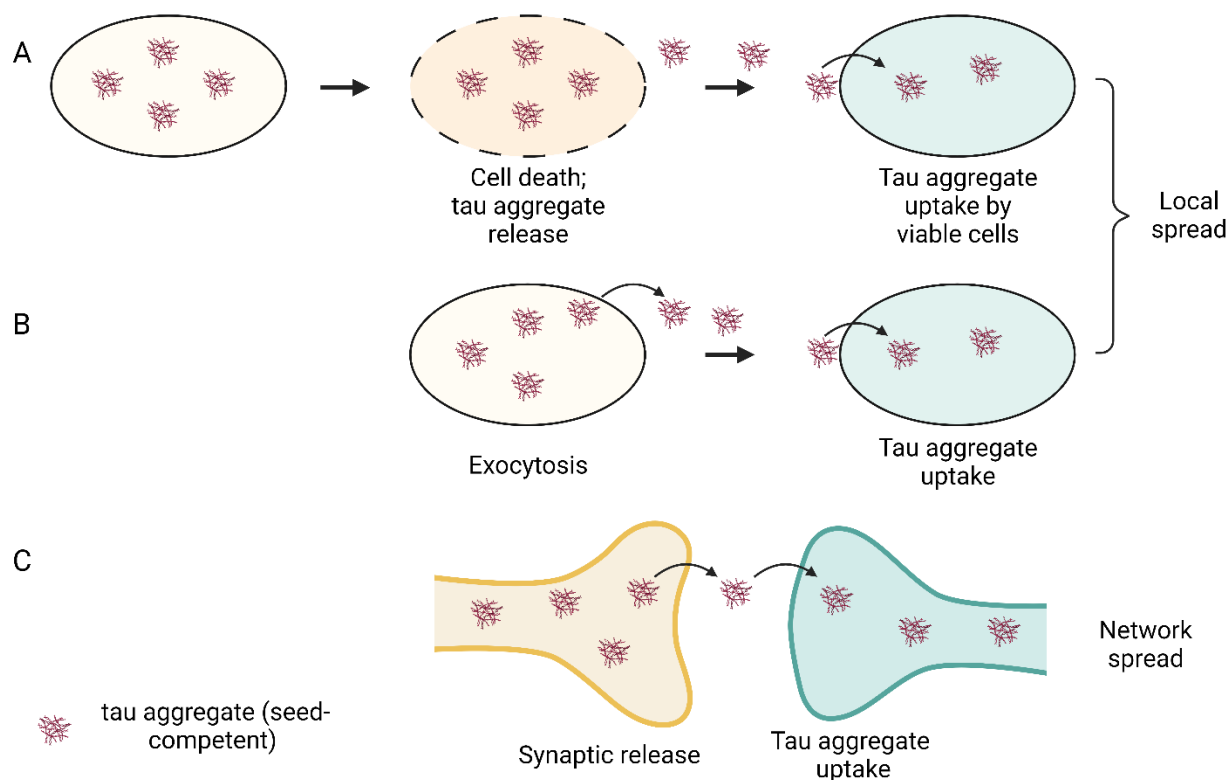


Fig. 1.9. Transcellular propagation of protein misfolding mechanism. (A) Cell death due to intracellular protein aggregation. Aggregates released into the extracellular space are taken up, aiding in protein misfolding in vulnerable cells. (B) Under normal physiological processes, protein aggregates are released from exosomes or through exocytosis. The presence of protein aggregates in extracellular spaces might be taken by adjacent cells. Both A and B processes account for the local propagation of misfolding. (C) Aggregates might cross synapses due to local synapse degeneration, which could be part of normal synaptic physiology or an exocytic process (as in B). This mechanism can explain network degeneration in neurodegenerative diseases. This figure is modified from Bess Frost *et al.* Prion-like mechanisms in neurodegenerative diseases, Nature Reviews Neuroscience, 2009²⁵⁸.

Nevertheless, the oligomers formed are proteolytically stable and could resist autophagic activity, enabling propagation between neurons and resulting in cytotoxicity. Thus, tau-induced neurodegeneration results from increased oligomers rather than an accumulation of PHFs in NFTs. This concept remains validated for AD and other neurodegenerative diseases. Studying the molecular mechanisms of protein self-assembly has been essential for further understanding neurodegeneration and identifying therapeutic targets. In addition, generating a reliable *in vitro* model that can accurately replicate cytotoxicity events associated with tauopathies will aid in understanding aggregation principles and identifying potential therapeutic targets (Fig. 1.9).

1.6.6 Tau spreading, toxicity and neurodegeneration

Growing evidence suggests that tauopathies spread between connected regions and cells involve complex processes, including secretion, cellular uptake, transcellular transfer, and seeding. However, the exact mechanism underlying tau pathological propagation remains unclear.

Followed by detachment from microtubules, tau undergoes structural transition, misfolding and degradation¹⁹. Tau can be secreted into extracellular space in its naked form or packaged in membranes/ exosomes, followed by neuronal activity in mature neurons, neuronal death or accumulation of tau reached beyond a certain level in non-neuronal cells^{281–284}. Similar to these findings, exogenous misfolded tau gets internalized by cells either through heparin sulphate proteoglycans (HSPGs) or cell membrane receptors, such as muscarinic (M1, M3) and α -amino-3-hydroxy-5-methyl-4-isoxazole propionic acid (AMPA) receptors-mediated processes or by endocytosis^{271,285,286}. After internalization, misfolded pathogenic tau proteins act as seeds, thereby recruiting soluble endogenous tau into larger aberrant conformations, which slowly propagate across the interconnected brain regions as confirmed by several animal models studies^{5,184,278,287}. Additionally, fibrillar tau species mediate transfer between cells and recruit endogenous tau proteins onto their ends, a mechanism responsible for the intracerebral spread of tau pathology²⁵⁷. The progressive accumulation of tau in brain regions in AD development is due to the spread of aggregated tau along anatomically connected regions^{288–290}. Accumulation of aggregate leads to neuronal loss and trans-synaptic spread of tau aggregates to more distal regions of the brain^{262,291}. Propagating neurofibrillary lesions and tau toxicity throughout different brain regions in neurodegenerative diseases are mediated by the spread of extracellular species^{260,292}.

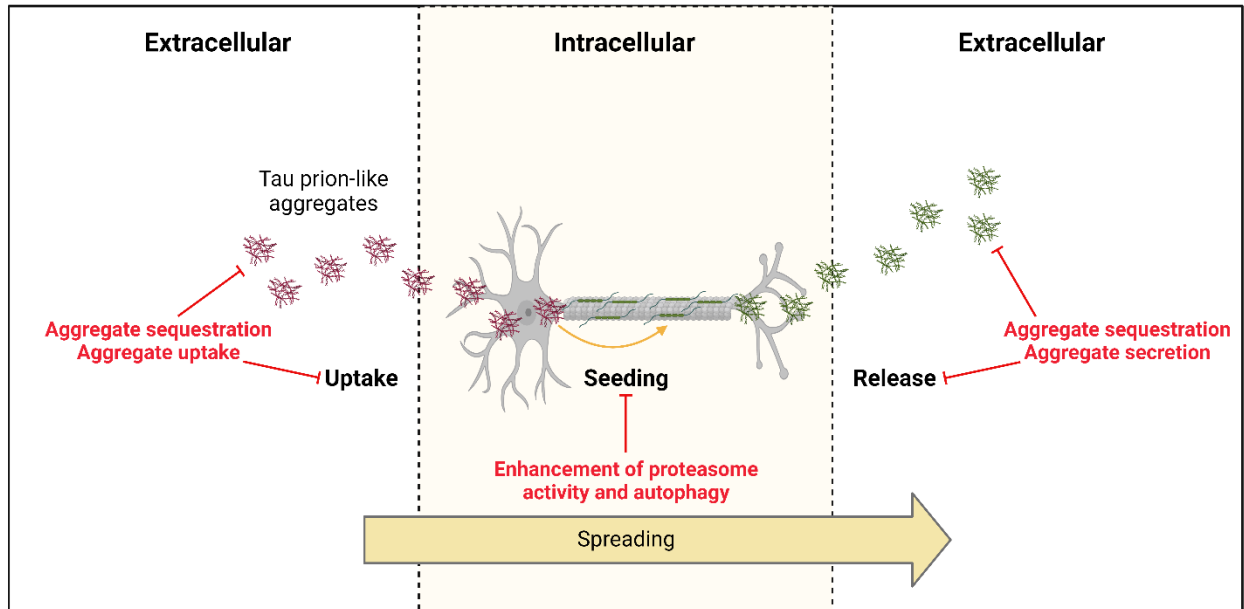


Fig. 1.10. Cell-to-cell tau spreading by prion-like mechanism and potential areas for therapeutic interventions (marked in red). This figure is modified from Annadurai N *et al.* Tau secretion and propagation: Perspectives for potential preventive interventions in Alzheimer's disease and other tauopathies, *Experimental Neurology*, 2021⁴.

A better understanding of the precise molecular mechanisms underlying tau propagation will contribute to developing new therapeutic approaches for halting this process and provide new perspectives for the early diagnosis and prevention of tau pathologies^{292,293}. The possible mechanisms involved in pathology propagation, such as tau detachment from microtubules, tau cleavage, tau degradation, and release, uptake, and movement of pathogenic tau along synaptically connected neurons, should be considered for understanding the mechanism²⁹⁴.

1.6.7 Toxicity associated with the spread of tau pathology

Neuronal transport disruption is thought as an underlying cause and early phenomenon in AD and other neurodegenerative conditions. Alteration of Ca^{2+} homeostasis by Tau phosphorylation, mislocalization, and conformational changes induces dendritic spine loss, impairs organelle trafficking, particularly in mitochondria, and leads to cell death^{76,116}. Three different hypotheses have been proposed to underlie tau-mediated toxicity: (1) insoluble NFTs might be toxic and lead to neuron death and cognitive dysfunction in AD, (2) misfolded soluble hyperphosphorylated tau might become toxic upon its accumulation in inappropriate cellular compartments, while NFTs exert a protective effect by serving as a sink for these toxic species, and (3) both insoluble NFTs and soluble pathological tau forms as toxic to cells²⁹⁵. Various works have favoured the third view. Recent studies observed that soluble tau species are linked to synaptic or neuronal dysfunction. These results indicate tau oligomers but not monomers or fibrils that act as aggregation seeds in the brains of wild-type mice, leading to mitochondrial dysfunction, synaptic deficits, and memory impairment²⁹⁴. Additionally, the interneuronal spread of soluble tau species may contribute to the spread of pathology in the brains of AD patients^{184,296,297}.

Besides, *in vivo* endogenous tau pathology arises from endocytosis of low molecular weight misfolded tau transported anterogradely and retrogradely by neurons. However, the neurons cannot endocytose fibrillar tau, brain-derived filamentous tau, or monomeric tau²⁶⁶. This substantiates that the cell-to-cell spread of trimeric and larger oligomeric forms in specific brain regions by endocytosis mediates tau toxicity²⁹⁸. Extracellular tau is considered neurotoxic²⁹⁹ and contributes to the pathological spread of AD. Thus, an increase in extracellular free tau levels compared to intracellular levels results in critical concentration wherein tau protein will self-aggregate and induce extracellular toxicity³⁰⁰. Thus, in comparison to free tau, PHFs are less toxic. Tau, upon interacting with muscarinic receptors, releases Ca^{2+} from its intracellular stores, thereby increasing

Ca²⁺ concentration. Toxicity and cell death associated with tau seeds can also be mediated through alteration in intracellular Ca²⁺ homeostasis resulting in tau phosphorylation and pathological progression of AD^{298,301,302}. Tau phosphorylation surges the detachment of tau from microtubules, increasing free tau levels, which in turn binds to muscarinic receptors on surrounding cells, inducing muscarinic toxicity and aggravating tau toxicity and transmission²⁸⁵. Through the different mechanisms, tau isoform variants are secreted into the extracellular space and play diverse roles in AD pathogenesis. For example, tau released through neuroactive stimulation or cell death events is considered non-toxic, while misfolded tau fragments or seeds (induced by A β , kinases, and hydrolases) exert toxic effects on the extracellular space. Tau protein in secreted vesicles impedes its binding to muscarinic receptors, thus reducing neurotoxicity.

Consequences of tau hyperphosphorylation include axonal transport impairment, synaptic loss and tau relocalization to the somatodendritic compartment³⁰³. Synaptic dysfunction can occur either presynaptically or postsynaptically, wherein the former involves synaptic vesicles to interfere with the transport of phosphorylated tau, whereas the latter involves the downregulation of AMPA receptors⁹⁹. Concerning the prion hypothesis, tau assemblies enter cytoplasm and seed native monomer aggregation, which gets released and spread to neighbouring cells^{184,304}. Aberrant post-translational modification events such as truncation, hyperphosphorylation and deamidation can induce tau detachment from microtubules under pathological conditions and promote its accumulation in free form¹⁵⁸. Once neurons degenerate and die, free tau enters extracellular space and gets diffused in all directions^{305,306}, which is in accordance with the observation made, wherein brain areas affected by degeneration pose progressive neuron loss, and without tangles, tau species can seed misfolding in human brains¹. This suggests that prior to neuronal death, tau seeds are released from intact neurons³⁰⁷. Similarly, extracellular NFTs or other substances released from degenerating neurons lead to their accumulation in extracellular space, damaging nearby cells³⁰⁸. These toxic compounds can act like extracellular A β peptides²⁹⁹. Thus, both soluble tau species and insoluble NFTs may contribute to the spread of tau toxicity.

1.7 Tau targeting therapy

Through screening, numerous compounds were identified, but only a few posed the potential to penetrate the brain or be non-toxic. An ideal approach for screening compounds involves utilizing cells expressing tau protein withholding mutations and selecting combinations among the group

with enhanced ability to prevent or revert the changes imposed by tau. For example, screens include kinase inhibitors, tau expression and aggregation modifiers, microtubule stabilizers and modifiers of neuronal tau interactors^{309–312}. In the latter case, the challenge is to achieve robust tau aggregation within the lifetime of a cell (a few days, compared to decades in the brain), observe the development of aggregation and toxicity using suitable readouts, and treat the cells with a library of promising compounds.

Recent drug discovery approaches focus on developing high and medium-molecular-weight drugs like antibodies or peptide-based drugs targeting alternative pathways to prevent abnormal tau formation. Approaches targeting tau-mediated toxicity reported so far include inhibition of tau post-translational modifications, pathological tau aggregation, propagation and microtubule stabilization. Recent findings illustrate that tau droplet formation by liquid-liquid phase separation might be the initial step in aberrant tau aggregation and explain the role of tau in dendritic and nuclear functions. Results from recent clinical trials should be considered to develop newer strategies focusing on the future direction of tau-targeted therapeutics³¹³.

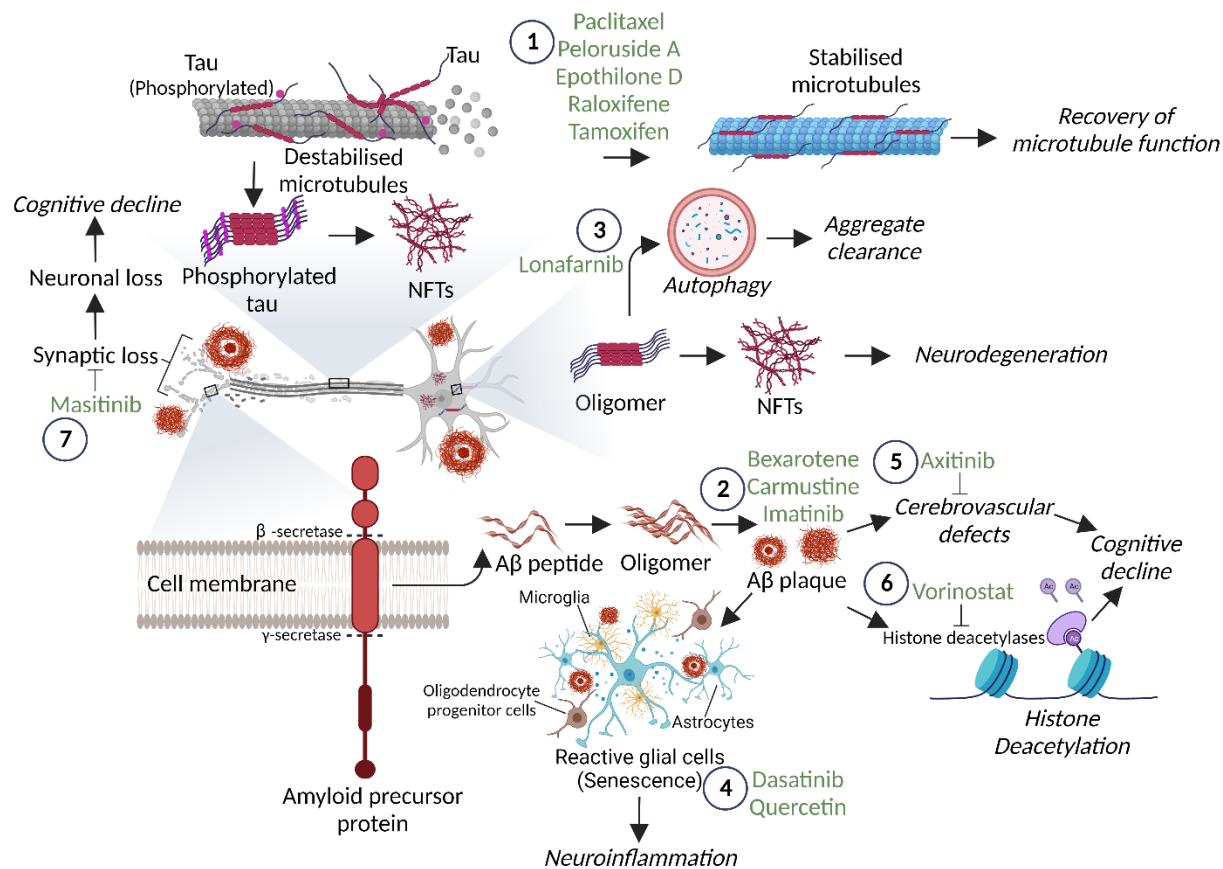


Fig. 1.11. Schematic diagram showing the mechanism of neuroprotective effects of antineoplastics in AD preclinical models. (1) Paclitaxel, peloruside A, epothilone D, and tamoxifen restore microtubule stability and dynamicity, resulting in the recovery of microtubule functions. (2) Aβ-targeting drugs (bexarotene, carmustine and imatinib) reduce the burden of Aβ plaques, reversing cognitive deficits. (3) Autophagy inducer lonafarnib-induced lysosomal clearance of tau pathology restores cognitive functions. (4) Extracellular Aβ plaques activate glial cells and induce senescence-like characteristics. Clearing senescent cells using senolytics (dasatinib and quercetin) reduce neuroinflammation, Aβ pathology, and cognitive deficits. (5) Axitinib modulates aberrant angiogenesis and corrects cerebrovascular defects. (6) HDAC inhibitor vorinostat restores epigenetic balance and reverses memory impairment. (7) Masitinib rescue of synaptic loss prevents cognitive decline. Created with BioRender.com.

1.7.1 Inhibition of tau aggregation

Tau aggregation remains detrimental to neurons; thus, inhibitors targeting tau aggregation could be protective. Compounds from different classes, including N-phenyl amines, phenylthiazolhydrazides, anthraquinones and rhodamines, are known to inhibit tau aggregation and disassemble existing filaments¹⁸⁰. For example, a tau aggregation inhibitor, bb14, inhibits tau aggregation in organotypic hippocampal slice culture expressing pro-aggregate tau RD Δ K280. In addition, the compound bb14 prevents calcium dysregulation and synapse loss³¹⁴. Similarly, N-phenylamine derivatives such as B1C11, B4D3, B4A1, and B4D5 inhibit tau aggregation and disassemble preformed aggregates^{315,316}. In addition, phenothiazines such as methylene blue are neuroprotective and known to inhibit A β oligomerization and tau aggregation along with reactive oxygen species production³¹⁷⁻³¹⁹. Another compound, CMP-16, inhibits tau aggregation in *Caenorhabditis elegans* models of tauopathy. However, whether they can remove tau oligomers remain unclear³²⁰. Recent reports indicate that curcumin can suppress soluble tau dimers by rescuing synaptic and behavioural deficits³²¹. Polyphenol epigallocatechin gallate inhibits α -synuclein and A β fibrillogenesis by directly binding to natively unfolded polypeptides. Epigallocatechin gallate prevents the formation of toxic aggregation intermediates, thereby reducing its cellular toxicity^{322,323}. Epigallocatechin gallate-coated nanoparticles efficiently reduce A β aggregation and cell toxicity³²⁴. Likewise, inhibitors targeted against tau aggregation might induce off-pathway oligomer formation. Thus, approaches targeting tau oligomers can aid in finding the cure for toxic tau species.

Though the pathway associated with AD remains a matter of debate, the aggregation of A β and tau are known to play a vital role in neurodegeneration^{93,325}. Therefore, low molecular weight antibodies or drugs targeted at inhibition or reversal of tau aggregation might serve as a potential therapeutic strategy currently undergoing clinical trials^{326,327}. So far, various tau aggregation inhibitors have been identified and evaluated in different test systems like transgenic mice, organotypic slices, and *Caenorhabditis elegans*^{314,317,320}. However rapid and cost-efficient evaluation of cellular effects, a cell model of tau aggregation would be desirable. Physiological tau poses a low aggregation propensity. Therefore, one problem is rapidly reducing aggregation within the cell's lifetime and observing its effects on cell behaviour and metabolism.

Insights about possible targets that mediate inhibition of tau aggregation, β -sheet fibrillisation intermediates or oligomers can be identified by preclinical studies³²⁸. Small molecules and compounds, including methylene blue, orange G, oleocanthal, diazodinitrophenol, polythiophene, curcumin, thiophene and phthalocyanine tetrasulphonate, are reported to inhibit tau aggregation *in vitro*^{183,329–335}. While only methylene blue derivative and curcumin are advanced to clinical trials, none of the other compounds characterized by *in vitro* studies is approved for further clinical use. Through the oxidation of cysteine residues, the phenothiazine compound methylene blue prevents tau fibrillisation¹⁷⁸. Furthermore, it mitigates tau-related neurodegeneration and pathology through autophagy induction, reduction of synaptotoxicity and tau phosphorylations by mitogen-associated kinase 4 and upregulation of NF-E2-related factor 2/antioxidant response element in mice³³⁶. In addition, Methylene blue functions as a redox cyler to stimulate mitochondrial metabolism and reduce the inflammatory response, which mediates its inhibitory activity for tau aggregation³³⁷. Despite the widespread use of methylene blue in various conditions, no epidemiological studies explaining dementia or AD-associated incidence rates have been done in these patient populations. Thus it is likely to have possible direct effects of methylene blue on tau fibrillisation. Additionally, LMTX, a reduced form of methylene blue, was unsuccessful in Phase III clinical trials (NCT01689246 and NCT01689233). However, LMTX is investigated as a monotherapy in early-stage AD patients (NCT03446001).

1.7.2 Drug repurposing for neurodegenerative diseases

Existing therapeutic approaches to treat AD are merely symptomatic, emphasizing the need for new molecular entities acting on the causes of the disease particularly urgent. The implication of compounds already in the market remains one of the potential solutions. Details about compound structures with known pharmacokinetics, toxicity profiles, pharmacodynamics and patient data are available in several countries. Several drugs have effectively treated diseases distinct from their primary purpose. Numerous retrospective studies reveal that cancer survivors have a reduced risk for dementia and AD compared to those without cancer^{338–341}. However, the mentioned inverse correlation due to common biological mechanisms between cancer and AD patients remains debatable, and mechanisms are primarily unknown^{21,339,342–344}. Drugs targeting AD follow different pathways. In retrospective studies, chemotherapy preceded AD diagnosis in cancer

survivors and may revoke tau seed formation and inhibit tau spreading and AD development (Fig. 1.10)^{340,345}. However, evidence implies that chemotherapy reduces AD risk in cancer survivors³⁴⁶.

Chapter 2

Aims of the study

The aims of the project were:

(1) To identify the minimal regions in the tau repeat microtubule-binding domain that defines seeding and its impact on intracellular tau phosphorylation and aggregation in tau-RD P301S FRET biosensor cells and Tau P301L (0N4R) HEK293 cells. To achieve Aim 1, the following were the objectives:

- a) In vitro characterisation of the aggregation and fibrillisation potential of tau repeat peptides (R1, R2, R3 and R4)*
- b) Characterisation of the prion-like seeding potential of aggregates of tau repeat peptides*
- c) Examine the effect of exogenous aggregates of tau repeat peptides on solubility and phosphorylation changes in intracellular seeded tau in cell models*

(2) To target the minimal regions with small molecules to abrogate the generation of seed-competent aggregates of tau and seeding in tau-RD P301S FRET biosensor cells. To achieve Aim 2, the following were the objectives:

- a) Examine the effect of small molecules on in vitro aggregation and fibrillisation of tau repeat peptides*
- b) Investigate the seeding activity of small molecule-treated aggregates in tau cell models*

(3) To compare the clearance of intracellular aggregates in tau cell models seeded with aggregates of tau repeat peptides. To achieve Aim 3, the following were the objectives:

- a) Analyse time-dependent build-up of intracellular tau aggregation in cells*
- b) Elucidate autophagy failure in cells seeded with tau repeat peptide aggregates*
- c) Induce autophagy-mediated clearance of intracellular tau aggregation in cells*

Chapter 3

Materials and methods

3.1 Chemicals and peptides

Paclitaxel, vincristine sulfate, bleomycin, resveratrol, polydatin, genistein and quercetin were purchased from Sigma-Aldrich and dissolved in DMSO to make a 10-mM stock. All other drugs were obtained from the University Hospital Olomouc (Table 3.1). Before the experiment, the drugs from injection vials or 10 mM DMSO stocks were reconstituted in 1× PBS (pH 7.2) to make fresh 1 mM intermediate stock. The intermediate drug stock was used to make working stocks for all experiments. Tau repeat peptides of the microtubule-binding domain of full-length 2N4R tau (Fig. 3.1 A, B), R1 (AS-65433-1), R2 (AS- 65435-1), R3 (AS-65435-1) and R4 (AS-65436-1) were purchased from Anaspec (Fremont, CA, USA). Mutant R3 peptide (C322A) was purchased from Genscript Biotech (Piscataway, NJ, USA). Tau R3 peptide was synthesized by Drs. Alfredo Cagnotto and Mario Salmona at the Department of Molecular Biochemistry and Pharmacology, Istituto di Ricerche Farmacologiche Mario Negri IRCCS, Milan, Italy, as described in the paper³⁴⁷. Peptides were dissolved in sterile deionised water and stored at -80° C until further use. The concentration of the peptides was quantified using Cary 60 UV-Vis Spectrophotometer (Agilent Technologies, USA).

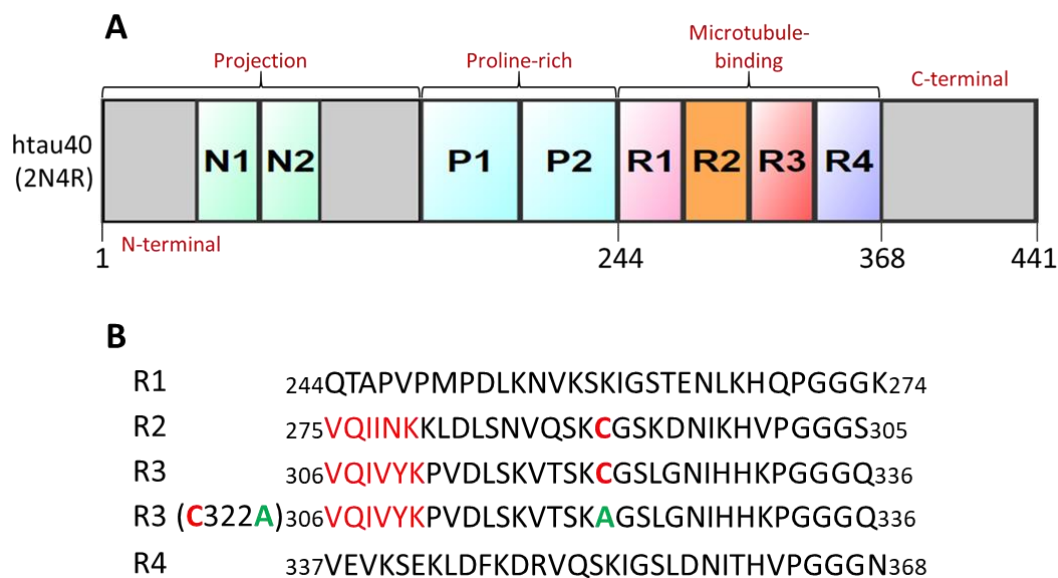


Fig. 3.1. Tau protein domain organization and tau repeat peptides sequence. (A) Schematic representation of 2N4R tau isoform (htau40), displaying the major domains (projection domain, proline-rich domain, microtubule-binding domain, and C-terminal domain). (B) Amino acid sequences of different tau peptides used in the thesis are shown. The N-terminal hexapeptide regions are marked in red, the cysteine residues are marked in bold red, and the cysteine to alanine substitution at position 322 in the R3 (C322A) peptide is shown in green in the amino acid sequences.

3.2 Tau aggregation assay

The aggregation of tau repeat peptides was monitored using an in vitro Thioflavin T (ThT) binding assay. To carry out aggregation assays, peptides stored at -80°C were thawed on ice and centrifuged at 13 000 rpm for 45 secs on a benchtop centrifuge. Throughout sample preparation, reagents and the assay plate were kept on ice. A reaction mixture consisting of 0–50 μM peptides and 15 μM ThT either in the presence or absence of 5 μM heparin (Sigma-Aldrich, Cat. #H4784–1G) was prepared in peptide aggregation buffer [20 mM Tris (pH 7.4), 100 mM NaCl and 1 mM EDTA]. The reaction mixture was dispensed into black and clear bottom 384 well plates (Cell Carrier, Cat. # 6007550; PerkinElmer, Waltham, MA, USA) and sealed with TopSealA-PLUS (PerkinElmer) adhesive to prevent evaporation. The assay plate was placed in an EnSpire Multimode Plate Reader (PerkinElmer), with the temperature of the measurement chamber set to 37°C . Within the plate reader, the upper temperature was set to 2°C warmer than the lower heater temperature to avoid condensation on the sealed plate surface. The plates were subjected to constant agitation of 1000 rpm during the resting period, and the fluorescence of ThT binding ($\lambda_{\text{exc}} = 460\text{--}490\text{ nm}$, $\lambda_{\text{em}} = 500\text{--}550\text{ nm}$) to aggregated peptide was recorded every 5 min up to 48 h. For normalised ThT fluorescence plots, the raw data (ThT fluorescence) were normalised to the lower and higher relative fluorescence intensity values in the data set using GraphPad Prism software (Version 7; San Diego, CA, USA).

Following the ThT binding assay protocol, the effect of antitumour drugs on R3 repeat peptide aggregation was determined in a two-step screening assay, which included peptide aggregation in the presence of drugs to identify active inhibitors. To this end, the reaction mixture containing 20 μM R3 repeat peptide, 5 μM heparin and 15 μM ThT was spiked with drugs at 1 μM concentration before dispensing into a 384-well assay plate to determine drug effects. To examine the effect of drugs on the polymerisation of preformed R3 aggregates into mature fibrils, R3 was first aggregated at 37°C for 24 h in the absence of drugs. The assay plate was then removed from the plate reader to add drugs from intermediate stocks to get the final desired concentration per well (0.1, 1 and 10 μM). The addition of drugs was performed in < 15 min. After adding drugs, the plate was placed back into the plate reader, and the fluorescence of ThT binding to aggregates was monitored for an additional 24 h. Control wells received an equal amount of aggregation buffer containing DMSO in all aggregation assays with drugs at a percentage present in drugged wells.

Unless otherwise mentioned, the final concentration of the drug solvent was always below 0.5%. All drug treatments were performed in duplicates per plate, and the assay was repeated at least 3 independent times. Note that all peptide aggregation assays in the presence or absence of drugs were carried out for cell and worm treatment experiments in the absence of ThT.

Similar to the protocol mentioned above for the ThT assay, 8-anilino-1-naphthalenesulfonic acid (ANS) fluorescence assay was performed with or without 5 μM heparin under similar aggregation conditions. For the assay, 25 μM tau repeat peptides were aggregated in a peptide aggregation buffer containing 40 μM ANS. The change in ANS fluorescence was recorded using EnSpire Multimode Plate Reader (PerkinElmer) at $\lambda_{\text{exc}} = 390 \text{ nm}$ and $\lambda_{\text{em}} = 475 \text{ nm}$.

3.3 Fluorescence imaging, atomic force microscopy, and Congo red absorbance

At the end of the ThT binding assay, the contents of the assay plates were embedded in 0.05% low-melting agarose (Sigma-Aldrich) and cooled to 40 $^{\circ}\text{C}$ for 10–15 min at room temperature (RT) to visualize the formation of tau repeat peptide fibrils. Likewise, the formation of β -sheet-rich tau repeat R3 peptide aggregates in the absence or presence of drugs was visualised by staining the content of assay wells with 15 μM ThT after the end of ThT-free aggregation assay and embedding in 0.05% low-melting agarose and imaged by the following protocol as mentioned earlier. The images of ThT-stained fibrils were captured on an Operetta™ High-Content Imaging System (PerkinElmer) using a 2 \times objective (numerical aperture: 0.08) and 488-laser line ($\lambda_{\text{exc}} = 460\text{--}490 \text{ nm}$, $\lambda_{\text{em}} = 500\text{--}550 \text{ nm}$). The captured images were processed using Harmony High-Content Analysis Software (PerkinElmer).

Morphological characterisation of fibrils formed post 24 h, and 48 h of tau repeat peptides aggregation and the effect of drugs on R3 fibril formation was confirmed by atomic force microscopy (AFM). To achieve this, samples were added dropwise onto a freshly cleaved 10 mm sized AFM mica disc (Ted Pella, Inc., Redding, CA, USA) and air-dried for 10 min at RT. Then, using a 0.22 μm sterile syringe filter (Merck Millipore, Burlington, MA)-sterilised deionised water, the mica discs were washed 5 \times times and dried for 10–15 min at RT. The discs were strapped using Cellotape on a glass slide to prevent them from moving during imaging.

Imaging of samples was done by Drs Lukáš Malina and Jakub Malohlava from the Department of Medical Biophysics, Faculty of Medicine and Dentistry, Palacký University in Olomouc, Czech

Republic. Briefly, images of aggregates were acquired on an Olympus IX81/Veeco BioScope™ Catalyst™ Atomic Force Microscope (Bruker, Billerica, CA, USA) using a 10 × objective under ambient conditions at a scan rate of 0.7 Hz (line/sec) and Peak Force amplitude of 150 nm. Antimony-doped silicon cantilever probes with a typical resonant frequency of 150 Hz and spring constant of 5.1 Nm⁻¹ were employed, and acquired images were processed in Gwyddion 2.40 freeware developed by the Czech Metrology Institute, Brno, Czech Republic³⁴⁸.

To validate the antifibrillation effect of drugs, 20 μM R3 was first allowed to fibrillise under a ThT-free pro-aggregation condition in the absence or presence of drugs at 10 μM concentration in a Spectra 384-well assay plate (PerkinElmer). After 48 h, the contents of the wells were stained with 40 μM Congo red (Sigma-Aldrich), and the absorbance was immediately measured in an EnSpire Multimode Plate Reader (PerkinElmer) at 540 nm wavelength.

3.4 Coomassie gel staining

R2 and R3 fibrils were collected, followed by aggregation assay of 24 and 48 h. Next, the collected samples were centrifuged at 65 000×g on a benchtop centrifuge for 60 min at 4 °C to pellet insoluble fractions. Next, the soluble fractions were removed, and the insoluble pellet fractions were washed twice with 1 × PBS and centrifugation at 65 000×g for 5 min. The insoluble fractions were then electrophoresed and processed for Coomassie staining as described below. For the drug-treated R3 repeat peptide aggregation experiments, the R3 repeat peptides aggregated in the presence or absence of drugs collected after the end of the aggregation assay were centrifuged to pellet insoluble fractions. In addition to non-centrifuged total fractions, the insoluble fractions were mixed with NuPAGE™ LDS Sample Buffer (Thermo Fisher Scientific, Waltham, CA, USA) without reducing agent and boiled for 5 min at 70 °C. The insoluble fractions were mixed with 10% β-ME in LDS Sample Buffer before boiling to denature disulfide bonds. The total and insoluble fractions were electrophoresed using NuPAGE™ 4–12% Bis-Tris gels (Thermo Fisher Scientific) at 200 V for 40 min at RT in 1× NuPAGE™ MES SDS Running Buffer (Thermo Fisher Scientific). Gels were fixed in a fixative solution [50% methanol (v/v) and 10% acetic acid (v/v) in deionised water] for 30 min and stained with Coomassie Brilliant Blue R-250 solution (Bio-Rad, Hercules, CA, USA) for 12 h at 4 °C. Gels were destained by washing multiple times in deionised water. Images of gels were acquired in a ChemiDoc MP imaging system (Bio-Rad).

3.5 Preparation of models for molecular dynamics simulation

Molecular dynamics simulation of drug-peptide interaction studies was performed by the groups of Prof. Michal Otyepka^a and Dr. Karel Berka^b from ^aCzech Advanced Technology and Research Institute (CATRIN), Regional Centre of Advanced Technologies and Materials (RCPTM), Palacký University Olomouc, Olomouc, Czech Republic and ^bDepartment of Physical Chemistry, Faculty of Science, Palacký University Olomouc, Olomouc, Czech Republic, as described in the paper³⁴⁷.

3.6 Cell culture and DNA transfection

All cell lines used in the study are from American Type Culture Collection (Manassas, VA, USA). Tau RD P301S FRET biosensor cells (ATCC; CRL-3275TM) were cultured in Dulbecco's Modified Eagle's medium (Lonza, Cat. # 12–604F) supplemented with 1% GlutaMAX (Lonza, Cat. # 12–604F), 10% fetal bovine serum (FBS; Capricorn Scientific GmbH, Ebsdorfergrund, Germany) or 10% fetal calf serum (Gibco, Cat. # 10270), and 1% penicillin/streptomycin (Diagnovum, Cat. # 910). Human embryonic kidney (HEK293) cells were cultured in Eagle's Minimum Essential Medium (Lonza, Cat. # 12–611F) supplemented with 10% fetal calf serum and 1% penicillin/streptomycin. Cells were maintained in a standard humidified 5% CO₂ atmospheric air incubator at 37° C. The cells were routinely tested for bacterial, fungal and mycoplasma contaminations and authenticated biweekly or monthly.

Tau P301L (0N4R) cloned in pCMV6 plasmid was a kind gift from Dr Jose F Abisambra of the University of Kentucky (Lexington, KY, USA). Then, the HEK293 cells were plated at a density of 1×10^6 /mL plated in a 100 mm tissue culture Petri dish. After overnight incubation in 5% CO₂ incubator, the cells were transfected with 2 µg/mL tau P301L plasmid diluted in jetPRIME® buffer supplemented with jetPRIME® reagent following the manufacturer's protocol for 18 h.

3.7 Tau seeding assay

Tau RD P301S biosensor cells and Tau P301L (0N4R) HEK293 cells were plated at a density of 50,000 cells/mL in a CellCarrier 96-well plate (PerkinElmer, Cat. # 6005550) for imaging experiments and at 1×10^6 cells/mL density for cellular fractionation in TPP Ø96mm, 60 cm² tissue culture Petri dishes (TPP Techno Plastic Products AG, Trasadingen, Switzerland). The next day, cells were transfected with 50 nM or 100 nM peptide fibrils, collected from the in vitro

aggregation assay carried out in the absence of ThT, premixed in jetPRIME® Buffer (Polyplus-transfection SA, New York, NY, USA) supplemented with jetPRIME® reagent (Polyplus-transfection SA) as described elsewhere. In addition, a transfection reagent mixture in peptide aggregation buffer without tau peptides was used as a negative seeding control. Post 24 h of transfection, the old medium was replaced with a fresh complete growth medium and allowed further for 48 h before processing for imaging and Triton X-100 cell fractionation experiments.

For studying the effect of drugs on the seeding effect of R3 repeat peptide aggregates, Tau-RD P301S FRET Biosensor cells were plated in a black, clear-bottom CellCarrier 96-well plate (PerkinElmer) at a density of 5×10^4 cells·mL⁻¹ in 100 µL of growth medium. The next day, cells were treated with R3 monomers or aggregates premixed in Lipofectamine LTX Plus transfection agent for 72 h.

For seeding assay with drug-capped aggregates, 1 µM fibrillar R3 repeat peptide aggregates were first incubated with 0.1 µM paclitaxel, 1 µM doxorubicin, and 4 µM resveratrol and quercetin in deionised water for 16 h at 37 °C to make an intermediate stock. Drug-capped fibrils were then sonicated for 1–2 min on a Cup Horn water bath to generate shorter aggregates, as described elsewhere, before adding to cells³⁴⁹. Alternatively, fibrillar R3 repeat peptide aggregates (1 µM) were first sonicated and then capped with drugs before adding to cells. The drug-capped aggregates were mixed with 1% Lipofectamine LTX and 0.5% Lipofectamine Plus in Opti-MEM reduced-serum medium and seeded to cells at a 1 : 1 ratio of transfectant to the growth medium. The drug concentrations for capping were chosen based on the concept that drugs required to block seeding by preformed fibrils are about 20 times greater than the amount required to inhibit monomeric tau aggregation³⁴⁹. The final concentration of R3 repeat peptide aggregates was 50 nM, whereas the concentration of paclitaxel was 5 nM, that of doxorubicin was 50 nM, and those of resveratrol and quercetin were 200 nM.

For seeding assay with drug-inhibited aggregates, 20 µM R3 peptide was first assembled in vitro in the presence of 2 µM paclitaxel, 20 µM doxorubicin, and 80 µM resveratrol and quercetin for 48 h. The R3 repeat peptide aggregates formed were then diluted into an Opti-MEM to make intermediate stocks. Five microlitres of intermediate stock of preinhibited R3 repeat peptide aggregates were mixed with 1% Lipofectamine LTX and 0.5% Lipofectamine Plus in Opti-MEM and seeded to cells at a 1 : 1 ratio. The final concentration of R3 repeat peptide aggregates was

50 nM, whereas the concentration of paclitaxel was 5 nM, that of doxorubicin was 50 nM, and those of resveratrol and quercetin were 200 nM.

For drug pretreatment seeding assay, cells were first pretreated with paclitaxel (1 nM), doxorubicin (10 nM), resveratrol (200 nM) and quercetin (200 nM) or just the aggregation buffer for 2 and 24 h at 37 °C. Following drug treatment, cells were washed twice with 1x PBS and seeded with sonicated R3 repeat peptide aggregates premixed with 1% Lipofectamine LTX and 0.5% Lipofectamine Plus in Opti-MEM reduced-serum medium and seeded to cells as per the tau seeding assay protocol mentioned above for 24 h.

In all seeding assays, the final concentration of drug solvent (DMSO) per well was always < 0.5%. Control cells were treated with aggregation buffer containing only Lipofectamine LTX Plus transfection agents. All treatments were performed in triplicate per experimental plate, and the experiments were repeated 3–5 independent times.

For autophagy-focused imaging studies, tau biosensor cells were plated at a density of 0.15×10^6 cells/mL in a CellCarrier 96-well plate (PerkinElmer, Cat. # 6005550). The next day, cells were transfected with 50 nM R3 fibrils premixed in Opti-MEM™ I Reduced Serum Medium (Gibco, Cat. # 11058021) supplemented with P3000™ reagent (0.25 µL/well) and Lipofectamine™ 3000 reagent (0.5 µL/well) and were allowed to grow before processed for imaging. The cells were seeded with 50 nM R3 fibrils, and after 6 h of seeding, the cells were rinsed with 1x PBS and treated with the compounds at the mentioned concentrations (Table 3.2) for 12 h.

3.8 Imaging and quantification of cell number and seeding

Prior to imaging, the biosensor cells were stained with 10 µM Hoechst-33342 nuclear dye (Invitrogen, Cat. #H21492) for 10–15 min at 37 °C in a humidified incubator and the cells were then washed twice with 1X PBS and replaced with phenol red-free growth media. Cells were imaged on an Operetta™ High-Content Imaging System (PerkinElmer) using a 20x objective and 488-laser line ($\lambda_{exc} = 460\text{--}490$ nm, $\lambda_{em} = 500\text{--}550$ nm) for CFP/YFP Tau-RD aggregates and 405-laser line ($\lambda_{exc} = 360\text{--}400$ nm, $\lambda_{em} = 410\text{--}480$ nm) for Hoechst-33342. At least 10–12 focal areas were imaged per well of experimental plates. Cell number was quantified by counting Hoechst-stained nuclei, and the seeding was determined by counting the number of intracellular CFP/YFP Tau-RD aggregates using Harmony Image Analysis Software. The aggregates were then

normalised to the total cell number per well and presented as ‘normalised seeding’ in our study. For morphology, the cells were imaged on the Cell Voyager CV7000S microscope (Yokogawa, Tokyo, Japan) using a 60x objective. Cells were maintained in a live-cell chamber at 37 °C and 5% CO₂/atmospheric air throughout imaging.

For autophagy-focused studies, prior to imaging, the tau biosensor cells were stained with 10 µM Hoechst 33342 nuclear dye (Invitrogen, Cat. #H21492) for 10–15 min at 37 °C in a CO₂ incubator. Then, the cells were replaced with phenol red-free growth media and imaged on the Cell Voyager CV7000S microscope (Yokogawa, Tokyo, Japan) using a 20x objective. The tau biosensor cells were maintained at 37 °C and 5% CO₂ atmospheric air incubator throughout imaging in a live-cell chamber. The intracellular CFP/YFP Tau RD P301S aggregates and cell numbers were quantified using Columbus Image Data Storage and Analysis System (PerkinElmer).

3.9 Quantification of internalised R3 fibrils

R3 fibrils were stained with 50 nM X-34 (Sigma-Aldrich, Cat. # SML1954) for 5 min at RT. HEK293 cells were then transfected with R3 fibrils prestained with X-34 premixed with or without transfection reagent as described above. After 12 h of transfection, cells were washed with 1 × PBS containing 20 U/mL heparin (Cat. #H4784-1G, Sigma-Aldrich) and then 0.25% trypsin (Gibco) in PBS for 2–3 min to remove any cell membrane-bound fibrils that were not internalised. Prior to imaging, the cells were stained with 1x BioTracker 650 Red Nuclear Dye (Merck Millipore, Cat. # SCT119) in a phenol red-free medium. Cells were imaged on a ZEISS Cell Observer SD Spinning Disk Confocal Microscope (Carl Zeiss AG, Oberkochen, Germany) using an oil-immersion 63 × objective (numerical aperture: 1.4). Images were acquired using ZEN 2 (blue edition) software (Carl Zeiss AG). X-34 was excited with a 405-nm laser line (λ_{exc} 350 nm/ λ_{em} 470 nm), and BioTracker 650 Red Nuclear Dye was excited using a 639-nm laser line (λ_{exc} 650 nm/ λ_{em} 665 nm). The laser intensity and exposure time were kept constant between different samples. The acquired images were processed using ZEN 2012 Black Edition imaging software (Carl Zeiss).

3.10 Cytotoxicity assay

R3 was assembled under a ThT-free pro-aggregation condition in the absence/presence of drugs for 48 h. The untreated/preinhibited R3 aggregates (R3Ag) were collected and diluted in 50 μ L Opti-MEM (Cat. # 11058021, Thermo Fisher Scientific) containing 1% Lipofectamine LTX (Cat. # 15338100, Thermo Fisher Scientific) and 0.5% Lipofectamine Plus (Cat. # 15338100, Thermo Fisher Scientific). The transfection mixture was incubated for 15 min at RT. These transfectants were then added to cells plated in a standard 24- or 96-well plate (Techno Plastic Products AG, Trasadingen, Switzerland) at a density of 0.1×10^6 cells/mL. Cell viability was analysed after 72 h of treatment using a standard MTT assay or trypan blue exclusion assay. Cell viability and the cell number and viability by trypan blue assay were measured using a Vi-CELL™ XR Cell Viability Analyser (Beckman Coulter, Brea, CA, USA) following the manufacturer's instructions.

3.11 Determining the IC₅₀ value of compounds

The cell viability of Tau biosensor cells in the presence of selected compounds (Table 3.2 and 6.14) was tested by a standard MTT assay. Cells were plated at a density of 0.1×10^6 cells/mL in 96-well plates and incubated at 37 °C in a 5% CO₂ incubator for overnight. After adding compounds, the cells were incubated at 37 °C in the 5% CO₂ incubator for 24, 48 and 72 h. Next, 10 μ L of MTT/well was added and incubated at 37 °C for 3 h. After 3 h of MTT treatment, 100 μ L of SDS was added to dissolve formazan crystals, and the plates were kept at 37 °C overnight. Absorbance at 570 nm was measured, and the IC₅₀ value was calculated using GraphPad Prism software.

3.12 Triton X-100 cell fractionation and Western blot analysis

Cells were harvested and resuspended in $1 \times$ Tris-Buffered Saline (TBS) containing 0.05% Triton X-100 supplemented with protease (Roche, Cat. # 04693116001) and phosphatase inhibitors (Roche, Cat. # 04906837001). The cell lysate was then clarified by two rounds of centrifugation, including 500 \times g for 5 min and 1000 \times g for another 5 min at 4 °C. The supernatant was collected, and 20% of the supernatant fraction was stored as a total fraction. The remaining supernatant was centrifuged at 65,000 \times g for 30 min at 4 °C. The resulting supernatant and pellet were collected as Triton X-100-soluble and insoluble fractions, respectively. Finally, the pellet fraction was resuspended in RIPA buffer supplemented with protease and phosphatase inhibitors. Thirty-five

µg of total fraction and an equal volume of Triton-soluble and -insoluble fractions were electrophoresed by 4–12% gradient PAGE and 10% SDS-PAGE.

Electrophoresed proteins were transferred onto a PVDF membrane (Blot™ 2 Transfer Stacks, PVDF, regular size, Invitrogen, Cat. # IB24001) using an iBlot™ 2 Gel Transfer Device (ThermoFisher Scientific). The blots were blocked with 5% BSA for 1 h in 1 × TBS containing 0.1% Tween® 20 Detergent (TBST) at RT and incubated with primary antibodies, anti-tau A10 antibody (1:1000; SCBT, Cat. #sc-390476) and anti-tau Tau-5 antibody (1:1000; Invitrogen, Cat. #AHB0042), anti-phospho Ser202/Thr205 tau (1:1000; Invitrogen, Cat. #MN1020), anti-phospho Ser262 tau (1:1000; Invitrogen, Cat. #OPA1-03142), anti-phospho Ser396 tau (1:1000; Invitrogen, Cat. #44-752G), anti-phospho Ser404 tau (1:1000; CST, Cat. #20194S) and anti-oligomeric tau T22 (1:1000; Merck Millipore, Cat. #ABN454), overnight at 4 °C and anti-GAPDH antibody (1:4000; SCBT, Cat. #sc-32233) for 1 h at RT. Primary antibody-stained blots were developed using anti-mouse (Cat. #A1134) or anti-rabbit (Cat. #A21202) Alexa Fluor 488-conjugated secondary antibodies (Invitrogen) at 1:2000 dilution for 1–2 h at RT in the dark. The blots were then imaged using a Gel Doc XR + Gel Documentation System (Bio-Rad) with appropriate filters for Alexa Fluor 488 to visualise protein bands.

For autophagy-focused studies, after preparing triton-soluble and –insoluble fractions as mentioned above, forty-five µg of Triton-soluble fraction and an equal volume of Triton-insoluble fractions were electrophoresed by 10% SDS-PAGE. Electrophoresed proteins were transferred onto a 0.2 µm Nitrocellulose membrane by using Trans-Blot Turbo Transfer System (Bio-Rad) as mentioned above. Blotted membranes were blocked as mentioned above and treated with primary antibodies such as Tau (1: 1000; Sigma-Aldrich, Cat. # 05-804) and anti-phospho Ser262 tau (1: 1000; Invitrogen, Cat. # PA5-85654) and incubated overnight at 4 °C. After incubation, the membranes were washed with 1x TBST and incubated with Alexa 488 fluorescent dye tagged secondary antibodies and processed for imaging as mentioned above.

3.13 Sample processing and protein quantification

For autophagy-focused Western blot analysis studies, the tau R2/R3 fibrils were prepared by aggregating for 48 h as described elsewhere^{347,350}. Tau biosensor cells were plated in a 6-well plate (0.5 × 10⁶ cells/mL, 2 mL of medium /well) and cultured at 37 °C in a 5 % CO₂ incubator overnight. The next day, cells were transfected with 50 nM fibrils collected from the *in vitro*

aggregation assay carried out without Thioflavin T using Lipofectamine™ 3000 Transfection Reagent kit. First, 50 nM of tau aggregates were mixed in Opti-MEM and supplemented with P3000™ reagent (1.5 µL/well) and Lipofectamine™ 3000 reagent (3 µL/well). Then, the transfection mixture was incubated for 15 min at RT. Next, the cells were replaced with a pre-warmed fresh complete growth medium and then treated with the transfection mixture containing tau repeat peptide aggregates. After 6 h of transfection, the transfection media was removed, and the cells were replaced with a pre-warmed fresh complete medium. Samples were collected at 3, 6, 9, 12, 24, 36, and 48 h after transfection. For compound treatment, the cells were seeded with 50 nM R3 fibrils in the presence or absence of selected compounds at the mentioned concentrations (Table 3.2) and incubated for 48 h.

When collecting the samples, the medium was collected, and cells were washed with 1x TBS and collected in the same centrifuge tube after washing. For cell detachment, 200 µL of TrypLE was used. When detached, TrypLE was inactivated by the complete growth medium, and the cell suspension was collected. Then, it was centrifuged at 1500 RPM for 5 min to pellet cells. Next, the sedimented cell pellet was resuspended in 1 mL of 1 x TBS, transferred into a 1.5 mL centrifuge tube, and centrifuged for 10 min at 500 x g. Finally, the supernatant was discarded, and the sedimented cell pellet was processed for protein extraction. RIPA lysis buffer (Thermo Scientific, Cat. # 89901) was mixed with protease (Roche, Cat. # 04693116001) and phosphatase (Roche, Cat. # 04906837001) inhibitors, and 100 µL of lysis buffer was added to cell pellets and mixed gently. Samples were sonicated using a water bath sonicator for 3 min at 25% Amplitude with a 15-sec pulse ON and 15-sec pulse OFF. After sonication, tubes were centrifuged at 12 000 RPM at 4 °C for 30 min, and the supernatant was transferred to a new chilled 1.5 mL centrifuge tube. The remaining cell pellet was discarded.

Protein concentration in samples was quantified using a BCA protein assay kit (ThermoFisher Scientific). A set of protein standards was used for calibration using bovine serum albumin (2 000, 1 500, 1000, 750, 500, 250, 125, 25 and 0 µg/mL). First, BCA reagent A and BCA reagent B were mixed at a 50:1 ratio. Then, 10 µL of each standard and 2.5 µL of samples were pipetted into separate wells, and 200 µL of BCA reagent A and B mixture/well was added and incubated at 37 °C for 30 min. Then, the absorbance was measured using an EnSpire Multimode Plate Reader

(PerkinElmer) at 562 nm. Microsoft Excel prepared the calibration curve, and sample protein concentration was calculated.

3.14 SDS-PAGE Electrophoresis and Western blotting

For autophagy- focused studies, the volume of a quantified sample containing 35 µg of protein was calculated and added into a new 1.5 mL centrifuge tube. 1x gel loading dye supplemented with 10% β-mercaptoethanol per protein sample (15 µL) was added to the protein sample containing tubes. RIPA buffer was added to bring the sample volume to 15 µL. This sample, dye, and buffer mixture was heated at 95 °C for 5 min in a dry thermal block. After heating and letting it cool down, samples were quickly spun for 10 seconds and loaded into gels. Samples were separated by 10% and 12% denaturing SDS polyacrylamide gel electrophoresis. Gels were hand cast using the Bio-Rad Mini-PROTEAN Tetra Cell system using Tris-Glycine-SDS buffer. Electrophoresis was run at 200 V for 1-1.5 h approximately until the dye hit the bottom of the gel.

Western blotting was done using the Trans-Blot Turbo Transfer System (Bio-Rad) and 0.2 µm Nitrocellulose membrane (Bio-Rad). The protein blot transfer was 10-15 min at 20-25 Volts. Blotted membranes were blocked in 5% BSA (diluted in 1x TBST buffer) for 1 hour. Membranes were quickly washed in 1x TBST for 1-2 min after blocking. Buffer was discarded after washing, and membranes were treated with primary antibodies such as anti-LC3A/B (1: 1000; Invitrogen, Cat. # PA1-16931), anti-p62 (1: 1000; CST, Cat. # 88588), anti-LAMP1 (1: 1000; CST, Cat. # 9091) and anti-β actin (1:4000; Sigma-Aldrich, Cat. #A2228) primary antibodies and incubated overnight at 4 °C. After incubation, membranes were washed with 1x TBST 4 times with each wash at 10 min intervals. The washing buffer was discarded after each wash. Then, membranes were treated with respective secondary antibodies (1:2000; Invitrogen) (anti-mouse (Cat. #A1134), anti-rabbit (Cat. #A21202)) conjugated with Alexa 488 fluorescent dye and incubated for 2 h at RT on a shaker. The shaker speed was maintained throughout this process at 120 RPM. Then, membranes were washed with 1x TBST 4 times with each wash at 10 min intervals. After the final wash, membranes were imaged in the Bio-Rad Gel Doc XR + Gel Documentation System, and images were processed using ImageJ (NIH) software.

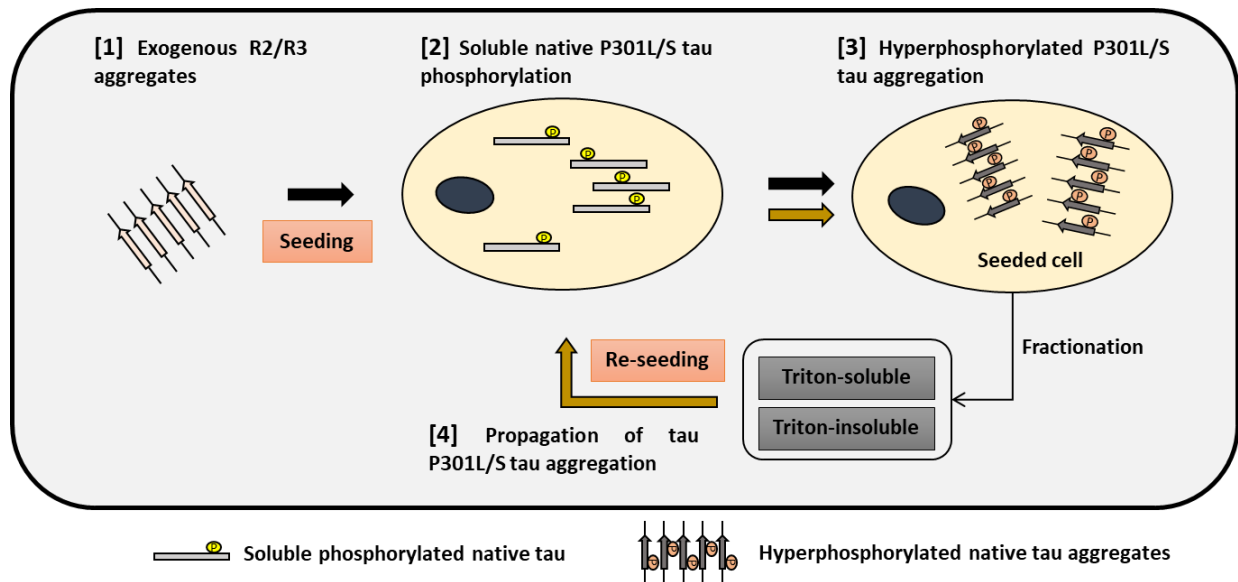


Fig. 3.2. Experimental procedure of seeding, fractionation, and re-seeding. Exogenous β -sheet rich aggregates of tau R2 and R3 peptides [1], when introduced into TauRD P301S biosensor cells and 0N4R tau over-expressing HEK293 cells [2], seed the aggregation of intracellular native tau aggregation by conversion of soluble tau into hyperphosphorylated and oligomerised forms [2, 3]. The triton-soluble and -insoluble fractions from seeded cells continue to propagate native tau aggregation when re-seeded into TauRD P301S biosensor cells [4].

3.15 Cellular reseeding assay

Tau RD P301S biosensor cells were plated at 0.1×10^6 cells/mL density in a CellCarrier 96-well plate (PerkinElmer). The next day, cells were transfected with 1 μ g/well total and Triton-soluble and -insoluble fractions prepared from biosensor cells (Fig. 3.2). After 24 h, the old medium containing transfection reagent was replaced with fresh complete growth media and cells were incubated for an additional 48 h before imaging. Imaging was done on an OperettaTM high-content imaging system, as described above, to quantify the cell number and intracellular Tau RD aggregates.

3.16 *Caenorhabditis elegans* studies

All *C. elegans* experiments were performed by Drs Luisa Diomedea and Margherita Romeo from the Department of Molecular Biochemistry and Pharmacology, Istituto di Ricerche Farmacologiche Mario Negri IRCCS, Milan, Italy, as described in the paper³⁴⁷.

3.17 Statistical analysis

All statistical analyses were performed using GraphPad Prism Software (Version 8; San Diego, CA, USA) and differences were considered significant at $P < 0.05$.

Table 3.1. Source of antitumour drugs and solvent concentrations.

| | Source | Actual concentraion (mg/mL) | Conversion to mM | Vehicle concentration (%) in drug dilutions | | | |
|-----------------------------------|---------------------------------|-----------------------------|------------------|---|-------------------|--------|--------|
| | | | | Intermediate (in 1× PBS) | Final (in 1× PBS) | | |
| | | | | | 1 mM | 10 µM | 1 µM |
| Paclitaxel | Sigma-Aldrich (Cat. No.: T7191) | 8.54 | 10 | 10 | 0.1 | 0.01 | 0.001 |
| Docetaxel | University Hospital Olomouc | 10 | 12.38 | 8.08 | 0.08 | 0.008 | 0.001 |
| Vincristine sulfate | Sigma-Aldrich (Cat. No.: V8879) | 5 | 5.42 | 18.45 | 0.184 | 0.018 | 0.001 |
| Vinorelbine tartrate | University Hospital Olomouc | 10 | 12.84 | 7.78 | 0.08 | 0.008 | 0.001 |
| Cisplatin | University Hospital Olomouc | 1 | 3.33 | 30.03 | 0.3 | 0.03 | 0.003 |
| Oxaliplatin | University Hospital Olomouc | 5 | 12.58 | 7.95 | 0.08 | 0.008 | 0.001 |
| Carboplatin | University Hospital Olomouc | 10 | 26.94 | 3.72 | 0.04 | 0.004 | <0.001 |
| Cyclophosphamide monohydrate | University Hospital Olomouc | 20 | 76.6 | 1.31 | 0.01 | 0.001 | <0.001 |
| 5-Fluorouracil | University Hospital Olomouc | 50 | 384.38 | 0.26 | <0.001 | <0.001 | <0.001 |
| Methotrexate | University Hospital Olomouc | 50 | 110.04 | 0.91 | 0.01 | 0.001 | <0.001 |
| Fludarabine phosphate | University Hospital Olomouc | 10 | 27.38 | 3.65 | 0.04 | 0.004 | <0.001 |
| Gemcitabine | University Hospital Olomouc | 40 | 151.97 | 0.66 | 0.01 | 0.001 | <0.001 |
| Doxorubicin hydrochloride | University Hospital Olomouc | 2 | 3.45 | 28.98 | 0.28 | 0.028 | 0.003 |
| Daunorubicin hydrochloride | University Hospital Olomouc | 5 | 9.48 | 10.55 | 0.11 | 0.011 | 0.001 |
| Bleomycin | Sigma-Aldrich (Cat. No.: B7216) | 10 | 7.06 | 14.16 | 0.141 | 0.014 | 0.001 |
| Mitomycin C | University Hospital Olomouc | 2 | 5.98 | 16.72 | 0.17 | 0.017 | 0.002 |
| Irinotecan hydrochloride Trihydra | University Hospital Olomouc | 20 | 29.54 | 3.39 | 0.03 | 0.003 | <0.001 |
| Etoposide | University Hospital Olomouc | 20 | 33.98 | 2.94 | 0.029 | 0.003 | <0.001 |
| Mitoxantrone | University Hospital Olomouc | 6 | 13.5 | 7.41 | 0.07 | 0.007 | 0.001 |
| Topotecan hydrochloride | University Hospital Olomouc | 1 | 2.2 | 45.45 | 0.45 | 0.045 | 0.005 |
| Resveratrol | Sigma-Aldrich (Cat. No.: R5010) | 16.24 | 71.13 | 1.41 | 0.01 | 0.001 | <0.001 |
| Polydatin | Sigma-Aldrich (Cat. No.: 15721) | 3.04 | 7.79 | 12.84 | 0.13 | 0.013 | 0.001 |
| Genistein | Sigma-Aldrich (Cat. No.: G6649) | 2.7 | 10 | 10 | 0.1 | 0.01 | 0.001 |
| Quercetin | Sigma-Aldrich (Cat. No.: Q4951) | 4.7 | 15.55 | 6.43 | 0.06 | 0.006 | 0.001 |

Table 3.2. Sources of compounds, stock and working concentrations.

| Name | Catalogue number | Vehicle | Stock (mM) | Intermediate stock (mM) | Working stock (μM) | | |
|--|-------------------------|----------------|-------------------|--------------------------------|--|------|------|
| Resveratrol (RSV) | R5010 (Sigma-Aldrich) | DMSO | 71.13 | 1 | 1 | 10 | 20 |
| Epigallocatechin gallate (EGCG) | E4143 (Sigma-Aldrich) | Water | 20 | 10 | 25 | 50 | 100 |
| L-Ascorbic acid (VITC) | A4403- (Sigma-Aldrich) | Water | 567.8 | 10 | 10 | 25 | 50 |
| Quercetin (QCT) | Q4951 (Sigma-Aldrich) | DMSO | 112.5 | 1 | 0.1 | 1 | 2 |
| Carbamazepine (CBZ) | C4024 (Sigma-Aldrich) | DMSO | 140.73 | 1 | 1 | 5 | 10 |
| Artemisinin (ART) | 361593 (Sigma-Aldrich) | DMSO | 97.6 | 1 | 1 | 5 | 10 |
| Dexamethasone (DEX) | D4902 (Sigma-Aldrich) | DMSO | 70.76 | 1 | 1 | 5 | 10 |
| Chloroquine (CQ) | C6628 (Sigma-Aldrich) | Water | 100 | 1 | 0.1 | 1 | 2 |
| Cycloheximide (CHX) | C7698 (Sigma-Aldrich) | Water | 66.05 | 0.1 | 0.001 | 0.01 | 0.02 |

Chapter 4

Identification of minimal regions in the tau repeat microtubule-binding domain that defines seeding and its impact on intracellular tau phosphorylation and aggregation

The data presented in this chapter have been published as “Annadurai N *et al.* Tau R2, and R3 are essential regions for tau aggregation, seeding and propagation. *Biochimie.* 2022, 200:79-86. doi: 10.1016/j.biochi.2022.05.013”.

4.1 R3 repeat region of the tau RD is essential for self-assembly of tau

In the presence of heparin, R2 and R3 peptides assemble time-dependently into β -sheet-rich fibrils, which are in corroboration with ThT fluorescence and morphological changes with fibrils (Fig. 4.1A and B). The ability of R2 and R3 to form β -sheet-rich fibrils was validated by fluorescence imaging (Fig. 4.1C).

Results from aggregation assays demonstrate that in comparison to R3, R2 aggregates faster, as implied by differences in their $t_{1/2}$ values (R2 vs R3, $p < 0.001$, paired t-test, $n = 3$; Fig. 4.1A), whereas R1 and R4 failed to assemble into fibrils (Fig. 4.1D and E). R2 and R3 displayed concentration-dependent growth kinetics (Fig. 4.2A). The findings are on par with earlier work wherein VQIINK of R2 is a more powerful driver of tau aggregation than VQIVYK of R3³⁴⁹. However, both R2 and R3 forms dimer in the presence of heparin upon aggregation (Fig. 4.2B).

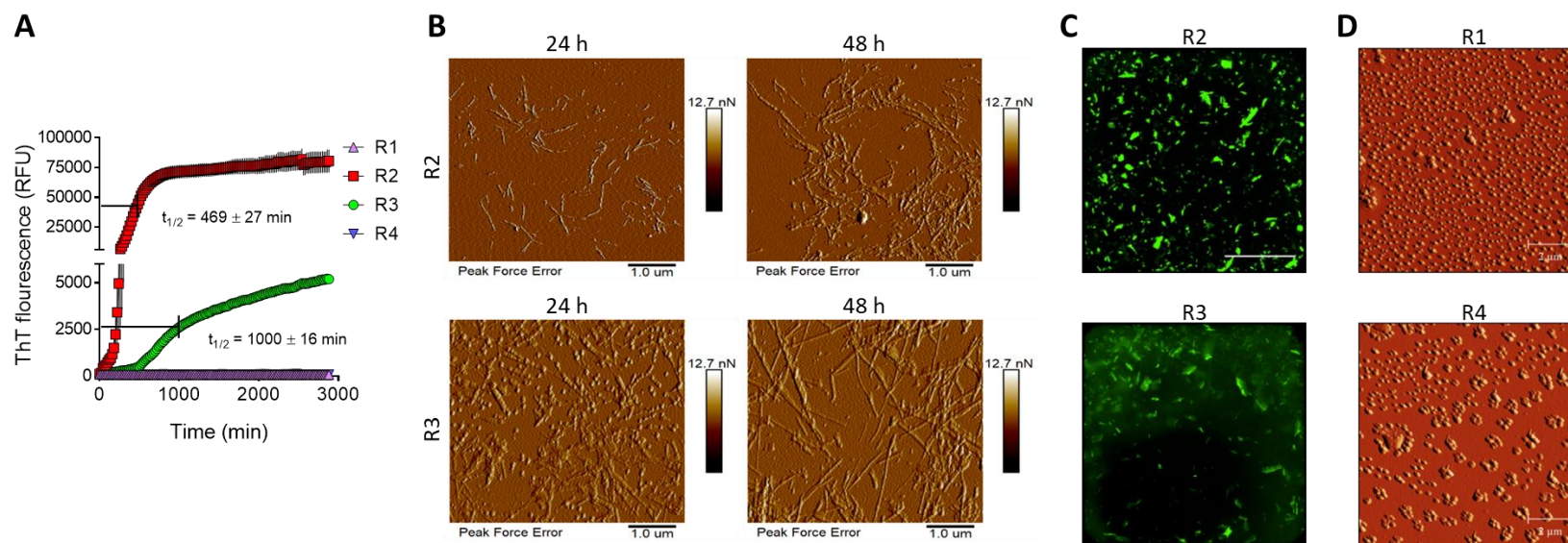


Fig. 4.1. *In vitro* aggregation of tau repeat peptides in the presence of heparin. (A) Aggregation of tau repeat peptides at 25 μM concentration in the presence of heparin. Data in A is mean \pm SEM of 3 independent replicates. (B) AFM images of R2 and R3 fibrils formed after 24 and 48 h of aggregation. (C) Fluorescence images of agarose gel-embedded ThT-stained R2 and R3 fibrils after 48 h of aggregation. Scale bar: 1 μm . (D) AFM images of R1 and R4 after 48 h of aggregation assay.

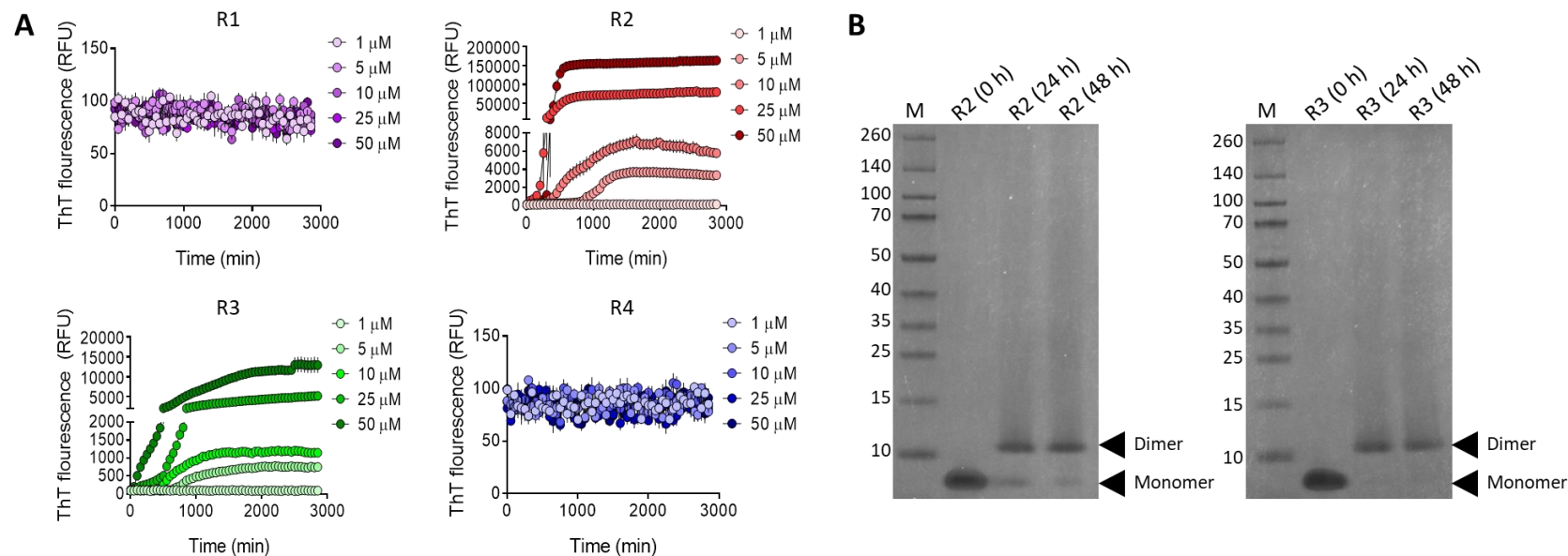


Fig. 4.2. Concentration-dependent aggregation of tau repeat peptides in the presence of heparin and Coomassie gel staining. (A) Aggregation kinetics of R1, R2, R3 and R4 peptides at different concentrations (1, 5, 10, 25 and 50 μ M) in the presence of heparin. Data is mean \pm SEM of 3 independent replicates. Gel images showing dimerisation of R2 and R3 peptides after 24 and 48 h of aggregation. Note the absence of dimer bands in R2 and R3 monomers (0 h).

In the absence of heparin, R2, despite its amyloid VQIINK motif and a cysteine residue, remarkably failed to self-assemble into fibrils (Fig. 4.3A and B), whereas R3 self-assembled and formed fibrils with highly aggregated morphology (Fig 4.3A and B). R3 formed fibrils with a twist compared to shorter and longer fibrils without a twist in the presence of heparin (Fig. 4.1B, Fig. 4.3B). To identify the necessity of cysteine residue in R3 self-assembly, a cysteine to alanine substituted R3 (C322A) peptide was utilised. Results from this study demonstrate R3 (C322A) aggregated and formed fibrils only in the presence of heparin (Fig. 4.3C and D). The fibrils comprised a mixture of shorter and longer fibrils, morphologically similar to those of R3 fibrils produced in the presence of heparin (Fig. 4.1B, Fig. 4.3D). R3 (C322A) also demonstrated concentration-dependent growth kinetics (Fig. 4.3E).

This data signifies the importance of cysteine residue in R3 self-assembly, which is accordant with the findings from Zweckstetter lab showing KXGS motifs in tau repeats promote aggregation³⁵¹. The data obtained from ThT data was confirmed by ANS assay, which assesses changes in hydrophobicity during protein aggregation. A similar time-dependent increase in ANS fluorescence was observed when peptides were aggregated in the presence [R2, R3, and R3 (C322A)] or absence (R3) of heparin (Fig. 4.3E and F).

4.2 Seed-competent R2 and R3 fibrils induce tau RD P301S aggregation

Next, a cell seeding assay was performed using biosensor cells to check the seeding potential of repeat peptides collected after 48 h of *in vitro* assembly. R2 and R3 fibrils, but not R1 and R4 samples, collected 48 h after assembly, seeded the aggregation of Tau RD P301S in biosensor cells (Fig. 4.4A and B). The presence or absence of heparin in the aggregation buffer (containing transfection reagents) did not affect seeding or cell number (Fig. 4.4A–E). R3 self-assembled fibrils demonstrated considerable seeding activity in contrast to R2 and R3 (C322A) formed without heparin, which did not seed Tau RD P301S aggregation (Figs. 4.4D and E). Regardless of the substitution of C→A, R3 (C322A) aggregated in the presence of heparin showed remarkable seeding activity (Fig. 4.4A and B). R2 and R3 assembled with heparin were consistently more seed-competent compared to fibrils of R3 assembled in the absence of heparin or R3 (C322A) in the presence of heparin.

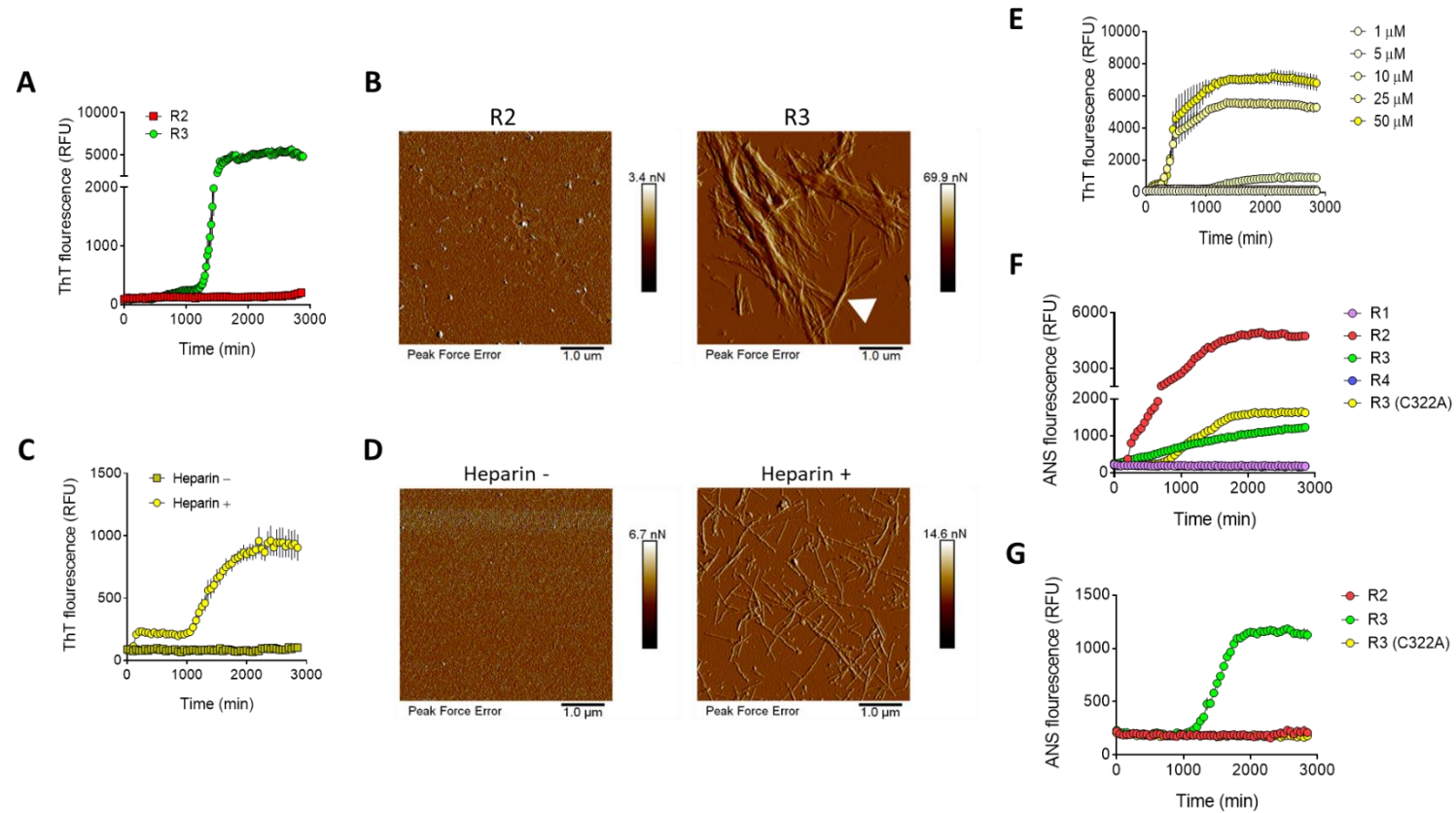


Fig. 4.3. R3 self-assembles in the absence of heparin. (A) Aggregation of 25 μM R2 and R3 peptides in the absence of heparin. Data in A is mean \pm SEM of 3 independent replicates. (B) R3, but not R2, forms fibrils of highly-aggregated morphology with twists (white arrowhead) when aggregated in the absence of heparin for 48 h. (C) Aggregation of 10 μM R3 (C322A) peptide in the absence or presence of heparin. Data in A is mean \pm SEM of 3 independent replicates. (D) R3 (C322A) forms fibrils when aggregated in the presence of heparin but not in the absence of heparin. (E) Aggregation kinetics of R3 (C322A) at different concentrations in the presence of heparin was monitored by ThT assay. Data is mean \pm SEM of 3 independent replicates. (F–G) Aggregation kinetics of indicated peptides at 10 μM concentration in the presence (E) and absence (F) of heparin monitored by ANS assay. Data is mean \pm SEM of 3 independent replicates.

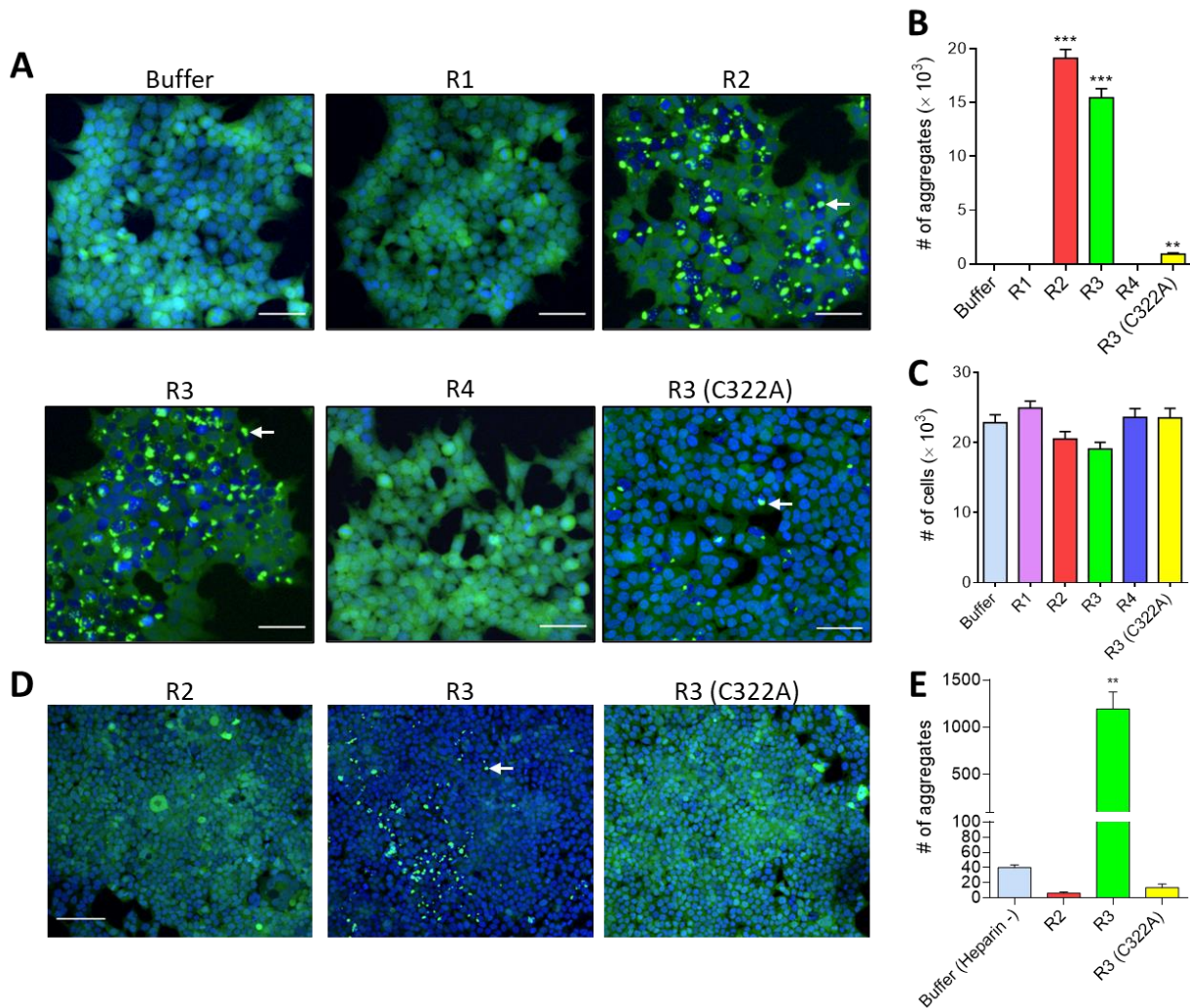


Fig. 4.4. Seeding potential of tau repeat peptide aggregates. (A) Seeding of Tau RD P301S in biosensor cells after 72 h of treatment with buffer (containing heparin) or 50 nM R1, R2, R3, R4 and R3 (C322A) samples or fibrils assembled in the presence of heparin. Scale bar: 50 μ m. (B–C) The number of seeded intracellular Tau RD P301S aggregates (B) and cells after treatment as indicated in (C). Data are mean \pm SEM of 3 independent experiments. ^{***} $p < 0.001$, ^{**} $p < 0.01$ vs buffer-treated cells, one-way ANOVA, Dunnett's posthoc test. (D) Biosensor cells after 72 h of treatment with R2, R3 and R3 (C322A) samples/fibrils after aggregation in the absence of heparin. Note that self-assembled R3 fibrils seed the intracellular tau aggregation. Scale bar: 100 μ m. (E) Intracellular Tau RD P301S aggregates in biosensor cells after seeding with buffer (without heparin) and 50 nM R2, R3, and R3 (C322A) samples/fibrils collected after 48 h of aggregation in the absence of heparin. ^{**} $p < 0.01$ vs buffer (Heparin -), one-way ANOVA, Dunnett's posthoc test.

R2 and R3 fibrils or R1 and R4 samples did not affect either cell number (Fig. 4.4C) or morphology (Fig. 4.5C) upon treatment with buffer alone comprising of transfection reagents. In addition, none of the peptides in monomeric forms affected seeding or cell number (data not shown). Overall, R2, R3 and R3 (C322A) fibrils assembled in the presence of heparin and R3 fibrils in the absence of heparin resulted in intracellular tau seeding. This data highlights the importance of the VQIVYK hexapeptide and cysteine-containing R3 repeat region on the prion-like seeding potential of tau in tauopathies.

We previously observed that seeding requires the accumulation of exogenous seeds within the cells³⁴⁷. Yet, we did not quantify the percentage of R3 fibrils internalised by cells. Our data show that in the presence of a transfection reagent, the cells take a significant fraction of R3 fibrils (Fig. 4.5A and B). However, it gets slower in the absence of transfection reagents (Fig. 4.2.2B), presumably not enough to trigger seeding, as noted in our previous study³⁴⁷.

4.3 R2 and R3 seeds increase triton-insoluble phospho-tau levels and reseed intracellular tau

Biosensor cells collected post 72 h of seeding with peptides assembled in the presence of heparin and fractionated into Triton X-100 soluble and insoluble fraction to study tau phosphorylation changes.

Though there was no change in tau phosphorylation in total protein (Fig. 4.6A), the presence of Ser262-phosphorylated tau was evident in triton-insoluble fractions of cells treated with R2 and R3 fibrils (Fig. 4.6B). These results indicate that extracellular R2 and R3 fibrils increase intracellular tau insolubility following pathological phosphorylation that enhances the accumulation of seeded tau inclusions. However, this result did not answer whether the phosphorylation per se enhanced intracellular tau aggregation following seeding with extracellular R2 and R3 fibrils.

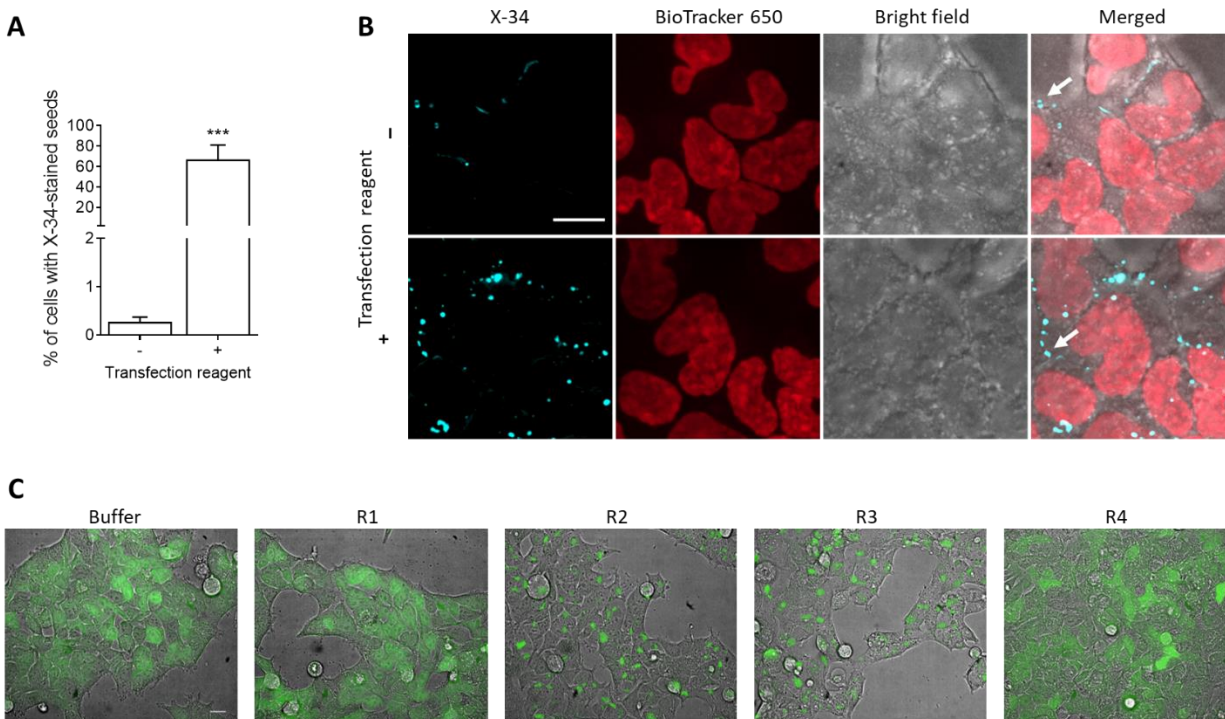


Fig. 4.5. Cellular internalisation of tau R3 aggregates. (A) Quantification of the percentage of cells with internalised X-34-stained R3 seeds in the absence (–) or presence (+) of transfection reagent. *** $p < 0.001$, two-tailed Student’s t-test, unpaired. (B) Images showing maximum internalisation of X-34-stained R3 fibrils in cells treated in the presence of transfection reagent. Arrows point to internalised X-34-stained seeds. X-34 is pseudocoloured in cyan. Scale bar: 10 μm . (C) Morphology of biosensor cells after 72 h of seeding with buffer (containing heparin) or R1, R2, R3 and R4 samples/fibrils. Scale bar: 20 μm .

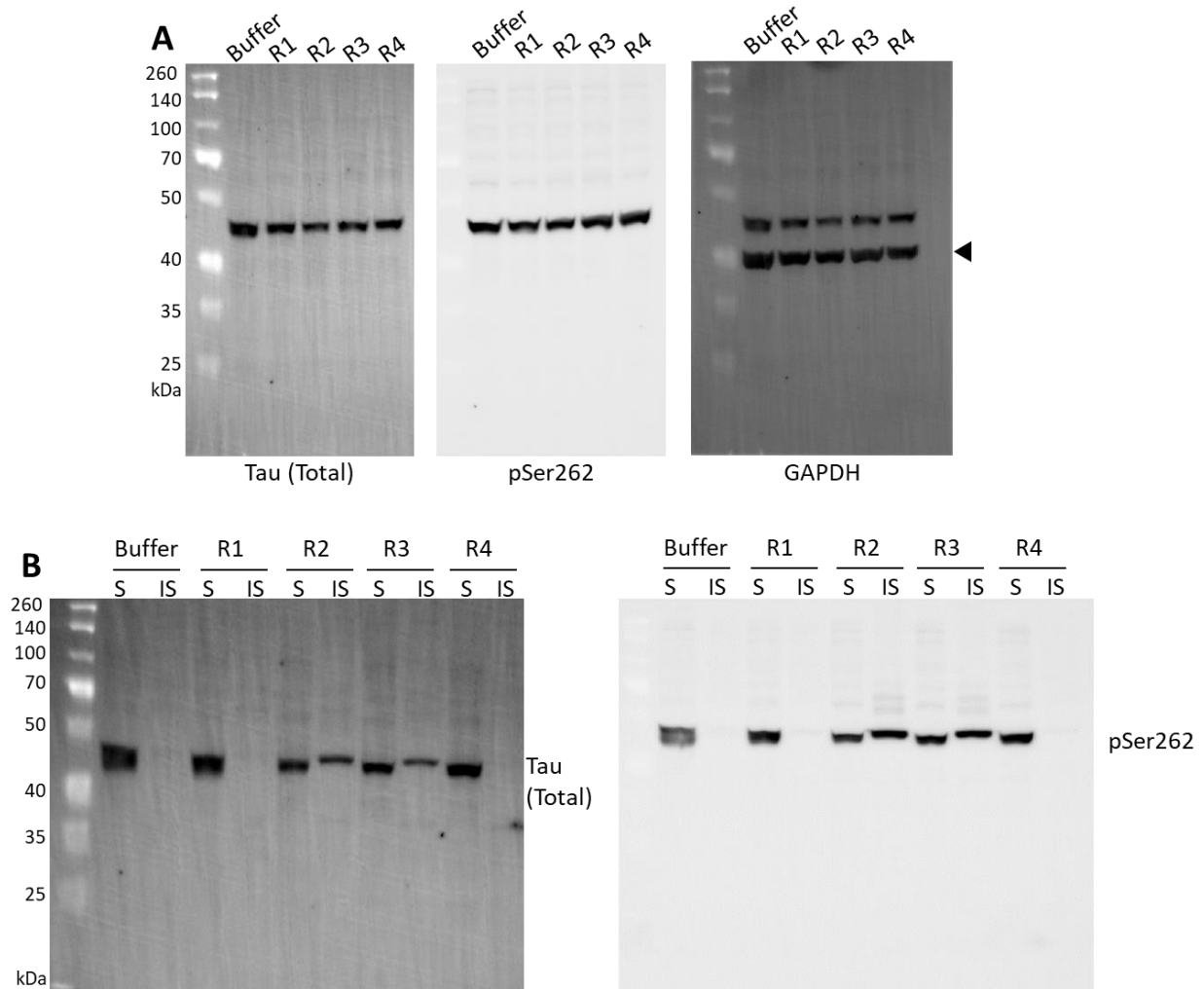


Fig. 4.6. Effect of tau R2 and R3 aggregates on intracellular tau phosphorylation and aggregation in Tau RD P301S biosensor cells. Changes in intracellular tau phosphorylation in Tau RD P301S biosensor cells. Representative western blots of total protein lysates (A) and triton-soluble and -insoluble fractions (B) from buffer-treated and R1, R2, R3 and R4 aggregate-treated cells. $n = 3-4$. Arrowheads show loading control GAPDH bands.

Biosensor cells express only the RD of tau (244–372 amino acids); thus, changes, including phosphorylation outside this domain, cannot be examined. This limitation has been overcome by transiently expressing P301L Tau (0N4R) in HEK293 cells and then seeding them with peptide fibrils/samples for 72 h before cellular fractionation, as described above. Similar to biosensor cells, no visible difference in tau phosphorylation in total protein was observed (Fig. 4.7A). However, apparent changes in total (Tau-5) and phosphorylated tau (Ser262, Ser396, Ser404) were observed in triton-insoluble fractions of cells treated with R2 and R3 fibrils (Fig. 4.7B). Additionally, both R2 and R3 fibrils resulted in tau oligomer (T22) formation in Tau P301L (0N4R) HEK293 cells (Fig. 4.7B). These findings suggest that only a few tau seeds derived from the minimum region are required to cause the formation of intracellular hyperphosphorylated tau aggregates.

Results reported so far suggest that both the size and seed confirmation influence the seeding activity of extracellular seeds^{18,239,352}. Thus, a reseeding assay was performed to seed a new set of biosensor cells with total, triton-soluble, and -insoluble fractions of biosensor cells that had previously been seeded with peptide fibrils/samples. The assay revealed that all three fractions of R2 and R3 fibrils-treated cells resulted in intracellular Tau RD P301S aggregation (Fig. 4.8). This data indicates seeded tau fibrils acquired seeding potency similar to extracellular R2 and R3 fibrils.

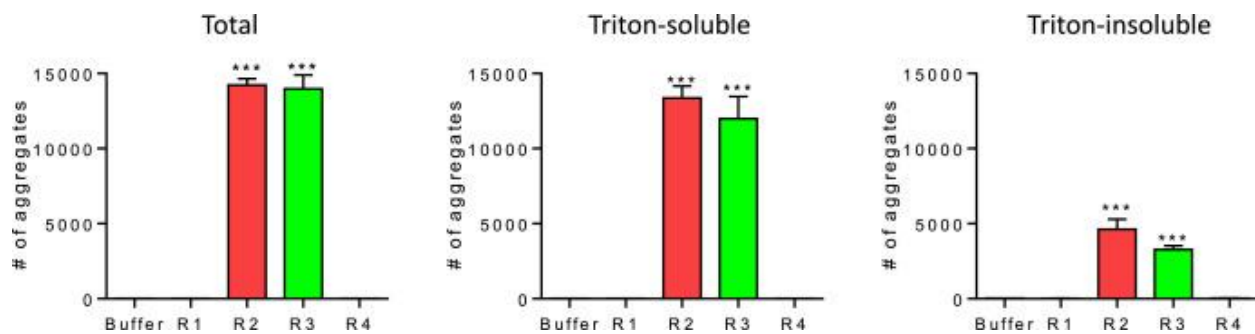


Fig. 4.8. Cellular reseeding assay. Quantification of intracellular Tau RD P301S aggregates in biosensor cells reseeded with the total, triton-soluble, and triton-insoluble fractions of cells seeded with buffer (containing heparin) or R1, R2, R3 and R4 samples or fibrils collected 48 h after heparin-supplemented in vitro aggregation assay. Data is mean \pm SEM of 3 independent experiments. *** $p < 0.001$ vs buffer-treated cells, one-way ANOVA, Dunnett's posthoc test.

Generally, tauopathies are distinguished based on the tau isoform within the filaments. While the presence of 4R is characterised in CBD, argyrophilic grain disease and PSP, Pick's disease (PiD) displays the presence of only 3R isoform³⁵³. On the contrary, AD and CTE show the presence of 3R and 4R tau isoforms³⁵³. Structural analysis of core filaments from tauopathy patients' brain tissues by Cryo-EM revealed that they all share a similar core area but diverse conformations³⁵⁴. The core structure comprises 10-13 amino acids of the C-terminal domain, R3 and R4, with different N-terminal extensions³⁵⁴. Structural and conformational differences between tau polymorphs in AD, PiD and other tauopathies, along with the effect of non-protein cofactors on tau aggregation, might affect the stability and propagation of aggregates³⁵⁵. Therefore, it is critical to identify tau regions that may play critical roles in differential tau aggregation and spread.

The hexapeptide amyloid motifs on R2 and R3 have been shown to assemble *in vitro* independently; however, they do not produce seed-competent fibrils¹⁴. Utilizing individual repeats peptides, we show that similar to R3, R2 forms seed-competent fibrils, indicating that R2 may be a separate nucleus for tau aggregation. Though R2 aggregates faster than R3, no difference in intracellular seeding ability was observed between R2 and R3 fibrils. This suggests that the aggregation rate does not give differential potency to R2 and R3 seeds. Though R2 and R3 hold identical N-terminal hexapeptide sequences and cysteine residues, R3, but not R2, fibrils assembled without heparin were seed-competent. These suggest that R3 may be the minimal region for pathological prion-like seed generation under physiological conditions, while R2 may need polyanionic cofactors to generate pathogenic seeds. The self-assembling R3 may nucleate tau aggregation without polyanionic cofactors, with R2 contributing in the later stages of the aggregation process.

Additionally, R3 (C322A) formed fibrils only upon aggregation in the presence of heparin, explaining the role of heparin in remodelling the R3 or tau towards fibril-prone conformations, as highlighted in a recent *in silico* study³⁵⁶. Seed-competent aggregates may contain a mixture of monomers, oligomers, and fibrils. These studies demonstrate that monomers do not seed intracellular tau aggregation, thus demanding further characterisation studies to identify species type, oligomers or fibrils in the aggregated sample responsible for the seeding effect.

Heparin-induced tau fibrils are polymorphic and different from fibrils derived from AD and PiD brains²²⁸. Several polyanionic cofactors, namely RNA, lipids, and DNA from several bacterial species, were found to promote tau aggregation *in vitro*^{229,357–359}. The potential role of RNA in producing unique tau strains and their stability is also suggested in a recent preprint article by M Diamond's group³⁶⁰. Interaction of tau with cofactors enables the formation of metastable complexes that remain inert and reversible until the interaction with seeds, triggering the formation of β -sheet-containing species³⁶¹. Despite studies demonstrating the co-localisation of cofactors such as heparan sulfate and RNA with NFTs, pick bodies, and neuritic plaques of AD and PiD, the role of polyanionic cofactors on tau pathological alterations has been overlooked^{362,363}

A conserved motif in the middle of each tau repeat domain, KXGS, mediates tau binding to microtubules, local structural stabilisation, and oligomerisation³⁵¹. *In vivo*, an intermolecular disulfide bond formed between two cysteine residues, C291 in R2 and C322 in R3 in KXGS motifs, is oxidised, leading to tau dimerisation and fibrillation. However, the two cysteine residues are functionally distinct and contribute differently to tau pathology²²². Further, their positions differ in the fibrillar core, with R3 in the fibril core and R2 in the fuzzy coat of fibrils³⁶⁴. Our data suggest that under physiological conditions, R3 (C322A) fibrils formed in the presence of heparin are seed-competent. This indicates that C322 at the KXGS motif may play an essential role in tau seed generation under pathological conditions.

Tau propagation following seeding occurs via template-dependent conformational changes or other unknown mechanisms²⁵⁷. Though PTMs are essential for a full-length tau to aggregate, hyperphosphorylation's role in seeded tau to aggregate remains unknown³⁶⁵. Thus, our study investigates the role of hyperphosphorylation or solubility changes in endogenous seeded tau following cell seeding with fibrils of R2 and R3. Serine 262 phosphorylation appears early in AD pathogenesis, suggesting this phosphorylation may contribute to tau seed formation³⁶⁶. Though we do not know which phosphorylations appeared first in our study, we can confirm that AD-specific phosphorylations in seeded tau appear in response to exogenous R2 and R3 fibrils. Our cell fractionation data show that cells seeded with R2 and R3 fibrils cause Ser262 phosphorylation in Tau RD P301S biosensor cells and other AD-specific phosphorylation, including Ser262, in Tau P301L (0N4R) HEK293 cells. In addition to phosphorylation, there is also oligomerisation of seeded P301L Tau. Soluble phosphorylated tau presence in both cell types implies enhanced

phosphorylation by mutation (Fig. 2A and B). They presumably make abnormally phosphorylated cytosolic tau prone to aggregate into insoluble inclusions upon seed-competent R2 and R3 fibrils exposure. These findings suggest that pathological phosphorylation is one of the unknown factors contributing to the aggregation of intracellular seeded tau.

Our reseeded assay confirms that cell fractions (total or Triton-soluble and -insoluble) of cells previously seeded with R2 and R3 fibrils continue to display seeding activity. This data confirms that tau propagation depends on initially generated fibrils and newly formed tau inclusions. The intracellular tau inclusions with pathological phosphorylations presumably result from the failure of cell clearance mechanisms and phosphatase functions that define the ageing-associated molecular mechanisms involved in AD and other tauopathies. However, since tau adopts disease-specific fibril polymorphs, a single inhibitor may not be capable of blocking seeding by all disease-associated polymorphs, possibly because both hexapeptide sequences contribute to differential seeding under different conditions²³⁹. Altogether, evidence from our previous study, this study and other studies support the importance of targeting the N-terminal hexapeptides or cysteines in R2 or R3 when developing tau aggregation and hyperphosphorylation inhibitors or antibodies for tau-targeted therapies^{222,347,349,364,367–369}.

Chapter 5

Targeting the minimal regions with small molecules to abrogate the generation of prion-like tau aggregates

The data presented in this chapter have been published as ‘‘Annadurai N. *et al.* Antitumour drugs targeting tau R3 VQIVYK and C322 prevent seeding of endogenous tau aggregates by exogenous seeds. *FEBS J.* 2022, 289(7):1929-1949. doi: 10.1111/febs.16270’.

5.1 R3 aggregation and effects of antitumour drugs on their fibrillisation

ThT binding assay was employed to monitor R3 peptide assembly under four different aggregation conditions and define an optimal condition for drug screening (Fig. 5.1A). R3 exhibited distinctive behaviour under reducing (+heparin/+DTT) aggregation conditions. Dithiothreitol (DTT) affected the assembly of R3 peptides even in the absence of heparin. The results from earlier studies demonstrate a differential effect of heparin and DTT on the fibrillisation kinetics of tau isoforms containing either C291 or C322 residue²¹⁹. Thus, drug effects on R3 peptide aggregation were evaluated in the absence of DTT. Oxidation of C322 by hydrogen peroxide generated by redox cycling compounds in the presence of reducing agents results in false positive results; thus, DTT was also excluded from drug screening³⁷⁰. AFM analysis showed R3 assembled into amyloidogenic fibrils 48 h after aggregation (Fig. 5.1B).

Based on availability in our laboratory, drugs were randomly selected, including 20 approved and four experimental or investigational antitumour drugs on *in vitro* aggregation of R3 (Table 5.1). Initially, R3 fibrillisation in the presence of drugs was monitored at a single concentration of 1 μM by ThT assay (Fig. 5.1C). In comparison to the control reaction without drugs, paclitaxel, docetaxel, cisplatin, oxaliplatin, doxorubicin, daunorubicin, resveratrol and quercetin at 1 μM tested concentration resulted in a significant decrease ($> 50\%$) in ThT fluorescence (Table 4.2). For subsequent *in vitro* studies, we selected paclitaxel, cisplatin, doxorubicin, resveratrol, and quercetin and tested the effect of the five drugs on R3 fibrillisation at two additional doses of 0.1 and 10 μM . The anti-fibrillisation effects of paclitaxel did not alter with the change in its concentration. However, cisplatin, doxorubicin, resveratrol, and quercetin were more effective only at a higher drug concentration of 10 μM in inhibiting R3 fibrillisation (Fig. 5.1D).

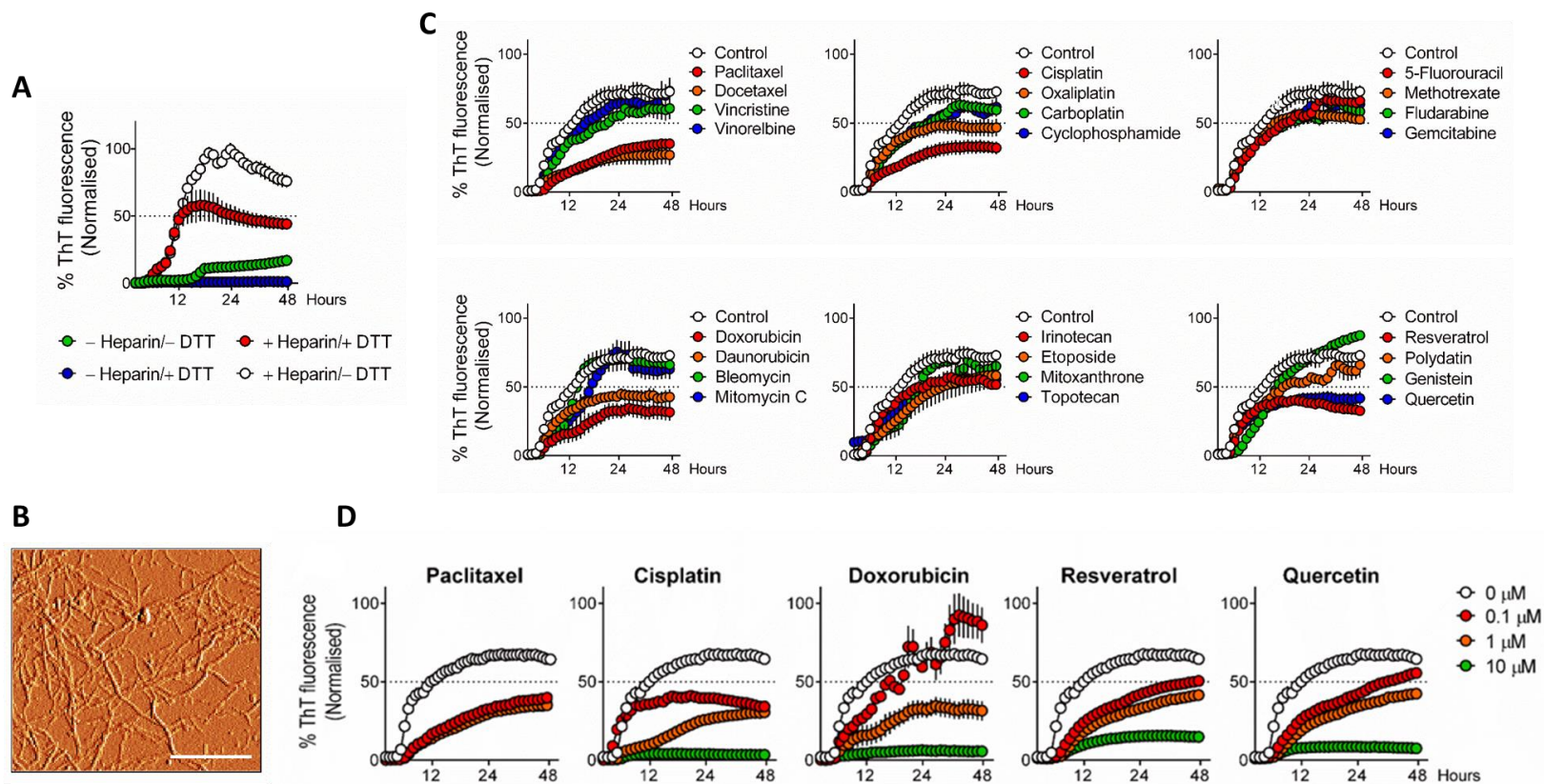


Fig. 5.1. Drug effect on R3 aggregation. (A) Graphs showing the rate of R3 aggregation under different conditions. (B) AFM image of R3 fibrils 48 h after incubation under nonreducing conditions. Scale bar: 2 μm . (C) Effect of antitumour drugs from groups 1 to 6 at a single concentration of 1 μM on R3 aggregation. Data in A and C are mean \pm SEM, $n = 3\text{--}4$ independent experiments. $***P < 0.001$ vs R3Ag; and $###P < 0.001$ vs R3 monomer, one-way ANOVA, Bonferroni's post hoc test. (D) Inhibition of R3 aggregation at different drug concentrations. Mean \pm SEM, $n = 3$.

Table 5.1. List of antitumor drugs classified into six groups based on their primary mechanism of action.

| | Approved | | | | | Preclinical/clinical |
|-------|-----------------------|----------------------|--------------------|----------------|------------------|----------------------|
| Group | 1. Antitubulin agents | 2. Alkylating agents | 3. Antimetabolites | 4. Antibiotics | 5. Topoisomerase | 6. Antioxidants |
| | Paclitaxel | Cisplatin | 5-fluorouracil | Doxorubicin | Irinotecan | Resveratrol |
| | Docetaxel | Oxaliplatin | Methotrexate | Daunorubicin | Etoposide | Polydatin |
| | Vincristine | Carboplatin | Fludarabine | Bleomycin | Mitoxanthrone | Lycopene |
| | Vinorelbine | Cyclophosphamide | Gemcitabine | Mitomycin C | Topotecan | Quercetin |

DMSO as a drug solvent did not affect R3 fibrillisation at the tested drug concentrations (Fig. 5.2A), and doxorubicin or daunorubicin-intrinsic fluorescence did not interfere with ThT fluorescence in our assay condition (Fig. 5.2B). Post 48h of aggregation in the presence of 10 μ M paclitaxel, cisplatin, resveratrol, and quercetin, R3 peptides displayed a complete absence of fibril formation as confirmed by AFM analysis (Fig. 5.2C). On the contrary, small granular to short fibril-like aggregates formed in the presence of doxorubicin (Fig. 5.2C). Overall, these results suggest that paclitaxel, cisplatin, doxorubicin, resveratrol, and quercetin limited the conversion of peptides from a soluble form to insoluble fibrillary aggregates. Although ThT assay is frequently used to detect amyloid fibrils, resveratrol and quercetin have been reported to compete with ThT for amyloid binding³⁷¹. Consequently, we also confirmed the anti-fibrillisation effects of drugs by an end-point fluorescence microscopy analysis. R3 peptide was assembled in the absence or presence of drugs under a pro-aggregation condition but without ThT. After 48 h of incubation, the content of the plate well was embedded in agarose, followed by imaging (Fig. 5.2D). We also performed an end-point Congo red binding assay to validate the anti-fibrillisation activity of drugs, particularly resveratrol and quercetin. A decreased Congo red absorbance in samples of R3Ag assembled in the presence of drugs substantiated the anti-fibrillisation activity of drugs (Fig. 5.2E). Overall, since ThT was added at the end of the aggregation assay for fluorescence microscopy analysis and Congo red binding assay, our findings confirm that drugs impede β -sheet-rich aggregates formation, and there is no interference of ThT to binding to R3 in the presence of drugs.

Table 5.2. Comparison of ThT fluorescence reading from Fig. 5.1C. The final (48th hour) normalised ThT fluorescence values following aggregation of R3 peptides in the presence of indicated drugs at a concentration of 1 μ m. Mean \pm SEM, drugs vs control, one-way ANOVA, Dunnett's post hoc test.

| | %ThT fluorescence (Normalised) | |
|-------------------------|--------------------------------|-----------------|
| | Mean \pm SEM | p-value summary |
| Control | 74 \pm 3 | |
| Paclitaxel | 35 \pm 2 | 0.002 |
| Docetaxel | 27 \pm 7 | <0.001 |
| Vincristine | 60 \pm 7 | 0.386 |
| Vinorelbine | 73 \pm 10 | >0.999 |
| Cisplatin | 32 \pm 5 | <0.001 |
| Oxaliplatin | 46 \pm 6 | 0.002 |
| Carboplatin | 69 \pm 10 | 0.149 |
| Cyclophosphamide | 84 \pm 15 | 0.422 |
| 5-flurouracil | 56 \pm 6 | 0.247 |
| Methotrexate | 51 \pm 2 | 0.089 |
| Fludarabine | 60 \pm 9 | 0.432 |
| Gemcitabine | 63 \pm 11 | 0.641 |
| Doxorubicin | 31 \pm 6 | <0.001 |
| Daunorubicin | 42 \pm 6 | 0.002 |
| Bleomycin | 70 \pm 7 | 0.976 |
| Mitomycin C | 61 \pm 8 | 0.353 |
| Irinotecan | 52 \pm 4 | 0.019 |
| Etoposide | 58 \pm 10 | 0.150 |
| Mitoxanthrone | 60 \pm 5 | 0.232 |
| Topotecan | 56 \pm 3 | 0.058 |
| Resveratrol | 32 \pm 2 | <0.001 |
| Polydatin | 59 \pm 7 | 0.054 |
| Genistein | 89 \pm 2 | 0.071 |
| Quercetin | 41 \pm 5 | <0.001 |

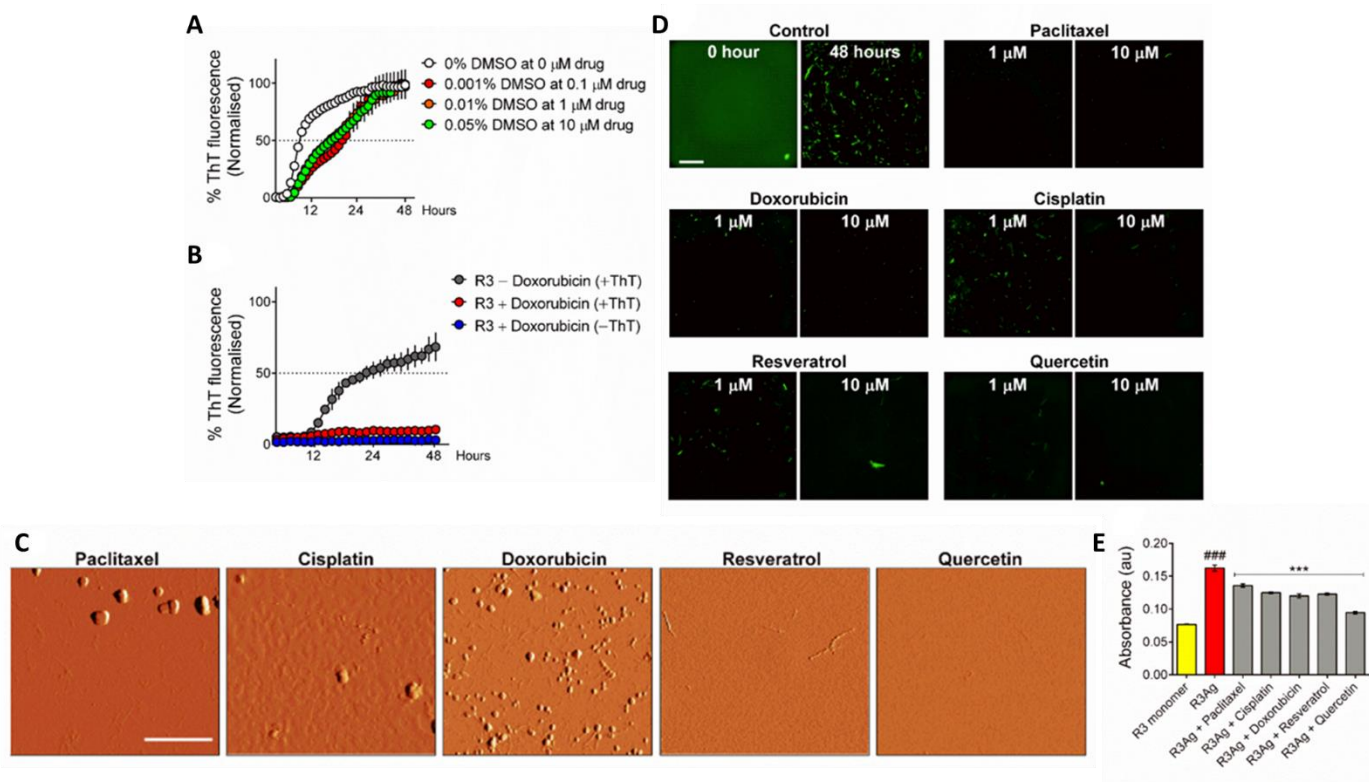


Fig. 5.2. Dose-dependent effect of DMSO and drugs on R3 aggregation. (A) Graphs showing no effect of DMSO on R3 aggregation. (B) R3 aggregation assay showed no interference of doxorubicin (10 μM) autofluorescence with the fluorescence of ThT binding to R3Ag. Data in A and B are mean \pm SEM, $n = 2$. (C) AFM images showing the morphology of R3Ag after 48 h of aggregation in the presence of indicated drugs at a concentration of 10 μM . Scale bar: 2 μm . (D) Images of ThT-stained assay plate wells at 0 h and 48 h after R3 aggregation and 48 h post aggregation in the presence of indicated drug concentrations. ThT was added after 48 h of aggregation, followed by embedding in low-melting agarose before imaging. Scale bar: 500 μm . (E) Congo red absorbance of R3 monomer and R3Ag after 48 h of aggregation in the absence or presence of indicated drugs at 10 μM concentration. Congo red was added immediately before reading the absorbance. Data in E is mean \pm SEM, $n = 3$ –4 independent experiments. *** $P < 0.001$ vs R3Ag; and ### $P < 0.001$ vs R3 monomer, one-way ANOVA, Bonferroni's post hoc test.

5.2 Inhibition of polymerisation of preformed R3 fibrils

Neurofibrillary tangles (NFTs) are formed in the advanced stages of the disease, whereas soluble oligomers generated at early stages are more toxic tau species responsible for neuronal death³⁷². Therefore, we next determined whether drugs that inhibited monomeric R3 fibrillisation also inhibited the growth of preformed R3 fibrils or dissociated them. R3 was first allowed to assemble for 24 h in the absence of drugs and then polymerise into mature fibrils for 24 additional h in the absence/presence of drugs. After 24 h of R3 aggregation, a highly heterogeneous morphological mixture of smaller protofibrils and granular aggregates was shown by AFM analysis (Fig. 5.3A).

A gradual decrease in the ThT signal following the addition of drugs at the 24th h indicated the dissociation of β -sheet-rich structures (Fig. 5.3B). These findings were verified by AFM analysis of samples collected 24 h after the addition of drugs. There was a complete dissociation of protofibrils into globular structures by doxorubicin or a mixture of granules and short fibril-like structures formed in the presence of paclitaxel, cisplatin, resveratrol, and quercetin (Fig. 5.3C). Overall, these data indicate that disaggregation of preformed aggregates is more evident following the addition of doxorubicin.

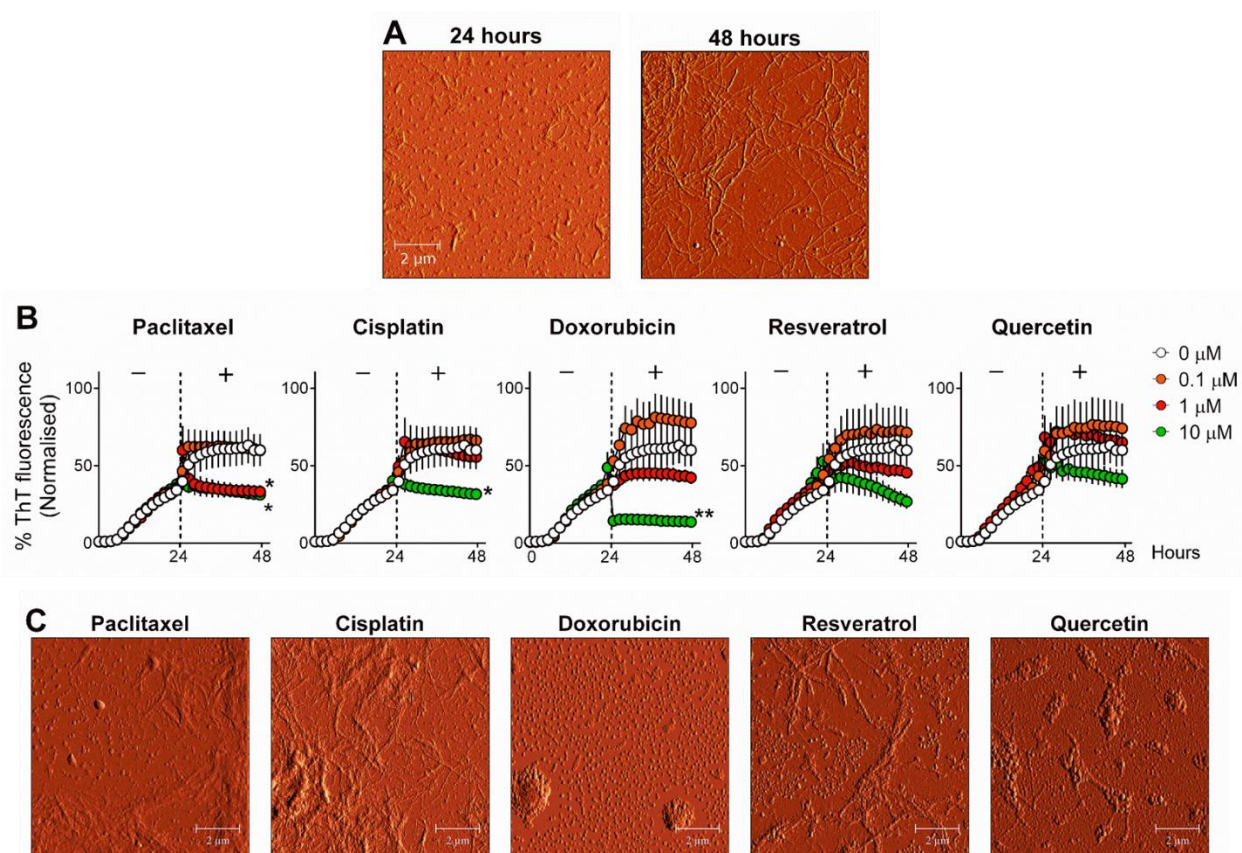


Fig. 5.3. Inhibition of elongation of preformed R3Ag or protofilaments. (A) AFM images of R3 (proto) fibrils formed after 24 and 48 h of aggregation under nonreducing conditions. (B) Graphs showing the effect of drugs on the elongation of R3 (proto) fibrils. Vertical dotted lines indicate the time at which the drugs were added. Mean \pm SEM, $n = 3$ independent experiments. ** $P < 0.01$ and * $P < 0.05$ vs 0 μ M (control), one-way ANOVA, Dunnett's post hoc test. (C) AFM images of R3 fibril morphology after 24 h of incubation in the presence of indicated drugs at 10 μ M concentration. See the morphology of drug-untreated fibrils formed after 24 and 48 h of aggregation in panel A.

5.3 Mechanisms of drug effect on R3 fibrillisation

Cysteine oxidation of wild-type tau results in the formation of disulfide-bonded dimers, and dimers with intermolecular disulfide bonds are highly prone to aggregation than those with intramolecular disulfide bonds²¹⁹.

Similar to wild-type three-repeat tau, R3 withholds a single cysteine residue and forms intermolecular disulfide-bonded dimers^{14,219}. We show that dimers are absent in monomeric samples and only appear when R3 peptides are aggregated under a nonreducing condition (Fig. 5.4A). This dimer band completely disappears when aggregates are treated with 10% β -mercaptoethanol before loading to gels (Fig. 5.4A). However, aggregating R3 under a reducing condition (+heparin/+DTT) affected dimerisation as indicated by the decrease in the dimer band (Fig. 5.4A, B). These data suggest that aggregating R3 peptide under reducing conditions inhibits intermolecular disulfide-bonded dimerisation, like inhibiting three-repeat tau dimerisation²¹⁹. To determine whether drugs inhibit R3 fibrillisation by affecting dimer formation, we analysed total aggregates and pelleted fractions by nonreducing SDS/PAGE (Fig. 5.4C, D). The quantification of dimer band intensity indicated that paclitaxel, doxorubicin, resveratrol and quercetin significantly inhibited dimer formation (Fig. 5.4E, F).

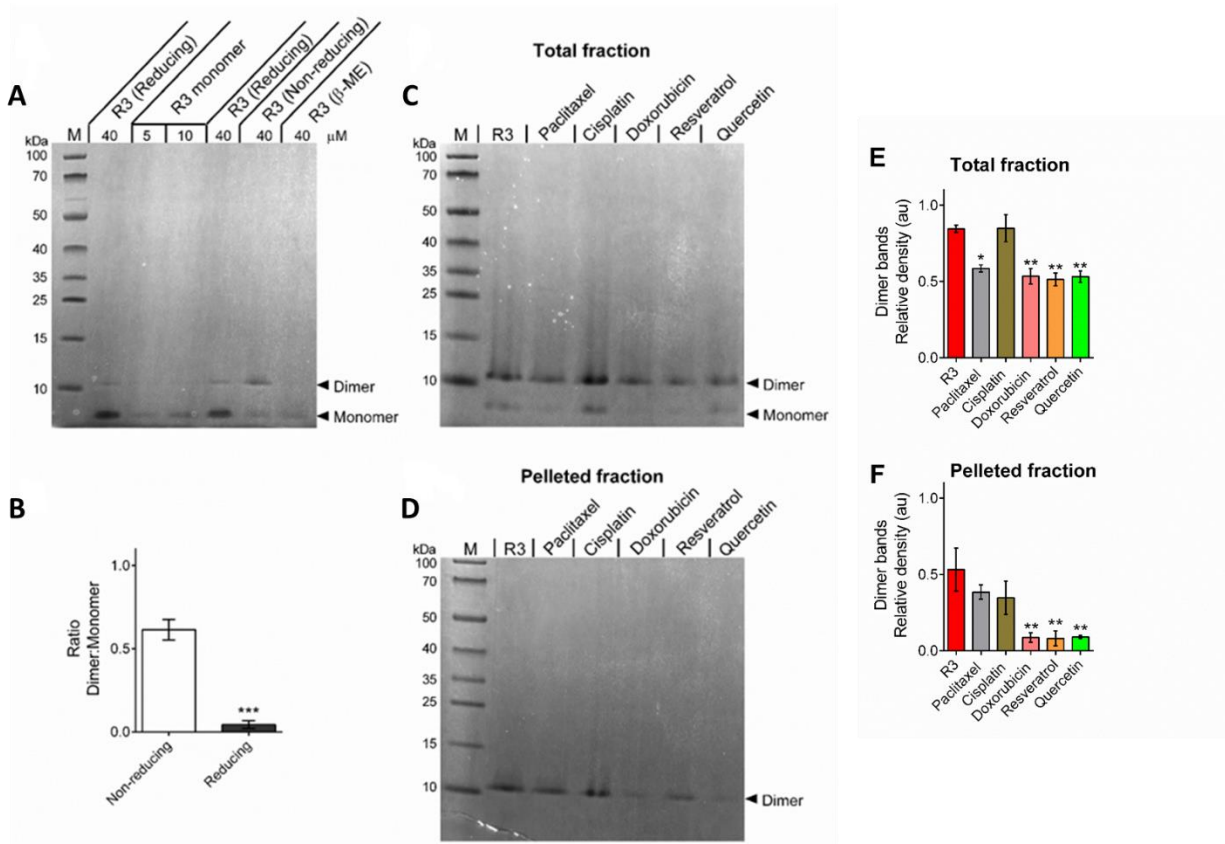


Fig. 5.4. Drug effect on R3 dimerisation. (A) Representative gel image showing the absence of dimer bands in R3 monomers electrophoresed at two concentrations (5 and 40 μM) and a strong dimerisation of 40 μM R3 under a nonreducing than reducing condition after 48 h of aggregation. The addition of β-ME (β-mercaptoethanol) to R3Ag formed under nonreducing conditions before gel loading abolishes the dimer band. $n=3-4$ independent experiments. M, marker. (B) A comparison of dimer to monomer bands under nonreducing and reducing aggregation. Mean \pm SEM, $n=3-4$ independent experiments, *** $P < 0.001$, two-tailed Student's t-test, unpaired. (C, D) Gel images showing dimer bands in total (C) and pelleted (D) fractions following R3 aggregation in the absence or presence of the shown drugs at the 10 μM concentration. M, marker. (E, F) Quantification of dimer band intensities in total (E) and pelleted (F) fractions shown in C and D. Mean \pm SEM, $n=3$ independent experiments, ** $P < 0.01$ and * $P < 0.05$ vs R3, one-way ANOVA, Dunnett's post hoc test.

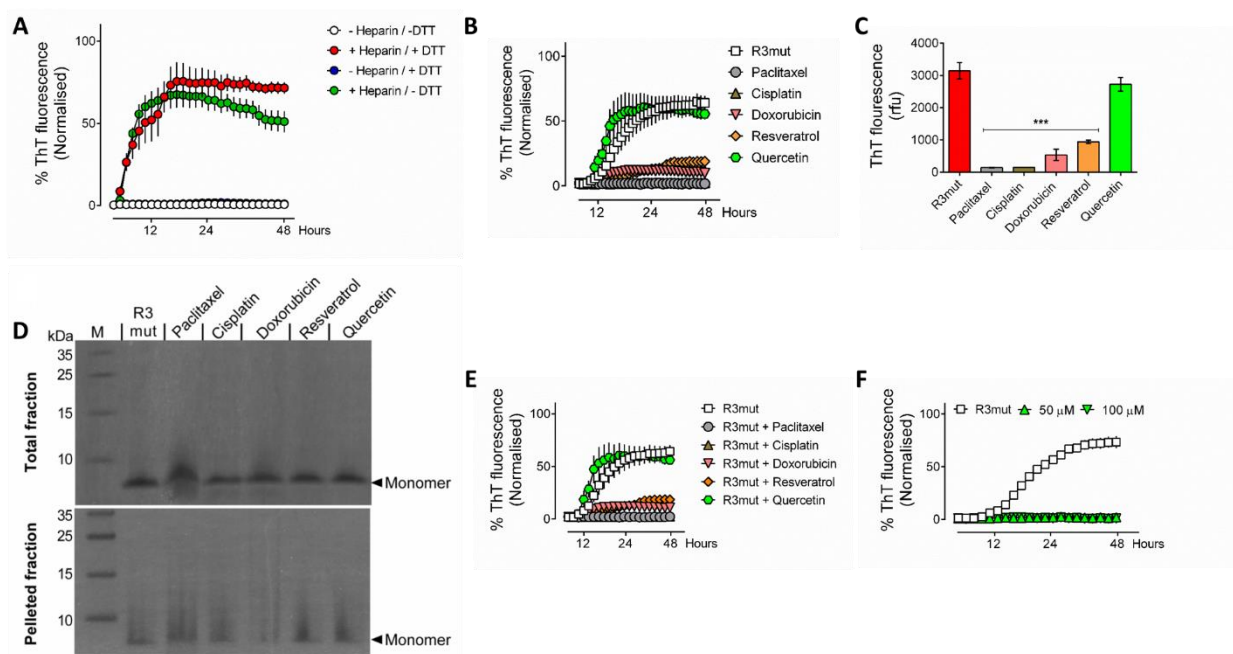


Fig. 5.5. Data on mutant R3 peptide aggregation. (A) Mutant R3 (R3mut) peptide does not aggregate in the absence of heparin. Mean \pm SEM, $n = 3$. (B) Aggregation of R3mut peptide in the absence or presence of indicated drugs at a $1 \mu\text{M}$ concentration under a nonreducing condition. Mean \pm SEM, $n = 3$ independent experiments. (C) Comparison of the final ThT fluorescence at the end of a 48 hour-aggregation assay shown in Panel B. Mean \pm SEM, $n = 3$, *** $p < 0.001$ vs R3mut, oneway ANOVA, Dunnett's post hoc test. (D) Gel images of total and pelleted fractions of aggregated R3mut (R3mut) showing the absence of dimer bands in the absence or presence of the indicated drugs ($10 \mu\text{M}$). M, marker. (E, F) Graphs showing the aggregation of R3mut peptide in the absence, or (E) presence of $10 \mu\text{M}$ concentration of indicated drugs and (F) $50 \mu\text{M}$ and $100 \mu\text{M}$ quercetin under a nonreducing condition. Mean \pm SEM, $n = 3$.

The C322 residue in R3 is essential for its dimerisation, and the binding of drugs to this site blocks the formation of toxic tau species^{219,222}. To determine whether inhibition of R3 dimerisation was due to the binding of drugs to C322, we used mutant R3 (R3mut) peptides containing Ala instead of Cys at position 322 (C322A). Aggregating R3mut peptides under different aggregation conditions indicated that heparin was essential for aggregation (Fig. 5.5A), indicating that C322, in addition to the hexapeptide sequence, defines the self-aggregation of R3. The Cys-to-Ala substitution only affected the anti-aggregation effect of quercetin, but not other drugs (Fig. 5.5B, C). Since R3mut did not dimerise, no effect of drugs was evident on dimerisation (Fig. 5.5D). The absence of a quercetin effect was also evident at a concentration of 10 μ M (Fig. 5.5E). However, oversaturating quercetin concentrations inhibited R3mut aggregation, presumably due to nonspecific binding or due to the effect of DMSO (Fig. 5.5F). DMSO was between 0.01% and 0.1% at 1–10 μ M concentrations of all drugs (Fig. 5.5B, E), and 0.30% and 0.60% at 50 and 100 μ M quercetin concentrations, respectively (Fig. 5.5F).

Overall, these data indicate that quercetin interaction with C322 residue results in the abrogation of dimerisation and, consequently, fibrillation of R3. The effect of paclitaxel, doxorubicin and resveratrol on R3 dimerisation and fibrillation results independently of C322 residue.

5.4 Molecular dynamics simulation of drug–peptide interaction

To gain a deeper insight into the mechanism of anti-fibrillation effects of drugs, molecular dynamics (MD) simulations were performed. In the absence of drugs, R3 monomers displayed high flexibility, in agreement with their nonstructured nature. R3 dimer, in the absence of drugs, was less flexible and preferred an extended β -sheet structure, housing the Cys residue in the loop (Fig. 5.6A). In the presence of drugs, the dimer became less stable, which is evident by fewer contacts formed between R3 chains and each drug bound to different regions of the R3 dimer. Paclitaxel interacted directly with the N-terminus of R3 that harbours the aggregation-prone sequence, VQIVYK. Whereas doxorubicin and resveratrol interacted mainly with the C-terminal region, quercetin stayed in contact with C-terminal and Cys residue (Fig. 5.6B), explaining the absence of quercetin effect on mutant R3 peptide aggregation (Figs. 5.5B, C, E and F).

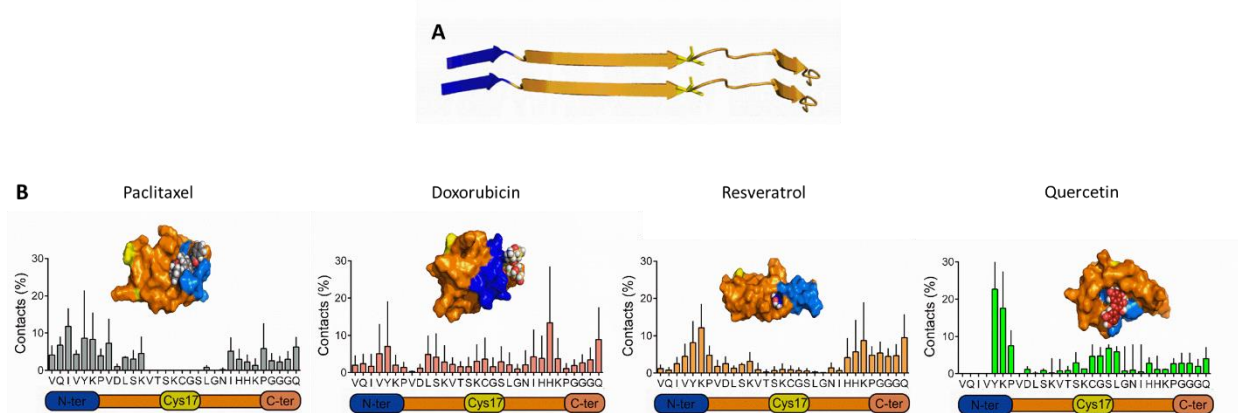


Fig. 5.6. Molecular dynamics simulation of drugs with R3 dimer. (A) A starting structure of R3 dimer for MD simulations prepared from X-ray structure (PDB ID: 5O3L). Stripes represent β -strands. (B) Graphs show the frequency of paclitaxel contact with the N-terminal, doxorubicin and resveratrol with the C-terminal, and quercetin with the C-terminal and the loop housing Cys residue. Error bars represent standard deviations of contact frequencies. Standard deviations were calculated with the block analysis for four separate blocks ($n=4$). Inset images show the R3 surface (N-terminal part in blue and Cys in yellow) and drugs in sphere models. Reported structures were generated using the PyMOL Molecular Graphics System, Version 2.0, Schrödinger, LLC (New York, NY, USA).

5.5 Exogenous R3Ag effect on intracellular Tau-RD seeding

Before investigating the effect of drugs on R3Ag-mediated seeding of intracellular tau, we first examined the effect of R3 monomer or R3Ag alone in Tau-RD P301S FRET biosensor cells³⁴⁵. R3 monomers did not induce seeding and were nontoxic to cells (Fig. 5.7A–C). Next, we determined the effect of R3Ag with and without sonication. We decided to check the effect of sonicated R3Ag because a recent study showed that smaller soluble aggregates formed after sonication of the fibrils of human Tau-441 have greater seeding activity than nonsonicated fibrils³⁷³. There was no difference in seeding between cells treated with nonsonicated or sonicated R3Ag (Fig. 5.7A, B). Furthermore, irrespective of sonication, R3Ag were nontoxic to cells when treated for over 72 h (Fig. 5.7C).

Interestingly, although R3Ag were nontoxic, we observed a significant reduction in the cell number after 72 h of cell treatment with aggregated but not monomeric R3 (Fig. 5.7D). To check whether R3Ag affected cell growth, we evaluated a time-dependent change in the total cell number (Fig. 5.7E). Compared with the untreated control, there was a significant decrease in the growth of cells treated with R3Ag (Fig. 5.7E). Monomeric R3 did not affect the cell number. Furthermore, there was no difference between the effect of nonsonicated and sonicated R3Ag on cell number (Fig. 5.7D, E). These findings indicate that R3Ag, irrespective of sonication, do not cause cell death by disrupting the cell membrane integrity but induce seeding and significantly reduce cell growth.

To determine whether the decrease in cell growth and seeding is related, we treated cells with sonicated R3Ag premixed with or without Lipofectamine and monitored them every 24 h for 72 h by imaging (Fig. 5.8A). The data show a time-dependent increase in seeding only in cells treated with R3Ag premixed with Lipofectamine (Fig. 5.8Bi), and correspondingly, these cells show reduced growth over time compared with control cells (Fig. 5.8Bii). In contrast, cells treated with R3Ag without premixing with Lipofectamine do not show seeding or a decrease in growth (Fig. 5.8B). Overall, these results indicate that R3Ag do not disrupt the cell membrane and affect cell viability but potentially cause alterations in metabolic activity and cell cycle due to cellular stress from protein aggregation^{374,375}.

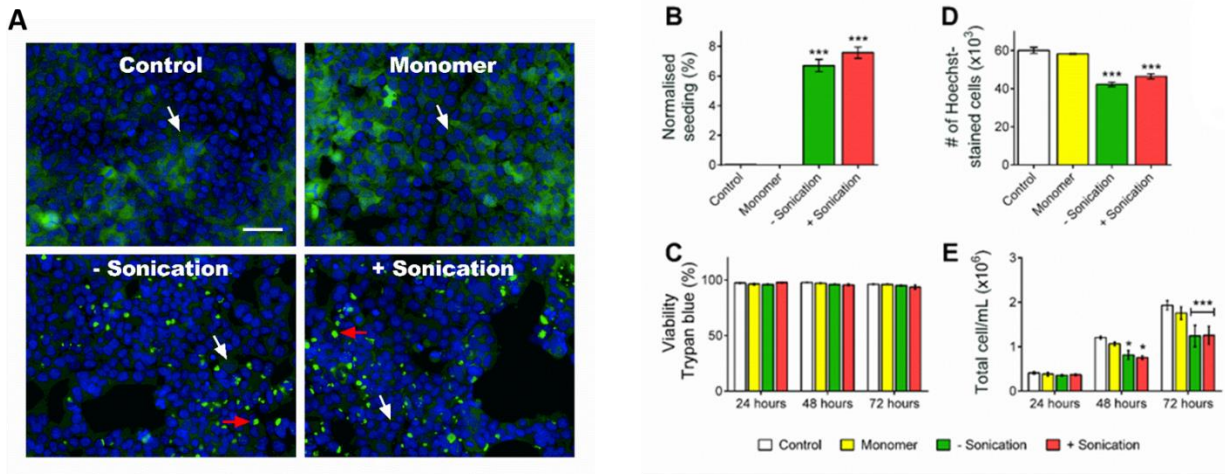


Fig. 5.7. Effect of R3Ag on seeding and viability. (A) Representative images displaying the effect of R3 monomer and nonsonicated (– sonication) and sonicated (+ sonication) R3Ag on seeding post 72 h of treatment. Nuclei are stained blue with Hoechst-33342. Red arrows indicate representative cells containing seeded intracellular Tau-RD aggregates, and white arrows indicate representative cells without aggregated Tau-RD. Scale bar: 50 μ m. (B) Quantification of seeding after 72 h of cell treatment with monomeric R3 (monomer), nonsonicated (– sonication) and sonicated (+ sonication) R3Ag. (C) Cell viability was quantified by trypan blue assay after treatment of cells with R3 monomer and nonsonicated and sonicated R3Ag for 24–72 h. (D) The number of Hoechst-stained cells after 72 h of indicated treatment of cells. (E) Time-dependent change in cell growth quantified by trypan blue assay following treatment of cells with R3 monomer and nonsonicated and sonicated R3Ag. Data in B–E are mean \pm SEM of 3–4 independent experiments, *** $P < 0.001$, ** $P < 0.01$ and * $P < 0.05$ vs control, one-way ANOVA, Tukey's post hoc test.

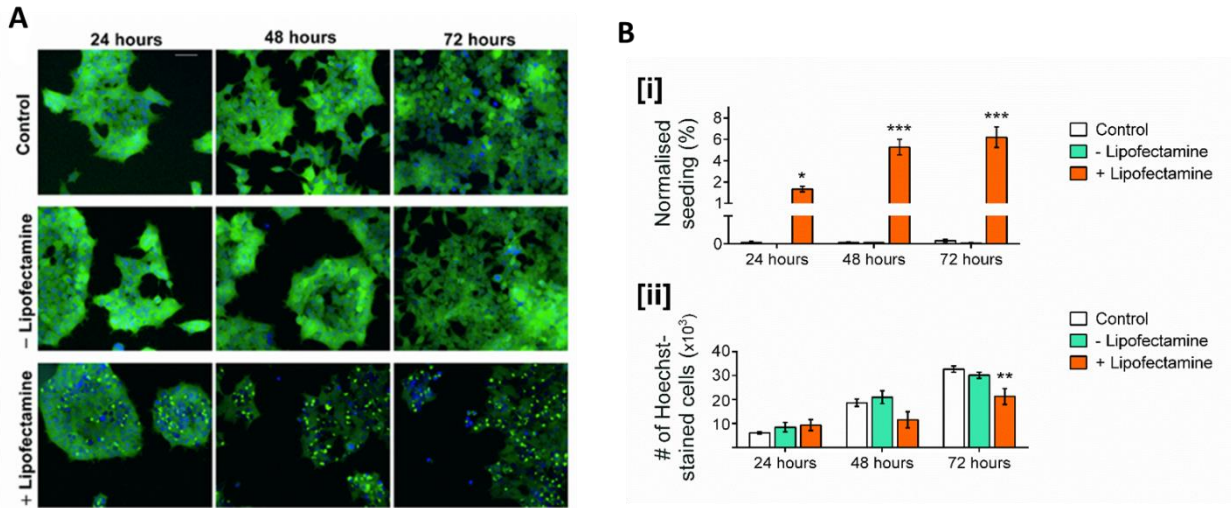


Fig. 5.8. Effect of Lipofectamine transfection reagent on cell density and seeding. (A) Representative images showed a time-dependent effect of R3Ag premixed (+ Lipofectamine) or not premixed (– Lipofectamine) with Lipofectamine transfection reagent on cell density and seeding. Scale bar: 50 μm . (B) Time-dependent increase in seeding (Bi) and decrease in the number of Hoechst-stained cells (Bii) after cell treatment with R3Ag premixed (+ Lipofectamine), but not premixed (– Lipofectamine), with Lipofectamine or control. Data are mean \pm SEM of 3 independent experiments, *** $P < 0.001$, ** $P < 0.01$ and * $P < 0.05$ vs control in each time-point, two-way ANOVA, Sidak's post hoc test.

5.6 Drug treatment abrogates R3Ag-mediated intracellular tau seeding

Tau pathology propagation by seed-competent tau species precedes NFTs formation in AD^{345,376}. Thus, we sought to determine whether pretreating exogenous R3Ags with drugs inhibits the native tau seeding when introduced in biosensor cells. Fig. 5.9 displays a scheme wherein two sets of cell treatments were carried out. In the first set (Fig. 5.9i), R3Ags were first incubated (capped) with drugs for 16 h, followed by sonication of capped R3Ags before treating cells, as described previously³⁷⁷. Alternatively, we first sonicated R3Ags and then capped them with drugs before treating the cells (Fig. 5.9ii). In the second set, we treated cells directly with R3Ags formed in the absence or presence of drugs, referred to as preinhibited R3Ags (Fig. 5.9iii).

We show that capping R3Ag with resveratrol and quercetin significantly abrogated seeding compared to cells treated with uncapped R3Ag (Fig. 5.10A, B; unnormalised aggregate and the cell number are in Fig. 5.11A, B). While capping with doxorubicin reduced seeding, the difference was insignificant (Fig. 5.10B). Interestingly, sonicating resveratrol or quercetin-capped R3Ag abolished the protective effect conferred by the drugs on Tau-RD seeding (Fig. 5.11C). Similarly, cells treated with pre-inhibited R3Ag formed in the presence of paclitaxel, resveratrol and quercetin were significantly less active in seeding the aggregation of Tau-RD in cells (Fig. 5.10A, C). None of the drugs at their final concentrations (paclitaxel 5 nM, doxorubicin 50 nM, and resveratrol and quercetin 200 nM), when administered alone, induced seeding (Fig. 5.12A) or affected the viability of cells (Fig. 5.12B). Our data from AFM analysis of drug-pre-inhibited R3Ag after 48 h of aggregation assay had shown the formation of a heterogeneous mixture of aggregates, particularly in the presence of doxorubicin (Fig. 5.2C).

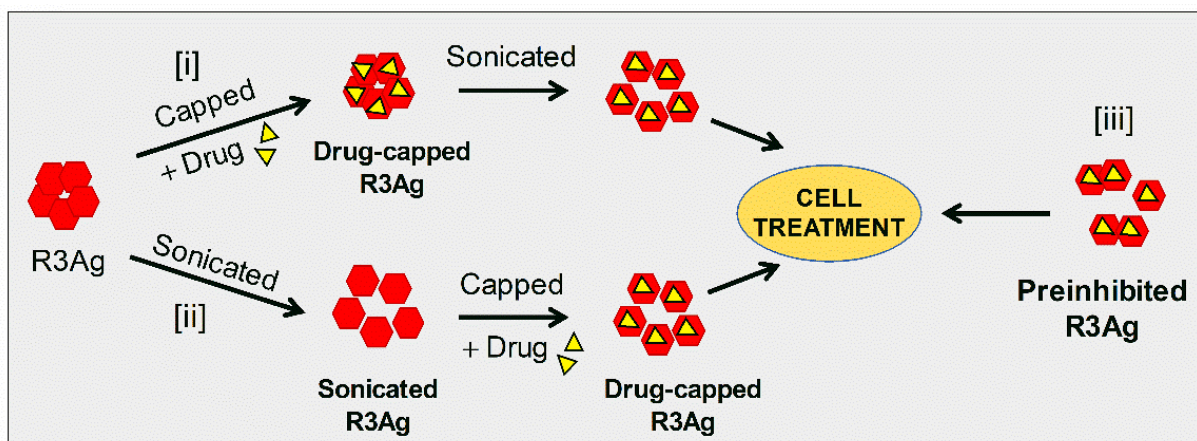


Fig. 5.9. Schematic representation of the seeding experiments.

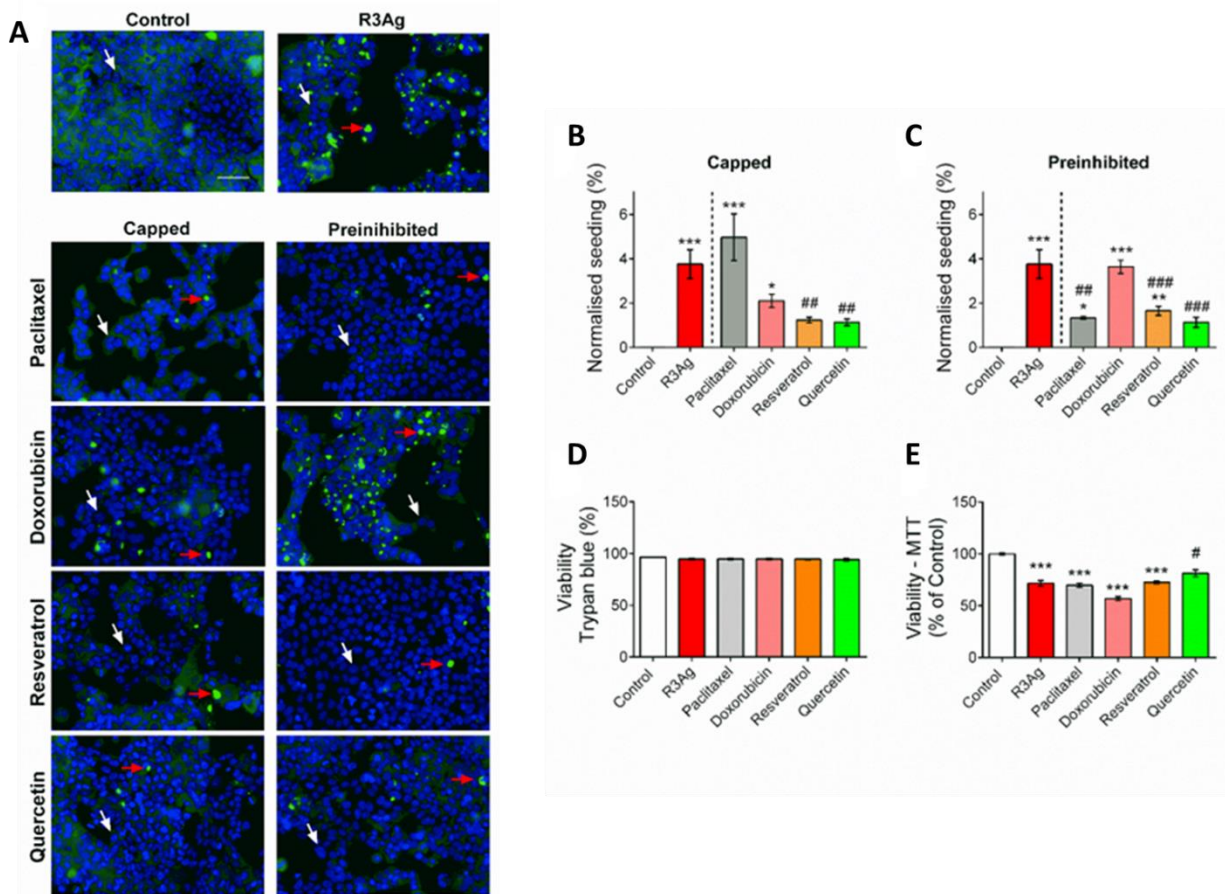


Fig. 5.10. Drug treatment abrogates seed-competent R3Ag formation. (A) Representative images show seeding post-72 h in untreated cells (control) and cells treated with R3Ag or R3Ag capped or pre-inhibited with the indicated drugs. Nuclei are stained blue with Hoechst-33342. Red arrows indicate representative cells containing seeded intracellular Tau-RD aggregates, and white arrows indicate representative cells without aggregated Tau-RD. Scale bar: 50 μ m. (B, C) Quantification of seeding following treatment of cells with R3Ag and drug-capped (B) or drug-pre-inhibited (C) R3Ag for 72 h. Data in B and C are mean \pm SEM of $n=4-5$ independent experiments, *** $P < 0.001$, ** $P < 0.01$ and * $P < 0.05$ vs control; and #### $P < 0.001$, ### $P < 0.01$ and # $P < 0.05$ vs R3Ag, one-way ANOVA, Tukey's post hoc test. Raw data showing unnormalised aggregate and cell numbers are shown in Fig. 11A, B. (D, E) Viability of cells measured by trypan blue (D) and MTT (E) assays following treatment with drug-untreated R3Ag and drug-pre-inhibited R3Ag for 72 h. Data are mean \pm SEM, $n=3$, *** $P < 0.001$ and ** $P < 0.01$ vs control; and # $P < 0.05$ vs R3Ag, one-way ANOVA, Tukey's post hoc test.

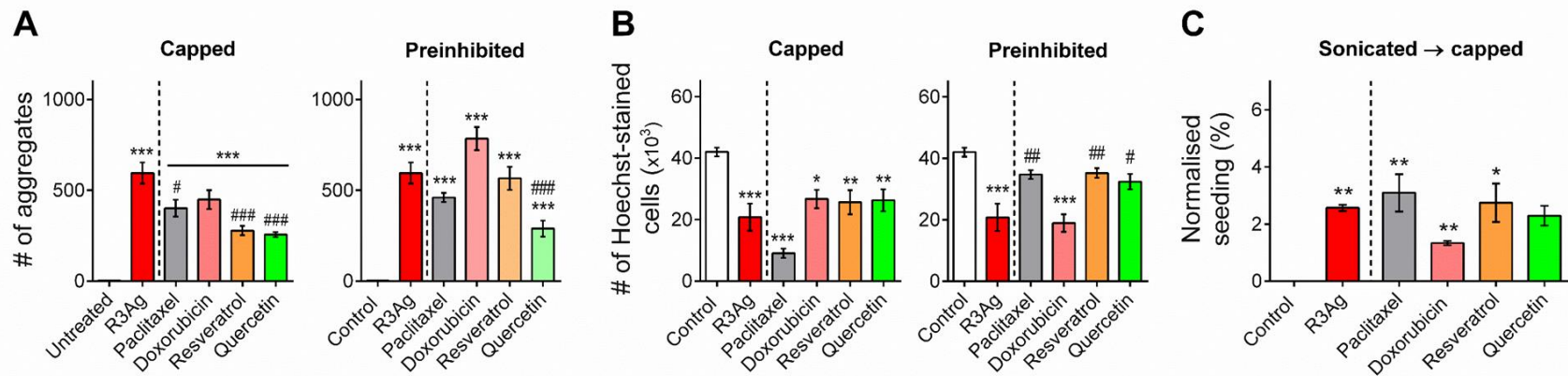


Fig. 5.11. Raw data of seeding from Fig. 5.10. (A, B) Graphs showing the number of aggregates (A) and cells (B) 72 h after seeding biosensor cells with R3Ag, drug-capped and drug-preinhibited R3Ag. (C) Seeding in cells treated with R3Ags first sonicated and then capped with the indicated drugs. Data in A-C are mean \pm SEM, $n = 3-5$ independent experiments, *** $p < 0.001$, ** $p < 0.01$, * $p < 0.05$ vs Control; ### $p < 0.001$, ## $p < 0.01$, # $p < 0.05$ vs R3Ag, one-way ANOVA, Tukey's post hoc test.

To check whether these globular assemblies formed in the presence of drugs are toxic, we treated cells with pre-inhibited R3Ag for 72 h and analysed cell viability by trypan blue exclusion and MTT assays. The trypan blue assay showed no change in viability following treatment with R3Ag or pre-inhibited R3Ag (Fig. 5.10D), indicating the absence of cell membrane perturbation. However, pre-inhibited R3Ag could not reverse the reduced cell growth compared with control cells (Fig. 5.12C). Except for doxorubicin (50 nM), none of the other drugs at their final concentrations (5 nM paclitaxel and 200 nM resveratrol and quercetin) inhibited cell growth compared with control cells (Fig. 5.12C).

Intriguingly, the MTT assay indicated a significant reduction in viability upon cell treatment with R3Ag and only pre-inhibited R3Ag formed in the presence of quercetin improved viability compared with R3Ag-treated cells (Fig. 5.10E). Except for doxorubicin, paclitaxel, resveratrol, and quercetin alone did not affect cell viability, as quantified by MTT assay (Fig. 5.12D). These data indicate that although aggregates do not disrupt the cell membrane, R3Ag affect the metabolic activity of cells, as indicated by the MTT assay. Quercetin abolished the formation of toxic R3 species and improved the viability of cells compared to cells treated with only R3Ag.

So far, our data indicated that the tested drugs prevent the formation of seeding-competent R3Ag *in vitro*. To show whether drugs prevented seeding activity in cells, we pretreated cells either with aggregation buffer (vehicle) (Fig. 5.12A) or drugs for 2 (Fig. 5.12B) and 24 h (Fig. 5.13A) and then exposed them to either aggregation buffer or R3Ag for an additional 24 h. We show that pretreating with all drugs for 2 h (Fig. 5.12C) or paclitaxel, resveratrol, and quercetin for 24 h (Fig. 5.13B) protected cells against R3Ag-mediated seeding. The quantification of the cell number by imaging indicated no statistically significant effect of drugs or R3Ag (Figs. 5.12D and 5.13C).

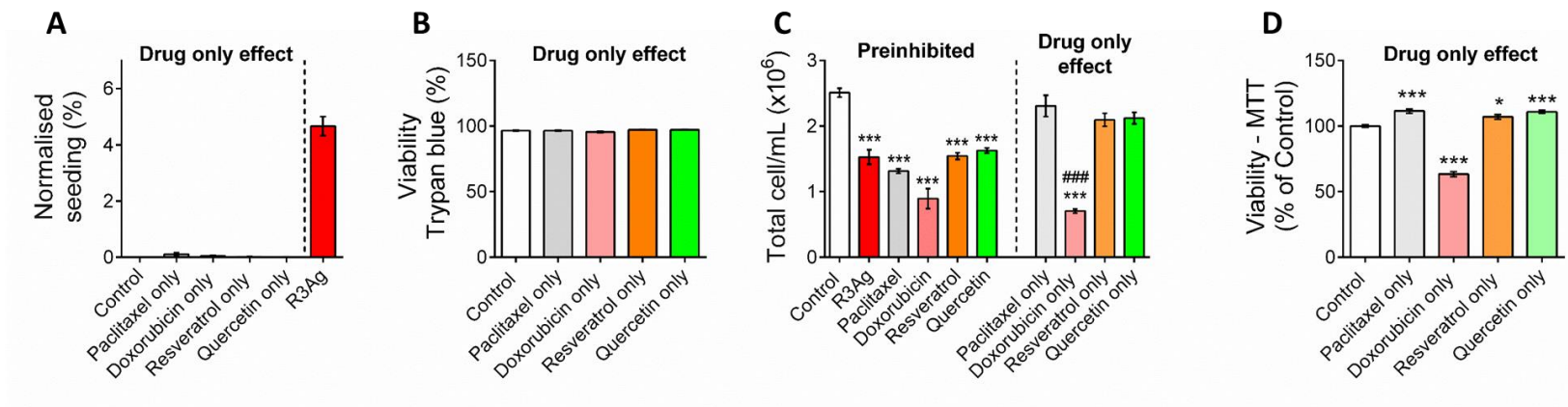


Fig. 5.12. Raw data of drug-only effect from Fig. 5.10. (A, B) Drug-only effect on seeding and viability of cells. Seeding by R3Ag in A is shown as a reference value. (C) Changes in the total cell number after treating cells with R3Ag, drug-preinhibited R3Ag or only drugs. (D) Drug-only effect on cell viability quantified by MTT assay. Data in A–D are mean \pm SEM, $n = 3$ –5 independent experiments, *** $p < 0.001$, ** $p < 0.01$, * $p < 0.05$ vs Control; ### $p < 0.001$, ## $p < 0.01$, # $p < 0.05$ vs R3Ag, one-way ANOVA, Tukey’s post hoc test.

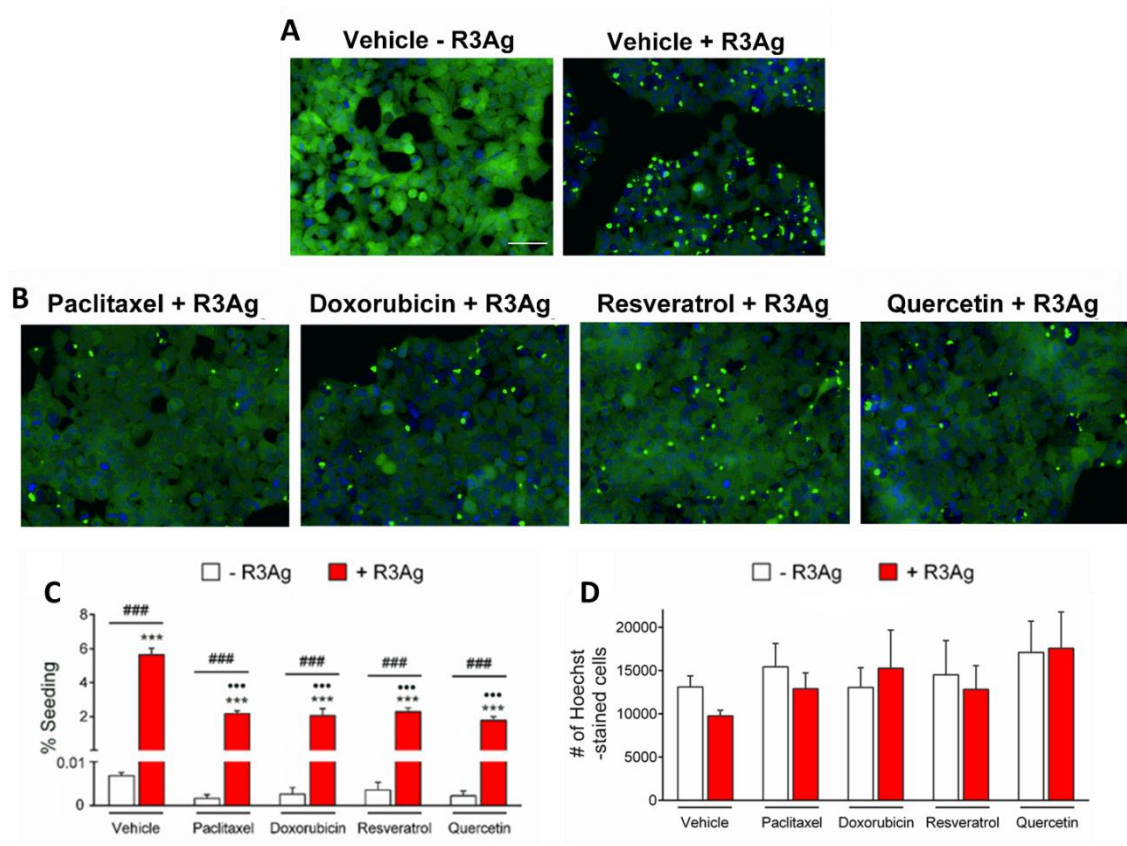


Fig. 5.13. Drug pretreatment (2 h) of cells prevents seeding by exogenous R3Ag. (A, B) Representative images showing pretreatment with paclitaxel, doxorubicin, resveratrol or quercetin for 2h (B), but not aggregation buffer (vehicle), protects cells from seeding by R3Ag. Nuclei are stained blue with Hoechst-33342. Scale bar: 50 μ m. (C) Quantification of seeding after cell treatment with aggregation buffer (vehicle), paclitaxel (1 nM), doxorubicin (10 nM), resveratrol (200 nM) or quercetin (200 nM) for 2 h followed (red bars, + R3Ag) or not followed (white bars, - R3Ag) by R3Ag. Data are mean \pm SEM of n = 3 independent experiments, ***P < 0.001 vs vehicle - R3Ag; **P < 0.001 and **P < 0.01 vs vehicle + R3Ag; and ####P < 0.001, - R3Ag vs + R3Ag, two-way ANOVA, Bonferroni's post hoc test. (D) Graphs showing the changes in the number of Hoechst-stained cells after pretreating cells with aggregation buffer (vehicle), paclitaxel (1 nM), doxorubicin (10 nM), resveratrol (200 nM) or quercetin (200 nM) for either 2 h (red bars, +R3Ag) or not followed (white bars, - R3Ag) by exposure to R3Ags. Data are mean \pm SEM of n = 3 independent experiments.

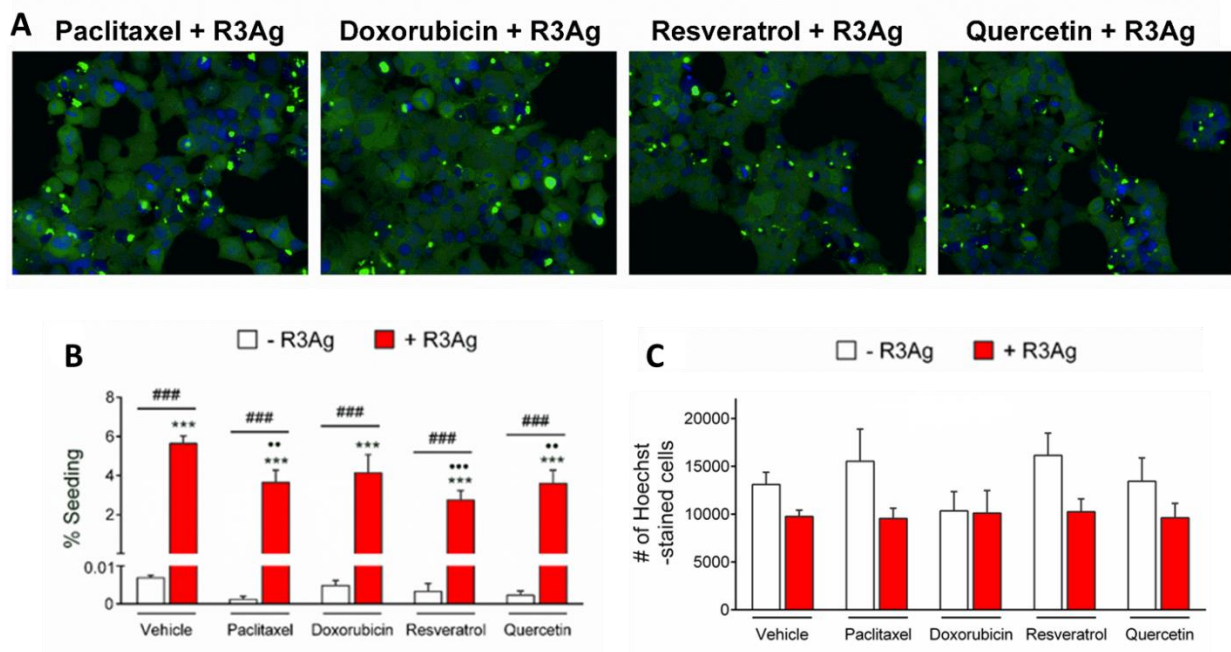


Fig. 5.14. Drug pretreatment (24 h) of cells prevents seeding by exogenous R3Ag. (A) Representative images showing pretreatment with paclitaxel, doxorubicin, resveratrol or quercetin for 24h protects cells from seeding by R3Ag. Nuclei are stained blue with Hoechst-33342. Scale bar: 50 μ m. (B) Quantification of seeding after cell treatment with aggregation buffer (vehicle), paclitaxel (1 nM), doxorubicin (10 nM), resveratrol (200 nM) or quercetin (200 nM) for 24 h followed (red bars, + R3Ag) or not followed (white bars, - R3Ag) by R3Ag. Data are mean \pm SEM of n = 3 independent experiments, ***P < 0.001 vs vehicle - R3Ag; ***P < 0.001 and **P < 0.01 vs vehicle + R3Ag; and ####P < 0.001, - R3Ag vs + R3Ag, two-way ANOVA, Bonferroni's post hoc test. (C) Graphs showing the changes in the number of Hoechst-stained cells after pretreating cells with aggregation buffer (vehicle), paclitaxel (1 nM), doxorubicin (10 nM), resveratrol (200 nM) or quercetin (200 nM) for either 24 h (red bars, +R3Ag) or not followed (white bars, - R3Ag) by exposure to R3Ags. Data are mean \pm SEM of n = 3 independent experiments.

5.7 Drugs protect *C. elegans* from R3Ag-mediated toxicity

C. elegans as a versatile *in vivo* model used to evaluate the toxicity of R3Ag with or without drug treatment^{378,379}. Drug-capped and drug-pre-inhibited R3Ag was administered to worms for 2 h, and the pharyngeal pumping was scored after an additional 2–24 h to determine whether the drug treatment affected aggregate-mediated toxicity *in vivo* (Fig. 5.14A). The administration of aggregation buffer (vehicle) alone did not cause any modification of the pharyngeal motility compared with worms fed with 1× phosphate-buffered saline (PBS; pH 7.4) (Fig. 5.14B).

However, 2 h after the administration of R3Ag, but not monomeric R3, a severe pharyngeal dysfunction was observed compared to nematodes fed with vehicle (Fig. 5.14B). Interestingly, the pharyngeal impairment caused by R3Ag is transient, as indicated by the absence of toxicity 24 h after administration (Fig. 5.14B). These results indicate that R3 monomers are nontoxic *in vitro* in cells (Fig. 5.7C) and *in vivo* in *C. elegans*. Capping-preformed R3Ag with paclitaxel and quercetin, but not resveratrol, significantly protected worms from pharyngeal dysfunctions scored 2 h post R3Ag administration (Fig. 5.15A; Table 5.3). R3Ag formed in the presence of paclitaxel, resveratrol, or quercetin resulted in less toxicity than R3Ag (Fig. 5.15B; Table 5.3).

In both capping and pre-inhibiting experiments, the effect of drugs alone was also considered by feeding worms with the final concentration of drugs. However, paclitaxel and resveratrol caused a minor but significant reduction of the pharyngeal function in pre-inhibited experiments (Fig. 5.15B); they exerted a significant protective effect against R3Ag toxicity (Table 5.3).

Although the above findings indicate that capping or inhibiting with drugs reverses the toxicity of R3Ag, the mechanisms underlying this protection remained unanswered. As depicted in scheme Fig. 5.15A, worms were pretreated with nontoxic concentrations of paclitaxel, resveratrol and quercetin for 24 h before administration with aggregation buffer or R3Ag for 2 h. Similar to previous experimentation, R3Ag significantly reduced the pharyngeal pumping rate in worms compared to those fed with aggregation buffer (Fig. 5.15B). Thus, the pretreatment of worms with paclitaxel, resveratrol and quercetin for 24 h offered a significant protective effect, making worms less susceptible to R3Ag toxicity (Fig. 5.15B; Table 5.3).

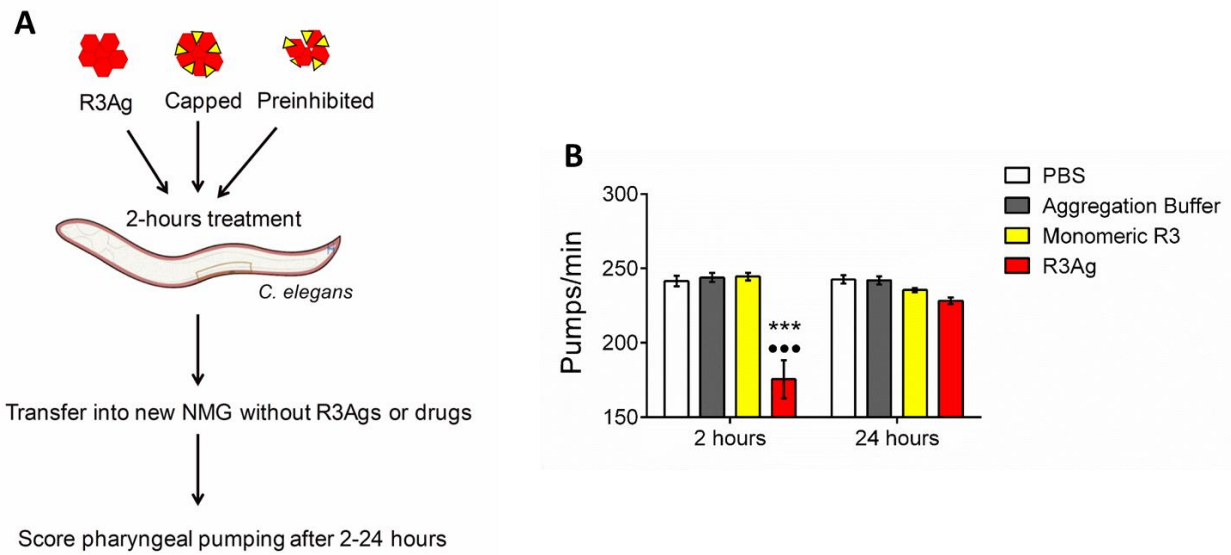


Fig. 5.15. R3Ag causes pharyngeal impairment in *C. elegans*. (A) Schematic representation of experimental set-up showing the feeding of *C. elegans* with R3Ag, drug-capped R3Ag or drug-preinhibited R3Ag. (B) Data showing pharyngeal impairment is transient. Effect of 1× PBS (pH 7.4), aggregation buffer, monomeric R3 and R3Ag on the pharyngeal function of worms, scored 2 and 24 h after the administration. Mean \pm SEM of at least ten experimental values from 3 independent experiments ($n = 30$). *** $p < 0.001$ vs Vehicle and Monomeric R3 at 2 h; *** $p < 0.001$ vs R3Ag at 24 h, two-way ANOVA, Bonferroni's post hoc test.

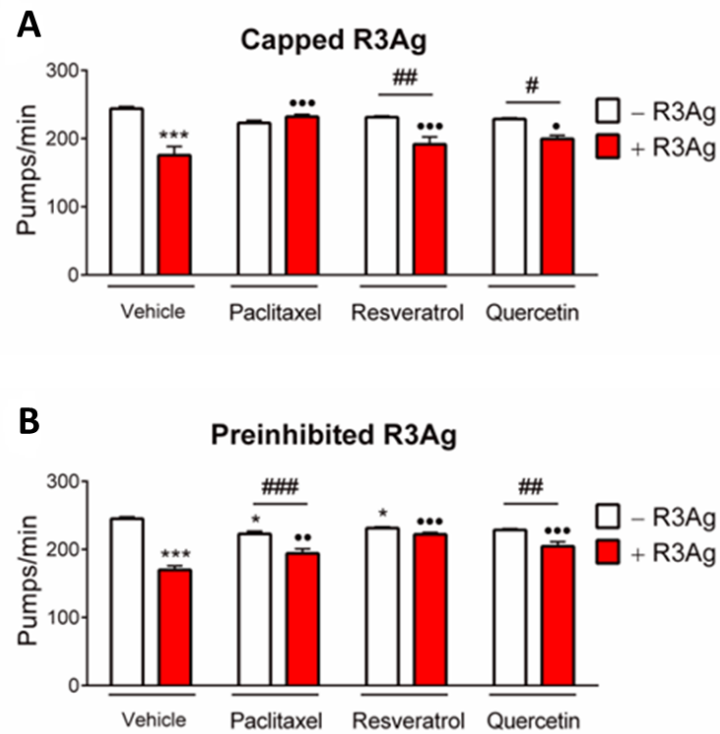


Fig. 5.16. Drug treatment reverses the toxicity of R3Ag in *C. elegans*. (A, B) Effect of R3Ag administered alone (vehicle) and drug-capped R3Ag (A) or drug-pre-inhibited R3Ag with 5 nM paclitaxel, 200 nM resveratrol or 200 nM quercetin (B) on pharyngeal function scored 2 h after administration (red bars, + R3Ag). The effect of aggregation buffer (vehicle) and 5 nM paclitaxel, 200 nM resveratrol or 200 nM quercetin was also evaluated (white bars, - R3Ag). Data in A and B are mean \pm SEM, n = 30, ***P < 0.001 and *P < 0.05 vs vehicle - R3Ag; ***P < 0.001, **P < 0.01 and •P < 0.05 vs vehicle + R3Ag; and ###P < 0.001, ##P < 0.01 and #P < 0.05 - R3Ag vs + R3Ag, two-way ANOVA, Bonferroni's post hoc test.

| | Two-way ANOVA Interaction (<i>p-values</i>) | | |
|-------------|--|------------------------|-------------------------------|
| | Drug-capped R3Ag | Drug-preinhibited R3Ag | Drug-pretreatment before R3Ag |
| Paclitaxel | <0.001 | <0.001 | 0.039 |
| Resveratrol | Not significant | <0.001 | 0.002 |
| Quercetin | 0.010 | <0.001 | <0.001 |

Table 5.3. P-value summary from Fig. 5.16 and 5.17. P-values of the interaction obtained from the two-way ANOVA and Bonferroni's *post hoc* analysis performed on data from the different experiments shown in Fig. 5.16 and 5.17, proving the protective effect exerted by some drugs on the R3Ag toxicity.

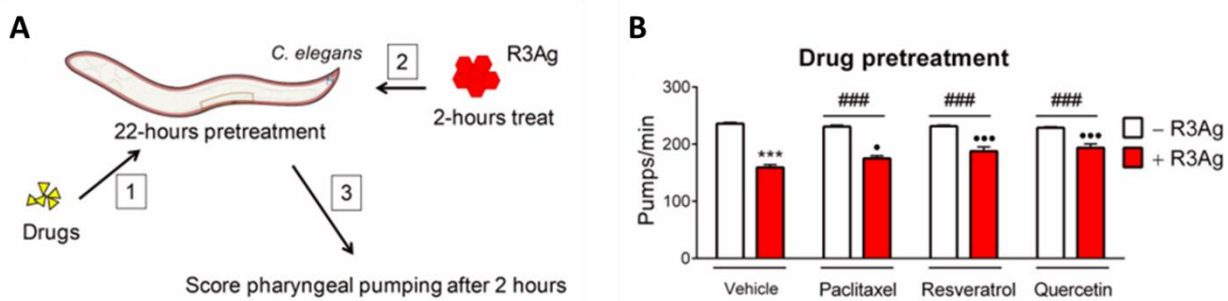


Fig. 5.17. Effect of drug pretreatment on R3Ag toxicity in *C. elegans*. (A) Schematic representation of experimental set-up showing the pretreatment of worms for 24 h with drugs or aggregation buffer (Vehicle) [1] followed by exposure to R3Ag for 2 h [2] and scoring of pharyngeal pumping post-2 h [3]. (E) Effect of aggregation buffer (vehicle), 5 nM paclitaxel, 200 nM resveratrol or 200 nM quercetin followed (red bars, + R3Ag) or not followed (white bars, - R3Ag) by the administration of R3Ag on the pharyngeal pumping. Data in B is mean \pm SEM, $n = 30$, *** $P < 0.001$ and * $P < 0.05$ vs vehicle - R3Ag; *** $P < 0.001$, ** $P < 0.01$ and * $P < 0.05$ vs vehicle + R3Ag; and ### $P < 0.001$, ## $P < 0.01$ and # $P < 0.05$ - R3Ag vs + R3Ag, two-way ANOVA, Bonferroni's post hoc test.

We identified N-terminal hexapeptides- and Cys- in R2 and R3 as the minimal regions of tau aggregation. Both R2 and R3 aggregates are also seed-competent. Targeting these R2 and R3 regions is vital for tau-based therapies for AD and other tauopathies. Thus, we used R3, a self-aggregating tau peptide, for screening potential R3 aggregation inhibitors. For example, we screened antitumour drugs for their effect on inhibiting R3 aggregation and prion-like seeding.

There is strong support for repurposing approved and experimental or investigational oncology drugs for AD therapy^{380,381}. Although the precise mechanisms remain elusive, different drugs may target various pathways, consequently protecting neurons against degeneration. For example, tamoxifen acts as an oestrogen-like agonist to enhance cholinergic and hippocampal activities, improving cognitive functions and reducing dementia risk in older women³⁸¹. Taxanes restore the damaged microtubule networks caused by tau loss of function, enhancing motor and cognitive functions in AD transgenic mice³⁸². Sunitinib has antiacetylcholinesterase activity and attenuates cognitive impairments in AD mice, similar to donepezil³⁸³. Bexarotene clears amyloids from AD mouse brains³⁸⁴, although, in later studies, it was not effective in AD treatment or prevention³⁸⁵. Carmustine and imatinib reduce the A β plaque burden by preventing altered processing of A β -precursor protein and AD-specific tau phosphorylation^{386,387}. Similarly, lonafarnib activates tau aggregate clearance via lysosomes, reducing tau pathology and behavioural abnormalities in AD mice³⁸⁸.

We used peptides of R3 to test our hypothesis that antitumour drugs may prevent the formation of prion-like seeds by inhibiting nucleation-dependent tau aggregation. Our data revealed that adding paclitaxel, docetaxel, cisplatin, doxorubicin, daunorubicin, resveratrol, and quercetin effectively inhibited fibrillisation of R3 peptides *in vitro* into β -sheet-rich aggregates (Fig. 5.1C, D). Furthermore, the anti-fibrillisation effect of drugs was validated further by Congo red dye and microscopic analysis of aggregates formed in the presence of drugs (Fig. 5.2C and E; Fig. 5.2D). These validation studies also ruled out the plausibility that the anti-fibrillisation effects of resveratrol and quercetin were due to the competitive interaction with ThT for binding to fibrils. Furthermore, in addition to inhibiting fibrillisation, these drugs also caused a complete-to-partial disaggregation of preformed fibrils (Fig. 5.3). The ability of drugs to disaggregate preformed

fibrils is an important feature, given the presence of pre-existing aggregates in the brain when patients are diagnosed with AD.

The anti-fibrillisation effect of paclitaxel, doxorubicin, resveratrol, and quercetin resulted from the inhibition of R3 dimerisation (Fig. 5.4C, D). Furthermore, we showed that the presence of Cys in the R3 was essential for the anti-fibrillisation effect of quercetin since R3mut, with a Cys-to-Ala substitution, continued to aggregate in the presence of optimal concentrations of quercetin (Fig. 5.4E; Fig. 5.5C–F). These findings were validated by MD simulation studies that showed the interaction of paclitaxel with the N-terminal VQIVYK sequence that plays a prominent role in self-aggregation of R3, and quercetin with Cys residue, involved in peptide dimerisation^{222,389} (Fig. 5.6). Additionally, interaction with the C-terminal of R3 by doxorubicin and resveratrol prevents dimerisation. The findings suggest that the drugs potentially trap R3 monomers or assembly-competent intermediate aggregates, affecting the dynamic equilibrium of R3 fibrillation²²⁷.

Previous studies have demonstrated that fibrils are generally nontoxic to cells^{390,391}; instead, oligomeric forms affect viability by disrupting the cell membrane³⁹². In agreement, we show that R3Ag does not affect cell viability by cell membrane disruption of the cell membrane (Fig. 5.7C). However, R3Ag-mediated seeding of intracellular tau reduces the growth of the seeded cells (Fig. 5.7E). The limited growth is related to the intracellular accumulation of Tau-RD aggregates, as indicated by the absence of seeding or cell growth inhibition in cells treated with R3Ag in the absence of Lipofectamine (Fig. 5.8B, green columns). Cells with intracellular NFTs or expressing aggregated proteins have been reported to have an aberrant cell cycle or proliferate more slowly than control cells^{374,375}.

Next, we demonstrated that the seeding competency of R3Ag is inhibited following capping with resveratrol and quercetin (Fig. 5.10A, B). Further, R3Ag formed in the presence of paclitaxel, resveratrol, and quercetin are significantly less competent in seeding native Tau-RD (Fig. 5.10A, C). These preinhibited R3Ag seem to have no additional effect on cell viability (Fig. 5.10D). However, although the drugs prevented seeding by R3Ag, they could not revert the limited cell growth (Fig. 5.12C). Interestingly, quercetin reversed the effect of R3Ag on the metabolic activity and, thus, the viability of cells, as quantified by the MTT assay (Fig. 5.10E). Cells with tau pathology display a senescence-like phenotype³⁷⁵. Given the senolytic activity of quercetin, it

could have improved metabolic functions, reversing the senescence-like phenotype. Though, future studies are needed to test this speculation³⁹³.

In addition to abrogating the formation of seeding-competent fibril *in vitro* (Fig. 5.10), the drugs also inhibited the seeding activity. This was shown following the pretreatment of cells with drugs followed by exposure to seeding-competent R3Ag (Fig. 5.13 and 5.14), suggesting that the drugs prevented the addition of monomers (intracellular P301S) to seeds (R3Ag) possibly by inhibiting template-assisted filament growth that inhibited the aggregation of intracellular tau. Like other amyloidogenic proteins, R3Ag also caused a specific pharyngeal dysfunction in *C. elegans*³⁹⁴ (Fig. 5.15, 5.16 and 5.17). This effect was reverted when the peptide was capped or its aggregation preinhibited with paclitaxel, resveratrol or quercetin, indicating that these drugs can mask residues relevant for the R3Ag proteotoxicity *in vivo* proteins³⁷⁸. Together with findings from *in vitro* assay, these data indicate that the drugs inhibited the primary nucleation of R3 fibrillisation that initiates the production of toxic R3 species, a process similar to inhibiting toxic A β 42 generation by bexarotene³⁹⁵.

AD is a dual proteinopathy of tau and A β proteins that act alone or in combination in the process of neurodegeneration¹⁰. A deeper understanding of how pathogenic seeds form and drive distinct structural polymorphs in tau spreading may reveal new insights for designing treatment strategies. A study using P301S Tg mice has shown that intracellular and extracellular tau levels are related, and low extracellular tau may mediate tau pathology³⁹⁶. Despite low concentrations, cells could take up extracellular tau, inducing intracellular tau aggregation and spreading. Several forms of pathogenic extracellular tau, either free or vesicle enclosed, are suspected of spreading tau pathology⁴. Therefore, therapeutic interventions, such as immunotherapy or small molecules that target extracellular tau, may halt disease progression. Like any model system, our study also has its inherent weaknesses. Although we have used simple models in our study, our findings present a rational approach for targeting the VQIVYK or cysteine that may block the nucleation-dependent tau aggregation and prion seed generation. We conclude that earlier detection of seed-competent tau inclusions in the brains of AD or susceptible patients and targeting these inclusions may prevent or slow tau spreading.

Chapter 6

Comparison of the clearance of intracellular aggregates in tau cell models seeded with aggregates of tau repeat peptides

The data presented in this chapter have been performed by Narendran Annadurai in collaboration with Jiří Hrubý and Agáta Kubíčková from the Institute of Molecular and Translational Medicine, Faculty of Medicine and Dentistry, Palacký University, Hněvotínská 5, 77900 Olomouc, Czech Republic.

6.1 R2 and R3 fibrils affect autophagy in tau biosensor cells

The changes in the levels of autophagy-related proteins in tau biosensor cells were measured upon seeding with R2/R3 fibrils. First, the autophagy induction was measured by quantifying the LC3A/B I to II conversion. R2 and R3 fibrils increased the p62 levels time-dependently (Fig. 6.1A, B and Fig. 6.2A, B). The increased level of p62 corresponds to the failure of autophagy, as LC3A/B I to II conversion was reduced in tau biosensor cells only upon seeding with R2/R3 fibrils (Fig. 6.1A, B and Fig. 6.2A, B). No changes in LAMP1 levels were observed in cells seeded with either R2 or R3 fibrils (Fig. 6.1A, B and Fig. 6.2A, B). The failure of autophagy induction in response to the fibrils-induced proteotoxic stress related p62 levels defines the build-up of intracellular aggregates in R2/R3 fibrils-seeded tau biosensor cells observed in our previous study³⁵⁰. Thus, we decided to explore the ability of compounds on autophagy induction to reduce the build-up of intracellular tau aggregates in tau biosensor cells.

6.2 Screening of autophagy-inducing compounds that reduce intracellular tau aggregation in R3 fibrils

We selected a list of compounds studied for their autophagy-inducing ability (Table 6.1). Then, using the MTT cell viability assay, we calculated the IC₅₀ and chose three non-cytotoxic concentrations for treating R3 fibrils seeded tau biosensor cells (Fig. 6.3). We also included autophagy inhibitors to further validate the role of autophagy on the clearance of intracellular tau aggregates (Fig. 6.3; Tables 6.1, 3.2).

Table 6.1 List of compounds and their mechanism of autophagy induction or inhibition.

| Compound | Autophagy activation/inhibition | Autophagy pathways |
|--|---------------------------------|---|
| Resveratrol (RSV) | Activation | mTOR inhibition/AMPK activation ³⁹⁷ |
| Epigallocatechin gallate (EGCG) | Activation | CaMKK β /AMPK-mediated mechanism, AMPK/mTOR ^{398,399} |
| L-Ascorbic acid (VITC) | Activation | AMPK activation |
| Quercetin (QCT) | Activation | AKT-mTOR pathway, LC3 turnover ⁴⁰⁰ |
| Carbamazepine (CBZ) | Activation | AMPK activation ^{401,402} |
| Artemisinin (ART) | Activation | AMPK pathway, PI3K-AKT-mTOR pathway ⁴⁰³ |
| Dexamethasone (DEX) | Activation | Increases expression of several autophagy genes, including ATG5, LC3, BECN1, and SQSTM1 ⁴⁰⁴ |
| Chloroquine (CQ) | Inhibition | Blocks binding of autophagosomes to lysosomes (altering the acidic environment of lysosomes) ⁴⁰⁵ |
| Cycloheximide (CHX) | Inhibition | Protein synthesis inhibitors/ modulation of mTORC1 signaling ⁴⁰⁶ |

6.3 EGCG and RSV reduced intracellular tau aggregation in R3 fibrils seeded tau biosensor cells

In this and previous studies, we showed that exogenous R3 fibrils induce intracellular tau aggregation in tau biosensor cells (Fig. 6.4A)^{347,350}. To study the effect of autophagy activators on the clearance of intracellular aggregates, we treated cells with compounds for 12 h post 6 h treatment with R3 fibrils. We found that EGCG (25, 50 and 100 μ M) and RSV (10 and 20 μ M) significantly reduced the levels of intracellular aggregates (Fig. 6.4B and D). EGCG is more effective than RSV at tested concentrations. As an autophagy inhibitor, CQ did not reduce intracellular tau aggregation (Fig. 6.4C and D).

6.4 EGCG and RSV induced autophagy in R3 fibrils seeded tau biosensor cells

To show the effect of EGCG and RSV, mediated through the induction of autophagy, on the reduction of intracellular tau aggregation, we measured the changes in LC3A/B II/I conversion and p62 and LAMP1 protein levels. Both EGCG and RSV treatments induced autophagy in tau biosensor cells (Fig. 6.5A, B and C), but the maximum effect of EGCG on LC3A/B II/I ratio was noted at 100 μ M concentration (Fig. 6.5A and B). With the induction of autophagy in EGCG- and RSV-treated cells, there was a decrease in R3 fibrils-induced p62 levels (Fig. 6.5A, B and C). EGCG at all three tested concentrations and RSV at 10 and 20 μ M tested concentrations decreased p62 level (Fig. 6.5A, B and C). In addition, the increase in LAMP1 was observed in 50 μ M EGCG- and 10 μ M RSV-treated cells (Fig. 6.5A, B and C). These results confirm that both EGCG and RSV induced autophagy that inhibited the buildup of intracellular tau aggregates in biosensor cells seeded with R3 fibrils (Fig. 6.4B and D).

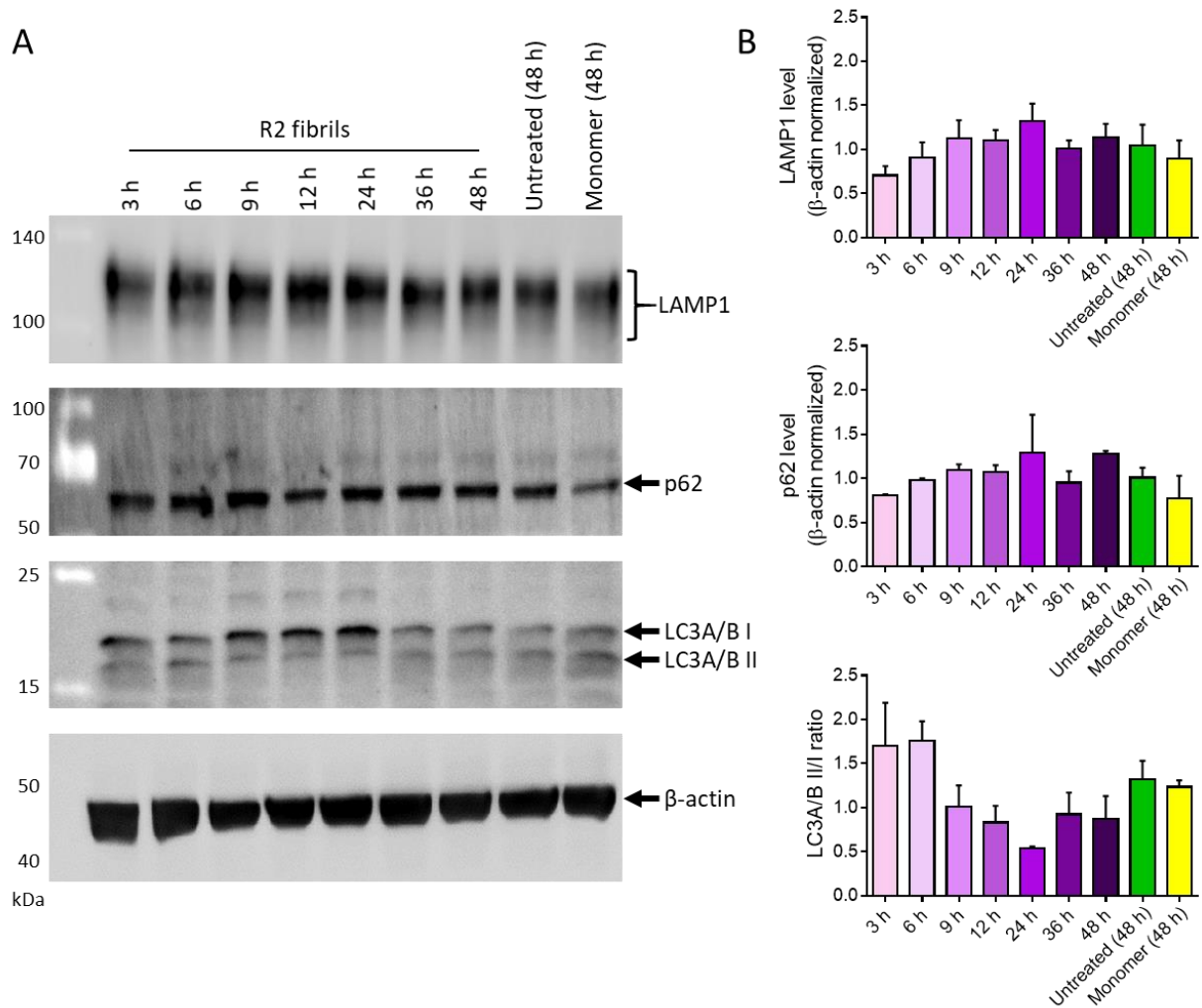


Fig. 6.1. Time-dependent changes in the autophagy-related proteins in biosensor cells seeded with R2 fibrils. (A) Representative Western blots and (B) quantitative analysis of the level of LC3A/B, LAMP1 and p62 after introducing tau R2 fibrils in tau biosensor cells. Time in hours is the time after the start of transfection with aggregates. Untreated (48 h) – Biosensor cells without treatment; Monomer (48 h) – Biosensor cells treated with R2 monomers. Data is mean \pm SEM of 2 independent experiments.

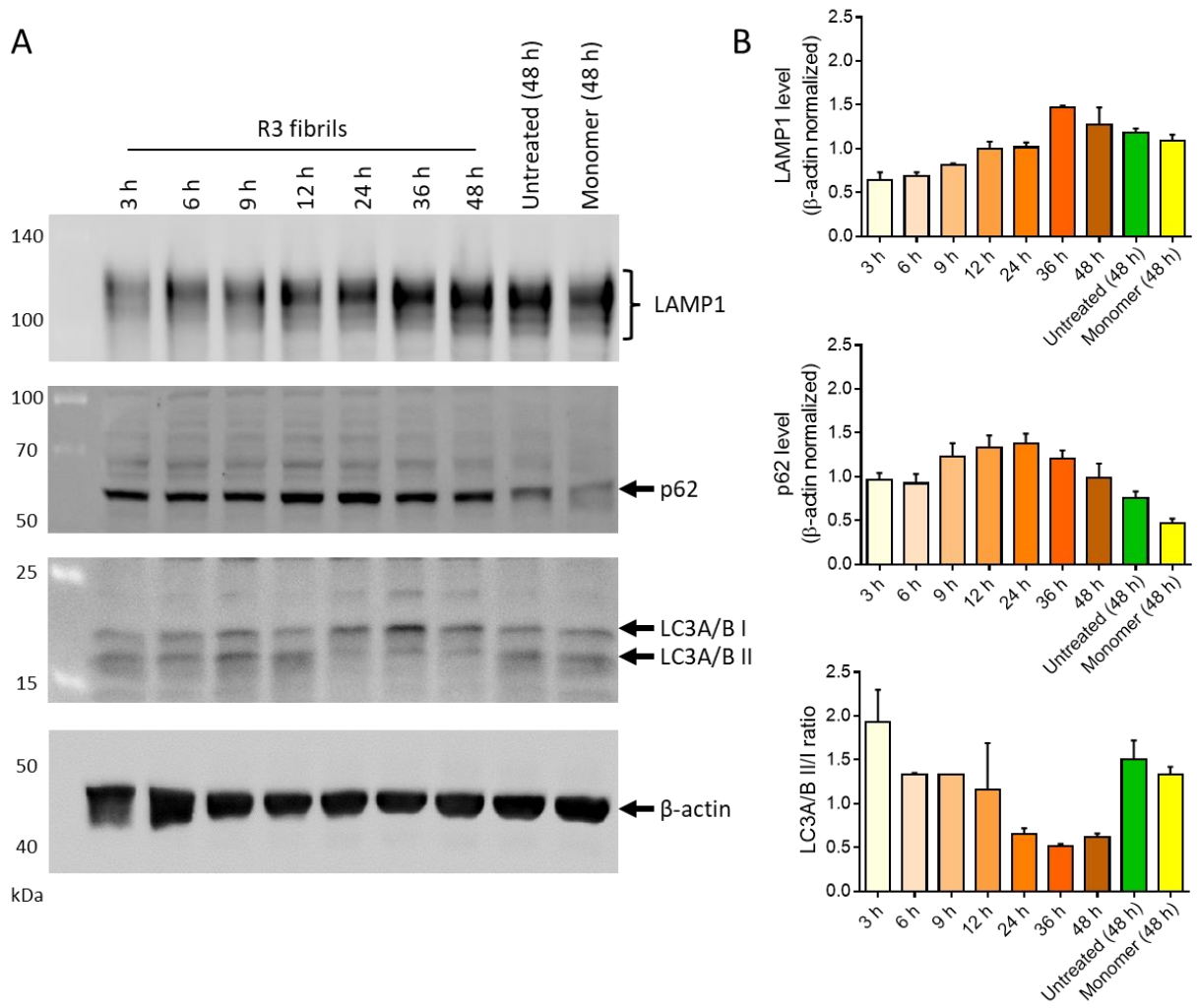


Fig. 6.2. Time-dependent changes in the autophagy-related proteins in biosensor cells seeded with R3 fibrils. (A) Representative Western blots and (B) quantitative analysis of the level of LC3A/B, LAMP1 and p62 after introducing tau R3 fibrils in biosensor cells. Time in hours is the time after the start of transfection with aggregates. Untreated (48 h) – Biosensor cells without treatment; Monomer (48 h) – Biosensor cells treated with R2 monomers. Data is mean ± SEM of 2 independent experiments.

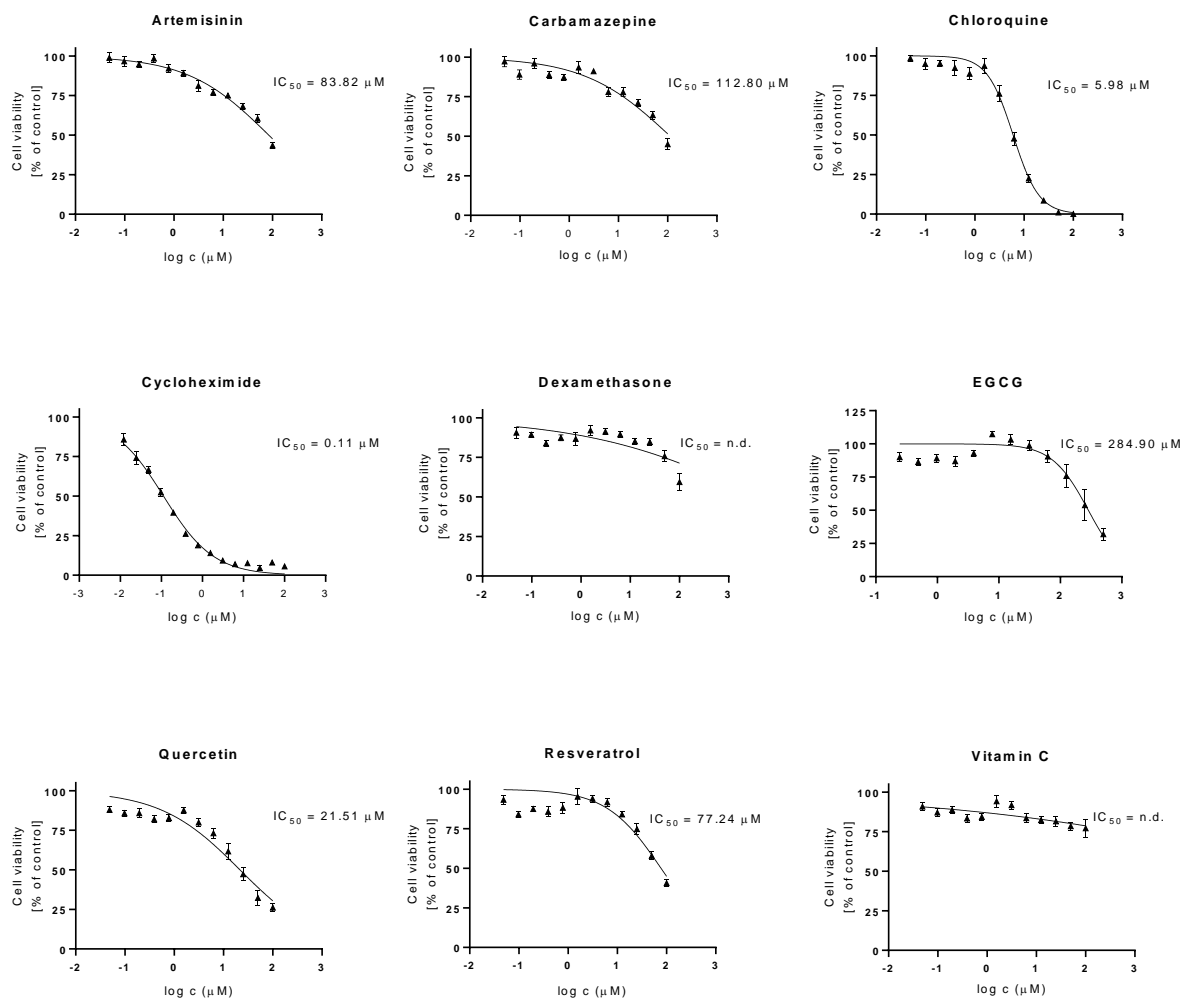


Fig. 6.3. Effect of compounds on the viability of tau biosensor cells. Data is mean \pm SEM of 2 independent experiments.

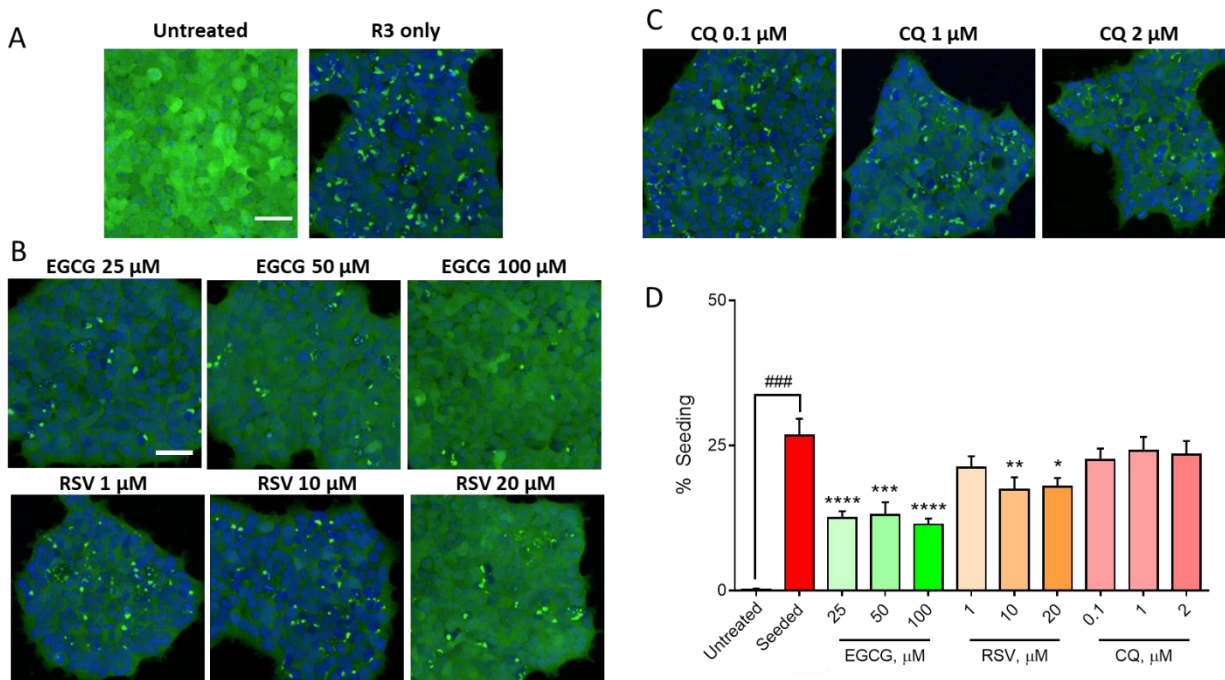


Fig. 6.4. EGCG and RSV reduced intracellular tau aggregation in R3 fibrils seeded cells. (A, B and D) Representative images showing the absence or presence of intracellular tau aggregates (green fluorescent inclusions) in unseeded (untreated) cells or seeded with R3 fibrils (A) and the effect of EGCG and RSV (B), but not CQ (C), treatment on reducing intracellular tau aggregates (B). Scale bar: 50 μ m. (D) Quantification of the % of intracellular seeding in the presence or absence of EGCG and RSV in R3 fibrils seeded cells. Data is mean \pm SEM of 3 independent experiments. ### p < 0.001; Untreated tau biosensor cells vs R3 fibrils seeded tau biosensor cells. * p < 0.05, ** p < 0.01, *** p < 0.001, **** p < 0.0001, R3 fibrils-seeded tau cells vs EGCG, RSV and CQ-treated cells, one-way ANOVA, Dunnett's posthoc test.

6.5 CQ inhibited autophagy in R3 fibrils seeded tau biosensor cells

To confirm our results, we next treated cells with CQ at three concentrations (0.1, 1 and 2 μM), resulting in significant inhibition of the conversion of LC3A/B I to II (Fig. 6.6A and B). The levels of p62 also increased in cells treated with 0.1 and 1 μM CQ (Fig. 6.6A and B). The level of LAMP1 increased at all tested CQ concentrations; however, this increase was not statistically significant (Fig. 6.6A, B and C). These results indicated that inhibited autophagy did not reduce/inhibit intracellular tau aggregation (Fig. 6.4B and C).

6.6 Effect of EGCG, RSV and CQ on triton-insoluble total and phosphorylated Ser262 tau

Our previous study showed an increase in total and phosphorylated Ser262 tau levels in the triton-insoluble fraction of cells seeded with R3 fibrils³⁵⁰. We show that EGCG reduced R3 fibrils seeding (Fig. 6.4B and C) and significantly reduced triton-insoluble total and phosphorylated Ser262 tau (Fig. 6.7A and C). Conversely, RSV treatment did not reduce the triton-insoluble total tau (Fig. 6.7A) but significantly decreased the triton-insoluble phosphorylated Ser262 tau (Fig. 6.7C). However, CQ, on the other hand, increased the triton-insoluble total and phosphorylated Ser262 tau levels (Fig. 6.7B and D).

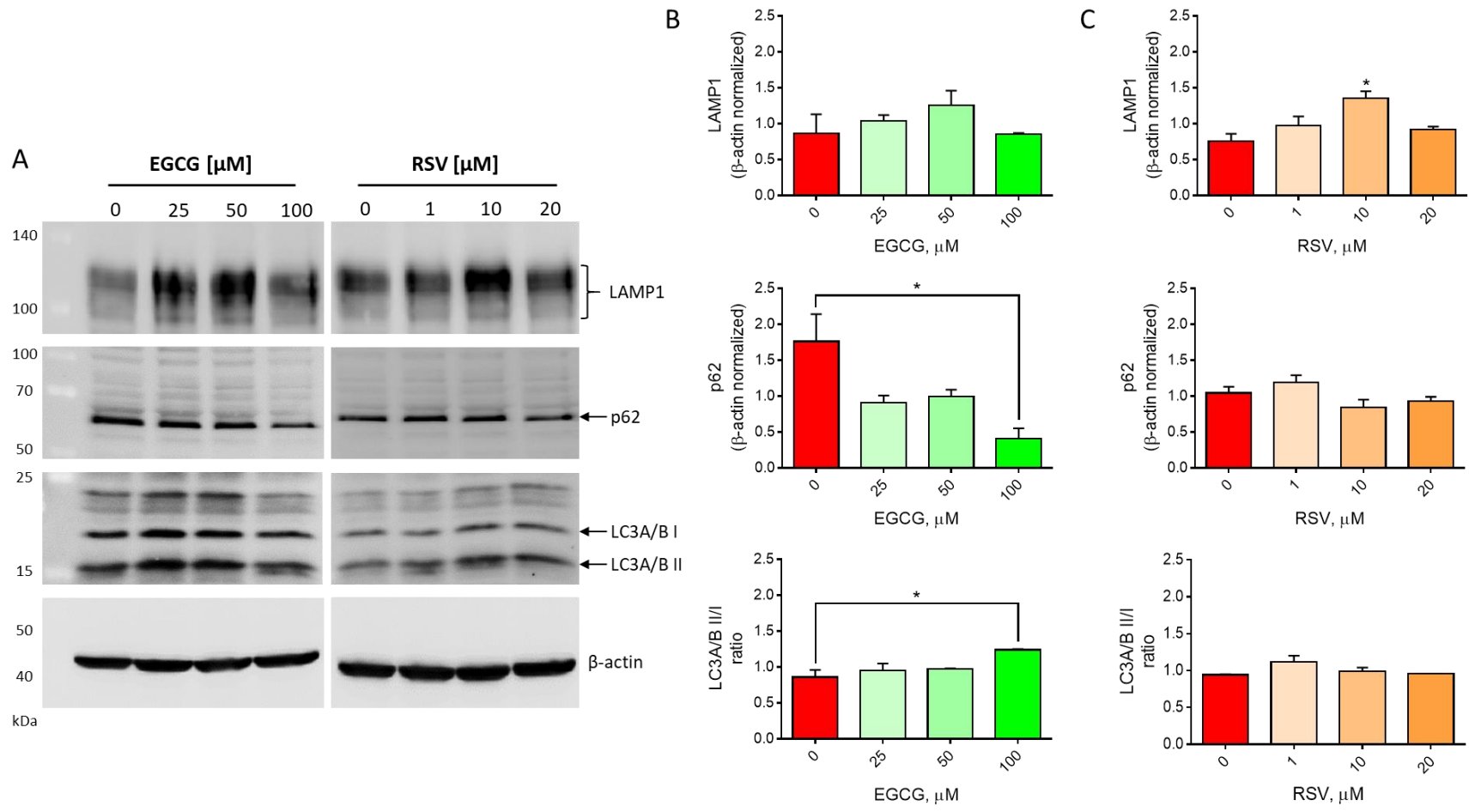


Fig. 6.5. EGCG and RSV induced autophagy in tau biosensor cells seeded with R3 fibrils. (A) Western blot analysis of the level of LC3A/B I, II, p62 and LAMP1 in R3 fibrils seeded tau biosensor cells treated with EGCG and RSV for 48 h. Quantitative analysis of EGCG (B) and RSV (C) treatment showed increased LC3A/B II/I ratio and LAMP1 level and decreased p62. Data is mean ± SEM of 2 independent experiments. * $p < 0.05$, one-way ANOVA, Dunnett's posthoc test.

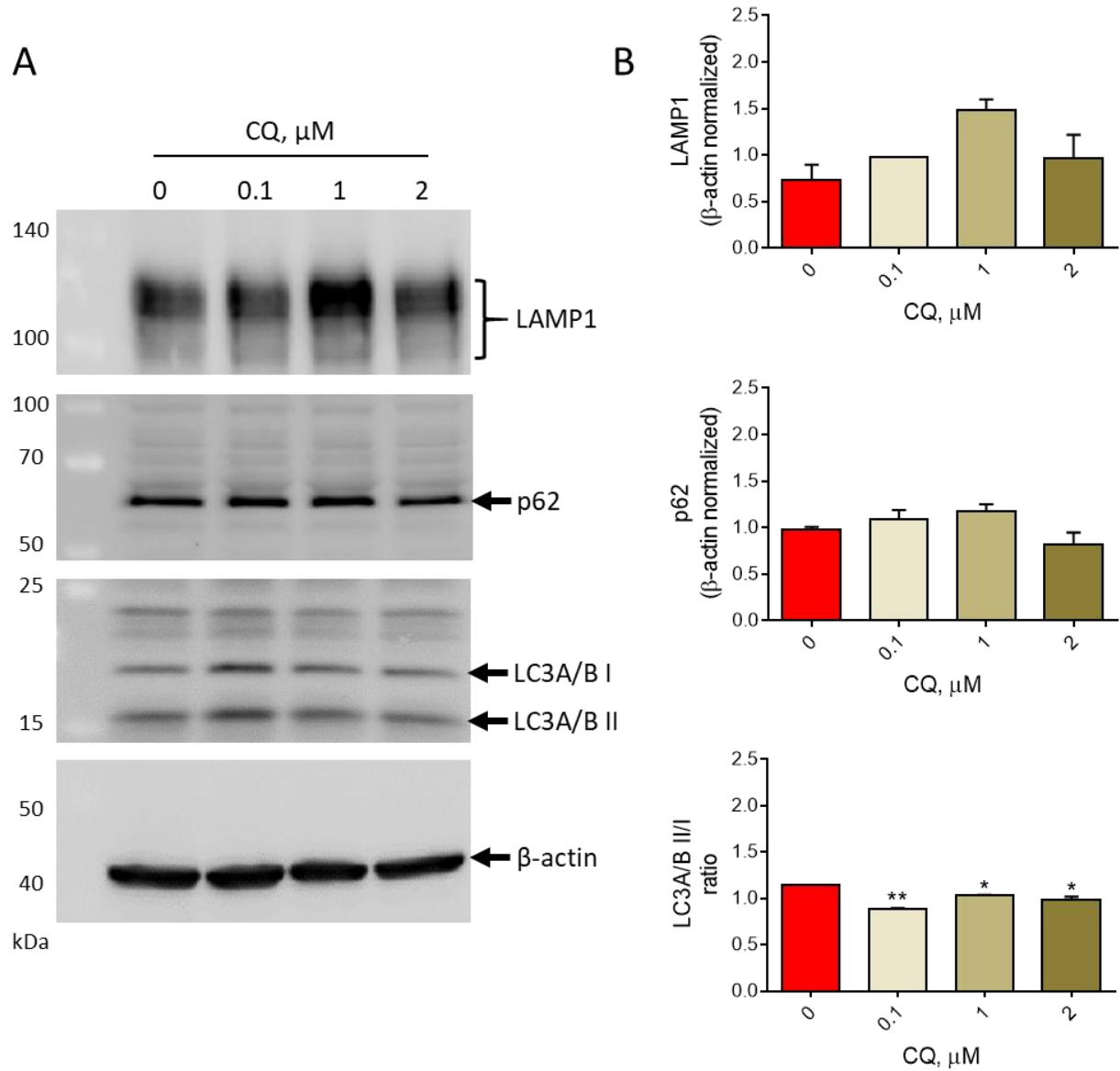


Fig. 6.6. CQ inhibited autophagy in R3 fibrils seeded tau biosensor cells. (A) Western blot and (B) Quantitative analysis of the levels of LC3A/B I, II, p62 and LAMP1 in R3 fibrils seeded tau biosensor cells treated with CQ for 48 h. Data is mean \pm SEM of 2 independent experiments. * $p < 0.05$, ** $p < 0.01$, 0 μM vs CQ-treated R3 fibril-seeded cells, one-way ANOVA, Dunnett's posthoc test.

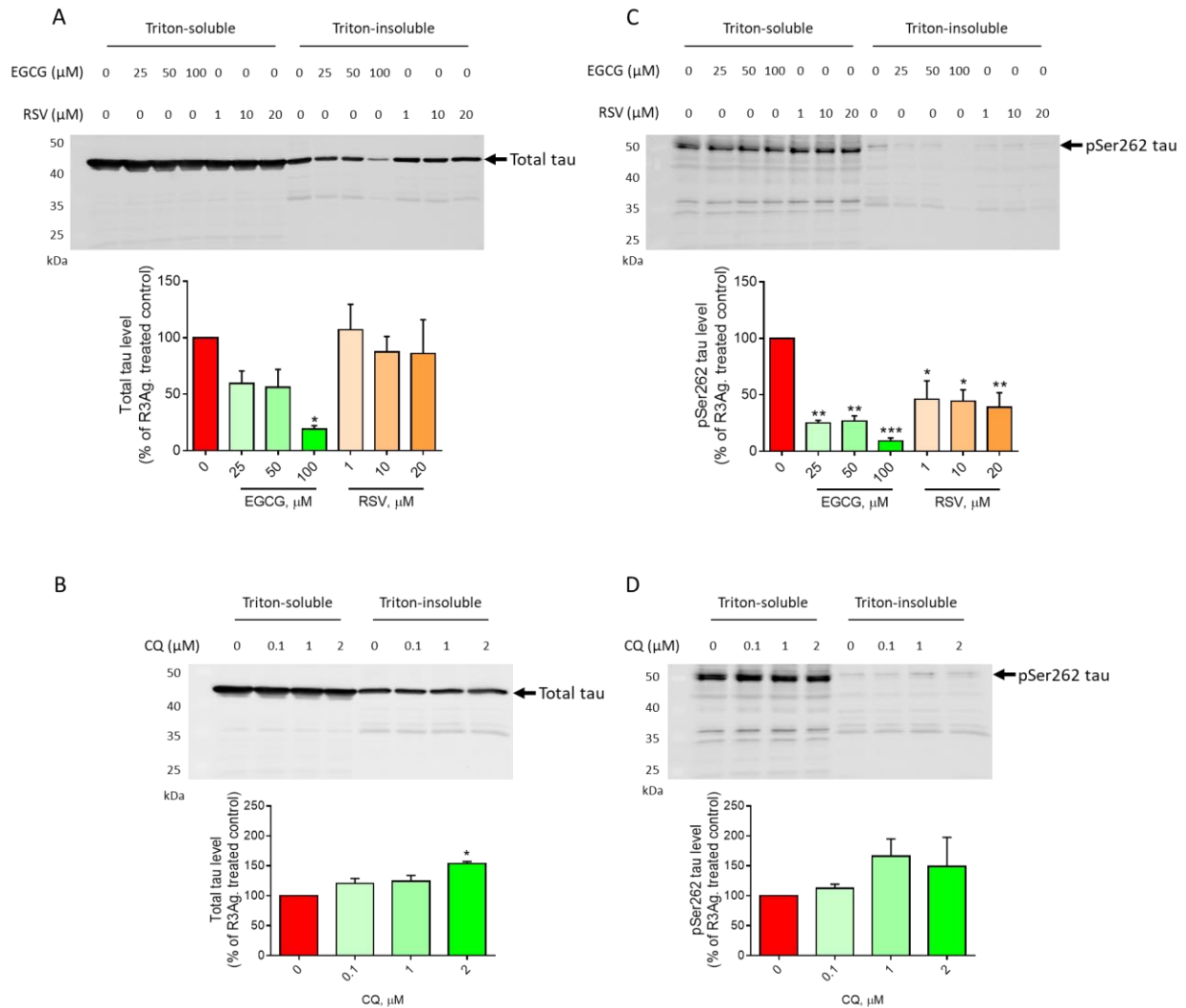


Fig. 6.7. Effect of EGCG, RSV and CQ on the solubility and phosphorylation of intracellular seeded tau. Western blot and quantitative analysis of levels of triton-soluble and -insoluble total tau (A, B) and phosphorylated Ser262 tau (C, D) in R3 fibrils-seeded biosensor cells following treatment with the indicated concentrations of EGCG, RSV and CQ for 48 h. Data are mean \pm SEM of 2 independent experiments. * $p < 0.05$, ** $p < 0.01$, *** $p < 0.001$, 0 μM vs drug-treated R3 fibril-seeded cells, one-way ANOVA, Dunnett's posthoc test.

Autophagy is a natural process involving aggregated protein clearance and worn-out organelles from cells⁴⁰⁷⁻⁴¹⁰. In most mammalian cells, autophagy is a general mechanism wherein its induction involves clearing aggregated or misfolded proteins⁴¹¹⁻⁴¹⁴. Compared to later-stage highly ordered tau filaments, evidence from various studies relates toxicity to early tau mislocalisation, oligomerisation and its solubility-associated changes^{295,415,416}. Another pathological hallmark of tauopathy is dysfunction of the autophagy-lysosomal pathway (ALP)^{417,418}. However, as autophagy remains the primary route associated with the clearance of tau in healthy neurons, thus consequences associated with autophagy impairment remain unclear^{140,419,420}.

Furthermore, studies of abnormal ALP function in the brain of tauopathy patients and animal and cellular models report that accumulation of autophagic vesicles, lysosomes, and tau correlates with neuronal toxicity^{417,421-425}. In these models, autophagy activators reduce misfolded and aggregated protein levels, mitigating tau spreading and neuronal loss^{411,426-430}, supporting autophagy modulators' therapeutic potential^{140,412,429}. Therefore, early tau clearance may help our understanding of disease aetiology and be a promising therapeutic strategy.

The relationship between tau degradation and the autophagy-lysosome system was unclear for a long time. Chloroquine, a malarial drug, interrupts autophagy by preventing autophagosome fusion with lysosomes rather than by perturbing the acidity or digestive function of lysosomes⁴⁰⁵. A study on chloroquine myopathy discovered that tau accumulated in rat muscle⁴³¹, implying that a lysosome autophagy system can degrade tau. Tau propagation through neurons is essential for the progress of tau-mediated neurodegeneration. Results from previous studies reported that tau is acetylated by the lysine acetyltransferase p300/CBP, and p300/CBP also controls the degradation and toxicity of tau. However, abnormal upregulation of P300/CBP in tauopathies interrupts the autophagy-lysosome pathway, leading to excessive tau secretion⁴³². In the mouse tauopathy model, human and rodent neocortex culture, p300 inhibitor SMDC37892 increased autophagic flux and reduced tau secretion. On the contrary, highly activated p300/CBP blocked the autophagic flux and enhanced tau secretion in neurons⁴³².

Furthermore, Tang *et al.* reported that activation of mTORC1 leads to autophagy inactivation, thereby promoting tau secretion in an exosome-independent manner into extracellular space in

neuroblastoma cells⁴³³. Recent reports state that CMA blockade upregulated cell-to-cell propagation in a rodent model of tauopathy⁴³⁴. Conversely, autophagy inducers increased total and phosphorylated tau secretion, which was reduced by Beclin1 knockdown or autophagy inhibitors in a hTau-overexpressing human neuroblastoma cell line⁴³⁵. In addition, six isoforms of tau were secreted in an autophagy-dependent manner⁴³⁵, and thus the issue remains controversial. Limited proteolysis of pathogenic proteins, namely α -synuclein, tau and polyglutamine proteins, is critical for the pathogenesis of neurodegenerative diseases^{436,437}. The hallmark lesions of tauopathies, including AD, are pathological neurofibrillary tangles composed of hyperphosphorylated filamentous tau aggregates⁴³⁸. Physiological tau is a highly soluble microtubule-associated protein essential for microtubule assembly and stability^{439,440}. A recent study utilising a cellular model of AD-like tau aggregate induction by preformed tau fibrils found that tau aggregates induced in the cells cleared by suppressing soluble-tau overexpression. In this study, the expression of aggregation-prone mutant tau is regulated. The study further mentioned that the autophagy-lysosome pathway partially mediates the tau aggregate clearance mechanisms. The ubiquitin-proteasome system and the ALP are deficient in handling large tau aggregates⁴⁴¹. In AD brains, abnormal accumulation of autophagosomes in neurons constituted the first sign of autophagy deficits⁴⁴².

Under pathological conditions, the insoluble hyperphosphorylated tau aggregates get disseminated in the brain, and the severity of the tauopathy correlates strongly with the tau aggregates propagation, which is also visible in the clinical phenotypes of tauopathy patients⁴⁴³⁻⁴⁴⁵. These insoluble tau aggregates and, more recently, the soluble pre-fibrillar tau species, like oligomeric tau, contribute to neuronal degeneration and its dysfunction⁴⁴⁶⁻⁴⁴⁹. Studies reported so far also confirm impairment of the ALP system in primary tauopathy patients, demonstrating that autophagy defects are a common feature of human tauopathies⁴⁵⁰. Several strategies have been discussed for inhibiting tau aggregation and clearing intracellular tau aggregates by compounds or antibodies that disassemble the tau aggregates. Ubiquitin-proteasome system⁴⁴⁰ is responsible for soluble and short-lived proteins turnover, and the autophagy-lysosome pathway involves the degradation of insoluble and long-lived proteins damaged by cellular organelles⁴⁵¹. Studies carried out in transgenic mice overexpressing mutant tau and cultured cells demonstrate that autophagy induction by trehalose or rapamycin could ameliorate tau pathology^{429,452,453}. A recent study found

that pathogenic P301L mutation inhibits tau degradation by autophagy, macroautophagy or chaperone-mediated autophagy.

In contrast, risk-associated A152T tau mutation directs the tau to distinct autophagy-mediated degradation pathways. As most of the tau mutation markedly reduced the degradation of defective tau at a different phase, finding or activating better pathogenic tau degradation pathways is essential⁴⁵⁴. However, it is unclear whether autophagy involves basal degradation of insoluble tau without pharmacological activation. Inhibition of the autophagy-lysosome pathway has been shown to induce tau deposition⁴⁵⁵⁻⁴⁵⁷, as the effect of tau aggregation on the autophagy-lysosome pathway has not been well studied. A recent study also shows that both normal and pathological tau is secreted in an autophagy-dependent manner. A recent study found that spleen tyrosine kinase (SYK) blocks the autophagy degradation of tau *in vitro* and *in vivo*, and SYK activation occurs upstream of the mTOR pathway. The pharmacological inhibition or knockdown of SYK increased the autophagic degradation of tau⁴⁵⁸. Therefore, it is crucial to determine whether pathways are getting activated or inactivated due to autophagic degradation failure of pathogenic tau. In our study, we want to discuss how the exogenous tau peptides aggregate seeded intracellular tau aggregates dysregulate the innate cellular mechanisms, including the lysosome-autophagy pathway or activate cellular degradation mechanisms as an effective strategy to eliminate the intracellular tau aggregates in Tau RD P301S FRET biosensor cells.

In our study, we want to discuss how the exogenous tau peptides aggregate seeded intracellular tau aggregates dysregulate the innate cellular mechanisms, including the lysosome-autophagy pathway or activate cellular degradation mechanisms as an effective strategy to eliminate the intracellular tau aggregates in tau biosensor cells. We have found that both R2 and R3 fibrils can induce proteotoxic stress and reduce autophagy in tau cells. The increased levels of p62 correspond to autophagy inhibition, which defines the failure of autophagy flux in tau biosensor cells seeded with R2/R3 fibrils⁴⁵⁹. We used R3 fibrils seeded tau biosensor cells for studying the effect of compounds with known autophagy-inducing function and also selected autophagy inhibitors (Table 6.1) to study their effect on the level of intracellular tau aggregates.

Overall, we found that EGCG and RSV significantly reduced intracellular tau aggregation and induced autophagy. Among other tested compounds, VITC, QCT, CBZ, and ART reduced intracellular tau aggregation compared to untreated R3 fibrils seeded tau biosensor cells. However,

the reduction in intracellular tau aggregation by these compounds (QCT, CBZ and ART) was not statistically significant, although VITC at 25 μ M significantly reduced intracellular tau aggregation (data not shown). We believe that the ability of both EGCG and RSV to reduce intracellular tau aggregation is not only because of autophagy but also because of their ability to inhibit tau aggregation and seeding^{460,461}. We have also shown that CQ treatment inhibited autophagy, thus inhibiting autophagic clearance of intracellular tau aggregates. From our study, we have also shown that compounds that induce autophagy can also reduce the triton-insoluble phosphorylated Ser262 tau, as our previous study explored that the hyperphosphorylation precedes the formation of intracellular tau aggregation³⁵⁰. Thus, our study provided information on how an autophagy-lysosomal pathway can be targeted for clearing intracellular tau aggregates in cells.

Chapter 7

General Discussion

General Discussion

Neurodegenerative tauopathies, including AD, are classified based on tau aggregation and the distinct composition of intracellular filaments with tau isoforms. Structural analysis of core filaments by Cryo-EM revealed a similar core area but with diverse conformations. The structural and conformational differences among the polymorphic tau fibrils of different tauopathies, with the effect of non-protein cofactors on tau aggregation, affect the stability and propagation of tau aggregates. Thus, it is crucial to identify and characterise tau regions critical for differential aggregation and conversion from inert to prion-like aggregates. Microtubule-binding domain plays a crucial role in tau aggregation in physiological and pathological conditions. The shorter R2 and R3 regions in the microtubule-binding domain share an aggregation potential similar to full-length tau protein. The N-terminal hexapeptides in R2 (VQIVYK) and R3 (VQIINK) aggregate *in vitro* into β -sheet rich fibrils, but these aggregates do not have prion-like properties. By utilising peptides of individual repeats (R1, R2, R3, and R4) in the microtubule-binding domain, we have shown that R2 and R3 assemble into prion-like aggregates or fibrils. On the other hand, R1 and R4 peptides are neither aggregates nor form seed-competent aggregates under defined physiological conditions. Though R2 aggregates faster than R3, no difference in intracellular seeding ability was observed, suggesting that differential aggregation rate does not influence the seeding potency of R2 and R3 seeds.

R3 but not R2 aggregates assemble into fibrils in the absence of heparin (a physiological condition), even though both R2 and R3 share similar N-terminal hexapeptide sequences and KXGS motifs containing cysteine residue. These data explain that R3 may be the minimal region that behaves as nuclei for pathological seed generation under physiological conditions. In contrast, R2 may need polyanionic cofactors to generate pathogenic seeds that may contribute to the later stages of the tau aggregation process. This finding is important because the latest evidence suggests that brain RNA may result in pathological tau strains and may contribute to the propagation of tau pathology in AD⁴⁶². When there is a cysteine to alanine mutation in the C-terminal region, R3 aggregates only in the presence of heparin and is seed-competent. Thus, cysteine residue at the KXGS motif of R3 might play an essential role in tau seed formation under pathological conditions. We also found that R2 and R3 monomers are not seed-competent, and only R2 and R3 aggregates seed the aggregation of intracellular tau. Therefore, there is also a need to analyse and

characterise the seed-competent species of the mixture of R2 and R3 aggregates, as seed-competent aggregates may contain dimers, oligomers and fibrils, including monomers.

Next, we explored the effect of exogenous aggregates of tau repeat peptides on the solubility and phosphorylation changes of intracellular seeded tau in cell models, as mechanisms associated with seeding are not yet known in detail. Our study found that AD-specific phosphorylations and oligomerisation are observed in cell models expressing mutant P301S and 0N4R (P301L) tau. Exogenous R2 or R3 fibrils-induced seeding enhanced insolubility of abnormally phosphorylated intracellular tau. These findings suggest that phosphorylation is one factor contributing to the aggregation of intracellular seeded tau. In addition, the seed-competent intracellular inclusions with pathological phosphorylations resulted from the failure of cell clearance mechanisms and phosphatase functions that define the ageing-associated molecular mechanisms observed in AD and other tauopathies.

Next, we targeted the minimal regions (VQIVYK and cysteine) of self-aggregating R3 with small molecules to abolish the seed-competency of R3 aggregates by inhibiting nucleation-dependent aggregation in tau P301S biosensor cells, thus inhibiting the prion-like seeding of R3 aggregates. Our study found that drugs like paclitaxel, docetaxel, cisplatin, doxorubicin, daunorubicin, resveratrol, and quercetin effectively inhibited the formation of β -sheet-rich aggregation and fibrillisation *in vitro*. We confirmed the anti-fibrillisation effect of paclitaxel, doxorubicin, resveratrol, and quercetin resulting from the inhibition of R3 dimerisation. In addition, these drugs also were able to disaggregate the preformed fibrils. The ability of drugs to inhibit fibrillisation and disaggregation is essential as patients diagnosed with AD have pre-existing aggregates in their brains.

Furthermore, we also showed that the interaction of paclitaxel with the N-terminal VQIVYK hexapeptide and quercetin with cysteine of R3 causes inhibition of R3 fibrillisation and dimerisation. In addition, we also showed the interaction of resveratrol and doxorubicin with the C-terminal of R3, thus preventing dimerisation. These findings suggest that drugs that can trap R3 monomers, preventing them from forming R3 aggregation nuclei or assembly-competent intermediate dimers or oligomers, affect R3 fibrillisation. Next, we showed that R3 aggregates capped (treated) with resveratrol or quercetin and R3 aggregates formed in the presence of paclitaxel, resveratrol, and quercetin are less-seed competent in seeding intracellular tau in cells.

In addition to abolishing the seed-competency of R3 aggregates, the drugs also conferred some protection against aggregate toxicity in cells pretreated with drugs before exposing them to R3 aggregates. These data prove that these drugs can prevent template-assisted filament growth. In addition, paclitaxel, resveratrol and quercetin pre-inhibition/capping reverted the R3 aggregates-induced pharyngeal dysfunction in *C. elegans*. These findings indicate that the drugs inhibited the primary nucleation of R3 fibrillisation, thus preventing the generation of seed-competent toxic R3 species. In addition, this study also presents a rational approach for targeting the VQIVYK or cysteine that may block the nucleation-dependent tau aggregation and prion seed generation.

Since we found the seeding potential of R2 and R3 fibrils in our previous study, we wanted to explore the mechanisms associated with the clearance of intracellular aggregates in tau biosensor cells seeded with aggregates of tau repeat peptides. From the time-dependent tau seeding assay, we found that exogenous R2 fibrils need less time in seeding intracellular tau aggregation than R3. Next, we elucidated the autophagy failure in tau cells upon seeding with R2 and R3 fibrils time-dependently. First, we found that both R2 and R3 fibrils-mediated seeding increased the p62 levels in response to the increased build-up of intracellular tau aggregates. Next, R2 and R3 fibrils reduced the autophagy marker LC3-II to-I ratio. In addition, there is increased lysosomal activity in cells seeded with R2 and R3 fibrils. These data indicate a failure in autophagy initiation and autophagy flux in tau biosensor cells, which failed to clear intracellular tau aggregates. Thus, we elucidated the mechanisms of autophagy induction on the clearance of intracellular tau aggregates. We have shown that autophagy inducers such as EGCG, RSV and VITC reduced intracellular tau aggregation in R3-seeded tau biosensor cells. We next confirmed the autophagy induction through increased LC3-II to-I ratio and decreased p62 levels corresponding to the reduced intracellular tau aggregates. We also found that CQ, an autophagy inhibitor, did not reduce intracellular tau aggregation. We have also confirmed that CQ did not induce autophagy and thus failed to induce the clearance of intracellular tau aggregates. As we found in our previous study, the seeding process involves the build-up of intracellular phosphorylated tau aggregates. Therefore, we checked the insoluble total and phosphorylated tau levels in the EGCG, RSV and CQ-treated R3-seeded biosensor cells. We found that EGCG reduced both triton-insoluble total and phosphorylated Ser262 tau. RSV treatment reduced phosphorylated Ser262 tau, and CQ treatment did not affect the triton-insoluble total and phosphorylated Ser262 tau levels.

Altogether, evidence from these studies supports the importance of targeting N-terminal hexapeptides or cysteines of R2 or R3 and enhancing cell clearance mechanisms for developing tau-targeted therapies.

References

1. DeVos, S. L. *et al.* Synaptic Tau Seeding Precedes Tau Pathology in Human Alzheimer's Disease Brain. *Front. Neurosci.* **12**, 267 (2018).
2. Kaufman, S. K., Thomas, T. L., Del Tredici, K., Braak, H. & Diamond, M. I. Characterization of tau prion seeding activity and strains from formaldehyde-fixed tissue. *Acta Neuropathol. Commun.* **5**, 41 (2017).
3. Vaquer-Alicea, J. & Diamond, M. I. Propagation of Protein Aggregation in Neurodegenerative Diseases. *Annu. Rev. Biochem.* **88**, 785–810 (2019).
4. Annadurai, N., De Sanctis, J. B., Hajdúch, M. & Das, V. Tau secretion and propagation: Perspectives for potential preventive interventions in Alzheimer's disease and other tauopathies. *Exp. Neurol.* **343**, 113756 (2021).
5. Clavaguera, F. *et al.* Transmission and spreading of tauopathy in transgenic mouse brain. *Nat. Cell Biol.* **11**, 909–913 (2009).
6. Dujardin, S. *et al.* Tau molecular diversity contributes to clinical heterogeneity in Alzheimer's disease. *Nat. Med.* **26**, 1256–1263 (2020).
7. Franzmeier, N. *et al.* Functional connectivity associated with tau levels in ageing, Alzheimer's, and small vessel disease. *Brain* **142**, 1093–1107 (2019).
8. Kaufman, S. K., Del Tredici, K., Thomas, T. L., Braak, H. & Diamond, M. I. Tau seeding activity begins in the transentorhinal/entorhinal regions and anticipates phospho-tau pathology in Alzheimer's disease and PART. *Acta Neuropathol. (Berl.)* **136**, 57–67 (2018).
9. Ossenkoppele, R. *et al.* Tau covariance patterns in Alzheimer's disease patients match intrinsic connectivity networks in the healthy brain. *NeuroImage Clin.* **23**, 101848 (2019).
10. Vogel, J. W. *et al.* Spread of pathological tau proteins through communicating neurons in human Alzheimer's disease. *Nat. Commun.* **11**, 2612 (2020).
11. La Joie, R. *et al.* Prospective longitudinal atrophy in Alzheimer's disease correlates with the intensity and topography of baseline tau-PET. *Sci. Transl. Med.* **12**, eaau5732 (2020).
12. Mukrasch, M. D. *et al.* Sites of Tau Important for Aggregation Populate β -Structure and Bind to Microtubules and Polyanions*. *J. Biol. Chem.* **280**, 24978–24986 (2005).
13. Tomoo, K. *et al.* Possible Role of Each Repeat Structure of the Microtubule-Binding Domain of the Tau Protein in In Vitro Aggregation. *J. Biochem. (Tokyo)* **138**, 413–423 (2005).
14. Ganguly, P. *et al.* Tau Assembly: The Dominant Role of PHF6 (VQIVYK) in Microtubule Binding Region Repeat R3. *J. Phys. Chem. B* **119**, 4582–4593 (2015).
15. Adamcik, J. *et al.* Microtubule-Binding R3 Fragment from Tau Self-Assembles into Giant Multistranded Amyloid Ribbons. *Angew. Chem. Int. Ed.* **55**, 618–622 (2016).
16. Stöhr, J. *et al.* A 31-residue peptide induces aggregation of tau's microtubule-binding region in cells. *Nat. Chem.* **9**, 874–881 (2017).
17. Despres Clément *et al.* Identification of the Tau phosphorylation pattern that drives its aggregation. *Proc. Natl. Acad. Sci.* **114**, 9080–9085 (2017).
18. Falcon, B. *et al.* Conformation Determines the Seeding Potencies of Native and Recombinant Tau Aggregates. *J. Biol. Chem.* **290**, 1049–1065 (2015).
19. Frost, B., Jacks, R. L. & Diamond, M. I. Propagation of Tau Misfolding from the Outside to the Inside of a Cell*. *J. Biol. Chem.* **284**, 12845–12852 (2009).
20. Tarutani, A. *et al.* Human tauopathy-derived tau strains determine the substrates recruited for templated amplification. *Brain* **144**, 2333–2348 (2021).
21. Mezencev, R. & Chernoff, Y. O. Risk of Alzheimer's Disease in Cancer Patients: Analysis of Mortality Data from the US SEER Population-Based Registries. *Cancers* **12**, (2020).
22. Savica, R. & Petersen, R. C. Prevention of Dementia. *Prev. Ment. Health Lifesp. Perspect.* **34**, 127–145 (2011).

23. Duyckaerts, C., Delatour, B. & Potier, M.-C. Classification and basic pathology of Alzheimer disease. *Acta Neuropathol. (Berl.)* **118**, 5–36 (2009).
24. World Health Organisation Dementia Fact sheet, 2022. <https://www.who.int/news-room/fact-sheets/detail/dementia> (2022).
25. Alzheimer's Research UK, 2022. <https://www.alzheimersresearchuk.org/dementia-information/types-of-dementia/rare-types-of-dementia/>.
26. Ott, A. *et al.* Diabetes mellitus and the risk of dementia. *Neurology* **53**, 1937 (1999).
27. Cholerton, B., Baker, L. D., Montine, T. J. & Craft, S. Type 2 Diabetes, Cognition, and Dementia in Older Adults: Toward a Precision Health Approach. *Diabetes Spectr.* **29**, 210–219 (2016).
28. Global Burden of Disease Study 2013. *The Lancet* **385**, 117–171 (2015).
29. Brookmeyer, R., Johnson, E., Ziegler-Graham, K. & Arrighi, H. M. Forecasting the global burden of Alzheimer's disease. *Alzheimers Dement.* **3**, 186–191 (2007).
30. Niu, H., Álvarez-Álvarez, I., Guillén-Grima, F. & Aguinaga-Ontoso, I. Prevalence and incidence of Alzheimer's disease in Europe: A meta-analysis. *Neurol. Engl. Ed.* **32**, 523–532 (2017).
31. Prince, M. *et al.* The global prevalence of dementia: A systematic review and metaanalysis. *Alzheimers Dement.* **9**, 63-75.e2 (2013).
32. Maresova, P. *et al.* Anticipated Social and Healthcare Economic Burden of People with Alzheimer's Disease in Two Selected Regions of the Czech Republic. *Healthcare* **8**, (2020).
33. Bertens, D. *et al.* Use of mild cognitive impairment and prodromal AD/MCI due to AD in clinical care: a European survey. *Alzheimers Res. Ther.* **11**, 74 (2019).
34. World Alzheimer Report 2015, The Global Impact of Dementia: An Analysis of Prevalence, Incidence, Cost and Trends. <https://www.alz.co.uk/research/WorldAlzheimerReport2015.pdf> (2015).
35. Bond, M. *et al.* The effectiveness and cost-effectiveness of donepezil, galantamine, rivastigmine and memantine for the treatment of Alzheimer's disease (review of Technology Appraisal No. 111): a systematic review and economic model. *Health Technol Assess* **16**, 21 (2012).
36. Loveman, E. *et al.* The clinical and cost-effectiveness of donepezil, rivastigmine, galantamine and memantine for Alzheimer's disease. *Health Technol. Assess.* **10**, (2006).
37. Cummings, J., Lee, G., Ritter, A., Sabbagh, M. & Zhong, K. Alzheimer's disease drug development pipeline: 2019. *Alzheimers Dement. Transl. Res. Clin. Interv.* **5**, 272–293 (2019).
38. Jellinger, K. A. Basic mechanisms of neurodegeneration: a critical update. *J. Cell. Mol. Med.* **14**, 457–487 (2010).
39. Stroo, E., Koopman, M., Nollen, E. A. A. & Mata-Cabana, A. Cellular Regulation of Amyloid Formation in Aging and Disease. *Front. Neurosci.* **11**, (2017).
40. Aguzzi, A. & O'Connor, T. Protein aggregation diseases: pathogenicity and therapeutic perspectives. *Nat. Rev. Drug Discov.* **9**, 237–248 (2010).
41. Sawaya, M. R. *et al.* Atomic structures of amyloid cross- β spines reveal varied steric zippers. *Nature* **447**, 453–457 (2007).
42. Sipe, J. D. & Cohen, A. S. Review: History of the Amyloid Fibril. *J. Struct. Biol.* **130**, 88–98 (2000).
43. Monsellier, E. *et al.* The Distribution of Residues in a Polypeptide Sequence Is a Determinant of Aggregation Optimized by Evolution. *Biophys. J.* **93**, 4382–4391 (2007).
44. Braak, H. & Del Tredici, K. Potential Pathways of Abnormal Tau and α -Synuclein Dissemination in Sporadic Alzheimer's and Parkinson's Diseases. *Cold Spring Harb. Perspect. Biol.* **8**, (2016).
45. Monaco, A. & Fraldi, A. Protein Aggregation and Dysfunction of Autophagy-Lysosomal Pathway: A Vicious Cycle in Lysosomal Storage Diseases. *Front. Mol. Neurosci.* **13**, (2020).
46. Menzies, F. M., Moreau, K. & Rubinsztein, D. C. Protein misfolding disorders and macroautophagy. *Cell Regul.* **23**, 190–197 (2011).
47. Taylor, J. P., Hardy, J. & Fischbeck, K. H. Toxic Proteins in Neurodegenerative Disease. *Science* **296**, 1991–1995 (2002).
48. Sin, O. & Nollen, E. A. A. Regulation of protein homeostasis in neurodegenerative diseases: the role of coding and non-coding genes. *Cell. Mol. Life Sci.* **72**, 4027–4047 (2015).

49. Yan, X., Wang, B., Hu, Y., Wang, S. & Zhang, X. Abnormal Mitochondrial Quality Control in Neurodegenerative Diseases. *Front. Cell. Neurosci.* **14**, (2020).
50. Chung, C. G., Lee, H. & Lee, S. B. Mechanisms of protein toxicity in neurodegenerative diseases. *Cell. Mol. Life Sci.* **75**, 3159–3180 (2018).
51. Guo, T., Noble, W. & Hanger, D. P. Roles of tau protein in health and disease. *Acta Neuropathol. (Berl.)* **133**, 665–704 (2017).
52. Mandelkow, E.-M. & Mandelkow, E. Biochemistry and Cell Biology of Tau Protein in Neurofibrillary Degeneration. *Cold Spring Harb. Perspect. Med.* **2**, (2012).
53. Morris, M., Maeda, S., Vossel, K. & Mucke, L. The Many Faces of Tau. *Neuron* **70**, 410–426 (2011).
54. Andreadis, A., Brown, W. M. & Kosik, K. S. Structure and novel exons of the human .tau. gene. *Biochemistry* **31**, 10626–10633 (1992).
55. Neve, R. L., Harris, P., Kosik, K. S., Kurnit, D. M. & Donlon, T. A. Identification of cDNA clones for the human microtubule-associated protein tau and chromosomal localization of the genes for tau and microtubule-associated protein 2. *Mol. Brain Res.* **1**, 271–280 (1986).
56. Couchie, D. *et al.* Primary structure of high molecular weight tau present in the peripheral nervous system. *Proc. Natl. Acad. Sci.* **89**, 4378–4381 (1992).
57. Jeganathan, S., von Bergen, M., Brutlach, H., Steinhoff, H.-J. & Mandelkow, E. Global Hairpin Folding of Tau in Solution. *Biochemistry* **45**, 2283–2293 (2006).
58. Hong, M. *et al.* Mutation-Specific Functional Impairments in Distinct Tau Isoforms of Hereditary FTDP-17. *Science* **282**, 1914–1917 (1998).
59. Goode, B. L., Chau, M., Denis, P. E. & Feinstein, S. C. Structural and Functional Differences between 3-Repeat and 4-Repeat Tau Isoforms: IMPLICATIONS FOR NORMAL TAU FUNCTION AND THE ONSET OF NEURODEGENERATIVE DISEASE *. *J. Biol. Chem.* **275**, 38182–38189 (2000).
60. Zhong, Q., Congdon, E. E., Nagaraja, H. N. & Kuret, J. Tau Isoform Composition Influences Rate and Extent of Filament Formation *. *J. Biol. Chem.* **287**, 20711–20719 (2012).
61. Goedert, M. & Jakes, R. Expression of separate isoforms of human tau protein: correlation with the tau pattern in brain and effects on tubulin polymerization. *EMBO J.* **9**, 4225–4230 (1990).
62. Trabzuni, D. *et al.* MAPT expression and splicing is differentially regulated by brain region: relation to genotype and implication for tauopathies. *Hum. Mol. Genet.* **21**, 4094–4103 (2012).
63. Wang, Y. P., Biernat, J., Pickhardt, M., Mandelkow, E. & Mandelkow, E.-M. Stepwise proteolysis liberates tau fragments that nucleate the Alzheimer-like aggregation of full-length tau in a neuronal cell model. *Proc. Natl. Acad. Sci.* **104**, 10252–10257 (2007).
64. Mukrasch, M. D. *et al.* Structural Polymorphism of 441-Residue Tau at Single Residue Resolution. *PLOS Biol.* **7**, e1000034 (2009).
65. Roman, A. Yu. *et al.* Zinc Induces Temperature-Dependent Reversible Self-Assembly of Tau. *J. Mol. Biol.* **431**, 687–695 (2019).
66. Leroy, K. *et al.* The active form of glycogen synthase kinase-3 β is associated with granulovacuolar degeneration in neurons in Alzheimer’s disease. *Acta Neuropathol. (Berl.)* **103**, 91–99 (2002).
67. Huang, Y. *et al.* Zinc Binding Directly Regulates Tau Toxicity Independent of Tau Hyperphosphorylation. *Cell Rep.* **8**, 831–842 (2014).
68. Gustke, N., Trinczek, B., Biernat, J., Mandelkow, E.-M. & Mandelkow, E. Domains of tau Protein and Interactions with Microtubules. *Biochemistry* **33**, 9511–9522 (1994).
69. Kadavath, H. *et al.* Tau stabilizes microtubules by binding at the interface between tubulin heterodimers. *Proc. Natl. Acad. Sci.* **112**, 7501–7506 (2015).
70. Brandt, R., Léger, J. & Lee, G. Interaction of tau with the neural plasma membrane mediated by tau’s amino-terminal projection domain. *J. Cell Biol.* **131**, 1327–1340 (1995).
71. Chen, J., Kanai, Y., Cowan, N. J. & Hirokawa, N. Projection domains of MAP2 and tau determine spacings between microtubules in dendrites and axons. *Nature* **360**, 674–677 (1992).
72. Bolkan, B. J. & Kretschmar, D. Loss of tau results in defects in photoreceptor development and progressive neuronal degeneration in *Drosophila*. *Dev. Neurobiol.* **74**, 1210–1225 (2014).

73. Yu, J.-Z. & Rasenick, M. M. Tau associates with actin in differentiating PC12 cells. *FASEB J.* **20**, 1452–1461 (2006).
74. Sultan, A. *et al.* Nuclear Tau, a Key Player in Neuronal DNA Protection *. *J. Biol. Chem.* **286**, 4566–4575 (2011).
75. Brandt, R., Hundelt, M. & Shahani, N. Tau alteration and neuronal degeneration in tauopathies: mechanisms and models. *Biol. Pathobiol. Tau* **1739**, 331–354 (2005).
76. Dixit, R., Ross, J. L., Goldman, Y. E. & Holzbaur, E. L. F. Differential Regulation of Dynein and Kinesin Motor Proteins by Tau. *Science* **319**, 1086–1089 (2008).
77. Stamer, K., Vogel, R., Thies, E., Mandelkow, E. & Mandelkow, E.-M. Tau blocks traffic of organelles, neurofilaments, and APP vesicles in neurons and enhances oxidative stress. *J. Cell Biol.* **156**, 1051–1063 (2002).
78. Kanaan, N. M. *et al.* Pathogenic Forms of Tau Inhibit Kinesin-Dependent Axonal Transport through a Mechanism Involving Activation of Axonal Phosphotransferases. *J. Neurosci.* **31**, 9858 (2011).
79. Magnani, E. *et al.* Interaction of tau protein with the dynactin complex. *EMBO J.* **26**, 4546–4554 (2007).
80. Belyy, V. *et al.* The mammalian dynein–dynactin complex is a strong opponent to kinesin in a tug-of-war competition. *Nat. Cell Biol.* **18**, 1018–1024 (2016).
81. Frandemiche, M. L. *et al.* Activity-Dependent Tau Protein Translocation to Excitatory Synapse Is Disrupted by Exposure to Amyloid-Beta Oligomers. *J. Neurosci.* **34**, 6084 (2014).
82. Barbier, P. *et al.* Role of Tau as a Microtubule-Associated Protein: Structural and Functional Aspects. *Front. Aging Neurosci.* **11**, 204 (2019).
83. Paonessa, F. *et al.* Microtubules Deform the Nuclear Membrane and Disrupt Nucleocytoplasmic Transport in Tau-Mediated Frontotemporal Dementia. *Cell Rep.* **26**, 582-593.e5 (2019).
84. Scott, C. W. *et al.* Differences in the abilities of human tau isoforms to promote microtubule assembly. *J. Neurosci. Res.* **30**, 154–162 (1991).
85. Mutreja, Y., Combs, B. & Gamblin, T. C. FTDP-17 Mutations Alter the Aggregation and Microtubule Stabilization Propensity of Tau in an Isoform-Specific Fashion. *Biochemistry* **58**, 742–754 (2019).
86. Liu, W. *et al.* IBS: an illustrator for the presentation and visualization of biological sequences. *Bioinformatics* **31**, 3359–3361 (2015).
87. DeTure, M. *et al.* Missense tau mutations identified in FTDP-17 have a small effect on tau–microtubule interactions. *Brain Res.* **853**, 5–14 (2000).
88. Sahara, N., Tomiyama, T. & Mori, H. Missense point mutations of tau to segregate with FTDP-17 exhibit site-specific effects on microtubule structure in COS cells: A novel action of R406W mutation. *J. Neurosci. Res.* **60**, 380–387 (2000).
89. Lei, P. *et al.* Motor and cognitive deficits in aged tau knockout mice in two background strains. *Mol. Neurodegener.* **9**, 29 (2014).
90. Seitz, A. *et al.* Single-molecule investigation of the interference between kinesin, tau and MAP2c. *EMBO J.* **21**, 4896–4905 (2002).
91. Millecamps, S. & Julien, J.-P. Axonal transport deficits and neurodegenerative diseases. *Nat. Rev. Neurosci.* **14**, 161–176 (2013).
92. Cowan, C. & Mudher, A. Are Tau Aggregates Toxic or Protective in Tauopathies? *Front. Neurol.* **4**, (2013).
93. Wang, Y. & Mandelkow, E. Tau in physiology and pathology. *Nat. Rev. Neurosci.* **17**, 22–35 (2016).
94. Andorfer, C. *et al.* Cell-Cycle Reentry and Cell Death in Transgenic Mice Expressing Nonmutant Human Tau Isoforms. *J. Neurosci.* **25**, 5446 (2005).
95. Spires-Jones, T. L. *et al.* *In Vivo* Imaging Reveals Dissociation between Caspase Activation and Acute Neuronal Death in Tangle-Bearing Neurons. *J. Neurosci.* **28**, 862 (2008).
96. Espuny-Camacho, I. *et al.* Hallmarks of Alzheimer’s Disease in Stem-Cell-Derived Human Neurons Transplanted into Mouse Brain. *Neuron* **93**, 1066-1081.e8 (2017).
97. Lasagna-Reeves, C. A. *et al.* Alzheimer brain-derived tau oligomers propagate pathology from endogenous tau. *Sci. Rep.* **2**, 700 (2012).

98. Maeda, S. *et al.* Granular Tau Oligomers as Intermediates of Tau Filaments. *Biochemistry* **46**, 3856–3861 (2007).
99. Hoover, B. R. *et al.* Tau Mislocalization to Dendritic Spines Mediates Synaptic Dysfunction Independently of Neurodegeneration. *Neuron* **68**, 1067–1081 (2010).
100. Tai, H.-C. *et al.* Frequent and symmetric deposition of misfolded tau oligomers within presynaptic and postsynaptic terminals in Alzheimer’s disease. *Acta Neuropathol. Commun.* **2**, 146 (2014).
101. Thies, E. & Mandelkow, E.-M. Missorting of Tau in Neurons Causes Degeneration of Synapses That Can Be Rescued by the Kinase MARK2/Par-1. *J. Neurosci.* **27**, 2896 (2007).
102. Zhou, L. *et al.* Tau association with synaptic vesicles causes presynaptic dysfunction. *Nat. Commun.* **8**, 15295 (2017).
103. Zempel, H. *et al.* Amyloid- β oligomers induce synaptic damage via Tau-dependent microtubule severing by TTL6 and spastin. *EMBO J.* **32**, 2920–2937 (2013).
104. Ittner, L. M. *et al.* Dendritic Function of Tau Mediates Amyloid- β Toxicity in Alzheimer’s Disease Mouse Models. *Cell* **142**, 387–397 (2010).
105. Roberson, E. D. *et al.* Amyloid- β /Fyn-Induced Synaptic, Network, and Cognitive Impairments Depend on Tau Levels in Multiple Mouse Models of Alzheimer’s Disease. *J. Neurosci.* **31**, 700 (2011).
106. Roberson Erik D. *et al.* Reducing Endogenous Tau Ameliorates Amyloid β -Induced Deficits in an Alzheimer’s Disease Mouse Model. *Science* **316**, 750–754 (2007).
107. SantaCruz, K. *et al.* Tau Suppression in a Neurodegenerative Mouse Model Improves Memory Function. *Science* **309**, 476 (2005).
108. Guo, J. L. *et al.* The Dynamics and Turnover of Tau Aggregates in Cultured Cells: INSIGHTS INTO THERAPIES FOR TAUOPATHIES *. *J. Biol. Chem.* **291**, 13175–13193 (2016).
109. Martin, L., Latypova, X. & Terro, F. Post-translational modifications of tau protein: Implications for Alzheimer’s disease. *Neurochem. Int.* **58**, 458–471 (2011).
110. Morris, M. *et al.* Tau post-translational modifications in wild-type and human amyloid precursor protein transgenic mice. *Nat. Neurosci.* **18**, 1183–1189 (2015).
111. Gendron, T. F. & Petrucelli, L. The role of tau in neurodegeneration. *Mol. Neurodegener.* **4**, 13 (2009).
112. Hanger, D. P., Anderton, B. H. & Noble, W. Tau phosphorylation: the therapeutic challenge for neurodegenerative disease. *Trends Mol. Med.* **15**, 112–119 (2009).
113. Mandelkow, E.-M. *et al.* Tau domains, phosphorylation, and interactions with microtubules. *Schmitt Symp. Cytoskelet. Alzheimers Dis.* **16**, 355–362 (1995).
114. Gong, C.-X. & Iqbal, K. Hyperphosphorylation of Microtubule-Associated Protein Tau: A Promising Therapeutic Target for Alzheimer Disease. *Curr. Med. Chem.* **15**, 2321–2328 (2008).
115. Lauretti, E. & Praticò, D. Alzheimer’s disease: phenotypic approaches using disease models and the targeting of tau protein. *Expert Opin. Ther. Targets* **24**, 319–330 (2020).
116. Zempel, H., Thies, E., Mandelkow, E. & Mandelkow, E.-M. A β Oligomers Cause Localized Ca²⁺ Elevation, Missorting of Endogenous Tau into Dendrites, Tau Phosphorylation, and Destruction of Microtubules and Spines. *J. Neurosci.* **30**, 11938 (2010).
117. Zempel, H. & Mandelkow, E. Mechanisms of Axonal Sorting of Tau and Influence of the Axon Initial Segment on Tau Cell Polarity. in *Tau Biology* (eds. Takashima, A., Wolozin, B. & Buee, L.) 69–77 (Springer Singapore, 2019). doi:10.1007/978-981-32-9358-8_6.
118. Iqbal, K. *et al.* Tau pathology in Alzheimer disease and other tauopathies. *Biol. Pathobiol. Tau* **1739**, 198–210 (2005).
119. Gong, C.-X. *et al.* Phosphatase Activity Toward Abnormally Phosphorylated τ : Decrease in Alzheimer Disease Brain. *J. Neurochem.* **65**, 732–738 (1995).
120. Gong, C.-X., Singh, T. J., Grundke-Iqbal, I. & Iqbal, K. Phosphoprotein Phosphatase Activities in Alzheimer Disease Brain. *J. Neurochem.* **61**, 921–927 (1993).
121. Liu, F., Grundke-Iqbal, I., Iqbal, K. & Gong, C.-X. Contributions of protein phosphatases PP1, PP2A, PP2B and PP5 to the regulation of tau phosphorylation. *Eur. J. Neurosci.* **22**, 1942–1950 (2005).

122. Sontag, E. *et al.* Altered Expression Levels of the Protein Phosphatase 2A AβC Enzyme Are Associated with Alzheimer Disease Pathology. *J. Neuropathol. Exp. Neurol.* **63**, 287–301 (2004).
123. Wesseling, H. *et al.* Tau PTM Profiles Identify Patient Heterogeneity and Stages of Alzheimer's Disease. *Cell* **183**, 1699–1713.e13 (2020).
124. Wegmann, S., Biernat, J. & Mandelkow, E. A current view on Tau protein phosphorylation in Alzheimer's disease. *Mol. Neurosci.* **69**, 131–138 (2021).
125. Kontaxi, C., Piccardo, P. & Gill, A. C. Lysine-Directed Post-translational Modifications of Tau Protein in Alzheimer's Disease and Related Tauopathies. *Front. Mol. Biosci.* **4**, (2017).
126. Cohen, T. J. *et al.* The acetylation of tau inhibits its function and promotes pathological tau aggregation. *Nat. Commun.* **2**, 252 (2011).
127. Cook, C. *et al.* Acetylation of the KXGS motifs in tau is a critical determinant in modulation of tau aggregation and clearance. *Hum. Mol. Genet.* **23**, 104–116 (2014).
128. Min, S.-W. *et al.* Acetylation of Tau Inhibits Its Degradation and Contributes to Tauopathy. *Neuron* **67**, 953–966 (2010).
129. Cohen, T. J., Friedmann, D., Hwang, A. W., Marmorstein, R. & Lee, V. M. Y. The microtubule-associated tau protein has intrinsic acetyltransferase activity. *Nat. Struct. Mol. Biol.* **20**, 756–762 (2013).
130. Irwin, D. J. *et al.* Acetylated Tau Neuropathology in Sporadic and Hereditary Tauopathies. *Am. J. Pathol.* **183**, 344–351 (2013).
131. Irwin, D. J. *et al.* Acetylated tau, a novel pathological signature in Alzheimer's disease and other tauopathies. *Brain* **135**, 807–818 (2012).
132. Trzeciakiewicz, H. *et al.* A Dual Pathogenic Mechanism Links Tau Acetylation to Sporadic Tauopathy. *Sci. Rep.* **7**, 44102 (2017).
133. Min, S.-W. *et al.* Critical role of acetylation in tau-mediated neurodegeneration and cognitive deficits. *Nat. Med.* **21**, 1154–1162 (2015).
134. Panza, F. *et al.* Disease-modifying therapies for tauopathies: agents in the pipeline. *Expert Rev. Neurother.* **19**, 397–408 (2019).
135. VandeVrede, L. *et al.* Open-Label Phase 1 Futility Studies of Salsalate and Young Plasma in Progressive Supranuclear Palsy. *Mov. Disord. Clin. Pract.* **7**, 440–447 (2020).
136. Cook, C., Stankowski, J. N., Carlomagno, Y., Stetler, C. & Petrucelli, L. Acetylation: a new key to unlock tau's role in neurodegeneration. *Alzheimers Res. Ther.* **6**, 29 (2014).
137. Cripps, D. *et al.* Alzheimer Disease-specific Conformation of Hyperphosphorylated Paired Helical Filament-Tau Is Polyubiquitinated through Lys-48, Lys-11, and Lys-6 Ubiquitin Conjugation *. *J. Biol. Chem.* **281**, 10825–10838 (2006).
138. Mori, H., Kondo, J. & Ihara, Y. Ubiquitin Is a Component of Paired Helical Filaments in Alzheimer's Disease. *Science* **235**, 1641–1644 (1987).
139. Perry, G., Friedman, R., Shaw, G. & Chau, V. Ubiquitin is detected in neurofibrillary tangles and senile plaque neurites of Alzheimer disease brains. *Proc. Natl. Acad. Sci.* **84**, 3033–3036 (1987).
140. Wang, Y. & Mandelkow, E. Degradation of tau protein by autophagy and proteasomal pathways. *Biochem. Soc. Trans.* **40**, 644–652 (2012).
141. Wang, J.-Z., Grundke-Iqbal, I. & Iqbal, K. Glycosylation of microtubule-associated protein tau: An abnormal posttranslational modification in Alzheimer's disease. *Nat. Med.* **2**, 871–875 (1996).
142. Arnold, C. S. *et al.* The Microtubule-associated Protein Tau Is Extensively Modified with O-linked N-acetylglucosamine *. *J. Biol. Chem.* **271**, 28741–28744 (1996).
143. Yuzwa, S. A. *et al.* Increasing O-GlcNAc slows neurodegeneration and stabilizes tau against aggregation. *Nat. Chem. Biol.* **8**, 393–399 (2012).
144. Liu, F. *et al.* Reduced O-GlcNAcylation links lower brain glucose metabolism and tau pathology in Alzheimer's disease. *Brain* **132**, 1820–1832 (2009).
145. Liu, F., Iqbal, K., Grundke-Iqbal, I., Hart, G. W. & Gong, C.-X. O-GlcNAcylation regulates phosphorylation of tau: A mechanism involved in Alzheimer's disease. *Proc. Natl. Acad. Sci.* **101**, 10804–10809 (2004).

146. Wang Andrew C., Jensen Elizabeth H., Rexach Jessica E., Vinters Harry V., & Hsieh-Wilson Linda C. Loss of O-GlcNAc glycosylation in forebrain excitatory neurons induces neurodegeneration. *Proc. Natl. Acad. Sci.* **113**, 15120–15125 (2016).
147. Borghgraef, P. *et al.* Increasing Brain Protein O-GlcNAc-ylation Mitigates Breathing Defects and Mortality of Tau.P301L Mice. *PLOS ONE* **8**, e84442 (2013).
148. Yu, Y. *et al.* Differential Effects of an O-GlcNAcase Inhibitor on Tau Phosphorylation. *PLOS ONE* **7**, e35277 (2012).
149. Wang, X. *et al.* MK-8719, a Novel and Selective O-GlcNAcase Inhibitor That Reduces the Formation of Pathological Tau and Ameliorates Neurodegeneration in a Mouse Model of Tauopathy. *J. Pharmacol. Exp. Ther.* **374**, 252 (2020).
150. Ballatore, C., Lee, V. M.-Y. & Trojanowski, J. Q. Tau-mediated neurodegeneration in Alzheimer's disease and related disorders. *Nat. Rev. Neurosci.* **8**, 663–672 (2007).
151. Goedert, M., Crowther, R. A. & Spillantini, M. G. Tau Mutations Cause Frontotemporal Dementias. *Neuron* **21**, 955–958 (1998).
152. Goedert, M. & Spillantini, M. G. Tau gene mutations and neurodegeneration. *Biochem. Soc. Symp.* **67**, 59–71 (2001).
153. Kovacs, G. G. Invited review: Neuropathology of tauopathies: principles and practice. *Neuropathol. Appl. Neurobiol.* **41**, 3–23 (2015).
154. Götz, J., Ittner, A. & Ittner, L. M. Tau-targeted treatment strategies in Alzheimer's disease. *Br. J. Pharmacol.* **165**, 1246–1259 (2012).
155. Medina, M. & Avila, J. New perspectives on the role of tau in Alzheimer's disease. Implications for therapy. *Alzheimer's Dis. – Amyloid Tau Beyond* **88**, 540–547 (2014).
156. Braak, H. & Braak, E. Staging of alzheimer's disease-related neurofibrillary changes. *Schmitt Symp. Cytoskelet. Alzheimers Dis.* **16**, 271–278 (1995).
157. Gerson, J. E., Castillo-Carranza, D. L. & Kaye, R. Advances in Therapeutics for Neurodegenerative Tauopathies: Moving toward the Specific Targeting of the Most Toxic Tau Species. *ACS Chem. Neurosci.* **5**, 752–769 (2014).
158. AVILA, J., LUCAS, J. J., PÉREZ, M. & HERNÁNDEZ, F. Role of Tau Protein in Both Physiological and Pathological Conditions. *Physiol. Rev.* **84**, 361–384 (2004).
159. Götz, J., Halliday, G. & Nisbet, R. M. Molecular Pathogenesis of the Tauopathies. *Annu. Rev. Pathol. Mech. Dis.* **14**, 239–261 (2019).
160. Lee, G. & Leugers, C. J. chapter 8 - Tau and Tauopathies. in *Progress in Molecular Biology and Translational Science* (ed. Teplow, D. B.) vol. 107 263–293 (Academic Press, 2012).
161. Braak, H. & Braak, E. Frequency of Stages of Alzheimer-Related Lesions in Different Age Categories. *Neurobiol. Aging* **18**, 351–357 (1997).
162. Raj, A., Kuceyeski, A. & Weiner, M. A Network Diffusion Model of Disease Progression in Dementia. *Neuron* **73**, 1204–1215 (2012).
163. Seeley, W. W., Crawford, R. K., Zhou, J., Miller, B. L. & Greicius, M. D. Neurodegenerative Diseases Target Large-Scale Human Brain Networks. *Neuron* **62**, 42–52 (2009).
164. Zhou, J., Gennatas, E. D., Kramer, J. H., Miller, B. L. & Seeley, W. W. Predicting Regional Neurodegeneration from the Healthy Brain Functional Connectome. *Neuron* **73**, 1216–1227 (2012).
165. Hyman Bradley T., Van Hoesen Gary W., Damasio Antonio R., & Barnes Clifford L. Alzheimer's Disease: Cell-Specific Pathology Isolates the Hippocampal Formation. *Science* **225**, 1168–1170 (1984).
166. Morrison, J. H. & Hof, P. R. Life and Death of Neurons in the Aging Brain. *Science* **278**, 412–419 (1997).
167. Bancher, C. *et al.* Accumulation of abnormally phosphorylated τ precedes the formation of neurofibrillary tangles in Alzheimer's disease. *Brain Res.* **477**, 90–99 (1989).
168. Glenner, G., Wong, C., Quaranta, V. & Eanes, E. The amyloid deposits in Alzheimer's disease: their nature and pathogenesis. *Appl Pathol.* **2**, (1984).

169. Glenner, G. G. & Wong, C. W. Alzheimer's disease: Initial report of the purification and characterization of a novel cerebrovascular amyloid protein. *Biochem. Biophys. Res. Commun.* **120**, 885–890 (1984).
170. Grundke-Iqbal, I. *et al.* Abnormal phosphorylation of the microtubule-associated protein tau (tau) in Alzheimer cytoskeletal pathology. *Proc. Natl. Acad. Sci.* **83**, 4913–4917 (1986).
171. Stelzmann, R. A., Norman Schnitzlein, H. & Reed Murtagh, F. An english translation of alzheimer's 1907 paper, "über eine eigenartige erkankung der hirnrinde". *Clin. Anat.* **8**, 429–431 (1995).
172. Forman, M. S., Trojanowski, J. Q. & Lee, V. M.-Y. Neurodegenerative diseases: a decade of discoveries paves the way for therapeutic breakthroughs. *Nat. Med.* **10**, 1055–1063 (2004).
173. Selkoe, D. J. Cell biology of protein misfolding: The examples of Alzheimer's and Parkinson's diseases. *Nat. Cell Biol.* **6**, 1054–1061 (2004).
174. Skovronsky, D. M., Lee, V. M.-Y. & Trojanowski, J. Q. NEURODEGENERATIVE DISEASES: New Concepts of Pathogenesis and Their Therapeutic Implications. *Annu. Rev. Pathol. Mech. Dis.* **1**, 151–170 (2006).
175. Goedert, M., Ghetti, B. & Spillantini, M. G. Frontotemporal Dementia: Implications for Understanding Alzheimer Disease. *Cold Spring Harb. Perspect. Med.* **2**, (2012).
176. Lee, V. M.-Y., Goedert, M. & Trojanowski, J. Q. Neurodegenerative Tauopathies. *Annu. Rev. Neurosci.* **24**, 1121–1159 (2001).
177. Ballatore, C. *et al.* Aminothienopyridazine inhibitors of tau aggregation: Evaluation of structure–activity relationship leads to selection of candidates with desirable in vivo properties. *Bioorg. Med. Chem.* **20**, 4451–4461 (2012).
178. Crowe, A. *et al.* Aminothienopyridazines and Methylene Blue Affect Tau Fibrillization via Cysteine Oxidation *. *J. Biol. Chem.* **288**, 11024–11037 (2013).
179. Pickhardt, M. *et al.* Identification of Small Molecule Inhibitors of Tau Aggregation by Targeting Monomeric Tau As a Potential Therapeutic Approach for Tauopathies. *Curr. Alzheimer Res.* **12**, 814–828 (2015).
180. Pickhardt, M. *et al.* Anthraquinones Inhibit Tau Aggregation and Dissolve Alzheimer's Paired Helical Filaments in Vitro and in Cells *. *J. Biol. Chem.* **280**, 3628–3635 (2005).
181. Schafer, K. N., Cisek, K., Huseby, C. J., Chang, E. & Kuret, J. Structural Determinants of Tau Aggregation Inhibitor Potency *. *J. Biol. Chem.* **288**, 32599–32611 (2013).
182. Taniguchi, S. *et al.* Inhibition of Heparin-induced Tau Filament Formation by Phenothiazines, Polyphenols, and Porphyrins *. *J. Biol. Chem.* **280**, 7614–7623 (2005).
183. Wischik, C. M., Edwards, P. C., Lai, R. Y., Roth, M. & Harrington, C. R. Selective inhibition of Alzheimer disease-like tau aggregation by phenothiazines. *Proc. Natl. Acad. Sci.* **93**, 11213–11218 (1996).
184. Clavaguera, F. *et al.* Brain homogenates from human tauopathies induce tau inclusions in mouse brain. *Proc. Natl. Acad. Sci.* **110**, 9535 (2013).
185. Murray, M. E. *et al.* Clinicopathologic assessment and imaging of tauopathies in neurodegenerative dementias. *Alzheimers Res. Ther.* **6**, 1 (2014).
186. Limorenko, G. & Lashuel, H. A. To target Tau pathologies, we must embrace and reconstruct their complexities. *Neurobiol. Dis.* **161**, 105536 (2021).
187. Goedert, M. Tau filaments in neurodegenerative diseases. *FEBS Lett.* **592**, 2383–2391 (2018).
188. Woerman Amanda L. *et al.* Tau prions from Alzheimer's disease and chronic traumatic encephalopathy patients propagate in cultured cells. *Proc. Natl. Acad. Sci.* **113**, E8187–E8196 (2016).
189. Ghetti, B., Wszolek, Z. K., Boeve, B. F., Spina, S. & Goedert, M. Frontotemporal Dementia and Parkinsonism Linked to Chromosome 17. in *Neurodegeneration: The Molecular Pathology of Dementia and Movement Disorders* 110–134 (2011). doi:10.1002/9781444341256.ch14.
190. Delacourte, A. *et al.* Specific Pathological Tau Protein Variants Characterize Pick's Disease. *J. Neuropathol. Exp. Neurol.* **55**, 159–168 (1996).
191. Arai, T. *et al.* Identification of amino-terminally cleaved tau fragments that distinguish progressive supranuclear palsy from corticobasal degeneration. *Ann. Neurol.* **55**, 72–79 (2004).

192. Tolnay, M. *et al.* Argyrophilic grain disease and Alzheimer's disease are distinguished by their different distribution of tau protein isoforms. *Acta Neuropathol. (Berl.)* **104**, 425–434 (2002).
193. Botez, G., Probst, A., Ipsen, S. & Tolnay, M. Astrocytes expressing hyperphosphorylated tau protein without glial fibrillary tangles in argyrophilic grain disease. *Acta Neuropathol. (Berl.)* **98**, 251–256 (1999).
194. Tolnay, M. & Clavaguera, F. Argyrophilic grain disease: A late-onset dementia with distinctive features among tauopathies. *Neuropathology* **24**, 269–283 (2004).
195. Nishimura, M., Namba, Y., Ikeda, K. & Oda, M. Glial fibrillary tangles with straight tubules in the brains of patients with progressive supranuclear palsy. *Neurosci. Lett.* **143**, 35–38 (1992).
196. Probst, A. *et al.* Progressive supranuclear palsy: extensive neuropil threads in addition to neurofibrillary tangles. *Acta Neuropathol. (Berl.)* **77**, 61–68 (1988).
197. Yamada, T., McGeer, P. L. & McGeer, E. G. Appearance of paired nucleated, Tau-positive glia in patients with progressive supranuclear palsy brain tissue. *Neurosci. Lett.* **135**, 99–102 (1992).
198. Komori, T. *et al.* Astrocytic plaques and tufts of abnormal fibers do not coexist in corticobasal degeneration and progressive supranuclear palsy. *Acta Neuropathol. (Berl.)* **96**, 401–408 (1998).
199. Probst, A., Tolnay, M., Langui, D., Goedert, M. & Spillantini, M. G. Pick's disease: hyperphosphorylated tau protein segregates to the somatoaxonal compartment. *Acta Neuropathol. (Berl.)* **92**, 588–596 (1996).
200. Goedert, M. & Spillantini, M. G. A Century of Alzheimer's Disease. *Science* **314**, 777–781 (2006).
201. Hardy, J. & Selkoe, D. J. The Amyloid Hypothesis of Alzheimer's Disease: Progress and Problems on the Road to Therapeutics. *Science* **297**, 353–356 (2002).
202. Baner, C., Jellinger, K., Lassmann, H., Fischer, P. & Leblhuber, F. Correlations between mental state and quantitative neuropathology in the Vienna Longitudinal Study on Dementia. *Eur. Arch. Psychiatry Clin. Neurosci.* **246**, 137–146 (1996).
203. Duyckaerts, C. *et al.* Modeling the Relation Between Neurofibrillary Tangles and Intellectual Status. *Neurobiol. Aging* **18**, 267–273 (1997).
204. Giannakopoulos, P., Hof, P. R., Michel, J.-P., Guimon, J. & Bouras, C. Cerebral cortex pathology in aging and Alzheimer's disease: a quantitative survey of large hospital-based geriatric and psychiatric cohorts. *Brain Res. Rev.* **25**, 217–245 (1997).
205. Grober, E. *et al.* Memory and mental status correlates of modified Braak staging. *Neurobiol. Aging* **20**, 573–579 (1999).
206. Braak, H. & Braak, E. Neuropathological staging of Alzheimer-related changes. *Acta Neuropathol. (Berl.)* **82**, 239–259 (1991).
207. Tepper, K. *et al.* Oligomer Formation of Tau Protein Hyperphosphorylated in Cells *. *J. Biol. Chem.* **289**, 34389–34407 (2014).
208. von Bergen, M. *et al.* Assembly of τ protein into Alzheimer paired helical filaments depends on a local sequence motif (³⁰⁶VQIVYK³¹¹) forming β structure. *Proc. Natl. Acad. Sci.* **97**, 5129 (2000).
209. Peterson, D. W., Zhou, H., Dahlquist, F. W. & Lew, J. A Soluble Oligomer of Tau Associated with Fiber Formation Analyzed by NMR. *Biochemistry* **47**, 7393–7404 (2008).
210. Barghorn, S. & Mandelkow, E. Toward a Unified Scheme for the Aggregation of Tau into Alzheimer Paired Helical Filaments. *Biochemistry* **41**, 14885–14896 (2002).
211. Barghorn, S., Davies, P. & Mandelkow, E. Tau Paired Helical Filaments from Alzheimer's Disease Brain and Assembled in Vitro Are Based on β -Structure in the Core Domain. *Biochemistry* **43**, 1694–1703 (2004).
212. von Bergen, M., Barghorn, S., Biernat, J., Mandelkow, E.-M. & Mandelkow, E. Tau aggregation is driven by a transition from random coil to beta sheet structure. *Biol. Pathobiol. Tau* **1739**, 158–166 (2005).
213. Crowther, R. A. & Wischik, C. M. Image reconstruction of the Alzheimer paired helical filament. *EMBO J.* **4**, 3661–3665 (1985).
214. Sillen, A. *et al.* Regions of Tau Implicated in the Paired Helical Fragment Core as Defined by NMR. *ChemBioChem* **6**, 1849–1856 (2005).

215. Wegmann, S. *et al.* Human Tau Isoforms Assemble into Ribbon-like Fibrils That Display Polymorphic Structure and Stability *. *J. Biol. Chem.* **285**, 27302–27313 (2010).
216. Wegmann Susanne, Medalsy Izhar D., Mandelkow Eckhard, & Müller Daniel J. The fuzzy coat of pathological human Tau fibrils is a two-layered polyelectrolyte brush. *Proc. Natl. Acad. Sci.* **110**, E313–E321 (2013).
217. von Bergen, M. *et al.* Mutations of Tau Protein in Frontotemporal Dementia Promote Aggregation of Paired Helical Filaments by Enhancing Local β -Structure *. *J. Biol. Chem.* **276**, 48165–48174 (2001).
218. Chen, D. *et al.* Tau local structure shields an amyloid-forming motif and controls aggregation propensity. *Nat. Commun.* **10**, 2493 (2019).
219. Bhattacharya, K., Rank, K. B., Evans, D. B. & Sharma, S. K. Role of Cysteine-291 and Cysteine-322 in the Polymerization of Human Tau into Alzheimer-like Filaments. *Biochem. Biophys. Res. Commun.* **285**, 20–26 (2001).
220. Sahara, N. *et al.* Assembly of two distinct dimers and higher-order oligomers from full-length tau. *Eur. J. Neurosci.* **25**, 3020–3029 (2007).
221. Schweers, O., Mandelkow, E. M., Biernat, J. & Mandelkow, E. Oxidation of cysteine-322 in the repeat domain of microtubule-associated protein tau controls the in vitro assembly of paired helical filaments. *Proc. Natl. Acad. Sci.* **92**, 8463–8467 (1995).
222. Soeda, Y. *et al.* Toxic tau oligomer formation blocked by capping of cysteine residues with 1,2-dihydroxybenzene groups. *Nat. Commun.* **6**, 10216 (2015).
223. Lee, V. M.-Y., Brunden, K. R., Hutton, M. & Trojanowski, J. Q. Developing Therapeutic Approaches to Tau, Selected Kinases, and Related Neuronal Protein Targets. *Cold Spring Harb. Perspect. Med.* **1**, (2011).
224. Noble, W., Jimenez-Sanchez, M., Perez-Nievas, B. G. & Hanger, D. P. Considerations for future tau-targeted therapeutics: can they deliver? *Expert Opin. Drug Discov.* **15**, 265–267 (2020).
225. Jeganathan, S. *et al.* Proline-directed Pseudo-phosphorylation at AT8 and PHF1 Epitopes Induces a Compaction of the Paperclip Folding of Tau and Generates a Pathological (MC-1) Conformation *. *J. Biol. Chem.* **283**, 32066–32076 (2008).
226. Schneider, A., Biernat, J., von Bergen, M., Mandelkow, E. & Mandelkow, E.-M. Phosphorylation that Detaches Tau Protein from Microtubules (Ser262, Ser214) Also Protects It against Aggregation into Alzheimer Paired Helical Filaments. *Biochemistry* **38**, 3549–3558 (1999).
227. Bulic, B. *et al.* Development of Tau Aggregation Inhibitors for Alzheimer’s Disease. *Angew. Chem. Int. Ed.* **48**, 1740–1752 (2009).
228. Zhang, W. *et al.* Heparin-induced tau filaments are polymorphic and differ from those in Alzheimer’s and Pick’s diseases. *eLife* **8**, e43584 (2019).
229. Fichou, Y. *et al.* Cofactors are essential constituents of stable and seeding-active tau fibrils. *Proc. Natl. Acad. Sci.* **115**, 13234 (2018).
230. Qi, H. *et al.* Characterization of Neuronal Tau Protein as a Target of Extracellular Signal-regulated Kinase *. *J. Biol. Chem.* **291**, 7742–7753 (2016).
231. Novak, M., Kabat, J. & Wischik, C. M. Molecular characterization of the minimal protease resistant tau unit of the Alzheimer’s disease paired helical filament. *EMBO J.* **12**, 365–370 (1993).
232. Rickard, J. E., Horsley, D., Wischik, C. M. & Harrington, C. R. Assays for the Screening and Characterization of Tau Aggregation Inhibitors. in *Tau Protein: Methods and Protocols* (ed. Smet-Nocca, C.) 129–140 (Springer New York, 2017). doi:10.1007/978-1-4939-6598-4_8.
233. Wille, H., Drewes, G., Biernat, J., Mandelkow, E. M. & Mandelkow, E. Alzheimer-like paired helical filaments and antiparallel dimers formed from microtubule-associated protein tau in vitro. *J. Cell Biol.* **118**, 573–584 (1992).
234. Wischik C M *et al.* Structural characterization of the core of the paired helical filament of Alzheimer disease. *Proc. Natl. Acad. Sci.* **85**, 4884–4888 (1988).
235. Goedert, M. *et al.* Assembly of microtubule-associated protein tau into Alzheimer-like filaments induced by sulphated glycosaminoglycans. *Nature* **383**, 550–553 (1996).

236. Crowe, A. *et al.* Identification of Aminothienopyridazine Inhibitors of Tau Assembly by Quantitative High-Throughput Screening. *Biochemistry* **48**, 7732–7745 (2009).
237. Fitzpatrick, A. W. P. *et al.* Cryo-EM structures of tau filaments from Alzheimer’s disease. *Nature* **547**, 185–190 (2017).
238. Fyfe, I. New in vivo evidence that different tau strains cause different diseases. *Nat. Rev. Neurol.* **12**, 677–677 (2016).
239. Sanders, D. W. *et al.* Distinct Tau Prion Strains Propagate in Cells and Mice and Define Different Tauopathies. *Neuron* **82**, 1271–1288 (2014).
240. Crowther, R. A., Olesen, O. F., Smith, M. J., Jakes, R. & Goedert, M. Assembly of Alzheimer-like filaments from full-length tau protein. *FEBS Lett.* **337**, 135–138 (1994).
241. del C. Alonso, A. *et al.* Interaction of Tau Isoforms with Alzheimer’s Disease Abnormally Hyperphosphorylated Tau and in Vitro Phosphorylation into the Disease-like Protein *. *J. Biol. Chem.* **276**, 37967–37973 (2001).
242. Eisenberg, D. S. & Sawaya, M. R. Structural Studies of Amyloid Proteins at the Molecular Level. *Annu. Rev. Biochem.* **86**, 69–95 (2017).
243. Knowles, T. P. J., Vendruscolo, M. & Dobson, C. M. The amyloid state and its association with protein misfolding diseases. *Nat. Rev. Mol. Cell Biol.* **15**, 384–396 (2014).
244. Collins, S. R., Douglass, A., Vale, R. D. & Weissman, J. S. Mechanism of Prion Propagation: Amyloid Growth Occurs by Monomer Addition. *PLOS Biol.* **2**, e321 (2004).
245. Harper, J. D. & Lansbury, P. T. MODELS OF AMYLOID SEEDING IN ALZHEIMER’S DISEASE AND SCRAPIE: Mechanistic Truths and Physiological Consequences of the Time-Dependent Solubility of Amyloid Proteins. *Annu. Rev. Biochem.* **66**, 385–407 (1997).
246. Jarrett, J. T. & Lansbury, P. T., Jr. Seeding “one-dimensional crystallization” of amyloid: A pathogenic mechanism in Alzheimer’s disease and scrapie? *Cell* **73**, 1055–1058 (1993).
247. Mirbaha, H. *et al.* Inert and seed-competent tau monomers suggest structural origins of aggregation. *eLife* **7**, e36584 (2018).
248. Chiti, F. & Dobson, C. M. Protein Misfolding, Amyloid Formation, and Human Disease: A Summary of Progress Over the Last Decade. *Annu. Rev. Biochem.* **86**, 27–68 (2017).
249. Labbadia, J. & Morimoto, R. I. The Biology of Proteostasis in Aging and Disease. *Annu. Rev. Biochem.* **84**, 435–464 (2015).
250. Kundra, R., Ciryam, P., Morimoto, R. I., Dobson, C. M. & Vendruscolo, M. Protein homeostasis of a metastable subproteome associated with Alzheimer’s disease. *Proc. Natl. Acad. Sci.* **114**, E5703–E5711 (2017).
251. Nedelsky, N. B., Todd, P. K. & Taylor, J. P. Autophagy and the ubiquitin-proteasome system: Collaborators in neuroprotection. *Ubiquitin Proteasomes Dis.* **1782**, 691–699 (2008).
252. Prusiner, S. B. Novel Proteinaceous Infectious Particles Cause Scrapie. *Science* **216**, 136–144 (1982).
253. Desplats, P. *et al.* Inclusion formation and neuronal cell death through neuron-to-neuron transmission of α -synuclein. *Proc. Natl. Acad. Sci.* **106**, 13010–13015 (2009).
254. Li, J.-Y. *et al.* Lewy bodies in grafted neurons in subjects with Parkinson’s disease suggest host-to-graft disease propagation. *Nat. Med.* **14**, 501–503 (2008).
255. Meyer-Luehmann, M. *et al.* Exogenous Induction of Cerebral β -Amyloidogenesis Is Governed by Agent and Host. *Science* **313**, 1781–1784 (2006).
256. Wischik, C. M., Schelter, B. O., Wischik, D. J., Storey, J. M. D. & Harrington, C. R. Modeling Prion-Like Processing of Tau Protein in Alzheimer’s Disease for Pharmaceutical Development. *J. Alzheimers Dis.* **62**, 1287–1303 (2018).
257. Kfoury, N., Holmes, B. B., Jiang, H., Holtzman, D. M. & Diamond, M. I. Trans-cellular Propagation of Tau Aggregation by Fibrillar Species*. *J. Biol. Chem.* **287**, 19440–19451 (2012).
258. Frost, B. & Diamond, M. I. Prion-like mechanisms in neurodegenerative diseases. *Nat. Rev. Neurosci.* **11**, 155–159 (2010).
259. Santa-Maria, I. *et al.* Paired Helical Filaments from Alzheimer Disease Brain Induce Intracellular Accumulation of Tau Protein in Aggresomes *. *J. Biol. Chem.* **287**, 20522–20533 (2012).

260. Iba, M. *et al.* Synthetic Tau Fibrils Mediate Transmission of Neurofibrillary Tangles in a Transgenic Mouse Model of Alzheimer's-Like Tauopathy. *J. Neurosci.* **33**, 1024 (2013).
261. de Calignon, A. *et al.* Propagation of Tau Pathology in a Model of Early Alzheimer's Disease. *Neuron* **73**, 685–697 (2012).
262. Liu, L. *et al.* Trans-Synaptic Spread of Tau Pathology In Vivo. *PLOS ONE* **7**, e31302 (2012).
263. Calafate, S. *et al.* Synaptic Contacts Enhance Cell-to-Cell Tau Pathology Propagation. *Cell Rep.* **11**, 1176–1183 (2015).
264. Dujardin, S. *et al.* Neuron-to-neuron wild-type Tau protein transfer through a trans-synaptic mechanism: relevance to sporadic tauopathies. *Acta Neuropathol. Commun.* **2**, 14 (2014).
265. Wu, J. W. *et al.* Neuronal activity enhances tau propagation and tau pathology in vivo. *Nat. Neurosci.* **19**, 1085–1092 (2016).
266. Wu, J. W. *et al.* Small Misfolded Tau Species Are Internalized via Bulk Endocytosis and Anterogradely and Retrogradely Transported in Neurons. *J. Biol. Chem.* **288**, 1856–1870 (2013).
267. Yamada, K. *et al.* Neuronal activity regulates extracellular tau in vivo. *J. Exp. Med.* **211**, 387–393 (2014).
268. Asai, H. *et al.* Depletion of microglia and inhibition of exosome synthesis halt tau propagation. *Nat. Neurosci.* **18**, 1584–1593 (2015).
269. Fontaine, S. N. *et al.* DnaJ/Hsc70 chaperone complexes control the extracellular release of neurodegenerative-associated proteins. *EMBO J.* **35**, 1537–1549 (2016).
270. Gómez-Ramos, A. *et al.* Characteristics and consequences of muscarinic receptor activation by tau protein. *Eur. Neuropsychopharmacol.* **19**, 708–717 (2009).
271. Holmes Brandon B. *et al.* Heparan sulfate proteoglycans mediate internalization and propagation of specific proteopathic seeds. *Proc. Natl. Acad. Sci.* **110**, E3138–E3147 (2013).
272. Jackson, S. J. *et al.* Short Fibrils Constitute the Major Species of Seed-Competent Tau in the Brains of Mice Transgenic for Human P301S Tau. *J. Neurosci.* **36**, 762 (2016).
273. Pollack, S. J. *et al.* Paired Helical Filament-Forming Region of Tau (297–391) Influences Endogenous Tau Protein and Accumulates in Acidic Compartments in Human Neuronal Cells. *J. Mol. Biol.* **432**, 4891–4907 (2020).
274. Tanemura, K. *et al.* Formation of Filamentous Tau Aggregations in Transgenic Mice Expressing V337M Human Tau. *Neurobiol. Dis.* **8**, 1036–1045 (2001).
275. Tatebayashi, Y. *et al.* Tau filament formation and associative memory deficit in aged mice expressing mutant (R406W) human tau. *Proc. Natl. Acad. Sci.* **99**, 13896–13901 (2002).
276. Wittmann, C. W. *et al.* Tauopathy in Drosophila: Neurodegeneration Without Neurofibrillary Tangles. *Science* **293**, 711–714 (2001).
277. Yoshiyama, Y. *et al.* Synapse Loss and Microglial Activation Precede Tangles in a P301S Tauopathy Mouse Model. *Neuron* **53**, 337–351 (2007).
278. Lasagna-Reeves, C. A. *et al.* Tau oligomers impair memory and induce synaptic and mitochondrial dysfunction in wild-type mice. *Mol. Neurodegener.* **6**, 39 (2011).
279. Arrasate, M., Mitra, S., Schweitzer, E. S., Segal, M. R. & Finkbeiner, S. Inclusion body formation reduces levels of mutant huntingtin and the risk of neuronal death. *Nature* **431**, 805–810 (2004).
280. Rubinsztein, D. C. The roles of intracellular protein-degradation pathways in neurodegeneration. *Nature* **443**, 780–786 (2006).
281. Barthélemy, N. R. *et al.* Differential Mass Spectrometry Profiles of Tau Protein in the Cerebrospinal Fluid of Patients with Alzheimer's Disease, Progressive Supranuclear Palsy, and Dementia with Lewy Bodies. *J. Alzheimers Dis.* **51**, 1033–1043 (2016).
282. Chai, X., Dage, J. L. & Citron, M. Constitutive secretion of tau protein by an unconventional mechanism. *Neurobiol. Dis.* **48**, 356–366 (2012).
283. Polanco, J. C., Scicluna, B. J., Hill, A. F. & Götz, J. Extracellular Vesicles Isolated from the Brains of rTg4510 Mice Seed Tau Protein Aggregation in a Threshold-dependent Manner. *J. Biol. Chem.* **291**, 12445–12466 (2016).

284. Simón, D., García-García, E., Royo, F., Falcón-Pérez, J. M. & Avila, J. Proteostasis of tau. Tau overexpression results in its secretion via membrane vesicles. *FEBS Lett.* **586**, 47–54 (2012).
285. Gómez-Ramos, A., Díaz-Hernández, M., Rubio, A., Miras-Portugal, M. T. & Avila, J. Extracellular tau promotes intracellular calcium increase through M1 and M3 muscarinic receptors in neuronal cells. *Mol. Cell. Neurosci.* **37**, 673–681 (2008).
286. Tian, T. *et al.* Dynamics of exosome internalization and trafficking. *J. Cell. Physiol.* **228**, 1487–1495 (2013).
287. Jucker, M. & Walker, L. C. Self-propagation of pathogenic protein aggregates in neurodegenerative diseases. *Nature* **501**, 45–51 (2013).
288. Clavaguera, F., Hench, J., Goedert, M. & Tolnay, M. Invited review: Prion-like transmission and spreading of tau pathology. *Neuropathol. Appl. Neurobiol.* **41**, 47–58 (2015).
289. Hanger, D. P. *et al.* Intracellular and Extracellular Roles for Tau in Neurodegenerative Disease. *J. Alzheimers Dis.* **40**, S37–S45 (2014).
290. Lewis, J. & Dickson, D. W. Propagation of tau pathology: hypotheses, discoveries, and yet unresolved questions from experimental and human brain studies. *Acta Neuropathol. (Berl.)* **131**, 27–48 (2016).
291. Croft, C. L. *et al.* Membrane association and release of wild-type and pathological tau from organotypic brain slice cultures. *Cell Death Dis.* **8**, e2671–e2671 (2017).
292. Pérez, M., Medina, M., Hernández, F. & Avila, J. Secretion of full-length Tau or Tau fragments in cell culture models. Propagation of Tau in vivo and in vitro. **9**, 1–11 (2018).
293. Fuster-Matanzo, A., Hernández, F. & Ávila, J. Tau Spreading Mechanisms; Implications for Dysfunctional Tauopathies. *Int. J. Mol. Sci.* **19**, (2018).
294. Usenovic, M. *et al.* Internalized Tau Oligomers Cause Neurodegeneration by Inducing Accumulation of Pathogenic Tau in Human Neurons Derived from Induced Pluripotent Stem Cells. *J. Neurosci.* **35**, 14234 (2015).
295. Kopeikina, K., Hyman, B. & Spires-Jones, T. Soluble forms of tau are toxic in Alzheimer’s disease. **3**, 223–233 (2012).
296. Braak, H. & Del Tredici, K. Alzheimer’s disease: Pathogenesis and prevention. *Alzheimers Dement.* **8**, 227–233 (2012).
297. de Calignon, A. *et al.* Propagation of Tau Pathology in a Model of Early Alzheimer’s Disease. *Neuron* **73**, 685–697 (2012).
298. Tian, H. *et al.* Trimeric Tau Is Toxic to Human Neuronal Cells at Low Nanomolar Concentrations. *Int. J. Cell Biol.* **2013**, 260787 (2013).
299. Gómez-Ramos, A., Díaz-Hernández, M., Cuadros, R., Hernández, F. & Avila, J. Extracellular tau is toxic to neuronal cells. *FEBS Lett.* **580**, 4842–4850 (2006).
300. Reynolds, M. R., Berry, R. W. & Binder, L. I. Site-Specific Nitration Differentially Influences τ Assembly in Vitro. *Biochemistry* **44**, 13997–14009 (2005).
301. Hallinan, G. I., Vargas-Caballero, M., West, J. & Deinhardt, K. Tau Misfolding Efficiently Propagates between Individual Intact Hippocampal Neurons. *J. Neurosci.* **39**, 9623 (2019).
302. Querfurth, H. W. & LaFerla, F. M. Alzheimer’s Disease. *N. Engl. J. Med.* **362**, 329–344 (2010).
303. Di, J. *et al.* Abnormal tau induces cognitive impairment through two different mechanisms: synaptic dysfunction and neuronal loss. *Sci. Rep.* **6**, 20833 (2016).
304. Kundel, F. *et al.* Measurement of Tau Filament Fragmentation Provides Insights into Prion-like Spreading. *ACS Chem. Neurosci.* **9**, 1276–1282 (2018).
305. Guo, J. L. & Lee, V. M.-Y. Seeding of Normal Tau by Pathological Tau Conformers Drives Pathogenesis of Alzheimer-like Tangles *. *J. Biol. Chem.* **286**, 15317–15331 (2011).
306. Hu, W. *et al.* Hyperphosphorylation determines both the spread and the morphology of tau pathology. *Alzheimers Dement.* **12**, 1066–1077 (2016).
307. Pickett, E. K. *et al.* Spread of tau down neural circuits precedes synapse and neuronal loss in the rTgTauEC mouse model of early Alzheimer’s disease. *Synapse* **71**, e21965 (2017).
308. Avila, J. Tau phosphorylation and aggregation in Alzheimer’s disease pathology. *FEBS Lett.* **580**, 2922–2927 (2006).

309. Ahn, J. S. *et al.* Defining Cdk5 Ligand Chemical Space with Small Molecule Inhibitors of Tau Phosphorylation. *Chem. Biol.* **12**, 811–823 (2005).
310. Brunden, K. R., Lee, V. M.-Y., Smith, A. B., Trojanowski, J. Q. & Ballatore, C. Altered microtubule dynamics in neurodegenerative disease: Therapeutic potential of microtubule-stabilizing drugs. *Neurobiol. Dis.* **105**, 328–335 (2017).
311. Cochran, J. N. *et al.* AlphaScreen HTS and Live-Cell Bioluminescence Resonance Energy Transfer (BRET) Assays for Identification of Tau–Fyn SH3 Interaction Inhibitors for Alzheimer Disease. *SLAS Discov.* **19**, 1338–1349 (2014).
312. Dehdashti, J. S. *et al.* A High-Throughput Screening Assay for Determining Cellular Levels of Total Tau Protein. *Curr. Alzheimer Res.* **10**, 679–687 (2013).
313. Soeda, Y. & Takashima, A. New Insights Into Drug Discovery Targeting Tau Protein. *Front. Mol. Neurosci.* **13**, (2020).
314. Messing, L., Decker, J. M., Joseph, M., Mandelkow, E. & Mandelkow, E.-M. Cascade of tau toxicity in inducible hippocampal brain slices and prevention by aggregation inhibitors. *Neurobiol. Aging* **34**, 1343–1354 (2013).
315. Khlistunova, I. *et al.* Inducible Expression of Tau Repeat Domain in Cell Models of Tauopathy: AGGREGATION IS TOXIC TO CELLS BUT CAN BE REVERSED BY INHIBITOR DRUGS *. *J. Biol. Chem.* **281**, 1205–1214 (2006).
316. Pickhardt, M. *et al.* N-Phenylamine Derivatives as Aggregation Inhibitors in Cell Models of Tauopathy. *Curr. Alzheimer Res.* **4**, 397–402 (2007).
317. Hochgräfe, K. *et al.* Preventive methylene blue treatment preserves cognition in mice expressing full-length pro-aggregant human Tau. *Acta Neuropathol. Commun.* **3**, 25 (2015).
318. Lira-De León, K. I. *et al.* Molecular Mechanism of Tau Aggregation Induced by Anionic and Cationic Dyes. *J. Alzheimers Dis.* **35**, 319–334 (2013).
319. Schirmer, R. H., Adler, H., Pickhardt, M. & Mandelkow, E. “Lest we forget you — methylene blue ...”. *Neurobiol. Aging* **32**, 2325.e7-2325.e16 (2011).
320. Fatouros, C. *et al.* Inhibition of tau aggregation in a novel *Caenorhabditis elegans* model of tauopathy mitigates proteotoxicity. *Hum. Mol. Genet.* **21**, 3587–3603 (2012).
321. Ma, Q.-L. *et al.* Curcumin Suppresses Soluble Tau Dimers and Corrects Molecular Chaperone, Synaptic, and Behavioral Deficits in Aged Human Tau Transgenic Mice *. *J. Biol. Chem.* **288**, 4056–4065 (2013).
322. Bieschke, J. *et al.* EGCG remodels mature α -synuclein and amyloid- β fibrils and reduces cellular toxicity. *Proc. Natl. Acad. Sci.* **107**, 7710–7715 (2010).
323. Ehrnhoefer, D. E. *et al.* EGCG redirects amyloidogenic polypeptides into unstructured, off-pathway oligomers. *Nat. Struct. Mol. Biol.* **15**, 558–566 (2008).
324. Zhang, J. *et al.* Epigallocatechin-3-gallate (EGCG)-Stabilized Selenium Nanoparticles Coated with Tet-1 Peptide To Reduce Amyloid- β Aggregation and Cytotoxicity. *ACS Appl. Mater. Interfaces* **6**, 8475–8487 (2014).
325. Selkoe, D. J. & Hardy, J. The amyloid hypothesis of Alzheimer’s disease at 25 years. *EMBO Mol. Med.* **8**, 595–608 (2016).
326. Kontsekova, E., Zilka, N., Kovacech, B., Novak, P. & Novak, M. First-in-man tau vaccine targeting structural determinants essential for pathological tau–tau interaction reduces tau oligomerisation and neurofibrillary degeneration in an Alzheimer’s disease model. *Alzheimers Res. Ther.* **6**, 44 (2014).
327. Wischik, C. M., Harrington, C. R. & Storey, J. M. D. Tau-aggregation inhibitor therapy for Alzheimer’s disease. *Alzheimer’s Dis. – Amyloid Tau Beyond* **88**, 529–539 (2014).
328. Cisek, K., Cooper, L. G., Huseby, J. C. & Kuret, J. Structure and Mechanism of Action of Tau Aggregation Inhibitors. *Curr. Alzheimer Res.* **11**, 918–927 (2014).
329. Akoury, E. *et al.* Inhibition of Tau Filament Formation by Conformational Modulation. *J. Am. Chem. Soc.* **135**, 2853–2862 (2013).
330. Dolai, S. *et al.* “Clicked” Sugar–Curcumin Conjugate: Modulator of Amyloid- β and Tau Peptide Aggregation at Ultralow Concentrations. *ACS Chem. Neurosci.* **2**, 694–699 (2011).

331. Fuse, S., Matsumura, K., Fujita, Y., Sugimoto, H. & Takahashi, T. Development of dual targeting inhibitors against aggregations of amyloid- β and tau protein. *Eur. J. Med. Chem.* **85**, 228–234 (2014).
332. Klingstedt, T. & Nilsson, K. P. R. Luminescent conjugated poly- and oligo-thiophenes: optical ligands for spectral assignment of a plethora of protein aggregates. *Biochem. Soc. Trans.* **40**, 704–710 (2012).
333. Landau, M. *et al.* Towards a Pharmacophore for Amyloid. *PLOS Biol.* **9**, e1001080 (2011).
334. Li, W. *et al.* Inhibition of tau fibrillization by oleocanthal via reaction with the amino groups of tau. *J. Neurochem.* **110**, 1339–1351 (2009).
335. Sinha, S. *et al.* Lysine-Specific Molecular Tweezers Are Broad-Spectrum Inhibitors of Assembly and Toxicity of Amyloid Proteins. *J. Am. Chem. Soc.* **133**, 16958–16969 (2011).
336. Huang, H.-C., Nguyen, T. & Pickett, C. B. Regulation of the antioxidant response element by protein kinase C-mediated phosphorylation of NF-E2-related factor 2. *Proc. Natl. Acad. Sci.* **97**, 12475–12480 (2000).
337. Stack, C. *et al.* Methylene blue upregulates Nrf2/ARE genes and prevents tau-related neurotoxicity. *Hum. Mol. Genet.* **23**, 3716–3732 (2014).
338. Driver, J. A. *et al.* Inverse association between cancer and Alzheimer’s disease: results from the Framingham Heart Study. *BMJ* **344**, e1442 (2012).
339. Frain, L. *et al.* Association of cancer and Alzheimer’s disease risk in a national cohort of veterans. *Alzheimers Dement.* **13**, 1364–1370 (2017).
340. Musicco, M. *et al.* Inverse occurrence of cancer and Alzheimer disease. *Neurology* **81**, 322 (2013).
341. Schmidt, S. A. J., Ording, A. G., Horváth-Puhó, E., Sørensen, H. T. & Henderson, V. W. Non-melanoma skin cancer and risk of Alzheimer’s disease and all-cause dementia. *PLOS ONE* **12**, e0171527 (2017).
342. Lanni, C., Masi, M., Racchi, M. & Govoni, S. Cancer and Alzheimer’s disease inverse relationship: an age-associated diverging derailment of shared pathways. *Mol. Psychiatry* **26**, 280–295 (2021).
343. Ospina-Romero, M. *et al.* Rate of Memory Change Before and After Cancer Diagnosis. *JAMA Netw. Open* **2**, e196160–e196160 (2019).
344. Sun, M., Wang, Y., Sundquist, J., Sundquist, K. & Ji, J. The Association Between Cancer and Dementia: A National Cohort Study in Sweden. *Front. Oncol.* **10**, (2020).
345. Holmes Brandon B. *et al.* Proteopathic tau seeding predicts tauopathy in vivo. *Proc. Natl. Acad. Sci.* **111**, E4376–E4385 (2014).
346. Kwok, M. K., Lin, S. L. & Schooling, C. M. Re-thinking Alzheimer’s disease therapeutic targets using gene-based tests. *eBioMedicine* **37**, 461–470 (2018).
347. Annadurai, N. *et al.* Antitumour drugs targeting tau R3 VQIVYK and Cys322 prevent seeding of endogenous tau aggregates by exogenous seeds. *FEBS J.* **289**, 1929–1949 (2022).
348. Nečas, D. & Klapetek, P. Gwyddion: an open-source software for SPM data analysis. **10**, 181–188 (2012).
349. Seidler, P. M. *et al.* Structure-based inhibitors of tau aggregation. *Nat. Chem.* **10**, 170–176 (2018).
350. Annadurai, N., Malina, L., Malohlava, J., Hajdúch, M. & Das, V. Tau R2 and R3 are essential regions for tau aggregation, seeding and propagation. *Biochimie* **200**, 79–86 (2022).
351. Ambadipudi, S., Reddy, J. G., Biernat, J., Mandelkow, E. & Zweckstetter, M. Residue-specific identification of phase separation hot spots of Alzheimer’s-related protein tau. *Chem. Sci.* **10**, 6503–6507 (2019).
352. Tanaka, Y. *et al.* Seeding Activity-Based Detection Uncovers the Different Release Mechanisms of Seed-Competent Tau Versus Inert Tau via Lysosomal Exocytosis. *Front. Neurosci.* **13**, 1258 (2019).
353. Shi, Y. *et al.* Structure-based classification of tauopathies. *Nature* **598**, 359–363 (2021).
354. Vaquer-Alicea, J., Diamond, M. I. & Joachimiak, L. A. Tau strains shape disease. *Acta Neuropathol. (Berl.)* **142**, 57–71 (2021).
355. Kim, C. *et al.* Distinct populations of highly potent TAU seed conformers in rapidly progressing Alzheimer’s disease. *Sci. Transl. Med.* **14**, eabg0253 (2022).
356. Dong, X. *et al.* Heparin remodels the microtubule-binding repeat R3 of Tau protein towards fibril-prone conformations. *Phys. Chem. Chem. Phys.* **23**, 20406–20418 (2021).

357. Barracchia, C. G. *et al.* Unsaturated Fatty Acid-Induced Conformational Transitions and Aggregation of the Repeat Domain of Tau. *Molecules* **25**, (2020).
358. Dinkel, P. D., Holden, M. R., Matin, N. & Margittai, M. RNA Binds to Tau Fibrils and Sustains Template-Assisted Growth. *Biochemistry* **54**, 4731–4740 (2015).
359. Tetz, G. *et al.* Bacterial DNA promotes Tau aggregation. *Sci. Rep.* **10**, 2369 (2020).
360. Zwierzchowski-Zarate, A. N., Kashmer, O. M., Collazo-Lopez, J. E., White, C. L. & Diamond, M. I. RNA induces unique tau strains and stabilizes Alzheimer’s disease seeds. *bioRxiv* 2022.01.29.478315 (2022) doi:10.1101/2022.01.29.478315.
361. Fichou, Y. *et al.* Tau-Cofactor Complexes as Building Blocks of Tau Fibrils. *Front. Neurosci.* **13**, (2019).
362. Ginsberg, S. D., Crino, P. B., Lee, V. M.-Y., Eberwine, J. H. & Trojanowski, J. Q. Sequestration of RNA in Alzheimer’s disease neurofibrillary tangles and senile plaques. *Ann. Neurol.* **41**, 200–209 (1997).
363. Su, J. H., Cummings, B. J. & Cotman, C. W. Localization of heparan sulfate glycosaminoglycan and proteoglycan core protein in aged brain and Alzheimer’s disease. *Neuroscience* **51**, 801–813 (1992).
364. Paul, A. *et al.* Inhibition of tau amyloid formation and disruption of its preformed fibrils by Naphthoquinone–Dopamine hybrid. *FEBS J.* **288**, 4267–4290 (2021).
365. Meraz-Ríos, M. A., Lira-De León, K. I., Campos-Peña, V., De Anda-Hernández, M. A. & Mena-López, R. Tau oligomers and aggregation in Alzheimer’s disease. *J. Neurochem.* **112**, 1353–1367 (2010).
366. Lund, H. *et al.* MARK4 and MARK3 associate with early tau phosphorylation in Alzheimer’s disease granulovacuolar degeneration bodies. *Acta Neuropathol. Commun.* **2**, 22 (2014).
367. Aillaud, I. *et al.* A novel D-amino acid peptide with therapeutic potential (ISAD1) inhibits aggregation of neurotoxic disease-relevant mutant Tau and prevents Tau toxicity in vitro. *Alzheimers Res. Ther.* **14**, 15 (2022).
368. Xia, Y., Prokop, S. & Giasson, B. I. “Don’t Phos Over Tau”: recent developments in clinical biomarkers and therapies targeting tau phosphorylation in Alzheimer’s disease and other tauopathies. *Mol. Neurodegener.* **16**, 37 (2021).
369. Liu, M. *et al.* Hyperphosphorylated tau aggregation and cytotoxicity modulators screen identified prescription drugs linked to Alzheimer’s disease and cognitive functions. *Sci. Rep.* **10**, 16551 (2020).
370. Johnston, P. A. Redox cycling compounds generate H₂O₂ in HTS buffers containing strong reducing reagents—real hits or promiscuous artifacts? *Omics* **15**, 174–182 (2011).
371. Hudson, S. A., Ecroyd, H., Kee, T. W. & Carver, J. A. The thioflavin T fluorescence assay for amyloid fibril detection can be biased by the presence of exogenous compounds. *FEBS J.* **276**, 5960–5972 (2009).
372. Berger, Z. *et al.* Accumulation of Pathological Tau Species and Memory Loss in a Conditional Model of Tauopathy. *J. Neurosci.* **27**, 3650 (2007).
373. Ghag, G. *et al.* Soluble tau aggregates, not large fibrils, are the toxic species that display seeding and cross-seeding behavior. *Protein Sci.* **27**, 1901–1909 (2018).
374. Miyazaki, Y. *et al.* A method to rapidly create protein aggregates in living cells. *Nat. Commun.* **7**, 11689 (2016).
375. Musi, N. *et al.* Tau protein aggregation is associated with cellular senescence in the brain. *Aging Cell* **17**, e12840 (2018).
376. DeVos, S. L. *et al.* Synaptic Tau Seeding Precedes Tau Pathology in Human Alzheimer’s Disease Brain. *Front. Neurosci.* **12**, 267 (2018).
377. Seidler, P. M. *et al.* Structure-based inhibitors halt prion-like seeding by Alzheimer’s disease–and tauopathy–derived brain tissue samples. *J. Biol. Chem.* **294**, 16451–16464 (2019).
378. Natale, C., Barzago, M. M. & Diomedea, L. *Caenorhabditis elegans* Models to Investigate the Mechanisms Underlying Tau Toxicity in Tauopathies. *Brain Sci.* **10**, (2020).
379. Sandhof, C. A., Hoppe, S. O., Tittelmeier, J. & Nussbaum-Krammer, C. C. *elegans* Models to Study the Propagation of Prions and Prion-Like Proteins. *Biomolecules* **10**, (2020).

380. Rodriguez, S. *et al.* Machine learning identifies candidates for drug repurposing in Alzheimer's disease. *Nat. Commun.* **12**, 1033 (2021).
381. Sun, L.-M., Chen, H.-J., Liang, J.-A. & Kao, C.-H. Long-term use of tamoxifen reduces the risk of dementia: a nationwide population-based cohort study. *QJM Int. J. Med.* **109**, 103–109 (2016).
382. Brunden, K. R. *et al.* The characterization of microtubule-stabilizing drugs as possible therapeutic agents for Alzheimer's disease and related tauopathies. *Pharmacol. Res.* **63**, 341–351 (2011).
383. Huang, L. *et al.* Sunitinib, a Clinically Used Anticancer Drug, Is a Potent AChE Inhibitor and Attenuates Cognitive Impairments in Mice. *ACS Chem. Neurosci.* **7**, 1047–1056 (2016).
384. Cramer, P. E. *et al.* ApoE-Directed Therapeutics Rapidly Clear β -Amyloid and Reverse Deficits in AD Mouse Models. *Science* **335**, 1503–1506 (2012).
385. O'Hare, E. *et al.* Lack of support for bexarotene as a treatment for Alzheimer's disease. *Synaptopathy – Biol. Ther.* **100**, 124–130 (2016).
386. Chu, J., Lauretti, E., Craige, C. P. & Praticò, D. Pharmacological Modulation of GSAP Reduces Amyloid- β Levels and Tau Phosphorylation in a Mouse Model of Alzheimer's Disease with Plaques and Tangles. *J. Alzheimers Dis.* **41**, 729–737 (2014).
387. Hayes, C. D. *et al.* Striking reduction of amyloid plaque burden in an Alzheimer's mouse model after chronic administration of carmustine. *BMC Med.* **11**, 81 (2013).
388. Hernandez, I. *et al.* A farnesyltransferase inhibitor activates lysosomes and reduces tau pathology in mice with tauopathy. *Sci. Transl. Med.* **11**, eaat3005 (2019).
389. Congdon, E. E. *et al.* Nucleation-dependent Tau Filament Formation: THE IMPORTANCE OF DIMERIZATION AND AN ESTIMATION OF ELEMENTARY RATE CONSTANTS *. *J. Biol. Chem.* **283**, 13806–13816 (2008).
390. Kaniyappan, S., Chandupatla, R. R., Mandelkow, E.-M. & Mandelkow, E. Extracellular low-n oligomers of tau cause selective synaptotoxicity without affecting cell viability. *Alzheimers Dement.* **13**, 1270–1291 (2017).
391. Lasagna-Reeves, C. A., Castillo-Carranza, D. L., Guerrero-Muñoz, M. J., Jackson, G. R. & Kaye, R. Preparation and Characterization of Neurotoxic Tau Oligomers. *Biochemistry* **49**, 10039–10041 (2010).
392. Flach, K. *et al.* Tau Oligomers Impair Artificial Membrane Integrity and Cellular Viability *. *J. Biol. Chem.* **287**, 43223–43233 (2012).
393. Xu, M. *et al.* Senolytics improve physical function and increase lifespan in old age. *Nat. Med.* **24**, 1246–1256 (2018).
394. Margittai, M. & Langen, R. Template-assisted filament growth by parallel stacking of tau. *Proc. Natl. Acad. Sci.* **101**, 10278–10283 (2004).
395. Habchi, J. *et al.* An anticancer drug suppresses the primary nucleation reaction that initiates the production of the toxic A β 42 aggregates linked with Alzheimer's disease. *Sci. Adv.* **2**, e1501244 (2016).
396. Yamada, K. *et al.* *In Vivo* Microdialysis Reveals Age-Dependent Decrease of Brain Interstitial Fluid Tau Levels in P301S Human Tau Transgenic Mice. *J. Neurosci.* **31**, 13110 (2011).
397. Park, D. *et al.* Resveratrol induces autophagy by directly inhibiting mTOR through ATP competition. *Sci. Rep.* **6**, 21772 (2016).
398. Kim, H.-S., Montana, V., Jang, H.-J., Parpura, V. & Kim, J. Epigallocatechin Gallate (EGCG) Stimulates Autophagy in Vascular Endothelial Cells: A POTENTIAL ROLE FOR REDUCING LIPID ACCUMULATION * \blacklozenge . *J. Biol. Chem.* **288**, 22693–22705 (2013).
399. Holczer, M. *et al.* Epigallocatechin-3-Gallate (EGCG) Promotes Autophagy-Dependent Survival via Influencing the Balance of mTOR-AMPK Pathways upon Endoplasmic Reticulum Stress. *Oxid. Med. Cell. Longev.* **2018**, 6721530 (2018).
400. Wang, K. *et al.* Quercetin induces protective autophagy in gastric cancer cells: Involvement of Akt-mTOR- and hypoxia-induced factor 1 α -mediated signaling. *Autophagy* **7**, 966–978 (2011).

401. Vasconcelos-Ferreira, A. *et al.* The autophagy-enhancing drug carbamazepine improves neuropathology and motor impairment in mouse models of Machado–Joseph disease. *Neuropathol. Appl. Neurobiol.* **48**, e12763 (2022).
402. Zhang, J.-J., Zhou, Q.-M., Chen, S. & Le, W.-D. Repurposing carbamazepine for the treatment of amyotrophic lateral sclerosis in SOD1-G93A mouse model. *CNS Neurosci. Ther.* **24**, 1163–1174 (2018).
403. Sun, X. *et al.* Targeting autophagy enhances the anticancer effect of artemisinin and its derivatives. *Med. Res. Rev.* **39**, 2172–2193 (2019).
404. Troncoso, R. *et al.* Dexamethasone-induced autophagy mediates muscle atrophy through mitochondrial clearance. *Cell Cycle* **13**, 2281–2295 (2014).
405. Mauthe, M. *et al.* Chloroquine inhibits autophagic flux by decreasing autophagosome-lysosome fusion. *Autophagy* **14**, 1435–1455 (2018).
406. Watanabe-Asano, T., Kuma, A. & Mizushima, N. Cycloheximide inhibits starvation-induced autophagy through mTORC1 activation. *Biochem. Biophys. Res. Commun.* **445**, 334–339 (2014).
407. Harris, H. & Rubinsztein, D. C. Control of autophagy as a therapy for neurodegenerative disease. *Nat. Rev. Neurol.* **8**, 108–117 (2012).
408. Kim, J. & Klionsky, D. J. Autophagy, Cytoplasm-to-Vacuole Targeting Pathway, and Pexophagy in Yeast and Mammalian Cells. *Annu. Rev. Biochem.* **69**, 303–342 (2000).
409. Mizushima, N. & Komatsu, M. Autophagy: Renovation of Cells and Tissues. *Cell* **147**, 728–741 (2011).
410. Seglen, P. O. & Bohley, P. Autophagy and other vacuolar protein degradation mechanisms. *Experientia* **48**, 158–172 (1992).
411. Berger, Z. *et al.* Rapamycin alleviates toxicity of different aggregate-prone proteins. *Hum. Mol. Genet.* **15**, 433–442 (2006).
412. Mandrioli, J. *et al.* Rapamycin treatment for amyotrophic lateral sclerosis: Protocol for a phase II randomized, double-blind, placebo-controlled, multicenter, clinical trial (RAP-ALS trial). *Medicine (Baltimore)* **97**, (2018).
413. Ravikumar, B. *et al.* Inhibition of mTOR induces autophagy and reduces toxicity of polyglutamine expansions in fly and mouse models of Huntington disease. *Nat. Genet.* **36**, 585–595 (2004).
414. Ciechanover, A. & Kwon, Y. T. Degradation of misfolded proteins in neurodegenerative diseases: therapeutic targets and strategies. *Exp. Mol. Med.* **47**, e147–e147 (2015).
415. Götz, J., Xia, D., Leinenga, G., Chew, Y. L. & Nicholas, H. What Renders TAU Toxic. *Front. Neurol.* **4**, (2013).
416. Spires, T. L. *et al.* Region-specific Dissociation of Neuronal Loss and Neurofibrillary Pathology in a Mouse Model of Tauopathy. *Am. J. Pathol.* **168**, 1598–1607 (2006).
417. Ikeda, K. *et al.* Alz-50/Gallyas-positive lysosome-like intraneuronal granules in Alzheimer’s disease and control brains. *Neurosci. Lett.* **258**, 113–116 (1998).
418. Nixon, R. A. & Yang, D.-S. Autophagy failure in Alzheimer’s disease—locating the primary defect. *Autophagy Protein Degrad. Neurol. Dis.* **43**, 38–45 (2011).
419. Lim, F. *et al.* FTDP-17 Mutations in tau Transgenic Mice Provoke Lysosomal Abnormalities and Tau Filaments in Forebrain. *Mol. Cell. Neurosci.* **18**, 702–714 (2001).
420. Wang, Y., Krüger, U., Mandelkow, E. & Mandelkow, E.-M. Generation of Tau Aggregates and Clearance by Autophagy in an Inducible Cell Model of Tauopathy. *Neurodegener. Dis.* **7**, 103–107 (2010).
421. Bain, H. D. C. *et al.* The role of lysosomes and autophagosomes in frontotemporal lobar degeneration. *Neuropathol. Appl. Neurobiol.* **45**, 244–261 (2019).
422. Caballero, B. *et al.* Interplay of pathogenic forms of human tau with different autophagic pathways. *Aging Cell* **17**, e12692 (2018).
423. Deng, Z., Sheehan, P., Chen, S. & Yue, Z. Is amyotrophic lateral sclerosis/frontotemporal dementia an autophagy disease? *Mol. Neurodegener.* **12**, 90 (2017).

424. Menzies, F. M., Fleming, A. & Rubinsztein, D. C. Compromised autophagy and neurodegenerative diseases. *Nat. Rev. Neurosci.* **16**, 345–357 (2015).
425. Rubinsztein, D. C. *et al.* Autophagy and Its Possible Roles in Nervous System Diseases, Damage and Repair. *Autophagy* **1**, 11–22 (2005).
426. Congdon, E. E. *et al.* Methylthioninium chloride (methylene blue) induces autophagy and attenuates tauopathy in vitro and in vivo. *Autophagy* **8**, 609–622 (2012).
427. Krüger, U., Wang, Y., Kumar, S. & Mandelkow, E.-M. Autophagic degradation of tau in primary neurons and its enhancement by trehalose. *Neurobiol. Aging* **33**, 2291–2305 (2012).
428. Ozcelik, S. *et al.* Rapamycin Attenuates the Progression of Tau Pathology in P301S Tau Transgenic Mice. *PLOS ONE* **8**, e62459 (2013).
429. Schaeffer, V. *et al.* Stimulation of autophagy reduces neurodegeneration in a mouse model of human tauopathy. *Brain* **135**, 2169–2177 (2012).
430. Siman, R., Cocca, R. & Dong, Y. The mTOR Inhibitor Rapamycin Mitigates Perforant Pathway Neurodegeneration and Synapse Loss in a Mouse Model of Early-Stage Alzheimer-Type Tauopathy. *PLOS ONE* **10**, e0142340 (2015).
431. Oyama, F., Murakami, N. & Ihara, Y. Chloroquine myopathy suggests that tau is degraded in lysosomes: implication for the formation of paired helical filaments in Alzheimer's disease. *Neurosci. Res.* **31**, 1–8 (1998).
432. Chen, X. *et al.* Promoting tau secretion and propagation by hyperactive p300/CBP via autophagy-lysosomal pathway in tauopathy. *Mol. Neurodegener.* **15**, 2 (2020).
433. Tang, Z. *et al.* mTor mediates tau localization and secretion: Implication for Alzheimer's disease. *Biochim. Biophys. Acta BBA - Mol. Cell Res.* **1853**, 1646–1657 (2015).
434. Caballero, B. *et al.* Acetylated tau inhibits chaperone-mediated autophagy and promotes tau pathology propagation in mice. *Nat. Commun.* **12**, 2238 (2021).
435. Kang, S., Son, S. M., Baik, S. H., Yang, J. & Mook-Jung, I. Autophagy-Mediated Secretory Pathway is Responsible for Both Normal and Pathological Tau in Neurons. *J. Alzheimers Dis.* **70**, 667–680 (2019).
436. Shao, J. & Diamond, M. I. Polyglutamine diseases: emerging concepts in pathogenesis and therapy. *Hum. Mol. Genet.* **16**, R115–R123 (2007).
437. Dufty, B. M. *et al.* Calpain-Cleavage of α -Synuclein: Connecting Proteolytic Processing to Disease-Linked Aggregation. *Am. J. Pathol.* **170**, 1725–1738 (2007).
438. Lee, V. M.-Y., Goedert, M. & Trojanowski, J. Q. Neurodegenerative Tauopathies. *Annu. Rev. Neurosci.* **24**, 1121–1159 (2001).
439. Cleveland, D. W., Hwo, S.-Y. & Kirschner, M. W. Purification of tau, a microtubule-associated protein that induces assembly of microtubules from purified tubulin. *J. Mol. Biol.* **116**, 207–225 (1977).
440. Drechsel, D. N., Hyman, A. A., Cobb, M. H. & Kirschner, M. W. Modulation of the dynamic instability of tubulin assembly by the microtubule-associated protein tau. *Mol. Biol. Cell* **3**, 1141–1154 (1992).
441. Guo, J. L. *et al.* The Dynamics and Turnover of Tau Aggregates in Cultured Cells: INSIGHTS INTO THERAPIES FOR TAUOPATHIES. *J. Biol. Chem.* **291**, 13175–13193 (2016).
442. Liang, J.-H. & Jia, J.-P. Dysfunctional autophagy in Alzheimer's disease: pathogenic roles and therapeutic implications. *Neurosci. Bull.* **30**, 308–316 (2014).
443. Arriagada, P. V., Growdon, J. H., Hedley-Whyte, T. & Hyman, B. T. Neurofibrillary tangles but not senile plaques parallel duration and severity of Alzheimer's disease. *Neurology* **42**, 631–639 (1992).
444. Ling, H. *et al.* Characteristics of progressive supranuclear palsy presenting with corticobasal syndrome: a cortical variant. *Neuropathol. Appl. Neurobiol.* **40**, 149–163 (2014).
445. Kouri, N. *et al.* Neuropathological features of corticobasal degeneration presenting as corticobasal syndrome or Richardson syndrome. *Brain* **134**, 3264–3275 (2011).
446. SantaCruz, K. *et al.* Tau Suppression in a Neurodegenerative Mouse Model Improves Memory Function. *Science* **309**, 476 (2005).

447. Wittmann, C. W. *et al.* Tauopathy in *Drosophila*: Neurodegeneration Without Neurofibrillary Tangles. *Science* **293**, 711 (2001).
448. Yoshiyama, Y. *et al.* Synapse Loss and Microglial Activation Precede Tangles in a P301S Tauopathy Mouse Model. *Neuron* **53**, 337–351 (2007).
449. Weingarten, M. D., Lockwood, A. H., Hwo, S. Y. & Kirschner, M. W. A protein factor essential for microtubule assembly. *Proc. Natl. Acad. Sci.* **72**, 1858 (1975).
450. Piras, A., Collin, L., Grüninger, F., Graff, C. & Rönnebeck, A. Autophagic and lysosomal defects in human tauopathies: analysis of post-mortem brain from patients with familial Alzheimer disease, corticobasal degeneration and progressive supranuclear palsy. *Acta Neuropathol. Commun.* **4**, 22 (2016).
451. Rubinsztein, D. C. The roles of intracellular protein-degradation pathways in neurodegeneration. *Nature* **443**, 780–786 (2006).
452. Caccamo, A. *et al.* mTOR regulates tau phosphorylation and degradation: implications for Alzheimer’s disease and other tauopathies. *Aging Cell* **12**, 370–380 (2013).
453. Krüger, U., Wang, Y., Kumar, S. & Mandelkow, E.-M. Autophagic degradation of tau in primary neurons and its enhancement by trehalose. *Neurobiol. Aging* **33**, 2291–2305 (2012).
454. Caballero, B. *et al.* Interplay of pathogenic forms of human tau with different autophagic pathways. *Aging Cell* **17**, e12692 (2018).
455. Bi, X. *et al.* Novel Cathepsin D Inhibitors Block the Formation of Hyperphosphorylated Tau Fragments in Hippocampus. *J. Neurochem.* **74**, 1469–1477 (2000).
456. Hamano, T. *et al.* Autophagic-lysosomal perturbation enhances tau aggregation in transfectants with induced wild-type tau expression. *Eur. J. Neurosci.* **27**, 1119–1130 (2008).
457. Inoue, K. *et al.* Macroautophagy deficiency mediates age-dependent neurodegeneration through a phospho-tau pathway. *Mol. Neurodegener.* **7**, 48 (2012).
458. Schweig, J. E. *et al.* Spleen tyrosine kinase (SYK) blocks autophagic Tau degradation in vitro and in vivo. *J. Biol. Chem.* **294**, 13378–13395 (2019).
459. Bjørkøy, G. *et al.* Chapter 12 Monitoring Autophagic Degradation of p62/SQSTM1. in *Methods in Enzymology* vol. 452 181–197 (Academic Press, 2009).
460. Annadurai, N. *et al.* Antitumour drugs targeting tau R3 VQIVYK and Cys322 prevent seeding of endogenous tau aggregates by exogenous seeds. *FEBS J.* **n/a**, (2021).
461. Seidler, P. M. *et al.* Structure-based discovery of small molecules that disaggregate Alzheimer’s disease tissue derived tau fibrils in vitro. *Nat. Commun.* **13**, 5451 (2022).
462. Zwierzchowski-Zarate, A. N. *et al.* RNA induces unique tau strains and stabilizes Alzheimer’s disease seeds. *J. Biol. Chem.* **298**, (2022).

Original articles, reviews

1. **N Annadurai**, L Malina, J Malohlava, M Hajdúch, V Das, Tau R2 and R3 are essential regions for tau aggregation, seeding and propagation, *Biochimie*, 2022, 200, 79-86, 0300-9084, PMID: 35623497.
2. **N Annadurai**, L Malina, M Salmona, L Diomede, A Diomede, A Cagnotto, M Romeo, M Šrejber, K Berka, M Otyepka, M Hajdúch, V Das. Antitumour drugs targeting Tau R3 VQIVYK and Cys322 Prevent Seeding of endogenous Tau aggregates by Exogenous Seeds. *FEBS Journal*, 2021 Nov 7. doi: 10.1111/febs.16270. Epub ahead of print. PMID: 34743390.
3. **N Annadurai**, JB De Sanctis, M Hajdúch, V Das. Tau secretion and propagation: Perspectives for potential preventive interventions in Alzheimer's disease and other tauopathies. *Experimental Neurology*, 2021, 343, 113756, PMID: 33989658.

Book chapter

1. **N Annadurai** and V Das. A combination of kinetic fluorometric assay and microscopy for the screening of potential anti-tau aggregating agents. K Agrawal, J Bouchal, V Das, J Drábek, P Džubák, M Hajdúch, K Koberna, A Ligasová, M Mistrík, JB De Sanctis, J Srovnal (Eds.). In: *Laboratory Techniques in Cellular and Molecular Medicine*, Palacký University Press. Chapter 41, pp: 340-348, 2021. ISBN 978-80-244-6049-9 (online: iPDF)

Aggregation buffer

20 mM Tris, pH 7.4, 100 mM NaCl, 1 mM EDTA

Dissolve appropriate amounts of the abovementioned chemicals in deionised water (eight-tenths of the final volume, e.g., 800 mL), adjust pH to 7.4 with 1 M NaOH and add deionised water to the final volume (e.g., to 1000 mL). Filter using a 0.22 µm sterile syringe filter. Store at 4 °C.

SDS gel composition

| Ingredients (for 10 mL) | 8% resolving gel | 10% resolving gel | 12% resolving gel | 4% stacking gel |
|--|-----------------------------|------------------------------|------------------------------|----------------------------|
| H ₂ O (mL) | 4.6 | 3.8 | 3.2 | 5.95 |
| 30% Acrylamide (mL) | 2.6 | 3.4 | 4 | 1.34 |
| 1.5 M Tris-HCl (pH 8.8) (mL) | 2.6 | 2.6 | 2.6 | |
| 0.5 M Tris-HCl (pH 6.8) mL | | | | 2.5 |
| 10% (w/v) SDS (mL) | 0.1 | 0.1 | 0.1 | 0.1 |
| 10% (w/v) ammonium persulfate (APS) (mL) | 0.1 | 0.1 | 0.1 | 0.1 |
| TEMED (mL) | 0.01 | 0.01 | 0.01 | 0.01 |

RIPA lysis buffer

150 mM NaCl, 0.5% sodium deoxycholate, 0.1% SDS (sodium dodecyl sulphate), 50 mM Tris-HCl, pH 8.0 supplemented with protease (Roche, Cat. # 04693116001) and phosphatase inhibitors (Roche, Cat. # 04906837001).

Triton X-100 cell fractionation buffer

1x Tris-Buffered Saline (TBS) containing 0.05% Triton X-100 supplemented with protease (Roche, Cat. # 04693116001) and phosphatase inhibitors (Roche, Cat. # 04906837001).

5x SDS sample buffer

Bromophenol blue (0.25 %), Glycerol (50 %), SDS (sodium dodecyl sulfate; 10 %), Tris-Cl (0.25 M, pH 6.8), β-Mercaptoethanol (10 %).

1x SDS running buffer

25 mM Tris base, 190 mM glycine and 0.1% SDS, Check the pH and adjust to 8.3. Makeup to 1000 mL with deionised water.

Gel fixation solution

50% methanol (v/v) and 10% acetic acid (v/v) in deionised water.

Western Blot Wet Transfer buffer (1x)

100 mL of 10x blotting buffer (Bio-rad, Cat. #1610771); 200 mL 100% methanol (working concentration 20%); Makeup to 1000 mL with deionised water.

Trans-Blot Turbo Transfer buffer (1x)

200 mL of 5x transfer buffer (Bio-rad, Cat. #10026938); with 600 ml of deionised water and 200 ml of ethanol (working concentration 20%).

10x TBS

200 mM Tris Base, 1500 mM NaCl, Adjust pH to 7.6. Makeup to 1000 mL with deionised water.

1x TBST

100 mL of 10x TBS with 1 mL of 0.1% Tween® 20 Detergent; Makeup to 1000 mL with deionised water.

Blocking buffer

5% BSA (bovine serum albumin; Add to TBST buffer (1x TBS + 0.1% Tween® 20 Detergent). Mix well and filter.

Materials (Instruments and equipment)

Centrifuges

| Name | Company |
|----------------------------|---------------------------|
| Eppendorf Centrifuge 5810R | Eppendorf, Germany |
| ROTINA 420R | Schoeller, Czech Republic |

Spectrophotometers

| Name | Company |
|----------------------------------|---------------------------|
| Enspire multimode plate reader | PerkinElmer, USA |
| Cary 60 UV-Vis Spectrophotometer | Agilent Technologies, USA |

Microscopes

| Name | Company |
|--|--------------------------------|
| Inverted Phase contrast tissue culture microscope (OLYMPUS IX51) | Olympus Corporation, Japan |
| AXIO Observer.D1 fluorescence Microscope | Carl Zeiss AG, Germany |
| Cell Voyager CV7000S microscope | Yokogawa, Japan |
| Operetta™ High-Content Imaging System | PerkinElmer, USA |
| ZEISS Cell Observer SD Spinning Disk Confocal Microscope | Carl Zeiss AG, German, Germany |

Cell culture equipment

| Name | Company |
|--|--|
| Vi-CELL™ XR Cell Viability Analyzer | Beckman Coulter, USA |
| Herasafe KS Class II biological safety cabinet | <i>Thermo Electron LED GmbH, Germany</i> |
| Heracell VIOS 160i CO ₂ Incubator | Thermo Fisher Scientific, USA |

Others

| Name | Company |
|-----------------------------------|---|
| Trans-Blot Turbo Transfer System | Bio-Rad, USA |
| ChemiDoc XRS+ System | Bio-Rad, USA |
| iBlot™ 2 Gel Transfer Device | Invitrogen by Thermo Fisher Scientific, USA |
| Unimax 1010 Shaker & Mixer | Heidolph, Germany |
| Vortex-Genie 2 mixer | Scientific Industries, USA |
| Roller mixers (Stuart SRT9) | Cole-Parmer®, UK |
| Bio TDB-100, Dry block thermostat | Biosan, Latvia |

| | |
|---|--|
| New Brunswick Ultra-low Temperature freezer (Innova® U725) | Eppendorf, Germany |
| Fridge/Freezer | Liebherr, Germany |
| Ice flaking machine | FRIGOPRO, Czech Republic |
| Laminar flow for bacterial inoculation (Herasafe KS Class II biological safety cabinet) | Thermo Electron LED GmbH, Germany |
| Weighing balance (Scaltec SBC 21) | SCALTEC INSTRUMENTS GmbH, Germany |
| pH meter (WTW™ inoLab™ 7110) | Xylem Analytics Germany Sales GmbH & Co. KG, Germany |
| Mica disc | Ted Pella Inc, USA |
| Gel apparatus for SDS-PAGE (Mini-PROTEAN® Tetra system) | Bio-Rad, USA |
| PVDF membrane (0.2 µm), Nitrocellulose Membrane (0.2 µm) | Bio-Rad, USA |
| Well plates (6,12,24, 96) | TPP Techno Plastic Products AG, Switzerland |
| Well plates (CellCarrier 96/384-well plate) | PerkinElmer, USA |
| Water bath | Memmert GmbH + Co. KG, Germany |
| Multidrop™ Combi Reagent Dispenser | Thermo Fisher Scientific, USA |
| Cup Horn (for sonication) | Qsonica L.L.C, USA |
| Branson 450 Digital Sonifier | Process Equipment & Supply Inc., USA |
| Glassware | SCHOTT AG, Germany |
| Microcentrifuge tubes 1.5 mL | Eppendorf, Germany |
| Conical Tubes 15 mL and 50 mL | TPP Techno Plastic Products AG, Switzerland |
| Pipette (0.1–2.5, 10, 20, 100, 200, 1000, 5000 µL) | Eppendorf, Germany |
| Multichannel Pipettes (0.5–10, 5–50, 10–100, 50–300 µL) | Eppendorf, Germany |
| Syringe filters (0.2 µm, 0.45 µm), Filtermax rapid bottle-top filter (capacity 500 mL) | TPP Techno Plastic Products AG, Switzerland |
| MSH-300, Magnetic Stirrer with hot plate | Biosan, Latvia |

Curriculum vitae

| | |
|---------------------------------------|--|
| Narendran Annadurai, M.Sc. | Institute of Molecular and Translational Medicine, Faculty of Medicine and Dentistry, Palacký University, Hněvotínská 1333/5 Olomouc (Czech Republic) E mail: narendran.annadurai01@upol.cz, ajnarendran@gmail.com Phone: +420-775 094 851 |
|---------------------------------------|--|

| RESEARCH EXPERIENCE | |
|--|--|
| 11/2015–Present | PhD student Institute of Molecular and Translational Medicine, Faculty of Medicine and Dentistry, Palacký University, Olomouc, Czech Republic <i>Identification and Characterisation of Tau minimal regions as Potential Pharmacological Targets against Tau Spreading in Tauopathies.</i> |
| 02/2014–07/2014 | Visiting Researcher Department of Immunity, Infection and Inflammation, University of Leicester, Leicester, United Kingdom <i>Bacterial genomics, pathogenesis and antimicrobial resistance (Klebsiella and Acinetobacter focused).</i> |
| 10/2011–06/2013 | Project Assistant CSIR- Central Drug Research Institute, Lucknow, Uttar Pradesh, India 1. <i>Combinatorial effect of Recombinant HIV-1 Protease and HIV-1 Nef proteins in cellular apoptosis regulation.</i> 2. <i>Mycobacterial clearance by human beta-casein hexapeptide in Balb/c mice model.</i> |
| EDUCATION AND TRAINING | |
| 06/2009-04/2011 | Master of Science in Biotechnology St. Joseph's College (Autonomous), Tiruchirappalli, Tamil Nadu, India Master's degree thesis: <i>Biochemical characterization of protease from a psychrophilic strain; Identification of the partial gene sequence encoding the protease</i> Microbial Biotechnology Division, CSIR-Indian Institute of Integrative Medicine, Jammu, India |
| 06/2006-04/2009 | Bachelor of Science in Biotechnology K.S.Rangasamy College of Arts and Science (Autonomous), Tiruchengode, Tamil Nadu, India |
| AWARDS | |
| <ol style="list-style-type: none"> 1. Dean's Award for Best Student Scientific Work, Faculty of Medicine and Dentistry, Palacký University, Olomouc, Czech Republic, 2022. 2. Recipient of PurSolutions' Reagent Scholarship by PurSolutions, LLC, Nashville, TN, USA, 2021. 3. Second prize in PhD Club Contest organized by the Cancer Research Foundation Czech Republic, Olomouc, | |

| |
|--|
| <p>Czech Republic, 2021.</p> <p>4. Dean's Award for Best Student Scientific Work, Faculty of Medicine and Dentistry, Palacký University, Olomouc, Czech Republic, 2018.</p> <p>5. Dean's Award for Best Student Scientific Work, Faculty of Medicine and Dentistry, Palacký University, Olomouc, Czech Republic, 2017.</p> <p>6. Indian Council of Medical Research and Department of Biotechnology Project Assistant Fellowships, CSIR-Central Drug Research Institute, Lucknow, Uttar Pradesh, India, 2011-2013.</p> <p>7. Certificate of Merit for first prize in Biotechnology (major), St. Joseph's College (Autonomous), Tiruchirappalli, Tamil Nadu, India, 2011.</p> <p>8. Merit certificate for the Second rank in the 10th standard State Board Examination in Government Higher Secondary School, Aravakurichi, Karur, Tamil Nadu, India, 2003-2004.</p> |
| PUBLICATIONS |
| <p>1. N Annadurai, L Malina, J Malohlava, M Hajdúch, V Das, Tau R2 and R3 are essential regions for tau aggregation, seeding and propagation, <i>Biochimie</i>, 2022, 200, 79-86, 0300-9084, PMID: 35623497.</p> <p>2. N Annadurai, L Malina, M Salmona, L Diomedea, A Diomedea, A Cagnotto, M Romeo, M Šrejber, K Berka, M Otyepka, M Hajdúch, V Das. Antitumour drugs targeting Tau R3 VQIVYK and Cys322 Prevent Seeding of endogenous Tau aggregates by Exogenous Seeds. <i>FEBS Journal</i>, 2021 Nov 7. doi: 10.1111/febs.16270. Epub ahead of print. PMID: 34743390.</p> <p>3. N Annadurai, JB De Sanctis, M Hajdúch, V Das. Tau secretion and propagation: Perspectives for potential preventive interventions in Alzheimer's disease and other tauopathies. <i>Experimental Neurology</i>, 2021, 343, 113756, PMID: 33989658.</p> <p>4. J Řehulka,[#] N Annadurai,[#] I Frydrych, P Džubák, JH Miller, M Hajdúch, V Das. Peloruside A-induced cell death in hypoxia is p53 dependent in HCT116 colorectal cancer cells. <i>Journal of Natural Products</i>, 2018, 81, 634-640, PMID: 29400463. ([#]equal contribution).</p> <p>5. N Annadurai, K Agrawal, P Džubák, M Hajdúch, V Das. Microtubule affinity-regulating kinases are potential druggable targets for Alzheimer's disease. <i>Cellular and Molecular Life Sciences</i>, 2017, 74, 4159-4169, PMID: 28634681.</p> <p>6. J Řehulka, N Annadurai, I Frydrych, P Znojek, P Džubák, P Northcote, JH Miller, M Hajdúch, V Das. Cellular effects of the microtubule-targeting agent peloruside A in hypoxia-conditioned colorectal carcinoma cells. <i>Biochimica et Biophysica Acta</i>, 2017, 17, 30124-1, PMID: 28366502.</p> |
| BOOK CHAPTERS |
| <p>1. N Annadurai and V Das. Microtubule Affinity Regulating Kinase 4: a potential drug target from cancers to neurodegenerative diseases. Md Imtaiyaz Hassan, S Noor (Eds.). In: <i>Protein Kinase Inhibitors: From Discovery to Therapeutics</i>. Elsevier Academic Press. Chapter 20, 2022. ISBN: 9780323912877 (paperback)</p> <p>2. N Annadurai and V Das. A combination of kinetic fluorometric assay and microscopy for the screening of potential anti-tau aggregating agents. K Agrawal, J Bouchal, V Das, J Drábek, P Džubák, M Hajdúch, K Koberna, A Ligasová, M Mistrík, JB De Sanctis, J Srovnal (Eds.). In: <i>Laboratory Techniques in Cellular and Molecular Medicine</i>, Palacký University Press. Chapter 41, pp: 340-348, 2021. ISBN 978-80-244-6049-9 (online: iPDF)</p> |
| CONFERENCE PRESENTATIONS |
| <p>1. Repurposing of anti-cancer drugs as potential inhibitors of toxic Tau aggregates. XIII Diagnostic, Predictive and Experimental Oncology Days, 2017 Czech Republic. (Oral)</p> <p>2. Identification of potential inhibitors of Tau aggregation for Alzheimer's disease therapy. XVII Interdisciplinary Meeting of Young Biologists, Biochemists and Chemists, 2017 Czech Republic. (Oral)</p> <p>3. Repurposing of anti-cancer drugs as potential inhibitors of toxic tau aggregates. Biomedical present: From basic</p> |

| |
|---|
| <p>research to clinical application. XXII Biological Days Conference, 2017 Slovak Republic. (Oral)</p> <ol style="list-style-type: none"> 4. Targeting the cellular uptake and processing of misfolded proteins: Example of tau aggregates. XIV Diagnostic, Predictive and Experimental Oncology Days, 2018 Czech Republic. (Oral) 5. Cellular uptake and processing of extracellular Tau aggregates: An implication for Neurodegenerative diseases. FENS Regional meeting, 2019 Serbia. (Poster) 6. Tau repeat peptide aggregates induce intracellular tau aggregation and phosphorylation. The 12th Conference of the Czech Neuroscience Society, 2019 Czech Republic. (Oral) 7. Seeding mechanisms of fibrillar tau repeat peptide aggregates. XX. Interdisciplinary Meeting of Young Biologists, Biochemists and Chemists, 2021 Czech Republic. (Oral) (Online) 8. Therapeutic targeting of repurposed anticancer drugs for protein aggregation: Example of tau aggregates. OL4PERMED, 2021 Czech Republic. (Oral) |
| RESEARCH SKILLS |
| <p>Eukaryotic cell culture and differentiation, Transfection/Co-transfection, Lentiviral particles preparation, transduction and stable cell line generation, 3D cell cultures (Cancer cell spheroids). Immunofluorescence technique. Fluorescence, Confocal microscopy. Immunoprecipitation, Native and SDS-PAGE, Protein gel staining methods, Western blot. Spectroscopic techniques. Handling and experimental procedures (intravenous injection, organ isolation) of BALB/c mice. Plasmid/Genomic DNA and RNA isolation, PCR, Gene cloning, Electrophoresis. Bacterial culture, transformation.</p> |
| SUPERVISION AND TEACHING EXPERIENCE |
| <ol style="list-style-type: none"> 1. Supervised one bachelor thesis. Jiří Hrubý. Dissertation title: Autophagy induction decreases the presence of endogenous P301S tau aggregates. Graduated: 2020. 2. Teaching assistant, Palacký University, Olomouc. 2018-2020. Exercises for bioorganic chemistry students (BSc, MSc): Isolation of RNA and reverse transcription, Isolation of DNA, spectrophotometry, gel electrophoresis. |